Author:
Alghazwani, Yahia S A

Title:
Characterisation of Compounds as Potential Inhibitors of G Protein-Coupled Receptor Kinases

University of BRISTOL

Characterisation of Compounds as Potential Inhibitors of G Protein-Coupled Receptor Kinases

Yahia Alghazwani

BSc, MSc

A dissertation submitted to the University of Bristol in accordance with the requirements for award of the degree of Doctor of Philosophy in the Faculty of Life Sciences

School of Physiology, Pharmacology and Neuroscience

August, 2020

Word count: 33602

Abstract

G-protein coupled receptor kinases (GRKs) are key regulators of GPCR signalling, and the search continues for potent and selective GRK inhibitors, for example, for the treatment of congestive heart failure. Compound101 (cmpd101), a GRK inhibitor, was developed by the Takeda Pharmaceuticals Company, and it exhibits some selectivity for the GRK2/3 subfamily. In this thesis, a number of novel cmpd101 analogues were investigated to determine their abilities to inhibit agonist-induced arrestin-3 recruitment to the μ opioid receptor (MOPr) and δ opioid receptor (DOPr) (as a proxy of GRK-induced phosphorylation of the receptor). In addition, the selectivity of cmpd101 and novel analogues towards different GRK isoforms was investigated following cellular overexpression of the GRK isoforms. To further explore the general selectivity of these novel analogues, their effects on agonist-induced G_i activation and MOPr internalisation were also explored. In DAMGO-stimulated cells, novel compounds BU14016, BU16005 and BU16007 showed significantly greater inhibition of arrestin-3 recruitment to MOPr than compound101, whilst compounds BU14013, BU14014 showed significantly less inhibition. In contrast, in cells treated with the lower efficacy MOPr agonist morphine, compound101 did not inhibit arrestin-3 recruitment, whilst only compounds BU16005 and BU14016 had any inhibitory capacity against morphine. Thus, the inhibitory effect of the novel analogues on GRK phosphorylation and following arrestin-3 recruitment to MOPr is apparently agonist-dependent. Interestingly, the novel analogues were not effective at reducing SNC80- or DADLE-induced arrestin-3 recruitment to DOPr. Thus, the effects of the novel analogues may also be GPCR subtype-dependent. Moreover, GRK isoform-overexpression studies with subsequent arrestin-3 recruitment measurements, suggested that the novel analogues show little or no selectivity between the isoforms, although this reflects the key role of GRK2 in promoting initial phosphorylation of MOPr. Overall, this thesis provides new evidence regarding the selectivity of cmpd101 and novel analogues for inhibition of GRK/arrestin function in HEK293 cells.

Acknowledgement

I cannot express enough thanks to my PhD supervisor, Prof. Eamonn Kelly, for his continuous support, encouragement, tireless guidance and patience. His guidance helped me throughout doing the research and writing of this thesis. Without his support, I would not have completed my PhD research. I am extremely grateful for what he has offered me. I could not have imagined having a better advisor for my PhD study.

Also, I would like to thank Prof. Graeme Henderson for his motivation, enthusiasm and immense knowledge, and for his constructive comments and support.

Special thanks to Dr. Alex Conibear for teaching me all the lab techniques, for the stimulating discussions and insightful comments.

Thank you to Dr. Gerda and Dr. Katy Sutcliffe for being supportive and cooperative and for helping me getting the lab work started.

Thank you Nokomis and all lab members for your kindness and support.

To my caring, loving and supportive wife, Fatimah, thanks from my deepest heart for your encouragement during tough times and during writing my thesis. Thank you for your great and successful management of the house and taking care of the kids while completing my work. Special thanks to my little daughters, Raseel and Samaya, for loving, supporting and understanding of my work.

I am extremely grateful to my mother, sisters and brothers for loving, caring, support and prayers along the way.

Special thanks to King Khalid University for sponsoring my PhD research and supporting me in my journey towards this degree.

This thesis is dedicated to .....

my Father's Soul

Yahia

Author’s Declaration

I declare that the work in this dissertation was carried out in accordance with the requirements of the University's *Regulations and Code of Practice for Research Degree Programmes* and that it has not been submitted for any other academic award. Except where indicated by specific reference in the text, the work is the candidate's own work. Work done in collaboration with, or with the assistance of, others, is indicated as such. Any views expressed in the dissertation are those of the author.

SIGNED: ..... DATE:.....

Abbreviations

AA	Amino acid
AC	Adenylyl cyclase
AMP	Adenosine monophosphate
ANOVA	Analysis of variance
AP2	Adaptor protein 2
β_2AR	Beta-2 adrenergic receptor
AT1R	Angiotensin II receptor type 1
ATP	Adenosine triphosphate
BRET	Bioluminescence resonance energy transfer
BSA	Bovine serum albumin
CaMKII	Calcium/calmodulin-dependent protein kinase II
CCP	Clathrin-coated pits
CCR5	C-C chemokine receptor type 5
CHO cells	Chinese hamster ovary cell
CNS	Central nervous system
CO_2	Carbon dioxide
CRISPR	Clustered regularly interspaced short palindromic repeats
DADLE	[D-Ala2, D-Leu5]-enkephalin
DAMGO	[D-Ala2, N-mephe4, Gly-ol]-enkephalin
DC assay	Detergent compatible protein assay
DFS	Differential scanning fluorimetry
DMEM	Dulbecco's Modified Eagle's Medium
DMSO	Dimethyl sulfoxide
DNM	Dominant-negative mutant
DOPr	Delta opioid receptor
DPDPE	[D-pen2,5]enkephalin
EC_{50}	Half maximal effective concentration
ECL	Extracellular loop
EDTA	Ethylenediaminetetraacetic acid
EGFR	Epidermal growth factor receptor
ELISA	Enzyme-linked immunosorbent assay
EM	Cryogenic electron microscopy

ERK	Extracellular signal-regulated kinase
FACS	Fluorescence-activated cell sorting
FBS	Foetal bovine serum
FDA	Food and Drug Administration
FITC	Fluorescein isothiocyanate
FRET	Fluorescence resonance energy transfer
FSC	Forward scatter
GABA	Gamma-aminobutyric acid
GDP	Guanosine-5'-diphosphate
GFP	Green fluorescent protein
GIRK	G protein-coupled inwardly-rectifying potassium channel
GLUT4	Glucose transporter protein type-4
GPCR	G protein-coupled receptor
GRK	G protein-coupled receptor kinase
GTP	Guanosine-5'-triphosphate
HA	Human influenza hemagglutinin
HDAC5	Class II histone deacetylase 5
HEK293	Human embryonic kidney 293
HEPES	4-(2-hydroxyethyl)-1-piperazineethanesulfonic acid
HRP	Horse-radish peroxidase
IC_{50}	He half maximal inhibitory concentration
ICL	Intracellular loop
IRS1	Insulin receptor substrate 1
JNK	C-Jun N-terminal kinase
KOPr	Kappa opioid receptor
LB	Lysogeny broth
LC	Locus coeruleus
MAPK	Insulin receptor substrate 1
ME	Met-enkephalin
MEF2	Myocyte enhancer factor 2
MOPr	Mu opioid receptor
MSK	Mitogen- and stress-activated kinases
NIH	National Institute of Health
NLS	Nuclear localisation sequence
U2OS CELL	U2-osteosarcoma

PBS	Phosphate-buffered saline
PDB	Protein data bank
PDGFR	Platelet-derived growth factor receptor β
PDVF	Polyvinylidene fluoride
PFA	Paraformaldehyde
PH	Pleckstrin homology
PI3K	Phosphoinositide 3-kinase
PIP2	Phosphatidylinositol 4,5, biphosphate
PKA	Protein kinase A
PKC	Protein kinase C
PRK2	Protein kinase C-related protein kinase
RH	Regulator of G protein signalling homology
RLuc2	Renilla luciferase
ROCK1	Rho-associated protein kinase 1
RSK1	P90 ribosomal protein S6 kinase
RVM	Rostral ventromedial medulla
SCG	Superior cervical ganglion
SDS	Sodium dodecyl sulfate
SELEX	Systematic evolution of ligands by exponential enrichment
SEM	Standard error of the mean
SERT	Serotonin transporters
SGK1	Serum and glucocorticoid-related kinase
SK-N-BE cells	Human neuroblastoma cell line
SOC	Super optimal broth with catabolite repression
SRC	Proto-oncogene tyrosine-protein kinase
SSRI	Selective serotonin reuptake inhibitor
TBS	Tris-buffered saline
TBST	Tris-buffered saline+Tween20
TM	Transmembrane domain
UTP	Uridine triphosphate
WB	Western blot
WT	Wild type
YFP	Yellow fluorescent protein

Table of Contents

List of Figures

List of Tables

CHAPTER 1 General Introduction

1.1 G protein-coupled receptors (GPCRs)

G protein-coupled receptors (GPCRs) are the largest protein family in mammals, comprising more than 800 receptors in the human genome (Fredriksson et al. 2003). GPCRs are localised on the plasma membrane of cells and they generally transduce external stimuli to the cell. They play a vital role in regulating many intracellular signalling pathways, which regulate many physiological functions including vision, smell, inflammatory response, neurotransmission and cellular differentiation and growth (Lefkowitz 2000). Therefore, any disturbance in GPCR signalling pathways has the potential to lead to diseases such as cancer, diabetes, inflammation, cardiac dysfunction and neuronal damage (Hu, Mai & Chen 2017). Also, GPCRs are pharmacologically important because around 30% of clinically used drugs target GPCRs (Hauser et al. 2017).

1.1.1 Classification of GPCRs

GPCRs are classified into six families based on sequence homology and similarity in function (Alexander et al. 2017; Hu, Mai & Chen 2017). The class A receptors, also known as the rhodopsin-like family, are the largest family of GPCRs including, light receptors, hormones, neurotransmitters, and includes the opioid receptors. Class B GPCRs, also called the secretin receptor family, includes 15 members, such as the secretin, glucagon and glucagon-like peptide1 receptor (Karageorgos et al. 2018). Class B is characterised by a long N-terminus with around 120 residues, which mostly interact with large peptide endogenous ligands (Hu, Mai & Chen 2017). Class C GPCRs includes metabotropic glutamate family, $GABA_B$ receptors and calcium-sensing receptors. Class C has a large N-terminus with about 600 residues (Hu, Mai & Chen 2017). Class C receptors are dimers with the ligand-binding pocket located on the extracellular Venus flytrap domain. Class D GPCRs includes fungal mating pheromone receptors, while class E includes cAMP receptors (Fredriksson et al. 2003). Class F GPCRs include frizzled/smoothened receptors, which consist of 10 frizzleds that are activated by Wnt signal, and smoothened, which regulates the hedgehog signal that plays an important role in embryonic development (Kozielewicz, Turku & Schulte 2020).

1.1.2 Structure of GPCRs

GPCRs have a conserved structure which consists of seven transmembrane α-helices (7TM) connected by three alternating intracellular (ICL1-3) and three extracellular (ECL1-3) loops followed by a cytoplasmic carboxyl-terminus tail (Figure 1.1) (Katritch, Cherezov & Stevens 2012). The extracellular region (ECL) includes an extracellular N-terminus, which varies in length between GPCR families (Katritch, Cherezov & Stevens 2012; Latek et al. 2012). The intercellular regions interact with G proteins, G protein-coupled receptor kinases (GRKs), arrestins and other downstream effectors (Latek et al. 2012).

1.1.3 GPCR Signalling

GPCRs transduce signal from the extracellular to the intracellular regions. Different efficacy ligands can modulate GPCRs signalling. The ligands of GPCR fall into these basic categories: a full agonist that induces a maximal signal response, a partial agonist that produces a submaximal signal response, an antagonist, which occupies the receptor binding site and does not produce a response, and an inverse agonist, which suppresses the basal activity of the receptor (Hilger, Masureel & Kobilka 2018).

Table 1.1 Classification of GPCRs

Family		Representative examples
Class A	Rhodopsin-like family	• Light receptors • Hormones • Neurotransmitters • Opioid receptors
Class B	Secretin receptor	• Secretin • Glucagon • Glucagon-like peptide1
Class C		• Metabotropic glutamate family • $GABA_B$ receptors • Calcium sensing receptors
Class D		• Fungal mating pheromone receptors
Class E		• cAMP receptors
Class F		• Frizzled/smoothened receptors

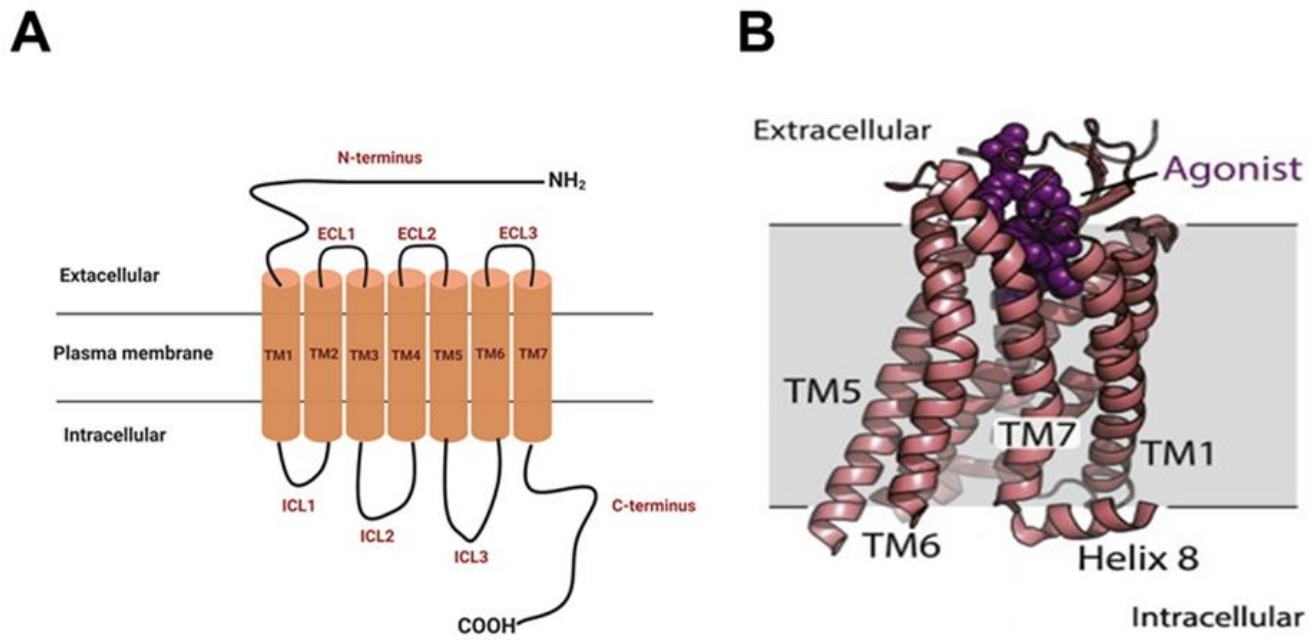

Figure 1.1 General structure of GPCRs

A) Schematic representation of the main features of GPCR structure. GPCR structure consists of seven transmembrane (TM1-TM7) domains connected by three intracellular (ICL1-ICL3) and three extracellular (ECL1-ECL3) loops, an extracellular N-terminus and intracellular C-terminus. B) The crystal structure of angiotensin II type 1 receptor (AT1R) (pink), an example of GPCR, bound to an agonist (purple) showing the arrangement of the seven transmembrane domains. Crystal structure of AT1R was taken from Wingler and Lefkowitz (2020).

Activation of GPCRs by an agonist is followed by the movement of transmembrane helices 5 and 6 (Gurevich, V. V. & Gurevich 2019), which creates a cavity on the cytoplasmic side of the receptor, which, in turn, becomes the docking site for G proteins, G protein-coupled receptor kinases (GRKs), and arrestins (Gurevich, V. V. & Gurevich 2019; Hilger, Masureel & Kobilka 2018). The heterotrimeric G proteins consist of G_{α}, G_{β} and G_{γ} subunits. G proteins are divided, based on the homology of G_{α}, into four major families: G_{s}, $G_{i/o}$, $G_{q/11}$ and $G_{12/13}$ (Downes & Gautam 1999).

Upon receptor activation, binding of G protein to the activated receptor resulting in the release of GDP and binding of GTP (Figure 1.2). Consequently, G_{α} subunit dissociates from the βγ dimer, where each subunit can bind to their effectors (Figure 1.2). The free GPCR can bind to another G protein and go through the same cycle, which leads to amplification of the signal. This ongoing activation must be controlled to ensure the cells are not over-activated and to maintain homeostasis; therefore, the signal needs to be turned off in due course. This occurs in two-step mechanism: phosphorylation of the serine/threonine (Ser/Thr) residues on the C-terminal and/or intracellular loop of the activated receptor by G protein-coupled receptor kinases (GRKs) that enhance the binding affinity of arrestins. Binding of arrestin to the activated receptor block G protein interaction with the receptor subjects it to desensitisation, internalisation, endocytosis and recycling.

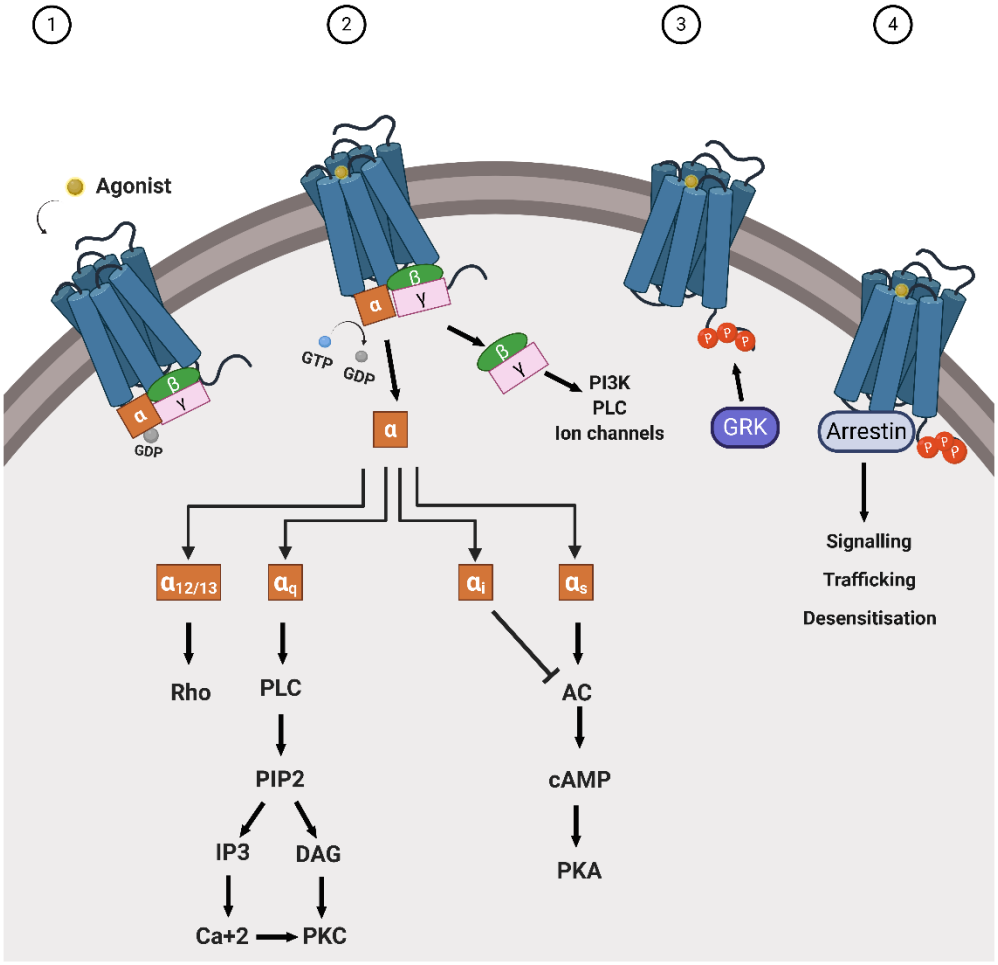

Figure 1.2 General schematic of GPCR signalling

Upon activation of a GPCR by an agonist, 1) the agonist-activated receptor couples to G proteins; 2) Coupling to G proteins triggers the exchange of GDP for GTP followed by the dissociation of G_{α} and $G_{\beta\gamma}$ subunits. Each subunit can activate downstream effectors; 3) The activated receptor is phosphorylated by GRKs which triggers the binding of arrestins; 4) Arrestin binding leads to block signalling of G protein and arrestin also activates downstream effectors.

1.1.4 Biased Agonism and Barcode Phosphorylation

Classically, GPCRs are considered on-off states that switch between two conformations, active and inactive (Gurevich, V. V. & Gurevich 2020). Based on this binary theory , agonists were believed to increase the signal by shifting the equilibrium towards the active conformation, where inverse agonists reduce basal activity by shifting the equilibrium towards the inactive conformation (Rang 2006). The neutral antagonists bind to the receptor without disturbing the equilibrium. Previously, it was thought that ligands could activate GPCR and initiate signalling pathways equally mediated by arrestins and G proteins. Since the discovery of ligands that can selectively activate particular pathways, the former theory cannot explain this phenomenon. Accumulating studies have shown that some ligands can preferentially activate particular pathways and block others (Rankovic, Brust & Bohn 2016). Therefore, the phenomenon of biased agonism or functional selectivity has been suggested. Biased agonism has been an active area of research because it can overcome some adverse effects of balance agonist such as respiratory depression produced by morphine (Kelly 2013).

A few years ago, two studies suggested the barcode phosphorylation based on the findings of the phosphorylation of β_2AR and M3-muscarinic acetylcholine receptor (Butcher et al. 2011; Nobles et al. 2011; Yang et al. 2017). The authors found that that β2AR was phosphorylated by different GRKs, which led to different cellular functions (Nobles et al. 2011). Similarly the M3-muscarinic acetylcholine receptor was shown to be differently phosphorylated in different cells (Butcher et al. 2011). These findings suggested that phosphorylation of a GPCR is dictating the cellular functions (Yang et al. 2017). There are only seven members of the GRK kinase family that phosphorylate hundreds of GPCRs. Previously, studies suggested that GRKs have no receptor specificity (Kohout & Lefkowitz 2003). However, some GRKs contribute differently in GPCR signalling. For instance, DOPr internalisation in HEK293 cells is governed by two different pathways: GRK2-dependent and GRK2-independent, with each mechanism having a different outcome (Zhang et al. 2008). In GRK2-dependent internalisation, this pathway is governed by arrestins 2 and 3 and results in DOPr recycling (Zhang et al. 2008). On the other hand, GRK2-

independent internalisation is mediated by arrestin-3 and causes DOPr degradation (Zhang et al. 2008).

1.2 Opioid Receptors

Opioid receptors are GPCRs that belong to the class A family of GPCRs. There are four subtypes of opioids receptors: mu (MOPr), delta (DOPr), kappa (KOPr), and opioid-related nociception receptors (Corder et al. 2018). In this thesis, I will mainly focus on MOPr and DOPr as examples of GPCRs, as they are the most important targets for pain therapy, in particular, morphine at MOPr (Williams et al. 2013).

Opioids are the best choice for treating acute being less effective in chronic pain. Morphine, oxycodone, fentanyl, methadone and other opioids are widely used in pain management. Morphine mainly exerts its analgesic activity through the activation of MOPr. However, acute use of morphine leads to the development of undesired side effects, such as respiratory depression, and prolonged use leads to development of tolerance, dependence and addiction (Bailey & Connor 2005; Waldhoer, Bartlett & Whistler 2004).

1.2.1 Opioid Receptor Signalling

Opioid receptors are widely expressed pre- and post-synaptically in the central and peripheral nervous system. Opioid receptors are also expressed in non-neuronal tissues. The highest levels of MOPr are in the thalamus, periaqueductal gray, locus coeruleus (LC), rostral ventromedial medulla (RVM), and dorsal horn of the spinal cord (Pasternak & Pan 2013). Traditionally, MOPr signals from the plasma membrane although recent studies have suggested that internalised receptors can signal from endosomes (Stoeber et al. 2018). Activation of MOPr leads to multiple physiological effects, such as analgesia, euphoria, respiratory depression and reduction on gastric motility (Toubia & Khalife 2019).

Activation of MOPr in the midbrain stimulates descending inhibitory impulses through inhibition of GABA to the periaqueductal gray, which activates descending

inhibitory neurons. Those neurons stimulate enkephalin-containing neurons that are connected directly to the dorsal horn in the spinal cord. Consequently, this leads to a reduction of the nociceptive transmission from the periphery to the thalamus (James & Williams 2020).

MOPr agonists induce euphoric actions through the mesolimbic system by decreasing GABA inhibition, resulting in excess release of dopamine, which is responsible for euphoric actions.

Activation of MOPr, like other GPCRs, by an agonist leads to conformational changes that allow the intracellular regions to adopt an open conformation to couple to G proteins (Figure 1.3) (Huang et al. 2015; Kelly, Bailey & Henderson 2008). The main G protein subtype that MOPr couples to is $G_{i/o}$ (Carter & Medzihradsky 1993). Activation of MOPr through G proteins promotes the opening of G protein-coupled inwardly rectifying potassium (GIRK) channels resulting in decreasing neuronal excitability (Ikeda, K et al. 2000; Nagi & Pineyro 2014). Also, MOPr inhibits voltage-gated calcium channels which leads to hyperpolarisation of the cell, in turn inhibiting action potential and decreasing the release of neurotransmitter (Schroeder et al. 1991; Seward, Hammond & Henderson 1991). In addition, activation of $G_{i/o}$ inhibits adenylyl cyclase (AC) and thereby reduces cyclic adenosine monophosphate (cAMP) levels (Carter & Medzihradsky 1993; Levine & Taiwo 1989). Moreover, MOPr can also signal through ERK, PKC and JNK pathways (Figure 1.3) (Belcheva et al. 1998; Gutstein et al. 1997; Kam, Chan & Wong 2004).

Table 1.2 Location and function of MOPr and DOPr

	Location in the CNS	Function	Selected endogenous ligands	Selected exogenous ligands
Mu (MOPr)	Thalamus, periaqueductal gray, locus coeruleus (LC), rostral ventromedial medulla (RVM), and dorsal horn of the spinal cord	Analgesia, gastrointestinal motility, mood, hormone secretion, thermoregulation	β-Endorphin, Met-enkephalins, endomorphin	Agonists: Morphine, DAMGO, fentanyl, hydromorphine, methadone Antagonists: Naloxone, Naltrexone
Delta (DOPr)	Cortex, olfactory bulb, thalamus, amygdala, caudate putamen, nucleus accumbens, dorsal horn	Analgesia, mood, gastrointestinal motility, behaviour	Dynorphin A, enkephalins, β-endorphin	Agonists: SNC80, DADLE, DPDPE Antagonists: Naloxone, Naltrindole,

Reference: Borsodi et al. (2019)

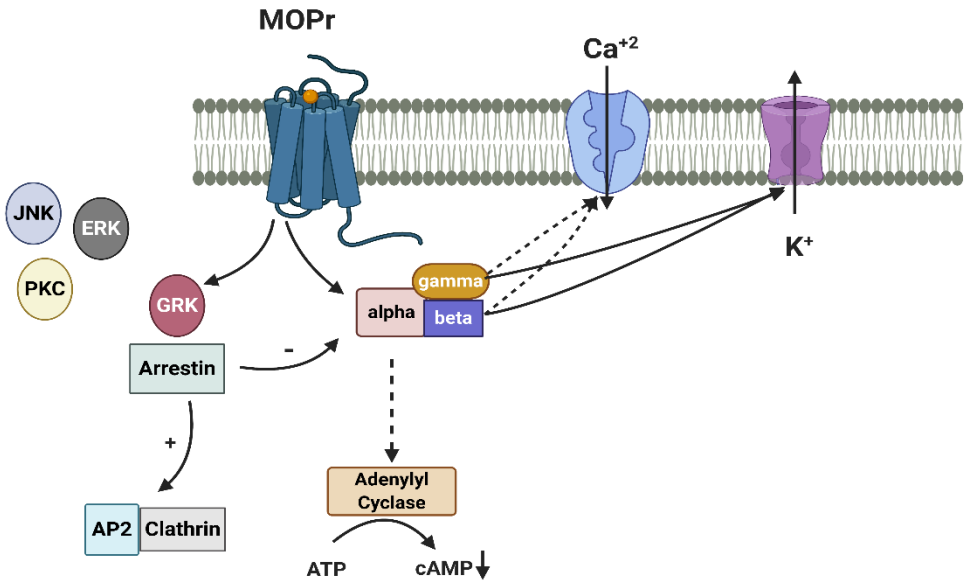

Figure 1.3 MOPr signalling

Activation of MOPr by an extracellular agonist results in coupling to $G_{i/o}$ that leads to a decrease in the influx of calcium (Ca^{+2}) and increases potassium (K^{+}) efflux and decreases cAMP levels through inhibition of adenylyl cyclase (AC) leading to decrease of neuronal excitability and signal transduction. MOPr is phosphorylated by GRK, which leads to the recruitment of arrestin that can initiate arrestin-dependent signalling and receptor internalisation. Other kinases also can regulate MOPr, such as PKC, ERK and JNK

1.2.2 Regulation of Opioid Receptor Signalling

Phosphorylation of proteins is one of the most important and frequent post-translational modifications. The most common cellular kinases that regulate GPCR phosphorylation are GRKs, protein kinase C (PKC), and possibly Ca^{2+}/calmodulin-dependent protein kinase II (CaMKII), proto-oncogene tyrosine-protein kinase (Src) (Chen, YJ et al. 2013; Just et al. 2013; Lowe et al. 2015).

Around 20 phosphorylation sites in MOPr have been predicted (Williams et al. 2013). The main kinases that phosphorylate particular MOPr residues are GRKs and studies also reported that MOPr can be phosphorylated by other kinases such as PKC, Src, CAMKII, ERK and JNK (Figure 1.4) (Dang, Napier & Christie 2009;

Koch, T et al. 1997; Melief et al. 2010; Schmidt et al. 2000). The important residues for MOPr phosphorylation are a cluster of serine and threonine within ^{370}TREHPSTANT^{379} motif in the C-terminal (Doll et al. 2011; Just et al. 2013).

It is established that distinct agonists differentially phosphorylate MOPr (Williams et al. 2013). Studies have shown that high efficacy opioids such as DAMGO and etonitazene initially induce phosphorylation of Ser^{375} followed by Thr^{370}, Thr^{376} and Thr^{379} (Just et al. 2013). This phosphorylation is mediated by GRK2/3 and subsequent recruitment of arrestin (Groer et al. 2011; Just et al. 2013; Miess et al. 2018). Treatment with morphine only induces phosphorylation of Thr^{375} and weak phosphorylation of Thr^{370}, Thr^{376} and Thr^{379} (Miess et al. 2018) where this phosphorylation is mainly mediated in part by GRK5 (Doll et al. 2012).

Receptor desensitisation, which is defined as a reduction in the signal transduction of the opioid receptor after stimulation with agonist (Allouche, Noble & Marie 2014), is a common event observed after prolonged agonist treatment and is readily observed with the opioid receptors. After prolonged treatment with an opioid agonist, the receptor undergoes desensitisation, which involves initial receptor phosphorylation and arrestin recruitment. In locus coeruleus neurons, mutation of serine and threonine residues of the receptor (Thr^{354}, Ser^{355}, Ser^{356}, Thr^{357}, Ser^{363}, Thr^{370}, Ser^{375}, Thr^{376}, Thr^{379} and Thr^{383}) greatly reduces acute desensitisation brought on by exposure to Met-enkephalin (ME) (Arttamangkul et al. 2019; Kliewer et al. 2019). Bailey, Llorente, et al. (2009) reported that ME and morphine-induced desensitisation of MOPr enhanced upon activation of PKC in locus coeruleus neurons. In AtT20 cells, mutation of all Ser/Thr at C-terminus of MOPr to alanine abolished ME-induced MOPr desensitisation but that induced by morphine (Yousuf et al. 2015). Morphine-induced desensitisation is only reduced by inhibition of PKC (Yousuf et al. 2015). Studies found that PKC is involved in morphine-induced desensitisation (Ingram & Traynor 2009; Levitt & Williams 2012; Yousuf et al. 2015).

There are two types of desensitisation of GPCR signalling. Homologous desensitisation, which is mainly mediated by GRKs, is recognised as an active receptor conformation. In homologous desensitisation, the agonist-activated

receptor undergoes desensitisation. On the other hand, in heterologous desensitisation, the second messenger-dependent kinases (PKA or PKC) phosphorylate non-activated receptor, which leads to desensitisation of the non-activated receptor. The phosphorylated receptor by GRKs enhances the affinity for arrestins.

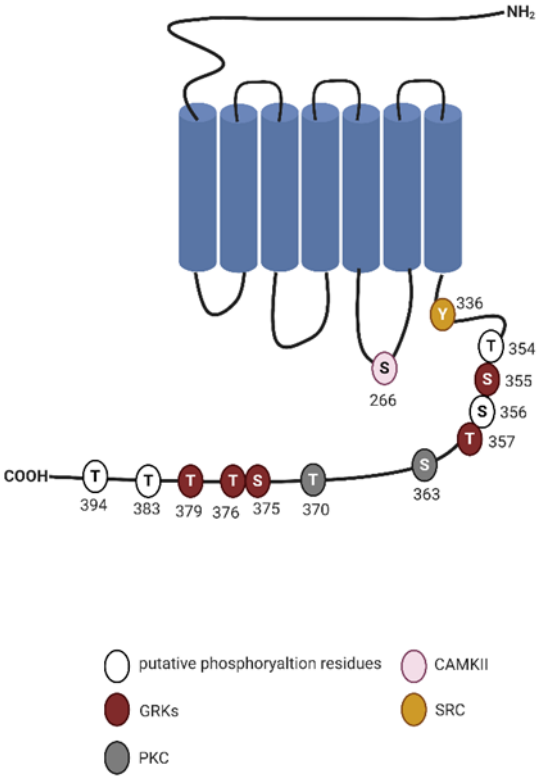

Figure 1.4 MOPr phosphorylation sites

A schematic illustration of rat MOPr phosphorylation residues. The residues probably phosphorylated by particular kinases are colour-coded; in red are residues phosphorylated by G protein-coupled receptors (GRKs), in grey are residues phosphorylated by protein kinase C (PKC), in yellow are residues possibly phosphorylated by proto-oncogene tyrosine-protein kinase (SRC), in pink are residues phosphorylated by Ca^{2+}/calmodulin kinase II (CaMKII), and white represents putative phosphorylation residues. (Adapted from Lemos Duarte and Devi (2020).

Binding of arrestins to phosphorylated GPCR results in blocking the G protein signalling, consequently, desensitising the receptor and terminating the signalling.

Opioid therapy remains the first choice for managing severe pain, but it is limited by developing tolerance over time. Tolerance to opioids is defined as the loss of receptor responsiveness following prolong administration of agonist (Williams et al. 2013). Despite all efforts to study the mechanism of developing tolerance, the exact mechanism has not been determined. Although the relationship between tolerance and desensitisation has been observed; its exact mechanism still unclear. It has been shown that the receptor phosphorylation might play a role in opioid tolerance. Studies have been shown that all 11 phosphorylation residues on the C-terminus of MOPr were involved in tolerance (Arttamangkul et al. 2019). Mutation of ^{375}STANT^{379} to alanine eliminated tolerance and only reduced desensitisation (Arttamangkul et al. 2019). Knock-in mice with mutation of Ser^{375} displayed desensitisation to ME and showed tolerance to morphine, but did not develop tolerance to fentanyl treatment (Kliewer et al. 2019). These findings show the complexity of the mechanism of tolerance and they also suggest that these phosphorylation sites could affect tolerance with different agonists (Birdsong & Williams 2020).

1.2.3 DOPr

DOPr plays a role in nociception, gastro-intestinal motility, olfaction and mood (Allouche, Noble & Marie 2014). DOPr is highly expressed in the olfactory tract, striatum, caudate, putamen, cerebral cortex, amygdala and dorsal horn (Table 1.2) (Allouche, Noble & Marie 2014; Le Merrer et al. 2009).

One advantage of DOPr agonists over MOPr agonists is that they are less likely prone to abuse (Brandt et al. 2001; Negus et al. 1998; Stevenson et al. 2005). Also, they do not cause side effects such as constipation or respiratory depression which are the main side effects caused by MOPr agonists (Vicente-Sanchez et al. 2018). Also, DOPr agonists are highly effective in chronic pain, but are weak in acute pain compared to MOPr agonists (Gallantine & Meert 2005; Vicente-Sanchez et al. 2018). However, DOPr agonists such as SNC80 have been shown to trigger convulsions, a major issue in the development of DOPr agonists as medicines (Comer et al. 1993; Vicente-Sanchez et al. 2018).

DOPr is phosphorylated at Thr^{361} and Ser^{363} in an agonist-induced manner (Kouhen et al. 2000), which is mediated by GRK2/3 (Qiu, Loh & Law 2007). Phosphorylation of DOPr at Ser^{344} is mediated by PKC in an agonist-independent manner (Xiang et al. 2001).

Studies have reported that different DOPr agonists preferentially recruit distinct arrestin isoform (Vicente-Sanchez et al. 2018). For instance, DPDPE, a higher efficacy peptide DOPr agonist, recruited arrestin-3 in the phosphorylation-dependent internalisation of DOPr in mouse embryonic fibroblasts (Qiu, Loh & Law 2007). On the other hand, etorphine-induced DOPr internalisation in SK-N-BE cells was mediated by arrestin-2 (Bowman et al. 2015). In addition, SNC80, a high efficacy DOPr agonist, preferentially recruited arrestin-2 resulting in DOPr desensitisation and acute tolerance (Vicente-Sanchez et al. 2018). In arrestin-2 knockout mice, an increased in SNC80 potency was observed and decreased in acute tolerance (Pradhan et al. 2016). On the other hand, the lower efficacy DOPr agonists ARM390 or JNJ20788560 recruited arrestin-3 resulting in receptor resensitisation (Pradhan et al. 2016). In arrestin-3 knock-in mice, it was observed that receptor resensitisation was impaired and increased acute tolerance upon stimulation with ARM390 or JNJ20788560 (Pradhan et al. 2016).

1.3 Arrestins

Arrestins are 48 kDa proteins and were discovered as proteins that bind to the phosphorylated rhodopsin (Kuhn, Hall & Wilden 1984). After that, arrestin subtypes were discovered and advancements in molecular studies revealed their structures and how they bind to GPCRs. Since the discovery of the role of arrestins in agonist-induced internalisation of β_2AR, many more studies have shown that arrestins regulate trafficking of GPCRs and non-GPCRs substrates such as ERK1/2, AKT and JNK3 (Gurevich, V. V. & Gurevich 2019; Moore, Milano & Benovic 2007; Shenoy & Lefkowitz 2011).

There are only four arrestins which are divided into two groups: visual and non-visual arrestins (Tian, Kang & Benovic 2014). Visual-specific arrestins are arrestin-

1 (rod arrestin) and arrestin-4 (cone arrestin). The widely expressed nonvisual arrestins are arrestin-2 (β-arresin1) and arrestin-3 (β-arrestin2) (Latek et al. 2012; Premont & Gainetdinov 2007). With the advancement in molecular structural studies using X-ray crystallography, arrestins structures have been reported. Arrestins have two main domains: the N-domain and C-domain, each consisting of antiparallel β-sheets which are joined by small flexible loops (Figure 1.5) (Tian, Kang & Benovic 2014). The N-domain and C-domain are connected by a small hinge region (Latek et al. 2012; Tian, Kang & Benovic 2014). The carboxyl-terminus of arrestins involves in maintaining the basal state of arrestins (Shukla & Dwivedi-Agnihotri 2020).

Arrestins are cytoplasmic proteins that play a critical role in regulating GPCRs signalling. Classically, the primary role of arrestins is thought to be the prevention of G protein binding to GPCRs, which leads to termination of G protein-mediated GPCRs signalling (Shukla & Dwivedi-Agnihotri 2020). In recent years, the role of arrestins has expanded and their importance in regulating downstream signalling of GPCRs demonstrated (Shukla & Dwivedi-Agnihotri 2020). For instance, arrestins can modulate ubiquitination and degradation by interacting with E3 ubiquitin ligases (Shenoy & Lefkowitz 2011; Shukla & Dwivedi-Agnihotri 2020). Also, arrestins have been shown to regulate GPCR internalisation. The overexpression of arrestins was found to enhance the agonist-induced internalisation of β_2AR (Kang, DS, Tian & Benovic 2014). Later, studies have shown that arrestins interact with clathrin and clathrin adapter protein-2 (AP2), key proteins involved in the assembly of clathrin-coated pits (CCPs) and which facilitate receptor trafficking (Kang, DS, Tian & Benovic 2014; Shukla & Dwivedi-Agnihotri 2020).

Recent structural studies revealed that arrestins and G proteins bind to the same interhelical cavity on the cytoplasmic tail of the receptor (Figure 1.5) (Gurevich, V. V. & Gurevich 2019; Kang, Y et al. 2015; Rasmussen et al. 2011; Zhou et al. 2017). Thus, binding of arrestins to the phosphorylated receptor precludes the binding of G protein, resulting in termination of G protein signalling. Arrestins bind to the phosphorylated receptor with a high affinity that is gained from binding tightly to the receptor phosphate group into its positive patches on arrestin surface (Zhou et al. 2017).

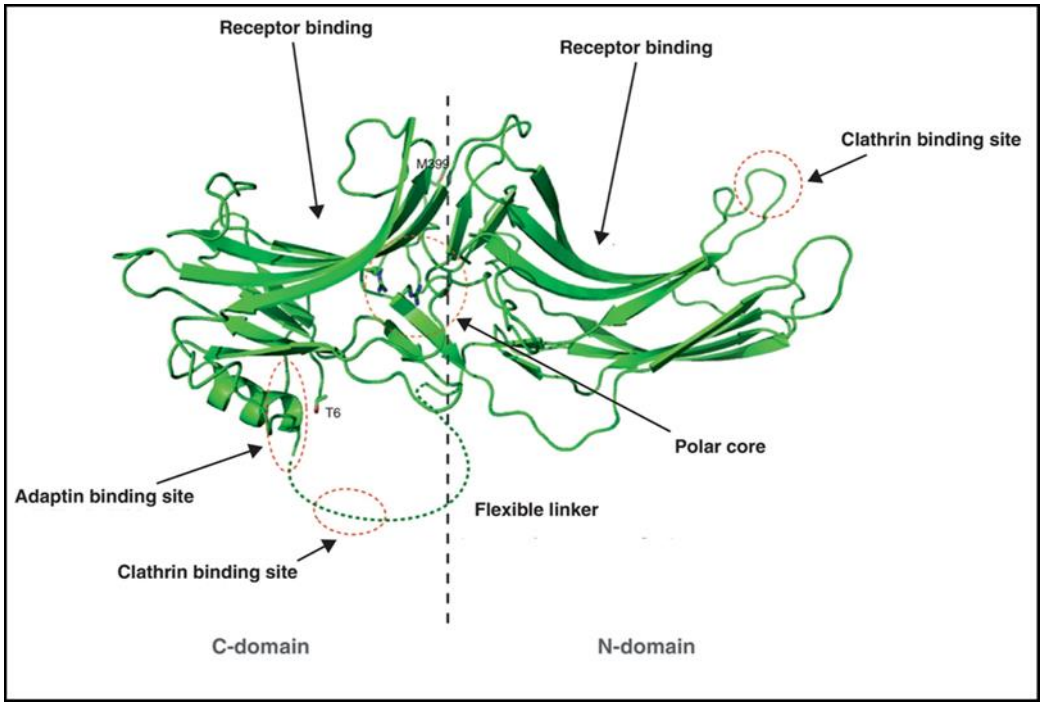

Figure 1.5 Structure of Arrestin

A ribbon structure of arrestin-2 showing the N-domain, C-domain, polar core, and the biding sites for GPCR, clathrin and adaptin. Taken from Kang, DS, Tian and Benovic (2014).

Non-visual arrestins bind to clathrin, a major component of clathrin-coated pits (CCPs) and clathrin-adaptor AP2, which regulate clathrin assembly and are a target receptor for CCPs (Kang, DS, Tian & Benovic 2014). The binding site in arrestins is a clathrin binding box, which is located in the c-terminal region of arrestins (Figure 1.5) (Kang, DS, Tian & Benovic 2014). The arrestin C-terminus becomes accessible for clathrin after binding to the phosphorylated receptor (Kang, DS, Tian & Benovic 2014).

Cahill et al. (2017) used a chimeric β_2V_2R construct, which consists of β_2AR with C-terminal tail exchanged with the vasopressin type 2 receptor (V_2R) C-terminal tail, to study the distinct conformations of receptor-arrestin complexes. This construct has the advantage of β_2AR, a class A GPCR which weakly and transiently binds to arrestins, and V_2R, a class B GPCR which tightly binds to arrestins (Cahill et al. 2017). It was found that the GPCR/arrestin-2 complex had two conformations: tail

conformation and core conformation. In tail conformation, arrestin-2 bound to the phosphorylated C-terminal of the receptor and this was involved in the internalisation of GPCR, while it did not block G protein binding to the receptor. In the core conformation, arrestin-2 made another interaction with the receptor transmembrane core that prevented G protein signalling and subsequently desensitisation of the receptor.

Several studies have reported cryo-EM and X-ray crystal structures of GPCR in complex with arrestin (Huang et al. 2020; Kang, Y et al. 2015; Lee et al. 2020; Staus et al. 2020; Yin et al. 2019). All these crystal structures provide mechanistic insights into the interaction of arrestin with the receptor. Briefly, the phosphorylated C-terminus of the receptor displaced the C-terminus of arrestin. The C-terminal end of helix8 of the receptor projects towards the N-terminal end of the arrestin. The receptor core engages the arrestin finger loop and the arrestin C-terminal domain C-edge loops diffuse through the lipid bilayer (Yoo, Bhardwaj & Benovic 2020).

1.4 G Protein-Coupled Receptor Kinases (GRKs)

The G protein-coupled receptor kinases (GRKs) are a family of seven kinases that phosphorylate serine and threonine residues normally in the third intracellular loop and/or carboxyl tail of activated GPCRs (Ferguson 2001; Guccione et al. 2016). This phosphorylation promotes the binding of arrestins, which leads to the uncoupling of G proteins from the receptor (Smith & Rajagopal 2016). The binding of arrestins leads to desensitisation of the G protein-mediated response and internalisation of the receptor (Hanyaloglu & von Zastrow 2008).

1.4.1 Classification of GRKs

The GRKs are grouped into three subfamilies; GRK1, GRK2 and GRK4 (Table 1.3) (Pierce, Premont & Lefkowitz 2002). The GRK1 subfamily consists of GRK1 and GRK7, and they are found almost exclusively in the retina (Homan & Tesmer 2015; Premont & Gainetdinov 2007; Thal et al. 2011). The GRK2 subfamily is composed of GRK2 and GRK3, both of which are widely distributed (Premont & Gainetdinov

2007; Thal et al. 2011). The GRK4 subfamily consists of GRK4, GRK5 and GRK6, whereas GRK5 and GRK6 are widely distributed. GRK4 is mainly expressed in the testis (Premont & Gainetdinov 2007). GRKs are also expressed differently in different cell types. For example, GRK6 and GRK3 expression levels in the heart are low compared to GRK2 and GRK5 expression levels.

1.4.2 Structure of GRKs

The crystal structures of bovine GRK2 with G_{α} (Tesmer, VM et al. 2005) and $G_{\beta\gamma}$ subunits (Lodowski et al. 2003) have been published as have the crystal structure of GRK2 with inhibitors such as balanol, compound101 (cmpd101), RNA aptamer paroxetine, CCG26584 and GSK180736A, have been reported (Homan et al. 2015; Homan et al. 2014; Tesmer, JJ et al. 2010; Tesmer, VM et al. 2012; Thal et al. 2012; Thal et al. 2011). All GRK isoforms share the general structure which consists of a conserved central catalytic domain (about 270 amino acids), which is shared with other AGC kinases such as PKA, PKC, an N-terminal domain (185 amino acids) and a C-terminal domain (100-230 amino acids) (Figures 1.6 and 1.7) (Penela et al. 2010; Pitcher, Freedman & Lefkowitz 1998).

The kinase domain consists of a small lobe (N) and a large lobe (C) (Figure 1.7). The small lobe is formed by six-stranded antiparallel β-sheets and three α-helices (αB, αC and αK) while the large lobe is composed of α-helices and four antiparallel β-strands. The ATP binding site, which is shared by about 500 different kinases, is located on the interface of the two lobes (Guccione et al. 2016; Lodowski et al. 2003; Thal et al. 2011). The ATP binding site of the kinase is composed of the adenine, ribose, triphosphate and hydrophobic subsites (Thal et al. 2011). The N-terminal domain anchors the kinase to the intracellular membrane which contains the regulator of G protein signalling homology (RH) domain (Dhami et al. 2002; Penela et al. 2010; Sallese, Mariggiò, et al. 2000). The C-terminal domain consists of a seven-stranded antiparallel β-barrel with a C-terminal helix on one end. In GRK2/3 isoforms, the C-terminal contains the pleckstrin homology (PH), which is unique to GRK2/3. The PH domain is the binding site for phosphatidylinositol 4, 5, biphosphate (PIP2), which binds directly to GRK and facilitates the membrane

association of GRK and $G_{\beta\gamma}$ subunits (Sallese, Iacovelli, et al. 2000). The binding of $G_{\beta\gamma}$ leads to an increase in the phosphorylation of GPCR and recruitment of GRK (Lodowski et al. 2003; Penela et al. 2010).

Table 1.3 GRK Subfamilies

Subfamily	Isoform	Tissue expression	No. of Amino Acids (human)	Size (kDa)
GRK1	GRK1	Retina (rods), pineal gland	563	63
	GRK7	Retina (cones)	553	62
GRK2	GRK2	Ubiquitous	689	79
	GRK3	Ubiquitous	688	80
GRK4	GRK4	testis, brain, thyroid nodes	578	66
	GRK5	Ubiquitous	590	68
	GRK6	Ubiquitous	576	66

References: Gurevich, Vsevolod V., Gurevich and Tesmer (2016); Santulli, Trimarco and Iaccarino (2013).

GRKs are soluble proteins; thus, their C-termini contain a particular element to able them to target the membrane. GRK1 and GRK7 are prenylated at their C-termini where GRK2 and GRK3 C-termini are composed of pleckstrin homology, which interacts with phosphatidylinositol 4, 5-biphosphate (PIP 2) and free $G_{\beta\gamma}$ subunits (Koch, WJ et al. 1993). This interaction facilitates the translocation of GRK2/3 from the cytoplasm to the plasma membrane to be able to phosphorylate agonist-activated GPCR (Gurevich, Vsevolod V., Gurevich & Tesmer 2016). However, GRK5 does not have a pleckstrin domain in its C-terminal; instead, it uses a C-terminal lipid-binding domain to facilitate membrane localisation (Pitcher et al. 1992;

Stoffel et al. 1994). The GRK4 and GRK6 isoforms rely on palmitoylation sites on their C-termini and/or on lipid binding positively charged elements.

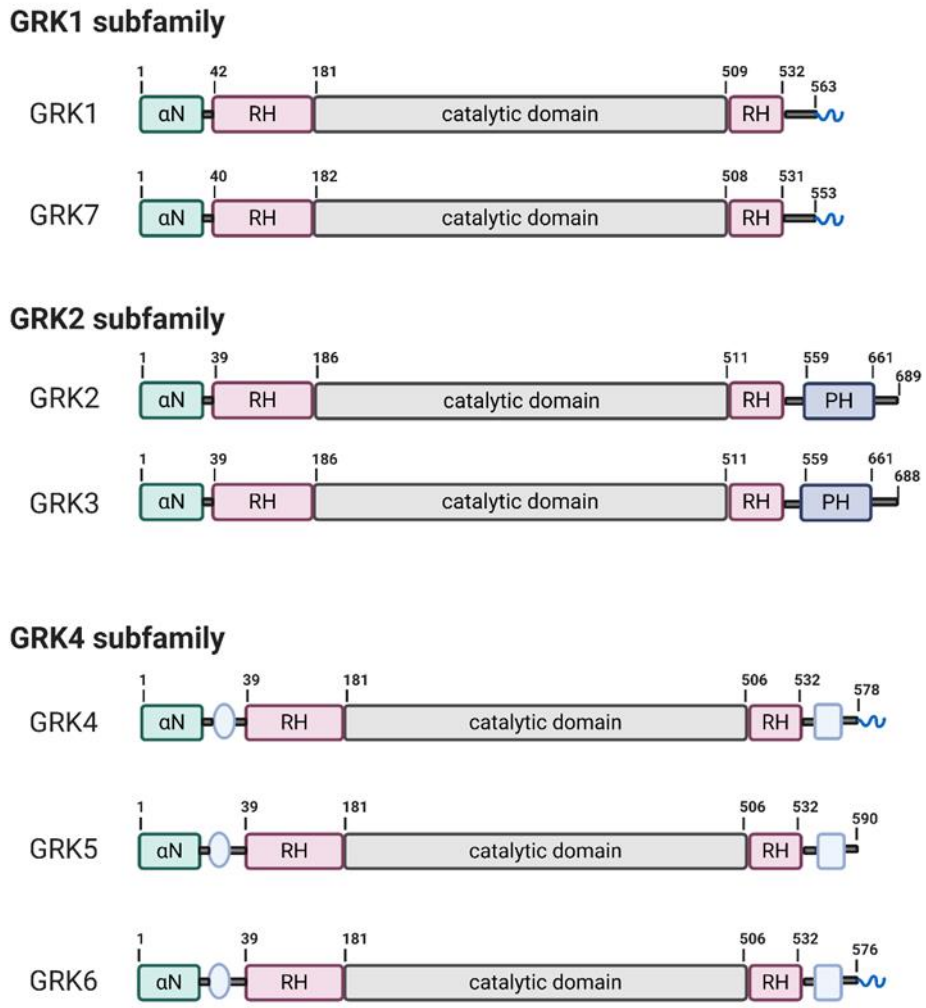

Figure 1.6 General structure of GRKs

General structure of the three GRK subfamilies. GRK structure is composed of the regulator of G protein signalling homology (RH) (pink) and catalytic domains (grey). The αN-helix (green) bridges the N- and C-lobes of the catalytic domain of the kinase. The C-terminal plays a role in membrane localisation and it varies between subfamilies. GRK1 subfamily has prenylated C-terminal where GRK2 subfamily has pleckstrin C-terminal. GRK4 and GRK6 C-termini are palmitoylated where GRK5 has polybasic regions in the C-terminus that help in interaction with negatively-charged phospholipids. Adapted from Komolov and Benovic (2018).

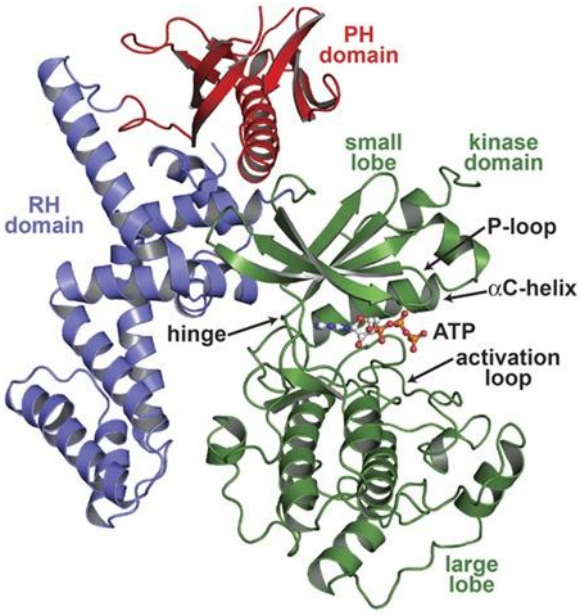

Figure 1.7 Crystal structure of GRK2

The main features of GRK2 structure are the kinase domain (green), the regulator of G protein signalling homology (RH) domain (purple), and pleckstrin homology (PH) domain (red). The ATP binding site is shown within the kinase domain, where most of small GRK inhibitors bind. Taken from Thal et al. (2011).

1.4.3 Regulation of GRK2 Activation and Function

The mechanism of GRK activation is complex and not fully understood. The interactions between αN-helix and the RH and PH domains keep the kinase in an open, nonactive state (Murga et al. 2019; Pack et al. 2018; Penela et al. 2006). Disruption of this binding and reorder of αN-helix and RH domain leads to activation of the kinase allosterically by agonist-activated GPCR (Yao et al. 2017).

Moreover, posttranslational modifications of GRKs influence kinase functionality. For example, c-Src and EGFR phosphorylate GRK2 on tyrosine residues in the α-N-helix and the RH region, which enhances the function of GRK2 (Murga et al. 2019). Also, GRK2 can be phosphorylated by PKC and PKA on Ser^{685}, which enhances the binding ability of GRK2 to $G_{\beta\gamma}$ and the activated receptor (Murga et al.

2019). Other kinases, such as ERK1/2 and MAPK, can also phosphorylate GRK2 (Penela et al. 2006).

GRK2 undergoes rapid degradation by the proteasome, which is enhanced upon agonist-stimulation of GPCR (Penela et al. 2006; Penela et al. 1998). The degradation of GRK2 requires arrestin to act as a scaffold for kinases such as c-Src and tyrosine kinase (Penela et al. 2006).

1.4.4 Physiological and Pathological Roles of GRK2 and GRK5

GRKs are not only involved in GPCR phosphorylation, but they also phosphorylate non-GPCR substrates (Gurevich, EV et al. 2012). Particularly, the ubiquitous and the most studied GRK2 isoform has been shown to be able to interact (mostly phosphorylate) with non-GPCR substrates. GRK2, the main GRK, which involves in the phosphorylation of MOPr, and GRK5 are the main focus of this section.

GRK2 and GRK5 phosphorylate synucleins, which consist of α-, β- and γ-synuclein, GRK2 phosphorylates α- and β-synuclein where GRK5 phosphorylates α-synuclein (Gurevich, EV et al. 2012). α-synuclein, the major component of Lewy bodies in the presynaptic terminals of the nervous system, plays a major role in sporadic Parkinson's disease (Gurevich, V. V. & Gurevich 2019).

As mentioned earlier, GRK2 is ubiquitously expressed in human tissues; it is highly expressed in the immune system. GRK2 phosphorylates chemokine receptors which induce leukocyte accumulation during inflammation. On the other hand, in rheumatoid arthritis, patients showed a reduction in the GRK2 expression and function (Vroon, Heijnen & Kavelaars 2006; Vroon et al. 2004).

GRK2/5 are associated with a failing heart; therefore, the role of GRKs in major disease area like heart failure is of importance. GRK2 has been shown to play an essential role in the development of embryo and heart function (Jaber et al. 1996; Metaye et al. 2005). GRK2 knockout is lethal in mice due to impairment in cardiac development (Matkovich et al. 2006), while cardiac GRK2-deleted mice showed unaffected heart structure and viable mice (Matkovich et al. 2006). GRK2-deficient

embryos displayed hypoplasia of the ventricular myocardium and dysplasia of the interventricular septum, which leads to heart failure (Jaber et al. 1996).

βARs represent about 90% of the adrenoceptors in the heart (O'Connell et al. 2014). Three βARs subtypes are expressed in the heart: β_1AR, β_2AR and β_3AR (Cannavo, Liccardo & Koch 2013), where the β_1AR represents around 80% (Siryk-Bathgate, Dabul & Lymperopoulos 2013). βARs are activated by endogenous catecholamines, adrenaline and noradrenaline (Wang, Gareri & Rockman 2018). Upon catecholamines stimulation, β_1AR and β_2AR couple to G_s which leads to stimulation of AC that results in increasing cAMP in cardiac myocyte and activation of protein kinase A (PKA) (Cannavo, Liccardo & Koch 2013). PKA phosphorylates many targets that regulate intracellular Ca^{+2} binding (Bristow et al. 1990; Woo & Xiao 2012). Also, activation of β_2AR leads to coupling with G_i, which inhibits AC and other β_2AR-independent pathways such as mitogen-activated protein kinase (MAPK) and PI3-kinase and Akt pathways (Cannavo, Liccardo & Koch 2013; Xiao 2001).

Continuous stimulation of βARs leads to desensitisation and loss of response to catecholamines, which can be contributed to the development of heart failure. Studies have shown that overexpression of GRKs in the heart leads to a decrease in isoproterenol, βARs agonist, -stimulated contractility and decreased cAMP production (Koch, WJ et al. 1995). Also, overexpression of GRK2 leads to impaired cardiac function and increased apoptosis (Brinks et al. 2010; Chen, EP et al. 1998). Among the expressed GRKs in the heart (Cannavo, Liccardo & Koch 2013), only GRK2 and GRK5 have been shown to involve in heart failure (Belmonte & Blaxall 2011).

GRK2 overexpression has been linked to reduced myocardial contractility and reduced βAR responsiveness (Anderson et al. 1999; Koch, WJ et al. 1995). Upregulation of GRK2 preceded the reduction in βAR number in spontaneously hypertensive heart failure rats (Anderson et al. 1999). Also, samples taken from human patients have shown an increase in GRK2 expression and activity with reduced βAR numbers and function (Ungerer et al. 1993; Ungerer et al. 1994). In animal studies, overexpression of GRK5 reduced βARs response to isoproterenol

(Rockman et al. 1996) and impaired cardiac function (Chen, EP et al. 2001). These findings suggest that GRK5 involves in the development of heart failure.

The ability of GRK5 to translocate was first shown in the cardiomyocytes of spontaneously hypertensive rats (Johnson, LR, Scott & Pitcher 2004; Yi et al. 2005). This was supported by the discovery of the nuclear localisation sequence (NLS) within GRK5 catalytic domain (Johnson, LR, Scott & Pitcher 2004; Sato et al. 2015; Yi et al. 2005). Cardiac hypertrophic stimulation causes activation of calcium-calmodulin, thereby translocating GRK5 to the nucleus where it targets class II histone deacetylase 5 (HDAC5). HDAC5 induces hypertrophic gene transcription and derepresses myocyte enhancer factor 2 (MEF2) (Galasinski et al. 2002; Sato et al. 2015).

The involvement of GRK2 in heart failure has led to the use of inhibition of GRK2 strategy to modulate heart failure. Inhibition of GRK2, but not GRK5 because it does not use $G_{\beta\gamma}$ to anchor to the plasma membrane, has been achieved through using a peptide from the C-terminal domain of GRK2 (βARKct), which competes with endogenous GRK2 for $G_{\beta\gamma}$ and blocks its translocation to the plasma membrane (Koch, WJ et al. 1993; Koch, WJ et al. 1995). The βARKct prevented and reversed the development of heart failure in mice and pig (Raake et al. 2013; Rockman et al. 1996). Recently, pharmacological inhibition of GRK2 by paroxetine, a GRK2 inhibitor, has shown an improvement in heart failure (Schumacher et al. 2015; Thal et al. 2012). Mice treated with paroxetine showed an increase in left ventricular inotropic reserve (Thal et al. 2012). Moreover, paroxetine treatment of heart failure mice model reversed cardiac dysfunction and completely restored the βAR system (Schumacher et al. 2015).

Studies have shown that the expression of GRK2 is altered in many pathological diseases, such as diabetes, Alzheimer's diseases (Gurevich, EV et al. 2012), and cancer (Penela et al. 2010). GRK2 plays a role in regulating insulin signalling, where upregulation level of GRK2 and increased activity leads to inhibition of insulin-induced glucose transport (Ciccarelli et al. 2011; Gurevich, EV et al. 2012). Overexpression of GRK2 impairs the translocation of glucose transporter protein

type-4 (GLUT4), while the injection of GRK2 antibody leads to increasing the GLUT4 translocation to the plasma membrane after insulin stimulation (Usui et al. 2004).

Moreover, the levels of GRK2 increase in the early stages of Alzheimer's disease (Steury, McCabe & Parameswaran 2017), which may lead to enhance the interaction of α- and β-synuclein, which has been linked to Alzheimer's and Parkinson's (Steury, McCabe & Parameswaran 2017). GRK2 also has been shown to play a role in controlling cell proliferation (Guccione et al. 2016). For example, GRK2 is upregulated in thyroid cancer and, hence, reduces cell proliferation (Metaye et al. 2008). In addition, overexpression of GRK2 inhibits the growth of human hepatocellular carcinoma cells (Wei et al. 2012). In summary, GRK2 regulates many signalling pathways, thus selectively targeting GRK2 is a critical strategy to develop therapeutic agents (Evron, Daigle & Caron 2012).

1.4.5 Small Molecule GRK Inhibitors

Studies have been conducted to develop potent and selective GRK inhibitors. However, all current GRK inhibitors lack selectivity among GRKs. The cumulating research on the role of GRK in GPCR signalling pathways, particularly GRK2, has elucidated that targeting GRK2 could be a promising strategy to treat many diseases and also use the inhibitors as research tools to understand cell physiology. A considerable effort has been made to develop potential GRK2 inhibitors, and the following are the most promising developed inhibitors of GRK2 and other GRKs:

Polyanions and Polycations

Polyanions and polycationic compounds were the first compounds to be examined for inhibition of GRK2 in the rhodopsin receptor. Heparin and dextran sulfate, examples of polyanions and polycations compounds, were most potent among tested compounds with an IC_{50} of 0.15 μM. However, heparin targeted other kinases such as casein kinase II and low-density lipoprotein receptor kinase (Hathaway, Lubben & Traugh 1980; Kishimoto et al. 1987). The other effective inhibitors are polyaspartic acid (1.3 μM), polyglutamic acid (2.0 μM) and inositol hexasulfate (13.5

μM) (Benovic et al. 1989; Guccione et al. 2016). However, these compounds are highly charged, which hinders cell penetration, thus limiting their usefulness.

Balanol

Balanol is a natural product synthesised by the fungus Verticillium balaniodes (Setyawan et al. 1999). It is a competitive inhibitor of ATP at the GRK kinase domain (Setyawan et al. 1999). It has an advantage over polyanions in that it is a cell permeable. Its structure is composed of four rings named A-D. Ring A is a 4-hydroxybenzoyl moiety and ring B is a hexahydroazepine ring connected to a benzophenone moiety (Figure 1.8A).

The crystal structure of balanol with GRK2 has revealed that the A ring occupies the hydrophobic adenine subsite of the GRK2 (Figure 1.8B). The B ring occupies the ribose subsite, the C ring binds to the polyphosphate subsite while the D ring binds to the hydrophobic subsite (Homan & Tesmer 2015).

Using a phosphorylation assay with biotinylated tubulin dimers to test the inhibitory capacity of balanol against GRK isoforms GRK1-7, balanol inhibited the isoforms with respective IC_{50} values of 340 nM, 42 nM, 47 nM, 260 nM, 160, 490 nM and 180 nM (Tesmer, JJ et al. 2010).

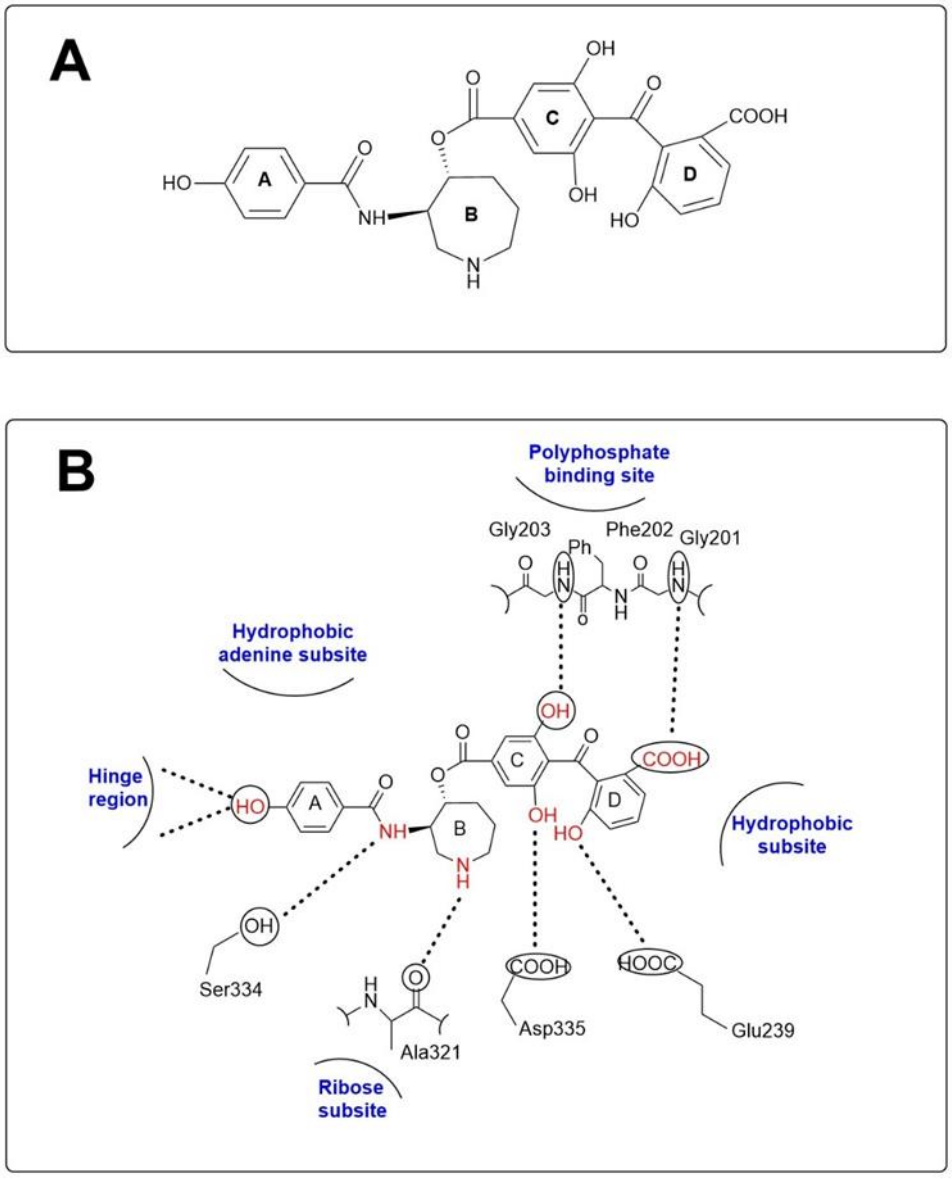

Figure 1.8 Chemical structure and GRK2 interaction of Balanol

Chemical structure of balanol (A), and an illustration of the binding of balanol moieties (red) in the GRK2 binding site (blue) (B). Adapted and modified from Guccione et al. (2016).

RNA Aptamers

Another approach of targeting GRK2 is the development of RNA aptamers. Aptamers are oligonucleotides that can be identified for many targets, such as small molecules, peptides, and proteins (Mayer et al. 2008). Aptamers are identified using

the SELEX process (systematic evolution of ligands by exponential enrichment) and have been used to target various protein targets. They can be prototype models for developing drug-like molecules that can be used in vivo (Mayer et al. 2008).

RNA aptamer C13 has been identified as selective for GRK2 with an IC_{50} of 4.1 nM in a rhodopsin phosphorylation assay (Mayer et al. 2008), and is less potent for inhibition of GRK5 with an IC_{50} of 79.4 nM (Mayer et al. 2008). The problem with RNA aptamers is that they are heavy molecules and cannot cross the cell membrane (Mayer et al. 2008).

Paroxetine

Paroxetine is a selective serotonin reuptake inhibitor (SSRI) approved by the FDA to treat depression-related disorders (Figure 1.9A). Paroxetine has been shown to inhibit GRK2-mediated phosphorylation of rhodopsin in the outer rod segment, with an IC_{50} for inhibition of GRK2 of 19.9 μM, and with lower potency against GRK1(316.2 μM) and GRK5 (25.2 μM) (Thal et al. 2012). Paroxetine restored the GRK2 expression in ipsilateral superior cervical ganglion (SCG) neurons using rat model (Tang et al. 2015).

The crystal structure of paroxetine in combination with GRK2 revealed that the dioxole moiety of paroxetine binds to the adenine subsite of GRK2 (Figure 1.9B) (Homan et al. 2014; Thal et al. 2012). Also, the methylene moiety interacts with the adenine subsite through van der Waal's interactions. The pyridine moiety binds in the ribose subsite of the GRK2 catalytic domain. The fluorophenyl ring formed a nonpolar interaction in the P-loop to stabilise GRK2 binding.

Paroxetine has shown modest inhibition of GRK2; however, it is not selective as it naturally selectively inhibits serotonin transporters (SERT). Paroxetine is already in the clinic and has good pharmacokinetic properties, so it was thought that paroxetine analogues would also have good pharmacokinetics parameters (Waldschmidt et al. 2017). Tesmer's group developed a benzolactam derivative of paroxetine, CCG206584, in order to obtain a more selective inhibitor (Homan et al.

2014). The crystal structure of CCG206584 with GRK2-$G_{\beta\gamma}$ showed less selectivity than paroxetine. It also displayed potent inhibition of PKA and PKC compared to paroxetine (Homan et al. 2014).

The same group developed other paroxetine derivatives as GRK inhibitors (Waldschmidt et al. 2017). The compound 14as was developed by ligation of amide moiety to the C-ring of paroxetine (Figure 1.10) (Waldschmidt et al. 2017). The compound 14as shows higher potency and better selectivity than paroxetine (IC_{50} of 1.38 µM) with an IC_{50} of 0.03 µM for GRK2 and more than 200-fold selectivity over other GRK isoforms as well as ROCK1 and PKA (Waldschmidt et al. 2017).

However, the stability of 14as in mouse liver microsomes was poor with a half-life of 7 min compared to 24.3 min of paroxetine (Waldschmidt et al. 2017).

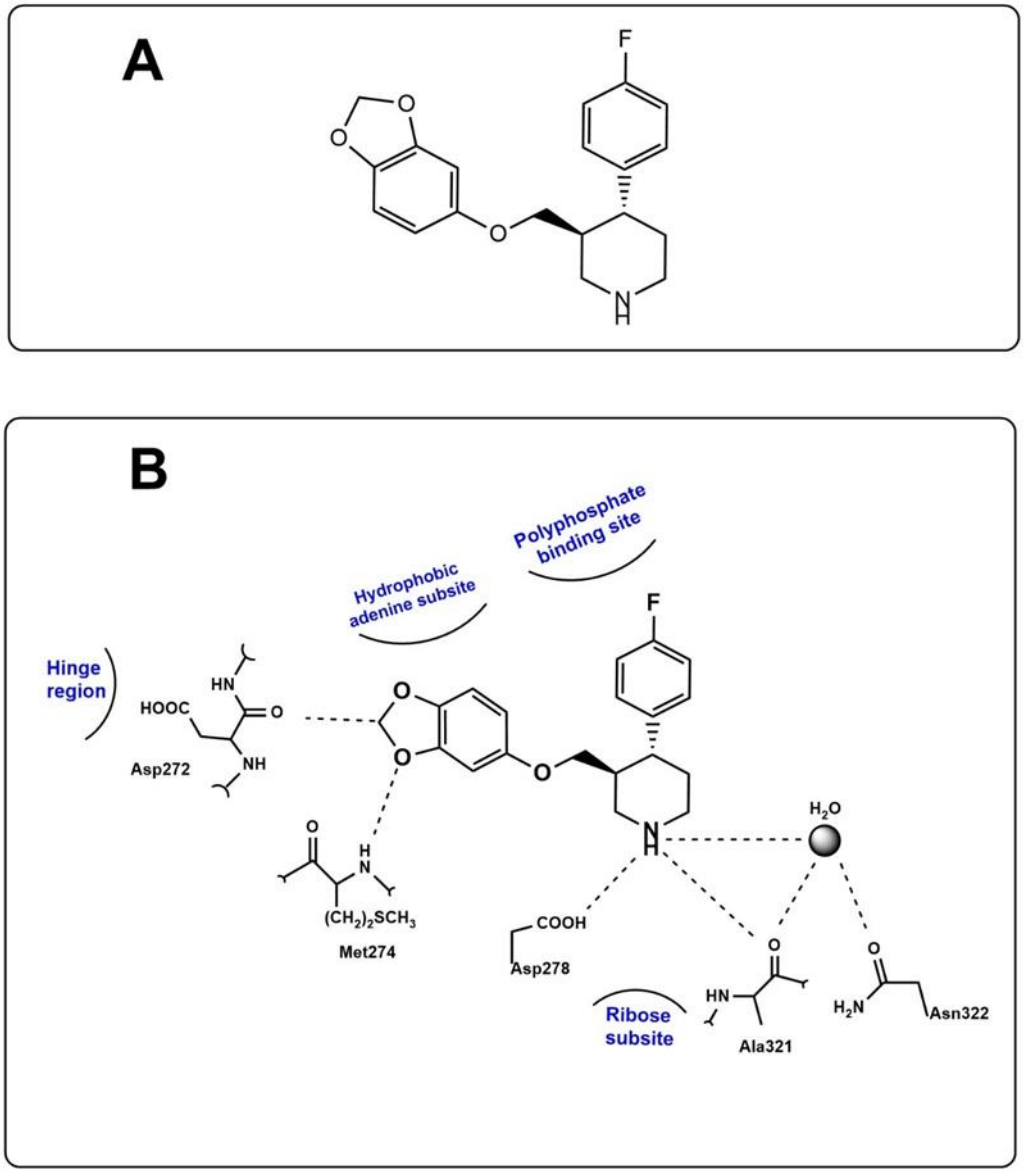

Figure 1.9 Paroxetine structure

Chemical structure of paroxetine (A), and an illustration of the binding of paroxetine moieties in the GRK2 binding site (blue) (B). Adapted and modified from Guccione et al. (2016).

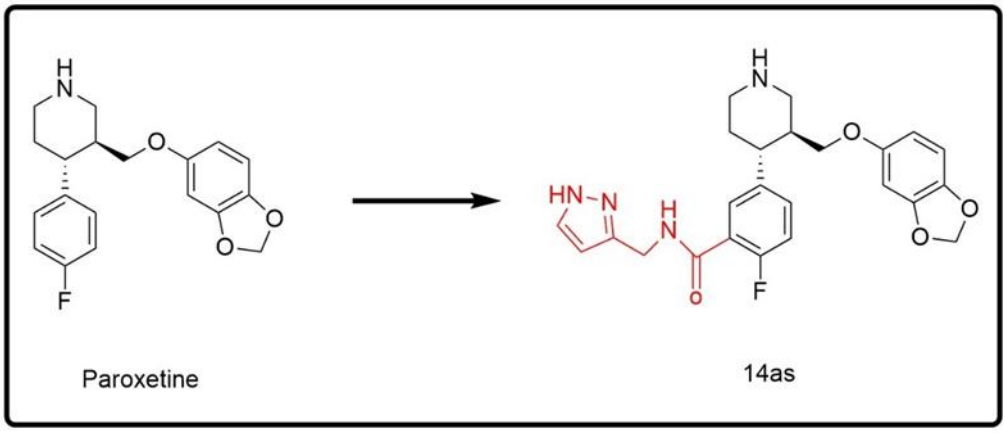

Figure 1.10 Chemical structure of 14as

Substitutions on paroxetine are coloured red.

Another attempt to increase the potency of GRK inhibitor was carried out by exchanging the benzodioxole moiety of paroxetine with indazole (Figure 1.11A) (Bouley, R et al. 2017). The resulting compounds showed improve potency in GRK2 inhibition compared to paroxetine; however, they lost the selectivity among other kinases (Bouley, R et al. 2017). Very recently, a compound derived from paroxetine (CCG258747) was developed which displayed very potent and selective inhibition of GRK2 (IC_{50}= 0.018 µM) over other GRK isoforms and other kinases, such as PKA and ROCK1 (Figure 1.11B) (Bouley, RA et al. 2020). In addition, CCG258747 has good stability in mouse liver microsomes with a half-life of 40 min compared to 23 min of paroxetine (Bouley, RA et al. 2020).

Screening of a collection of kinase inhibitors known as the structural genomics consortium at the University of Oxford resulted in identifying potential GRK inhibitors (Homan et al. 2015). Using a differential scanning fluorimetry (DFS) method to screen compounds that increase the melting point (T_m) of the GRK2 or GRK5 (Homan et al. 2015), this screening resulted in the identification of GSK180736A, which was initially developed as a ROCK1 inhibitor (Homan et al. 2015). In a tubulin phosphorylation assay, GSK180736A had an IC_{50} of 0.25 µM for GRK2 and was 4,000- and 400-fold more potent over GRK1 and GRK5, respectively (Guccione et al. 2016; Homan et al. 2015). Also, GSK180736A showed potent inhibition of ROCK1 and weak inhibition of PKA (Waldschmidt et al. 2018). Thus, GSK180736A

is not an ideal GRK inhibitor, which is in addition to its poor bioavailability (Waldschmidt et al. 2018). Compound 12n was a derivative of GSK180736A and showed to be both potent and selective (Waldschmidt et al. 2016). Using a different strategy to develop potent and selective GRK5/6 subfamily inhibitors enabled researchers to produce very potent and selective inhibitors over the GRK2/3 subfamily (Rowlands et al. 2019). Compounds CCG258903 and CCG265328 were developed that covalently interact with Cys^{474}, which is unique to the GRK4 subfamily; GRK5/6. CCG258903 and CCG265328 showed inhibition of GRK5 and GRK6 with IC_{50} of 0.22, 0.41 and 1.1 and 1.8 µM, respectively (Rowlands et al. 2019). They showed IC_{50} values of >100 µM for GRK1 and GRK2 (Rowlands et al. 2019). However, the IC_{50} of CCG258903 and CCG265328 was determined using purified GRK enzyme, which does not reflect the cell-based assay values. It is important to note that the covalent inhibitors are not favoured as drugs due to their hepatotoxicity and idiosyncratic drug reactions (Singh et al. 2011).

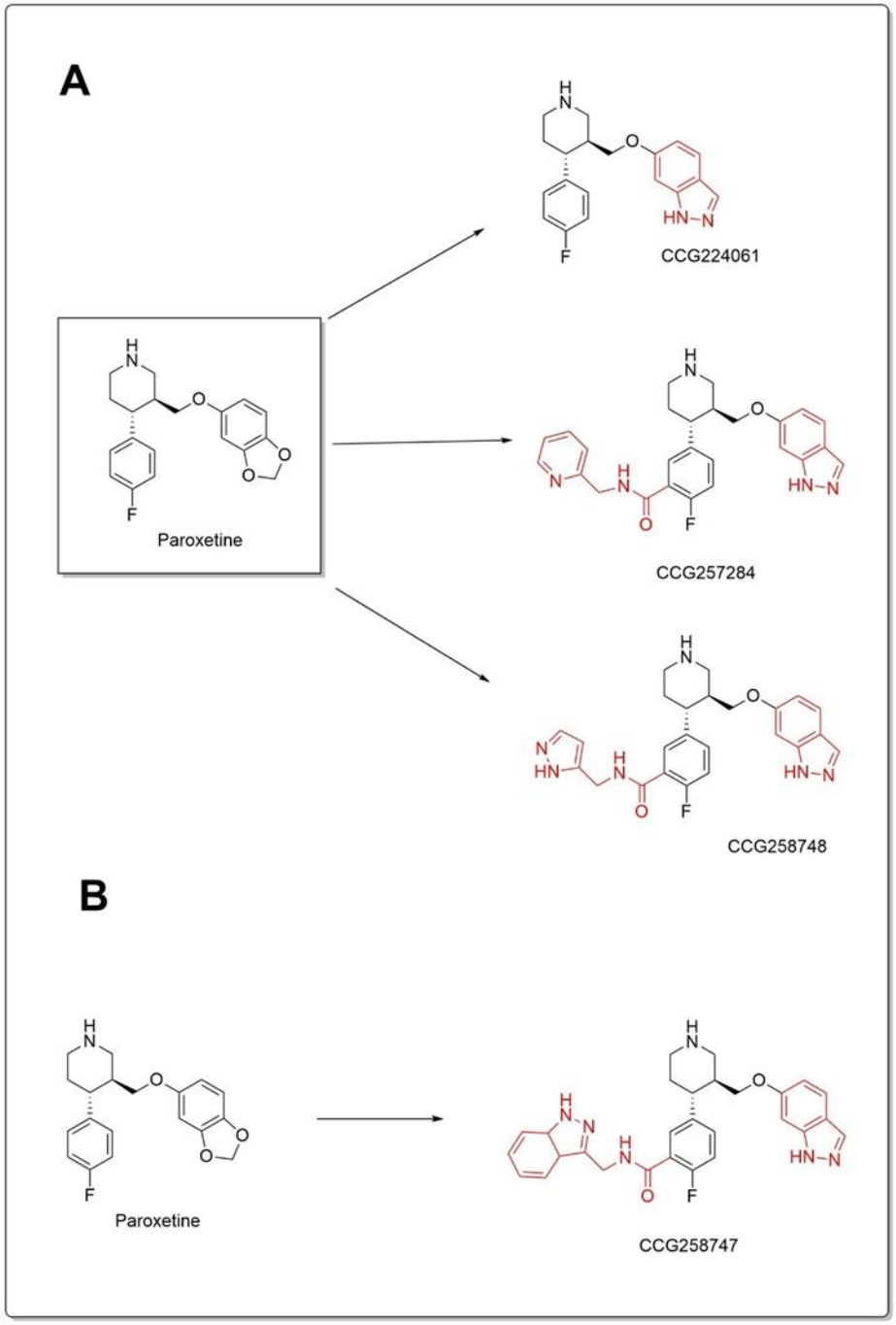

Figure 1.11 Chemical structures of paroxetine derivatives

Substitutions on paroxetine are shown in red.

Takeda Inhibitors

In 2007, the Takeda Pharmaceutical Company developed compound101 (cmpd101) and compound103A (cmpd103A) as GRK2/3 inhibitors (Ikeda, S, Keneko & Fujiwara 2007). Their structures are composed of four rings named A-D (Figure 1.12A). When these compounds crystallised with GRK2-$G_{\beta\gamma}$, they showed a slightly different interaction with the catalytic site of GRK2 from that of balanol (Figures 1.9B and 1.12B) (Thal et al. 2011). The A rings of cmpd101 and cmpd103 bind to the adenine subsite whereas the B rings bind to the ribose subsite. The C rings bind in the triphosphate subsite of the kinase catalytic domain whilst the D rings bind to the hydrophobic subsite, making nonpolar interactions with Gly^{201}, Phe^{202}, Leu^{235}, Glu^{239}, Gly^{337} and Leu^{338} (Thal et al. 2011).

Cmpd101 and cmpd103 bind to an open, noncatalytic conformation of GRK2 with a slight closure of the kinase domain towards the small lobe by 2.4 A° and 3.6 A°, respectively (Thal et al. 2011). Both compounds show inhibition of GRK2 with an IC_{50} of 290 and 54 nM, respectively. They show no inhibition against GRK1 and GRK5 up to a concentration of 125 µM (Thal et al. 2011).

Recently, Professor Steve Husbands at the University of Bath has developed a series of novel cmpd101 analogues. They were designed based on the idea that the selectivity of cmpd101 is due to forming van der Waals interaction (Homan & Tesmer 2015) through the A-ring and more hydrogen bonds can lead to a loss in the selectivity. To explore the idea, the A/B rings of cmpd101 were replaced by naphthyl rings as in compounds BU16007 and BU16006 or quinolone ring as in compound BU16005 (Figure 1.13). Also, the amide and CH_2NH groups were replaced by double bonds, as in compounds BU14013 and BU14014, respectively (Figure 1.13). These compounds will be the subject of this thesis.

Finally, at the time of starting my research, most of the potent and selective GRK2 inhibitors are paroxetine derivatives have not been developed. The only GRK2/3 inhibitors being used are paroxetine, balalnol, cmpd101 in most of the studies. Cmpd101 is a promising inhibitor and can be a scaffold for developing new potent and selective inhibitors. However, there are as yet no clinically used selective GRK inhibitors.

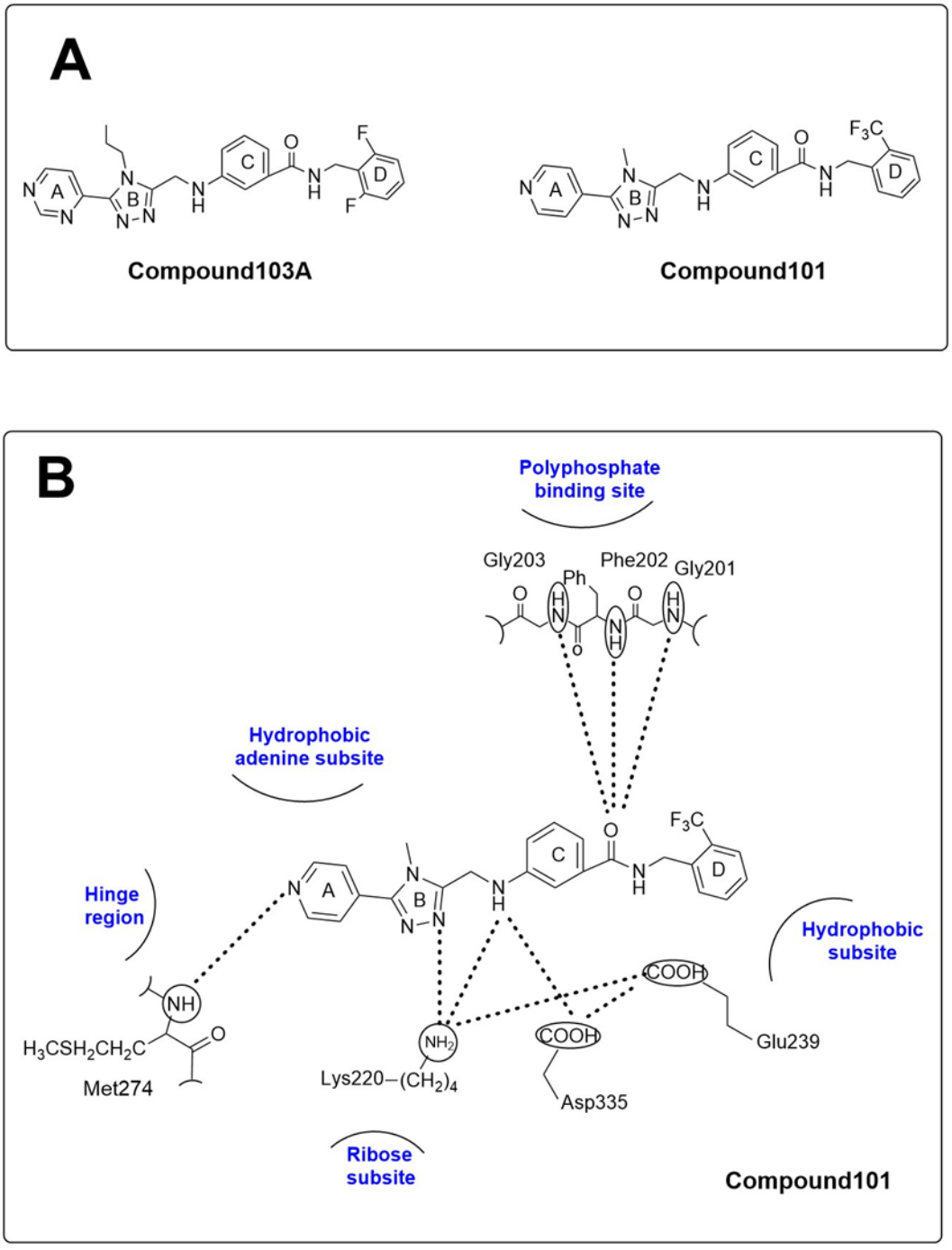

Figure 1.12 Chemical structures of cmpd101 and cmpd103A

Chemical structures of cmpd101 and cmpd103A (A), and an illustration of the binding of cmpd101 in the GRK2 binding site (blue) (B). Adapted and modified from Guccione et al. (2016)

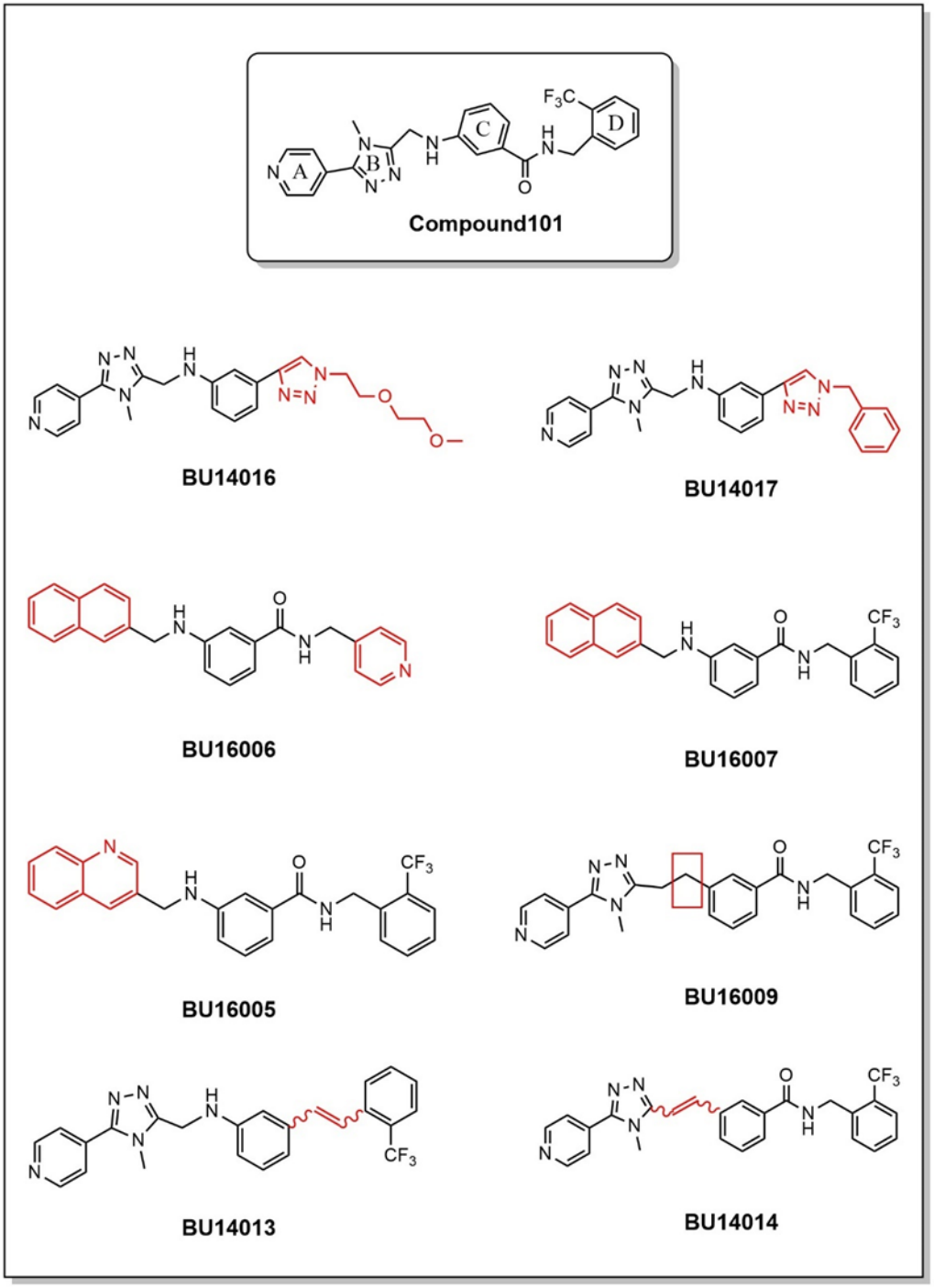

Figure 1.13 Chemical structures of novel inhibitors

The modifications on cmpd101 are shown in red.

1.4.6 Application of GRK Inhibitors in GPCR Signalling

While RNAi and animal gene knockout studies have increased our understanding of GRKs (Fan et al. 2013; Matkovich et al. 2006; Mundell, S. J., Benovic & Kelly 1997), the introduction of small GRKs inhibitors (Bouley, RA et al. 2020; Ikeda, S, Keneko & Fujiwara 2007; Rowlands et al. 2019) has brought further insight into the role of GRKs in modulating GPCR signalling. Using GRK inhibitors to study GPCRs has identified role of GRKs, in particular GRK2, in regulating various signalling pathways. In this section, I will give some examples of utilising GRK inhibitors in studying the role of GRK in GPCR signalling.

Paroxetine has been used in investigating the role of GRK2 in GPCR signalling. Recently, a study used most potential GRK2 inhibitors, including paroxetine, cmpd101, and two paroxetine derivatives, CCG215022 and CCG224063, to investigate GRK2-mediated desensitisation of uridine triphosphate (UTP) and angiotensin II (AngII)-stimulated cells. These GRK2 inhibitors attenuated UTP- and AngII-induced desensitisation in isolated smooth muscle cells (Rainbow et al. 2018).Using these inhibitors confirmed that GRK2 plays a central role in regulating vasoconstrictor-mediated arterial contraction (Rainbow et al. 2018).

In MOPr, Lowe et al. (2015) investigated the role of GRK2 in desensitisation of MOPr using GIRK current in LC neurons. LC slices were pretreated with cmpd101 (30 μM), a selective GRK2/3 inhibitor, and then stimulated with methionine-enkephalin (Met-Enk), DAMGO, endomorphin-2, and morphine to induce MOPr desensitisation. Cmpd101 inhibited the Met-Enk-, DAMGO-, endomorphin-2- and morphine-induced desensitisation of the G protein–activated inwardly-rectifying potassium (GIRK) current. The authors concluded that GRK2/3 played a role in MOPr desensitisation in LC neurons.

Another study looked at the role of GRK2 in insulin and βAR signalling pathways in fibroblasts (Cannavo et al. 2019). Aldosterone blocks insulin signalling in vascular smooth muscle cells (Cannavo et al. 2019). The authors wanted to study whether GRK2 has a role in this pathway. Fibroblast cells (3T3) were pretreated with cmpd101 (3 μM) in the presence or absence of aldosterone. Then cells were

stimulated with insulin. They looked at the phosphorylation of insulin receptor substrate 1 (IRS1) at Ser^{307}, which is the GRK2 phosphorylation site resulting in blocking insulin signalling. They found that cmpd101 blocked the effect of aldosterone on the insulin signalling. These results indicate the role of GRK2 in aldosterone signalling pathway.

In a mouse myocardial infarction model, treatment with paroxetine after 2 weeks of myocardial infarction improved left ventricular function and structure when compared to fluoxetine, an analogue of paroxetine with no effect of GRK activity (Schumacher et al. 2015). The use of genetically engineered mice further suggested that paroxetine was working through inhibition of GRK2 (Schumacher et al. 2015).

In summary, these and other functional studies are revealing interesting insights into the role of GRKs in GPCR signalling pathways and the possibility of using GRK inhibitors as potential therapeutic agents.

1.5 Bioluminescence Resonance Energy Transfer (BRET)

Over the years, many methods have been developed to study protein interaction with GPCRs, including bioluminescence resonance energy transfer (BRET), fluorescence resonance energy transfer (FRET), and other biochemical methods. GPCRs are well known to function in dimer/oligomer forms and to interact with various effectors in a ligand-driven manner or constitutively. Therefore, studying protein-protein interaction is essential in finding and developing targeted therapy. In this thesis, I will use the BRET technique, in particular $BRET^2$, to study arrestin-3 recruitment to MOPr and DOPr.

1.5.1 Principle of BRET

BRET was initially adapted from marine animals (sea pansy *Renilla reniformis* and jellyfish *Aequoria victoria*) and has subsequently been used to study protein-protein interaction in living cells (El Khamlichi et al. 2019). It generates non-radiating energy so that it can avoid the complication of radiation when using a radiolabelled agent

(Pfleger, Seeber & Eidne 2006). The energy is transferred from the donor, usually Renilla Luciferase, to the acceptor protein, such as Yellow Fluorescent Protein (YFP) (Figure 1.14) (El Khamlichi et al. 2019). A protein of interest can be generated by fusing donor protein to one protein and the acceptor protein to the other protein of interest. Then, both proteins are cotransfected into suitable cell lines (e.g., HEK293, CHO). Once the proteins of interest are coexpressed in the chosen cell line, the substrate coelenterazine, a cell-permeable substrate that is oxidised, is added (Figure 1.14). When the two proteins of interest come in close proximity (<10 nm) (Pfleger & Eidne 2006), the energy resulting from the catalytic degradation of the coelenterazine substrate from the donor (luciferase) to the acceptor (e.g., YFP) generates light emission at 530 nm (El Khamlichi et al. 2019). The intensity of BRET is influenced by many factors, such as 1) the distance between the two BRET proteins; 2) the overlap of the emission of the donor with excitation of the acceptor; 3) the orientation of the BRET proteins; and 4) the ratio of a donor to an acceptor (Ayoub & Pfleger 2010; Pfleger & Eidne 2006). Specific interaction between the two proteins shows a hyperbolic relationship and reaches a plateau once all donors bind to the acceptor (Ayoub & Pfleger 2010). In nonspecific interaction, the relationship is dictated by increasing linearly upon increasing the donor concentration (Ayoub & Pfleger 2010). In the last few years, a growing number of BRET systems have been developed to increase the BRET signal or the stability of BRET partners.

More systems have been developed to overcome the drawbacks of BRET^1, such as the high spectral ratio of a donor to the acceptor and high signal/noise ratio. BRET^2 using a coelenterazine derivative, DeepBlue C or coelenterazine 400a has improved the RLuc emission, but its luminescence signal last for only a few seconds making it less sensitive than BRET^1 (El Khamlichi et al. 2019). Also, it requires the increasing of the protein expression level, which may detect nonspecific protein-protein interaction (El Khamlichi et al. 2019).

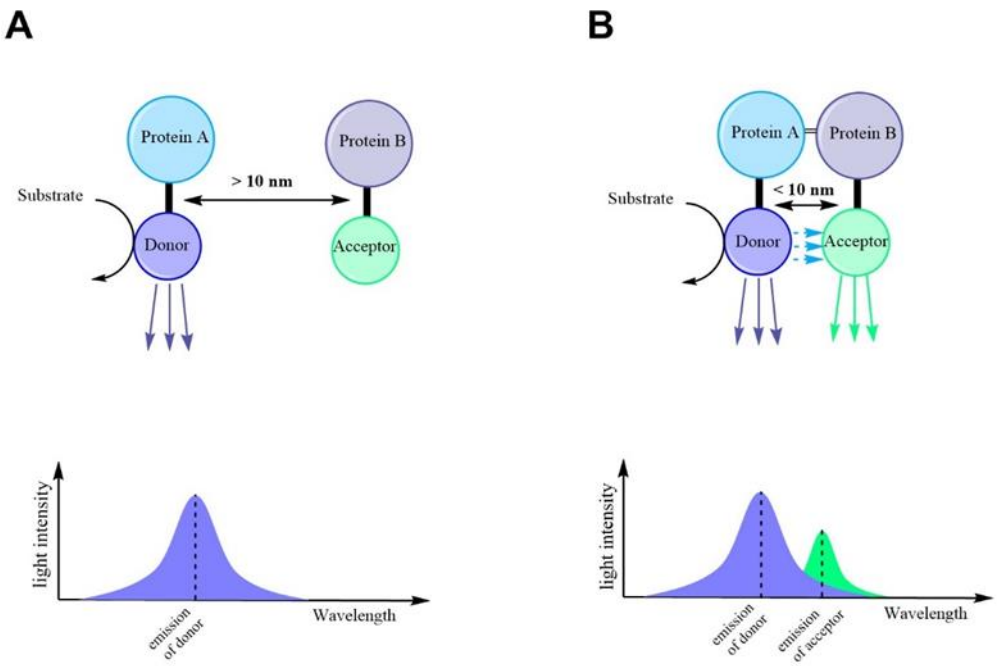

Figure 1.14 BRET principle

A schematic representation of the principle of BRET. BRET technology involves the fusion of donor (e.g., RLuc) and acceptor (e.g., GFP) to proteins of interest (Protein A and Protein B). Co-transfection of the donor and the acceptor into cell lines enables to study their interaction. A) When the distance between a donor and an acceptor is more than 10 nm i.e., no interaction, there is no transfer of energy and no emission from the acceptor. B) the donor comes in close proximity to the acceptor (<10 nm), and the energy transfers from the donor to the acceptor result in light emission from the acceptor at a specific wavelength. The energy emitted by the acceptor relative to the energy emitted by the donor is the BRET ratio.

1.5.2 BRET Application in Cellular Signalling

BRET technology has been used extensively in studying protein-protein interaction. One area that has been applied to is studying the GPCR signalling and identifying new mechanisms. Also, it helps in elucidating downstream signalling of GPCRs. BRET is of help in studying dimerisation of GPCR and oligomerisation (Issad & Jockers 2006; Massoud et al. 2007). It has also been applied in studying GPCR and G protein interaction. For example, our lab has used BRET to study the interaction of MOPr and G protein, which helps in understanding the morphine and MOPr agonists (Hill et al. 2018).

GPCR interactions with G protein have been studied in living cells by using BRET. BRET has allowed the determination of full agonists, partial agonist and antagonists. Also, BRET has been utilised in the characterisation of different receptor conformations induced by distinct ligands by means of agonist biased. Moreover, BRET is used to monitor the dissociation of G proteins subunits after receptor activation.

Expanding the application of BRET to be used in determining the interactions between GPCR and GRK, which a direct way to study the recruitment of GRK to the activated receptor (Miess et al. 2018). Agonist-induced arrestin recruitment to the phosphorylated GPCR is one common BRET assay. One of the first studies used arrestin BRET assay where the receptor was fused with Venus and arrestin-3 with RLuc in HEK293 cells. This screening resulted in finding compounds that inhibit agonist-induced arrestin-3 recruitment to C-C chemokine receptor type 5 (CCR5) (Hamdan et al. 2006). Hill et al. (2018) used BRET to determine the functionality of PZM21 in arrestin and G protein activation assay in HEK293 cell expressing MOPr. This showed that PZM21 is low efficacy MOPr agonist in both assays.

1.6 Thesis Aims

The growing body of research on GRKs shows their importance in regulating the signalling and trafficking of GPCRs. In addition, GRKs regulate GPCR-independent signalling pathways that play a key role in important cellular functions, such as platelet-derived growth factor receptor β (PDGFRβ) and EGFR (Gurevich, EV et al. 2012). There is a need for a better understanding of the role of GRKs in regulating phosphorylation of GPCRs and the functional consequences this produces in the cell and organism. Until recently, there have been few if any selective inhibitors for GRKs. The recent development of Takeda compounds and the promising findings make it possible to study the function of individual GRKs.

There has been some progress on the development of potent and selective GRK inhibitors. However, the selectivity, in particular, has not been resolved. Understanding the structure and functions of GRKs will facilitate the development

of potent and selective inhibitors. In this thesis, I aim to study the ability of cmpd101 and some novel structural analogues to inhibit GRKs, principally by assessing their ability to inhibit agonist-induced arrestin-3 recruitment to μ and δ opioid receptors. Inhibitors of GRK phosphorylation of opioid receptors could represent drugs that suppress tolerance, a common problem observed with the use of opioid receptor agonists. The long-term goal of our research is to investigate the role of GRK phosphorylation in the function of μ opioid receptor and other GPCRs. Particularly, the specific aims of this thesis are:

1. To use the mu-opioid receptor (MOPr) and an arrestin-3 recruitment assay as a readout of GRK phosphorylation to identify and characterise potential novel inhibitors of GRK function.
2. To investigate whether inhibition of arrestin-3 recruitment to MOPr by potential GRK inhibitors is agonist-dependent.
3. To investigate whether inhibition of agonist-dependent arrestin-3 recruitment by potential GRK inhibitors is receptor-dependent (MOPr versus DOPr).
4. To investigate the selectivity of potential GRK inhibitors of different GRKs by assessing their ability to inhibit arrestin-3 recruitment to MOPr following cellular overexpression of individual GRK isoforms.

CHAPTER 2 Materials and Methods

2.1 Materials

2.1.1 Compounds and Reagents

Cmpd101 was purchased from Hello Bio (Bristol, UK) and all other analogues were synthesised by Professor Steve Husbands at the University of Bath (Bath, UK). DAMGO ([d-Ala^2-MePhe^4-Gly-ol] enkephalin) was purchased from Bachem (Bubendorf, Switzerland); SNC80 ((+)-4-[(α*R*)-α-((2*S*,5*R*)-4-Allyl-2,5-dimethyl-1-piperazinyl)-3-methoxybenzyl]-*N*,*N*-diethylbenzamide), DADLE ([D-Ala^2, D-Leu^5]-Enkephalin), GF109203X, PD98059, KN-93 and SP600125 were from Tocris Bioscience (Bristol, UK). Morphine hydrochloride was purchased from MacFarlan Smith (Edinburgh, UK). Lipofectamine 2000 was purchased from Invitrogen and coelenterazine 400a (DeepBlueC) was from Insight Biotechnology (Wembley, UK). All other reagents were purchased from Sigma-Aldrich (Dorset, UK).

2.1.2 Antibodies

The primary and secondary antibodies used in this thesis are listed in Table 2.1. The primary antibodies, anti-GRK2, anti-GRK3, anti-GRK5 and anti-GRK6, were purchased from Santa Cruz Biotechnology (Insight Biotechnology, Wembley, UK); anti-α-tubulin was from Sigma-Aldrich (Dorset, UK), and anti-HA.11 was from BioLegend (London, UK). The secondary antibodies: anti-mouse IgG horse-radish peroxidase linked antibody was from GE Healthcare (Buckinghamshire, UK), anti-mouse IgG-alkaline phosphatase was from Sigma-Aldrich (Dorset, UK). All the concentrations of the antibodies (Table 2.1) were determined based on a combination of the manufacturer recommendation and published literature.

Table 2.1 Primary and secondary antibodies

Antibody	Assay	Species	Dilution	Supplier	Catalogue number
Primary antibodies					
Anti-α-tubulin	WB	Mouse	1:10,000	Sigma	T6074
Anti-GRK2 (C-15)	WB	Rabbit	1:200	Santa Cruz	Sc-562
Anti-GRK3 (C-14)	WB	Rabbit	1:300	Santa Cruz	Sc-563
Anti-GRK5 (C-20)	WB	Rabbit	1:500	Santa Cruz	Sc-565
Anti-GRK6 (C-20)	WB	Rabbit	1:300	Santa Cruz	Sc-566
Anti-HA.11	ELISA	Mouse	1:1,000	Biolegend	901514
Secondary antibodies					
Rabbit-HRP	WB	Sheep	1:7,500	GE Healthcare	NA934V
Mouse-HRP	WB	Sheep	1:10,000	GE Healthcare	NXA931
Mouse-IgG AP	ELISA	Goat	1:1,000	Sigma	A5153

All primary and secondary antibodies were used for western blotting (WB) or enzyme-linked immunosorbent assay (ELISA). Horse-radish peroxidase (HRP)-conjugated antibodies, alkaline phosphatase (AP).

2.2 Methods

2.2.1 Preparation of the Plasmids

The hMOPr-RLuc2 (MOPr-RLuc2) in the pQCXIN vector and DOPr-RLuc2 in the pQCXIN vector and arrestin-3-GFP10 (Arr3-GFP) in the pQCXIH vector constructs were a gift from Dr Tomasso Costa, Institute Superiore di Sanita, Italy. The $G_{\alpha i}$-RLuc2 and G_{γ}-GFP plasmids in the pcDNA3.1 vector were a gift from Dr Michel Bouvier, University of Montreal, Canada. The HA-tagged rMOPr construct in the pcDNA3 vector was from Dr Helen Sanderson, University of Bristol. GRK2, GRK3, GRK5, GRK6 in the pcDNA3.1 vector and pcDNA3.1 constructs were from Dr Michael Bouvier, University of Montreal, Canada. The purified DNAs were obtained as follows: the subcloning efficiency DH5α competent cells (Invitrogen) were divided into 20 µl aliquots and stored in -80°C when required the aliquot of DH5α competent cells was thawed on ice. The plasmid DNA (1 µg) was added to the 20 µl DH5α competent aliquot and incubated on ice for 30 min. Then, the mixture was heat shocked in a water bath at 42°C for 45 seconds and then incubated on ice for 2 min. Next, 200 µl of SOC (super optimal broth with catabolite repression) medium was added to the mixture and incubated in a shaking incubator at 180 rpm and 37°C for 1 h. The transformed cells were then plated on LB agar (Luria-Bertani) plates containing an appropriate antibiotic (e.g., Ampicillin 100 µg/ml or kanamycin 50 µg /ml). The LB agar plate was then placed in an incubator at 37°C overnight. The next morning, well separated bacterial colonies were picked up by a sterile glass hook and added into 3 ml tubes containing an appropriate antibiotic (Ampicillin 100 µg/ml or kanamycin 50 µg /ml) and incubated in a shaker incubator at 37°C overnight. The following day, the bacteria cultures were expanded into 200 ml LB agar flasks containing the appropriate antibiotic (Ampicillin 100 µg/ml or kanamycin 50 µg /ml) and incubated in the shaking incubator at 37°C overnight.

The next day, the bacterial cells were pelleted by centrifugation at 6,000 x g for 15 min at 4ºC. We used the HighSpeed Plasmid Preparation Kit (Qiagen®), which is based on modified alkaline lysis, to prepare high-quality DNA for transfection. The steps of the protocol were given by the manufacturer as follows: the pellet was resuspended in Buffer P1 (10 ml) and then added to Buffer P2 (10 ml). Next, the DNA was precipitated with chilled Buffer P3 (10 ml) and incubated on ice for 20 min and then centrifuged at 20,000 x g for 30 min at 4ºC. The supernatant was

then filtered using QIAGEN-tip that had been equilibrated with Buffer QBT (10 ml). Following this, the DNA was eluted using Buffer QF (15 ml) and then the DNA precipitated by adding 10.5 ml 100% isopropranolol and centrifuged for 30 min. The DNA pellet was then washed with 2 ml 70% ethanol and centrifuged for 10 min. Finally, the DNA pellet was resuspended in a suitable volume of TE buffer. The DNA concentration was measured by NanoDrop™ 2000 Spectrophotometer at 260 nm (Thermo Scientific). The DNA constructs were store at -20ºC. All DNA constructs were sequenced by Source BioScience, Nottingham, UK.

2.2.2 Cell Culture

Human Embryonic Kidney 293 (HEK293) cells were cultured at 37°C in 5% CO_2 in Dulbecco's Modified Eagle's Medium (DMEM, Gibco) supplemented with 10% fetal bovine serum (FBS, Corning), 10 U/ml penicillin and 10 mg/ml streptomycin (Invitrogen/Life Technologies, Paisley, UK). Cells were seeded onto 100 mm dishes and grown to 80-90% confluence, then subjected to splitting. To do this, media was removed, and cells were washed with phosphate-buffered saline (PBS, Oxoid Limited, Basingstoke, UK). Cells were then detached by adding 0.25% trypsin (Gibco). Cells were then collected by adding 5 ml media and transferred to centrifuge tubes. Cells were centrifuged at 300 x g for 3 min. The pelleted were resuspended in DMEM and transferred to new sterilised dishes or plates and cultured in the incubator until required for further splitting or experimentation. All cell culture procedures were undertaken in an aseptic cell culture hood.

2.2.3 cDNA Transfection

For the arrestin-3 recruitment assay, we used two BRET configurations. The required DNA constructs were diluted in Opti-MEM media (Gibco) to a total volume of 500 ml. We used $BRET^2$ where HEK293 cells cotransfected with MOPr-Rluc2 (5 µg) and Arr3-GFP (5 µg). Another set of cells was only transfected with MOPr-Rluc2 to correct for the basal luciferase signal in cells (Borroto-Escuela et al. 2013). For the G_i activation assay, HEK293 cells were transfected with HA-MOPr (3 µg), $G_{\alpha i}$-RLuc2 (3 µg) and G_{γ}-GFP (3 µg).

The ratio of donor to acceptor was determined previously in our laboratory (Gasiunaite G 2017). cDNA construct transfections were carried out using Lipofectamine® 2000 according to the manufacturer's instructions. The DNA of

interest was diluted with Opti-MEM media (Gibco) to a final concentration of 5 µg/ml in a total volume of 500 ml and mixed gently. Also, lipofectamine® 2000 was diluted with Opti-MEM media in a total volume of 500 ml and mixed gently. The ratio of DNA (µg) to lipofectamine® 2000 (µl) was 1:2.7; this ratio was determined previously by Dr Gerda Gausinuaite in our laboratory through a saturation assay, where a fixed amount of DNA was coexpressed with an increasing concentration of lipofectamine® 2000. The DNA dilution and lipofectamine dilution were incubated for 5 min at room temperature. During the incubation, the culture media of the dishes that were intended for transfection was removed and replaced with 9 ml Opti-MEM media. After 5 min incubation, the diluted lipofectamine was added slowly to the diluted DNA and mixed gently and incubated for a further 10 min at room temperature. After, the complex was added to cells and the cells incubated at 37°C in a CO_2 incubator for 24 h. Following this, the Opti-MEM media was removed and fresh DMEM media (10 ml) was added. All assays were performed 48 h after transfection.

2.2.4 Bioluminescence Resonance Energy Transfer (BRET) Measurements

BRET assays were used to measure agonist-induced arrestin-3 recruitment to MOPr or DOPr and also to measure the dissociation (activation) of G-protein subunits ($G_{\alpha i}$ and G_{γ}). HEK293 cells were transfected with MOPr-RLuc2 (a BRET donor) along with Arr3-GFP (a BRET acceptor), as described in Section 2.2.3. On the day of the BRET experiment, the cell media was aspirated and the cells washed with sterile 5 ml PBS. Then, the PBS was removed and 1 ml 0.25% trypsin was added to help detach the cells. Then, 5 ml of medium was added to each dish and the cells and medium transferred into 10 ml centrifuge tubes and the cells pelleted by centrifugation at 300 x g for 3 min. The pellet was resuspended in 5 ml clear media and re-seeded onto white 96-well plates. Cmpd101 and its analogues were dissolved in DMSO and the final concentration of DMSO was 0.3% in all BRET assays.

To construct agonist concentration-response curves (Figures 3.3 and 3.4), cells were stimulated with MOPr agonists DAMGO (0.001-30 µM), morphine (0.01-100 µM), or DOPr agonists SNC80 (0.001-100 µM), or DADLE (0.001-100 µM) for 10 min. For DAMGO or morphine time courses, the BRET measurements were taken every 2 min up to 20 min (Figure 3.5). Three minutes after starting the

measurements, DAMGO (10 µM) or morphine (30 µM) was added. In the time course experiments, naloxone (10 µM) was added 4 min after the addition of DAMGO or morphine.

To investigate the effect of compounds on the agonist-induced arrestin-3 recruitment, HEK293 cells were preincubated with cmpd101 or test compounds for 30 min (Figures 3.7A, 3.8 and 4.6) and then DAMGO (10 µM), morphine (30 µM), SNC80 (10 µM), or DADLE (10 µM) was added. For time course experiments, BRET measurements were taken at every 2 min up to 16 min (Figures 3.7A, 3.8,) or 18 min (Figure 4.6). To investigate the cmpd101-induced inhibition of established DAMGO- or morphine-induced arrestin-3 recruitment, BRET measurements were taken at every 2 min up to 16 min up to 20 min (Figure 3.7B) or 18 min (Figure 3.11), cmpd101 was added 4 min after the agonist stimulation (Figures 3.7B and 3.11).

For concentration-dependent inhibition of agonist-stimulated arrestin-3 recruitment by cmpd101 and test compounds, cells were preincubated with various concentrations of cmpd101 or test compound (0.01-100 µM) for 30 min at 37ºC. Then, cells were stimulated with the addition of DAMGO (10 µM), morphine (30 µM) or SNC80 (10 µM) for 10 min before BRET measurement.

To measure the effect of different kinase inhibitors on the DAMGO-induced arrestin-3 recruitment, cells were preincubated with GF109203X (1 µM), a PKC inhibitor; SP600125 (30 µM), a JNK inhibitor; PD998059 (10 µM), an ERK1/2 inhibitor; KN-93 (1 µM), a CaMKII inhibitor or cmpd101 (30 µM) as a positive control and cells then stimulated with DAMGO (10 µM) for a further 10 min.

To measure G_i activation, cells were transfected with HA-MOPr, $G_{\alpha i}$-RLuc2 and G_{γ}-GFP, as described in Section 2.2.3. For experimentation, cells were preincubated with cmpd101 (30 µM) or test compounds for 30 min. Then, cells were stimulated with DAMGO (0.001- 30 µM) for a further 2 min. Coelenterazine 400a (final concentration of 5 µM) was prepared 10 min before BRET measurements. All the BRET measurements were performed using a FLUOstar Omega (BMG LABTECH, Germany) microplate reader with a filter set of 410/80 nm (donor) and 515/30 nm (acceptor). The BRET ratio was determined by (dividing the intensity of acceptor luminescence emission at 515 nm by the intensity of donor luminescence emission at 410 nm) times 1000.

2.2.5 Western Blotting

Sample Preparation

HEK293 cells were transfected (as described in Section 2.2.3) with MOPr-RLuc2, Arr3-GFP and GRK2, GRK3, GRK5 or GRK6, and another 100 mm cell dish was transfected with MOPr-RLuc2, Arr3-GFP, and pcDNA3.1 as a control. After 48 h of the transfection, cell dishes were placed on ice and the media was aspirated. Cells were washed two times with ice-cold PBS. Then, 400 µl RIPA buffer (150 mM NaCl, 5 mM EDTA, 50 mM Tris, 1% Triton-X100, 0.5% Sodium deoxycholate, 0.1% SDS, pH 7.5) was added to the dishes to lyse cells and the cells were then scraped into and transferred to sterile Eppendorf tubes. Tubes were placed in a slow rotator for 30 min in a cold room. Next, cells were centrifuged at 2,000 x g for 10 min at 4ºC. The pellets were discarded and the clear solution was transferred to new sterile Eppendorf tubes and stored at -20 ºC. The protein concentration in each sample was then determined as below.

Measurement of Protein Concentration by DC Assay

Protein concertation was determined by DC (detergent compatible) protein assay using a DC™ Protein assay kit (Bio-Rad, cat# 500-d114). A range of BSA concentrations (0-2 mg/ml) was prepared in RIPA buffer as a standard curve. For this, 5 µl of the standards and the samples were added to a 96-well plate. Then, 25 µl of reagent A and then 200 µl of reagent B was added to each well. The plate was incubated at room temperature for 15 min and the absorbances in each well were read at 595 nm in a microplate reader (Tecan infinite M200Pro, Tecan Austria GmbH). The unknown protein concentrations of the samples were determined by interpolation of the BSA standard curve. The curves were constructed using GraphPad Prism v8. All curves were carried out in triplicate.

Immunoblotting

Equal amounts of proteins (50 µg) were resolved by running buffer [25 mM Tris, 200 mM glycine and containing 0.1% (w/v) sodium dodecyl sulphate (SDS)] on 10% SDS-polyacrylamide gel at 120V for 90 min. Prestained markers (PageRuler™ Plus, Thermo Scientific) (7 µl) were added to estimate the molecular weights of the proteins. Proteins were then transferred onto polyvinylidene fluoride (PDVF) membranes (Millipore) at 100V for 90 min. Membranes were then blocked with 5% (w/v) non-fat dried milk in TBST buffer (20 mM Tris, pH 7.5, 100 mM NaCl,

containing 0.1% (v/v) Tween 20) and placed on a rocker for 1 h. Following that, membranes were incubated with primary antibodies in 5% (w/v) non-fat dried milk in TBST buffer in sealed bags overnight at 4°C on shaking rocker. The next morning, membranes were washed three times with TBST, first time 15 min the next two 5 min each at room temperature. Membranes were then incubated with horseradish-peroxidase (HRP)-conjugated secondary antibody prepared in 5% (w/v) non-fat dried milk in 10 ml TBST buffer on shaking rocker at room temperature for 1 hr. Then, membranes were washed three times with TBST. After that, the protein on membranes was subjected to detection using western blotting detection reagents (ELC™, GE Healthcare) for 2 min. Membranes were exposed to Hyperfillm ECL (GE Healthcare) for about 1 min in a dark room and the films were processed by an SRX-101A developer (Konika Minolta). Pictures were finally processed by ImageJ software (NIH).

2.2.6 Enzyme-linked Immunosorbent Assay (ELISA)

The surface expression of MOPr was determined by ELISA, according to Mundell, Stuart J., Nisar and Kelly (2010) with minor modifications. HEK293 cells were transfected with HA-MOPr, as described in Section 2.2.3. After 24 h of transfection, cells were plated in a 24-well plate precoated with 400 µl poly-L-lysine. Cells transfected with pcDNA3.1 were plated in parallel and used as background controls. Plates were kept at 37°C in a CO_2 incubator overnight. The following morning, the DMEM medium was replaced by serum-free DMEM and incubated at 37°C in a CO_2 incubator for 10 min. Cmpd101 or test compound (30 µM) were added to the plates and incubated at 37°C in a CO_2 incubator for 30 min. Then, DAMGO (10 µM), morphine (30 µM) or vehicle was added for a further 30 min; this time point was chosen based on Figure 3.14A, which indicates that peak agonist-induced surface receptor loss was reached by this time point. Cells were then fixed with 3.9% paraformaldehyde (PFA) (VWR) for 5 min. Cells were washed three times with TBS (20 mM Tris, 100 mM NaCl, pH 7.5) at room temperature in a cell culture hood. After this, cells were blocked with 1% BSA prepared in TBS for 45 min at room temperature on a rocker. Following this, cells were further incubated with primary antibody (mouse anti-HA monoclonal antibody, Biolegend) at a dilution of 1:1,000 (250 µl/well) for 1 hr. Cells were then washed a further three times with TBS and then were incubated with 1% BSA at room temperature for 15 min. After that, they were incubated with secondary antibody (goat anti-mouse IgG alkaline phosphatase conjugate, Sigma) at 1:1,000

dilution for 1 hr. After that, cells were again washed three times with TBS. Cells were finally incubated at 37°C with 250 µl/well alkaline phosphatase substrate (Thermo scientific) until the colour changed to yellow. The reaction was stopped by transferring the substrate to 96-well plates containing 2N NaOH. The absorbance was then measured at 405 nm using Tecan Infinite plate reader (Tecan). All experiments were performed four times in triplicate.

2.2.7 Fluorescence-activated Cell Sorting (FACS)

Flow cytometry was used to determine the percentage of GFP positive cells in HEK293 cells transfected with MOPr-RLuc2 and Arr3-GFP, as described in Section 2.2.3 and cultured for 48 hr. Following this, the DMEM media was removed and cells were washed with 5 ml PBS. Then, cells were detached by adding 1 ml 0.25% trypsin. Cells were then collected by adding 5 ml of medium and transferred to centrifuge tubes. Cells were then centrifuged at 300 x g at room temperature for 3 min. The pelleted cells were then resuspended in FACS buffer (Ca^{+2} and Mg^{+2} free PBS, 25 mM HEPES pH 7.0, 2.5 mM EDTA and 0.5% BSA), which is designed to prevent cell clumping. Following this, the cells were transferred to new sterile Eppendorf tubes at a density of $1x10^5$ cells/ml and kept on ice until analysis. The actual FACS analysis was carried out by the Faculty of Life Science, the Flow Cytometry Facility, University of Bristol led by Dr Andrew Herman. The fluorescence was analysed by Novocyte 3000 Flow Cytometer (Acea Biosciences, San Diego, CA, USA).

2.2.8 Data Analysis

The BRET ratio was determined by dividing the intensity of acceptor luminescence emission at 515 nm by the intensity of donor luminescence emission at 410 nm times 1000. These values were then subtracted from the no agonist-treated cells and normalised to the agonist-induced stimulation and fitted to a curve by nonlinear regression using GraphPad Prism v8.0 software (San Diego, CA, USA). A snapshot of the raw data obtained from the machine is shown in Figure 2.1. For the G_i activation assay, the data were plotted as a percentage decrease from vehicle-treated wells. ELISA data were measured in triplicate and the values were averaged. The averaged values were then subtracted from the empty vector (pcDNA3.1) value. Then, the subtracted values were divided by the control (untreated cells) to obtain the percentage of the cell surface receptor loss. A

snapshot of the raw data obtained from the machine is shown in Figure 2.2. The EC_{50}, maximum response and IC_{50} values were obtained by averaging the values of individual experiment and were fitted to three or four parameters nonlinear regression model based on which gave the best r^2 and narrow 95% confidence interval (CI). All inhibition curves were fitted to a three parameters model with a fixed slope of -1. Standard curves of the DC protein assay were fitted by linear regression analysis. Figures 1.1- 6 and 5.16 were created with BioRender.com. All data are presented as mean ± SEM from at least three independent experiments performed in duplicate for the BRET assay and in triplicate for the ELISA assay. The logP values were calculated using ChemDraw Professional 16 software. It estimates logP of a compound based on its chemical structure. The software calculates the logP value using specific logarithms based on the formula:

$$\mathrm{logP_{oct/wat}} = \log\left(\frac{[\mathrm{solute}]_{\mathrm{octanol}}}{[\mathrm{solute}]_{\mathrm{un-ionized\ water}}}\right)$$

Statistical analysis was carried out with one-sample Student's t-test, one-way ANOVA, or two-way ANOVA followed by Tukey's or Dunnett's post-hoc test. Post-hoc tests were chosen based on the type of analysis required. For instance, Tukey's test was used to compare between all means of the groups while Dunnett's was used to compare selected group mean, such as control or vehicle mean, to the other group means. *P*-values of < 0.05 were considered as statistically significant.

Figure 2.1 Representative example of raw data of BRET readout

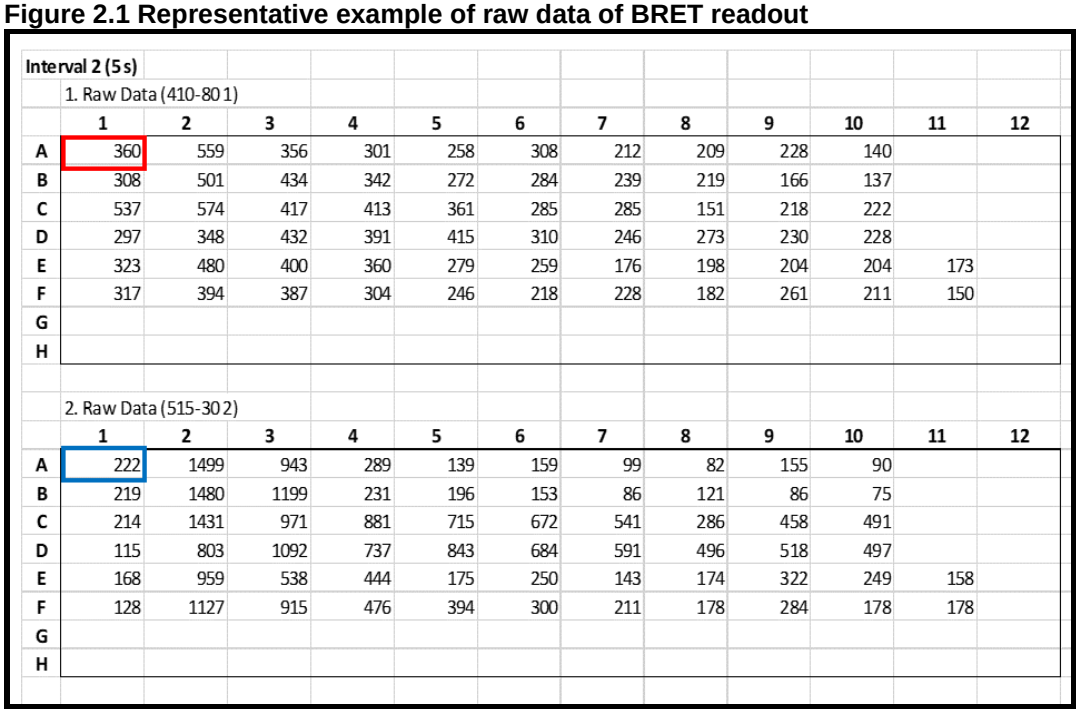

Interval 2 (5 s)

1. Raw Data (410-80 1)

	1	2	3	4	5	6	7	8	9	10	11	12
A	360	559	356	301	258	308	212	209	228	140		
B	308	501	434	342	272	284	239	219	166	137		
C	537	574	417	413	361	285	285	151	218	222		
D	297	348	432	391	415	310	246	273	230	228		
E	323	480	400	360	279	259	176	198	204	204	173	
F	317	394	387	304	246	218	228	182	261	211	150	
G												
H												

2. Raw Data (515-30 2)

	1	2	3	4	5	6	7	8	9	10	11	12
A	222	1499	943	289	139	159	99	82	155	90		
B	219	1480	1199	231	196	153	86	121	86	75		
C	214	1431	971	881	715	672	541	286	458	491		
D	115	803	1092	737	843	684	591	496	518	497		
E	168	959	538	444	175	250	143	174	322	249	158	
F	128	1127	915	476	394	300	211	178	284	178	178	
G												
H												

The snapshot represents the plate layout. Each row represents one run. The upper box is the donor emission readouts and the below box is the acceptor readout. During data analysis, donor emission (highlighted in red) is divided by the acceptor emission (highlighted in blue) to give the BRET ratio.

Figure 2.2 Representative example of ELISA raw data

User				UOB\ya16916			
Plate				Greiner 96 Flat Bottom Transparent Polystyrol [GRE96ft.pdfx]			
Plate-ID (Stacker)							
Label: BCA							
Mode				Absorbance			
Wavelength				405	nm		
Bandwidth				9	nm		
Number of Flashes				25			
Settle Time				0	ms		
Part of Plate				E7-H12			
Start Time	19/09/2019 02:22:26 PM						
	Temperature: 25.1 °C						
<>	7	8	9	10	11	12	
E	1.6409	1.6446	1.5183	1.328	1.3109	1.3578	
F	1.5642	1.5735	1.519	1.3058	1.2762	1.2414	
G	1.4829	1.4341	1.512	1.2147	1.2639	1.3401	
H	1.4077	1.5098	1.2944	0.1625	0.1613	0.1568	

The snapshot represents a 24-well plate layout for ELISA assay. The first row which marked in red is the control samples, the green cells are the samples, the blue cells are the non-transfected cells.

CHAPTER 3 Inhibition of Agonist-stimulated Arrestin-3 Recruitment to MOPr and DOPr by GRK Inhibitor Compound101

3.1 Introduction

There has been great interest in developing selective GRK inhibitors due to the significant role played by GRKs in the regulation of GPCR signalling. Particularly, GRK2 and GRK5 have been shown to be upregulated in heart failure (Dzimiri et al. 2004; Monto et al. 2012). A number of GRK inhibitors have been developed (Mayer et al. 2008; Setyawan et al. 1999; Tesmer, JJ et al. 2010); however, many of them are either nonselective between kinases or have weak potency (Thal et al. 2012). On the other hand, the Takeda Pharmaceuticals Company developed compound 101 (cmpd101; (Ikeda, S, Keneko & Fujiwara 2007), which was reported to be a selective GRK2/3 inhibitor (Thal et al. 2011). Recently, a new compound, CCG258747, has been developed which is potent and selective GRK inhibitor over other kinases (Bouley, RA et al. 2020).

Cmpd101 has been used as GRK2/3 inhibitor in a number of *in vitro* and *in vivo* studies (Abraham et al. 2018; Li, H et al. 2016; Lowe et al. 2015; Pack et al. 2018). For example, Lowe et al. (2015) reported that cmpd101 inhibited DAMGO-induced MOPr desensitisation in locus coeruleus (LC) neurons, implying that the desensitisation is mediated by GRK2/3. Moreover, cmpd101 partially blocked the agonist-induced internalisation of galanin receptor 2 (Reyes-Alcaraz et al. 2018) and did not block GPCR-mediated 14-3-3 signalling, a multifunctional signal adaptor protein (Li, H et al. 2016). The latter signalling pathway is not thought to involve GRK/arrestins.

A fundamental step towards determining the role of GRKs in GPCR signalling is to establish selective inhibitors for GRKs to be used in standard assays. Thus, the main goal of this chapter is to characterise the ability of cmpd101 to inhibit arrestin-3 recruitment upon addition of different agonists using HEK293 cells expressing MOPr or DOPr. We used two MOPr agonists, DAMGO, a full agonist, and morphine, a partial agonist, in the arrestin assay as well as DOPr agonists, SNC80 and DADLE. We used arrestin-3 recruitment as a proxy assay for GRK phosphorylation of the receptor. Also, we utilised a G_i activation BRET assay to examine the selectivity of cmpd101 for the GRK/arrestin pathway.

MOPrs, like most GPCRs, are significantly regulated following agonist activation, particularly prolonged agonist activation. For example, MOPr gets phosphorylated by GRKs leading to receptor desensitisation. This process is called homologous desensitisation and is a GRK-dependent mechanism. Subsequently, the phosphorylated MOPr recruits arrestins which leads to receptor internalisation. Another desensitisation pathway for MOPr is heterologous desensitisation, which can be mediated by second messenger-dependent protein kinases such as PKC (Illing, Mann & Schulz 2014). It has been known for some time that the MOPr internalisation and desensitisation mechanisms are determined partially by the agonist (Johnson, EA et al. 2006). For example, DAMGO and etorphine, which are high efficacy MOPr agonists, induce significant receptor desensitisation mediated by a GRK-arrestin mechanism (Groer et al. 2011). Thus, they induce extensive receptor internalisation. However, morphine, a partial MOPr agonist, induces desensitisation, which is mediated in part by PKC and induces little internalisation, at least in HEK293 cells (McPherson et al. 2010). Therefore, the activity of GRKs plays a pivotal role in determining the GPCR desensitisation and internalisation. Thus, we also explored the effect of cmpd101 on the internalisation of MOPr upon stimulation with MOPr agonist, using an ELISA technique.

Another important opioid receptor is the δ opioid receptor (DOPr), whose sequence is closely related to MOPr, but has distinct physiological and pharmacological properties (Al-Hasani & Bruchas 2011; Gendron et al. 2015). We focused on MOPr and DOPr as examples of GPCRs and because they are important targets for the treatment of moderate to severe pain (Evans 2004; Williams et al. 2013). Accordingly, we thought it useful to study the effect of cmpd101 on agonist-induced arrestin-3 recruitment to both MOPr and DOPr. This chapter will address a number of basic background experiments to provide data for comparison with that in later chapters, for example, the actions of cmpd101 to compare to the novel GRK inhibitors to be tested later. The experiments would also provide information on the optimum conditions under which to undertake future experiments.

3.2 Results

3.2.1 Agonist-induced Arrestin-3 Recruitment to MOPr and DOPr

Firstly, the expression of the GFP construct Arr3-GFP was assessed to get some idea of the efficiency of the transient transfection. Accordingly, the expression of Arr3-GFP in transfected HEK293 cells was determined using fluorescence activating cell sorting (FACS, the actual analysis was undertaken by Faculty of Life Science flow cytometry facility, University of Bristol led by Dr. Andy Herman); the results are shown in Figure 3.1. This FACS analysis indicated that GFP- positive cells represented about 22% of the whole cells compared to the untransfected cells (Figure 3.1, A & C). For BRET experiments, the recruitment of arrestin-3 to the MOPr or DOPr was assessed in HEK293 cells expressing human MOPr-RLuc2 or DOPr-RLuc2 and Arr3-GFP. An increase in the BRET ratio is an indication of the arrestin coming into close proximity to the receptor, i.e., being recruited. As a control, we transfected HEK293 cells with MOPr-RLuc2 only and compared it to HEK293 cells expressing human MOPr-RLuc2 and Arr3-GFP, as shown in Figure 3.2. DMSO was the vehicle and was used at a final concentration of 0.3% for all BRET assays. This concentration of DMSO had no effect on DAMGO-induced arrestin-3 recruitment, as shown in Figure 3.2A. Concentration-response curves for agonist-induced arrestin-3 recruitment to MOPr or DOPr are shown in Figures 3.3 and 3.4.

DAMGO appeared to be a full agonist in the arrestin-3 assay with an EC_{50} of 0.84 ± 0.35 µM and E_{max} of 2,085 ±163 (BRET ratio; no units), as shown in Figure 3.3B. However, this response to DAMGO was completely absent in HEK293 cells expressing MOPr-RLuc2 without arrestin-3 (Figure 3.2B). Morphine was a partial agonist compared to DAMGO with an EC_{50} of 1.30 ± 0.36 µM and E_{max} of 603 ± 50 (BRET ratio) (Figure 3.3B). We next investigated the activity of SNC80 and DADLE, DOPr agonists, using HEK293 cells cotransfected with DOPr. The results showed that SNC80 induced a high maximal level of arrestin-3 recruitment with an EC_{50} of 0.52 ± 0.10 µM and E_{max} of 5,112 ± 475 (BRET ratio) as compared to DADLE with an EC_{50} of 0.05 ± 0.01 µM and E_{max} of 2,648 ± 222 (BRET ratio) (Figures 3.4).

To further investigate the responses to DAMGO and morphine at MOPr, we undertook time-course experiments for both agonists. The responses were measured by BRET and, after 3 min of the beginning of the recording, the cells were stimulated with maximal concentrations (for arrestin-3 recruitment) of DAMGO (10 µM) or morphine (30 µM). Each agonist stimulated the peak arrestin-3 recruitment after around 1 min of stimulation and the response then remained level over the following 16 min, the duration of the experiment (Figure 3.5). In some experiments, naloxone (10 µM), a MOPr antagonist, was added after 4 min of the agonist stimulation. The responses of DAMGO and morphine were rapidly and completely blocked by naloxone (Figure 3.5).

GRKs play a crucial role in GPCR desensitisation and are involved in other downstream signal pathways. Whilst we do not have the tool for measuring GRK phosphorylation, we used an arrestin-3 recruitment assay instead. We next studied the effect of cmpd101 on arrestin-3 recruitment using the BRET arrestin-3 assay. Cmpd101 concentration-dependently reduced DAMGO-induced (10 µM) arrestin-3 recruitment to MOPr, as well as SNC80-induced (10 µM) arrestin-3 recruitment to DOPr by a maximum of around 60% and 50% with an IC_{50} 8.0 ± 3.5 µM and 5.8 ± 0.9 µM, respectively (Figure 3.6, A and B). To further study the kinetics of cmpd101 inhibition of arrestin-3 recruitment to MOPr, we undertook a time-course experiment. HEK293 cells were incubated with cmpd101 (100 µM) for 30 min and then stimulated with DAMGO (10 µM) for 10 min. Figure 3.7A shows that preincubation with cmpd101 strongly inhibited DAMGO-induced arrestin-3 recruitment for the period of the experiment. In addition, we investigated the rate at which cmpd101 is able to inhibit established DAMGO-induced arrestin-3 recruitment. Cells were stimulated with DAMGO (10 µM) and responses measured by BRET; 4 min later, cmpd101 (30 µM) was added. The results (Figure 3.7B) showed that cmpd101 inhibited DAMGO-induced arrestin-3 recruitment relatively rapidly following the addition of cmpd101 and reached the maximum inhibition (~60%) after around 10 min (Figure 3.7B). We also undertook a time-course experiment to investigate the kinetics of cmpd101 inhibition of arrestin-3 recruitment to DOPr. HEK293 cells were incubated with cmpd101 (30 µM) for 30 min and then stimulated with SNC80 (10

μM) for 10 min. Figure 3.8 shows that preincubation of cmpd101 inhibited SNC80-induced arrestin-3 recruitment by around 50% for the period of the experiment.

We further investigated whether the inhibition of arrestin-3 recruitment to MOPr or DOPr would be different when employing different MOPr or DOPr agonists. To determine this, HEK293 cells expressing MOPr or DOPr were preincubated with cmpd101 at 30 or 100 μM and were then stimulated with the MOPr agonists; DAMGO (10 μM) or morphine (30 μM), or the DOPr agonists; SNC80 (10 μM) or DADLE (10 μM), designed to produce maximal arrestin-3 recruitment for that agonist. As expected, the maximum arrestin-3 recruitment induced by morphine was significantly lower than that of DAMGO (Figure 3.9A). Cmpd101 at 30 and 100 μM showed similar maximal inhibition (approximately 65%) of DAMGO-induced arrestin-3 recruitment to MOPr (Figure 3.9, A and B). SNC80-induced arrestin-3 recruitment to DOPr was also inhibited by cmpd101 (maximum approximately 50%) (Figure 3.10, A, B and C). On the other hand, cmpd101 inhibited DADLE-induced arrestin-3 recruitment by only about 33% (Figure 3.10D). Surprisingly, cmpd101 at 30 or 100 μM did not significantly inhibit morphine-induced arrestin-3 recruitment, although, cmpd101 at 30 μM displayed a trend for reduction (Figure 3.9, A and B).

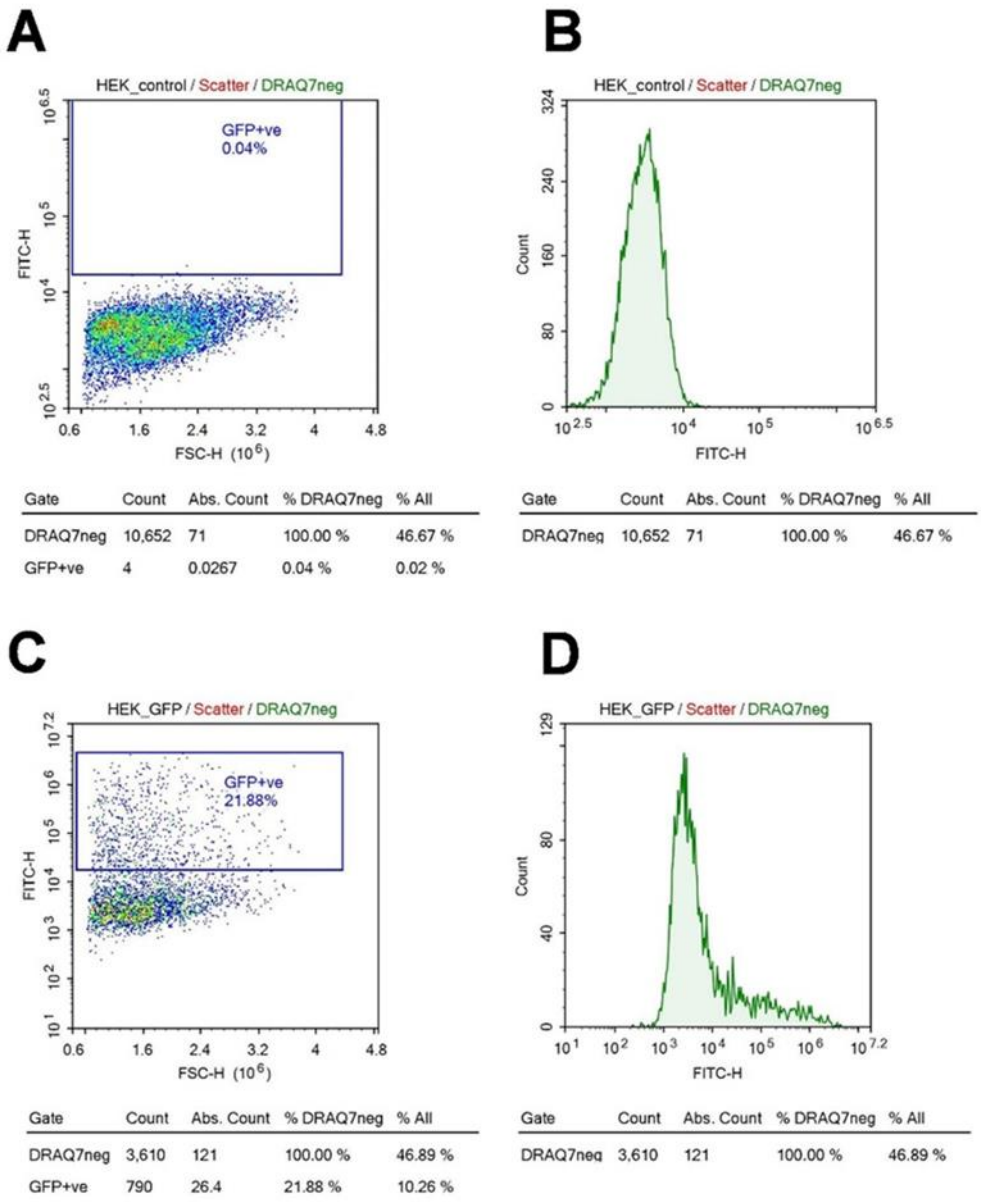

Figure 3.1 Detection of GFP by flow cytometry.

HEK293 cells were transiently transfected with Arr3-GFP (C, D) whilst untransfected (GFP^-) cells (A, B) were used as control. They gated based on forward scatter (FSC-H) and FITC fluorescence. Wild type HEK293 cells showed no signal for GFP^+ cells (A and B) whilst GFP transfected cells showed 22% of the total cells (C and D). The FACS analysis was carried out by Dr Andrew Herman, Flow Cytometry Facility, University of Bristol.

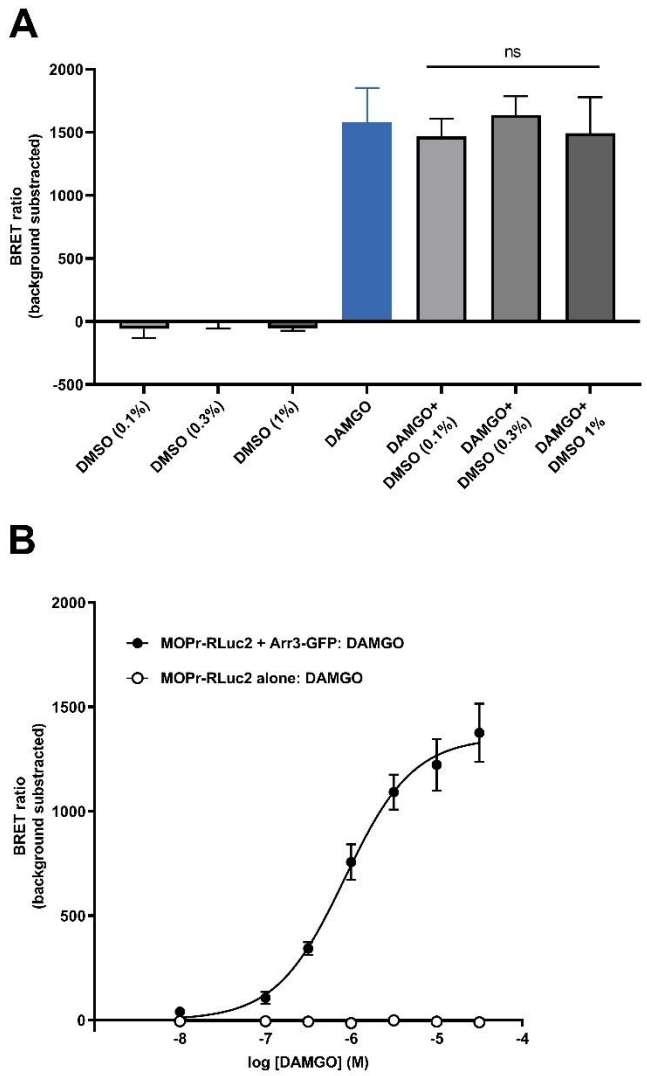

Figure 3.2 Log concentration-response curve for DAMGO-induced arrestin-3 recruitment to MOPr.

A) The effect of (or lack of) different concentrations of DMSO on DAMGO-induced arrestin-3 recruitment to MOPr. HEK293 cells were transiently transfected with MOPr-RLuc2 and Arr3-GFP, cells were then pretreated with 0.1, 0.3, or 1% DMSO for 30 min. Cells were then stimulated with DAMGO (10 µM) for a further 10 min. B) HEK293 cells were transiently transfected with MOPr-RLuc2 and Arr3-GFP (●) or MOPr-RLuc2 alone (○). Cells were then stimulated with DAMGO (0.01- 30 µM) for 10 min. DAMGO-induced arrestin-3 recruitment to MOPr was measured by BRET assay. ns, not statistically different, one-way ANOVA. Data were fitted to a four-parameter non-linear regression model for a sigmoidal curve with variable slope (slope = 1.1 ± 0.1). Data are presented as mean ± SEM from three (A) or five (B) independent experiments.

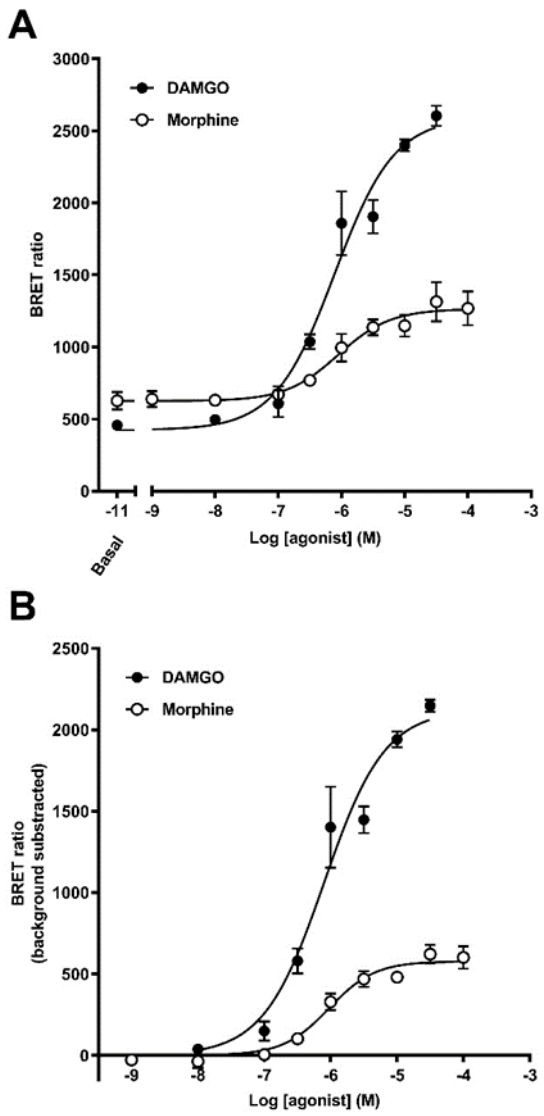

Figure 3.3 Log concentration-response curves of DAMGO- and morphine-induced arrestin-3 recruitment to MOPr.

HEK293 cells were transfected with MOPr-RLuc2 and Arr3-GFP and incubated with DAMGO (10 µM, ●) or morphine (30 µM, ○) for 10 min and Arr3-GFP recruitment and subsequent BRET measurements taken. Data were plotted with the basal values included (A) or following subtraction of the basal value (B) and fitted to a four-parameter non-linear regression model for a sigmoidal curve with variable slope (slope = 0.95 ± 0.6 for DAMGO and 1.2 ± 0.3 for morphine). Data are presented as mean ± SEM from three independent experiments.

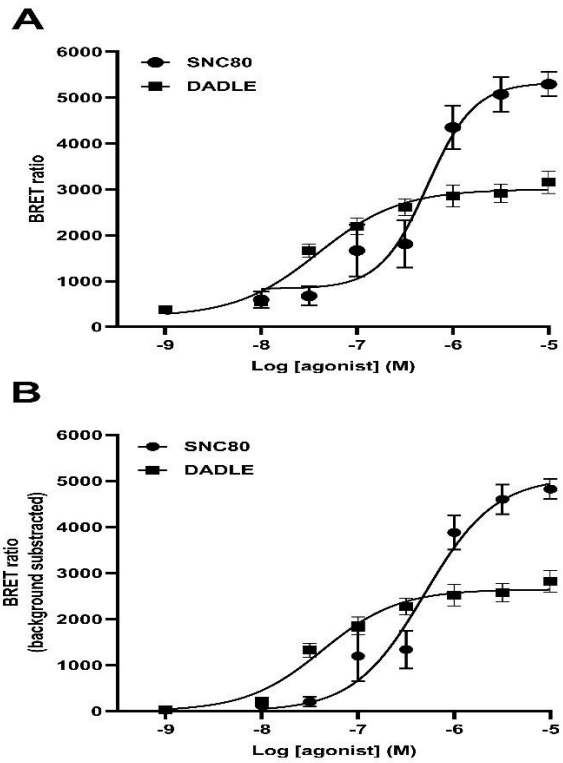

Figure 3.4 Log concentration-response curves of SNC80- and DADLE-induced arrestin-3 recruitment to DOPr.

HEK293 cells were transfected with DOPr-RLuc2 and Arr3-GFP and incubated with SNC80 (10 μM, ●) or DADLE (10 μM, ■) for 10 min and Arr3-GFP recruitment and subsequent BRET measurements taken. Data were plotted with the basal value included (A) or (B) following subtraction of the basal value and fitted to a four-parameter non-linear regression model for a sigmoidal curve with variable slope (slope = 1.2 ± 0.3 for SNC80 and 1.1 ± 0.1 for DADLE). Data are presented as mean ± SEM from three (SNC80) or four (DADLE) independent experiments.

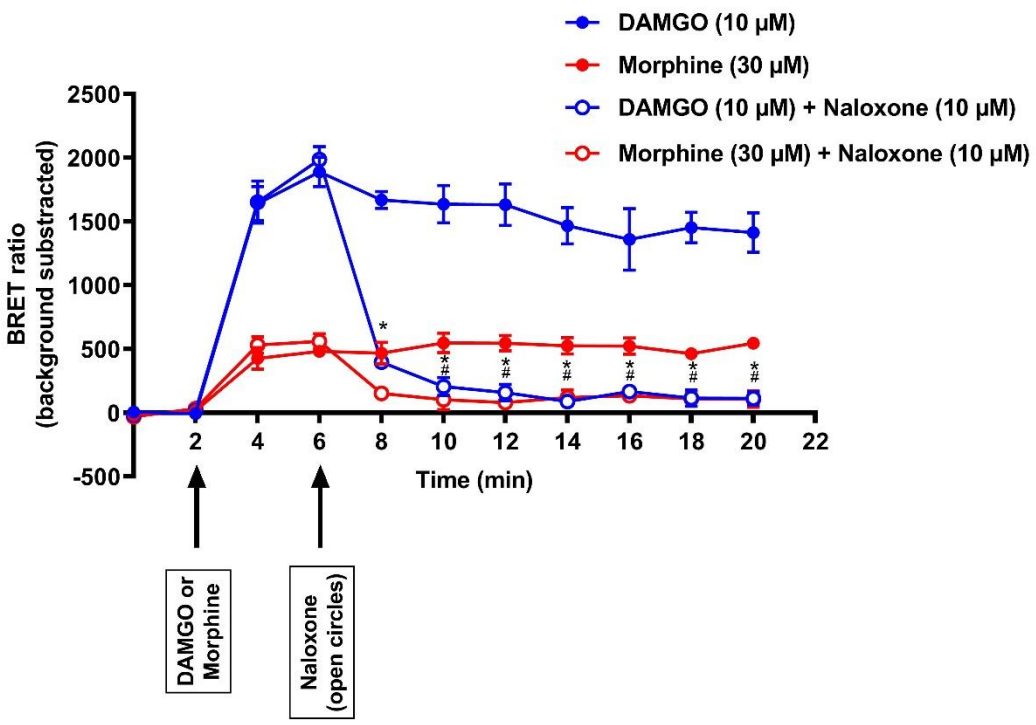

Figure 3.5 Time course of DAMGO- and morphine-induced arrestin-3 recruitment to MOPr and effects of naloxone.

HEK293 cells were transiently transfected with MOPr-RLuc2 and Arr3-GFP and stimulated with DAMGO (10 μM) or morphine (30 μM) and Arr3 recruitment to MOPr measured by BRET assay. Kinetic traces after DAMGO or morphine stimulation at 3 min (●) and followed by the addition of 10 μM naloxone at 7 min (○). The BRET ratio of vehicle-treated cells was subtracted from agonist-stimulated values and the data are presented as mean ± SEM of non-normalised results from four independent experiments. * $P < 0.05$ DAMGO compared to no naloxone treatment at the same time point, $^{\#}$ $P < 0.05$ morphine compared to no naloxone treatment at the same time point; two-way ANOVA followed by Tukey post hoc test for multiple comparisons.

To further investigate morphine-induced arrestin-3 recruitment to MOPr, we undertook a time-course experiment. Cmpd101 (100 μM) was added at 4 min after stimulation of the cells with morphine (30 μM) (Figure 3.11). As above, the results indicated that cmpd101 does not inhibit morphine-induced arrestin-3 recruitment over the time course of the experiment (Figure 3.11).

We observed an increase in arrestin-3 recruitment in the presence of 100 µM cmpd101 when applied on its own. Therefore, we used cmpd101 at 30 µM in the majority of further experiments. We also used 10 µM DAMGO and 30 µM morphine as these concentrations produce maximum BRET readings for these agonists. Furthermore, we measured arrestin-3 recruitment at 10 min after agonist stimulation for all BRET assays as this provided a stable signal at this point.

To rule out the possible involvement of various cell kinases associated with signalling (e.g., PKC, JNK, ERK1/2 and CaMKII) in agonist-induced arrestin-3 recruitment to MOPr, we pretreated HEK293 cells with kinase inhibitors. These kinase inhibitors were GF109203X (1 µM, a PKC inhibitor), SP600125 (30 µM, a JNK inhibitor), PD998059 (10 µM, an ERK1/2 inhibitor), or KN-93 (1 µM, a CaMKII inhibitor) as well as cmpd101 (30 µM) as a positive control, and then cells were stimulated with DAMGO (10 µM) (Lowe et al. 2015; Rezazadeh, Claydon & Fedida 2006). We did not observe any significant inhibitory effect on DAMGO-induced arrestin-3 recruitment in the presence of the PKC, JNK, ERK1/2 and CaMKII inhibitors (Figure 3.12). In addition, none of the kinase inhibitors applied on their own significantly affected basal arrestin-3 recruitment (Figure 3.12).

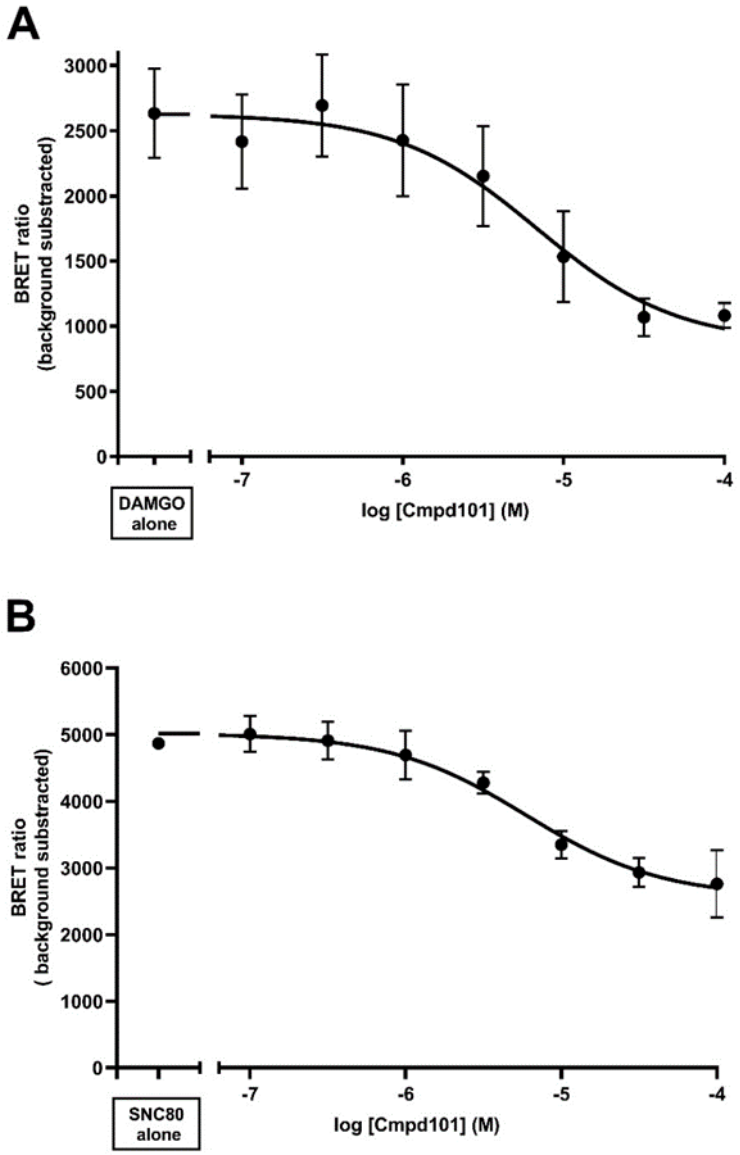

Figure 3.6 Concentration-dependent inhibition of DAMGO- and SNC80-induced arrestin-3 recruitment to MOPr and DOPr by cmpd101.

HEK293 cells were transiently transfected with MOPr-RLuc2 (A) or DOPr-RLuc2 (B) and Arr3-GFP. Cells were preincubated with cmpd101 (0.1-100 µM) for 30 min and then stimulated with (A) DAMGO (10 µM) or (B) SNC80 (10 µM) for 10 min and Arr3-GFP recruitment was measured by BRET assay. Data were fitted to a non-linear regression model with three parameters. Data are presented as mean ± SEM from four independent experiments performed in duplicate.

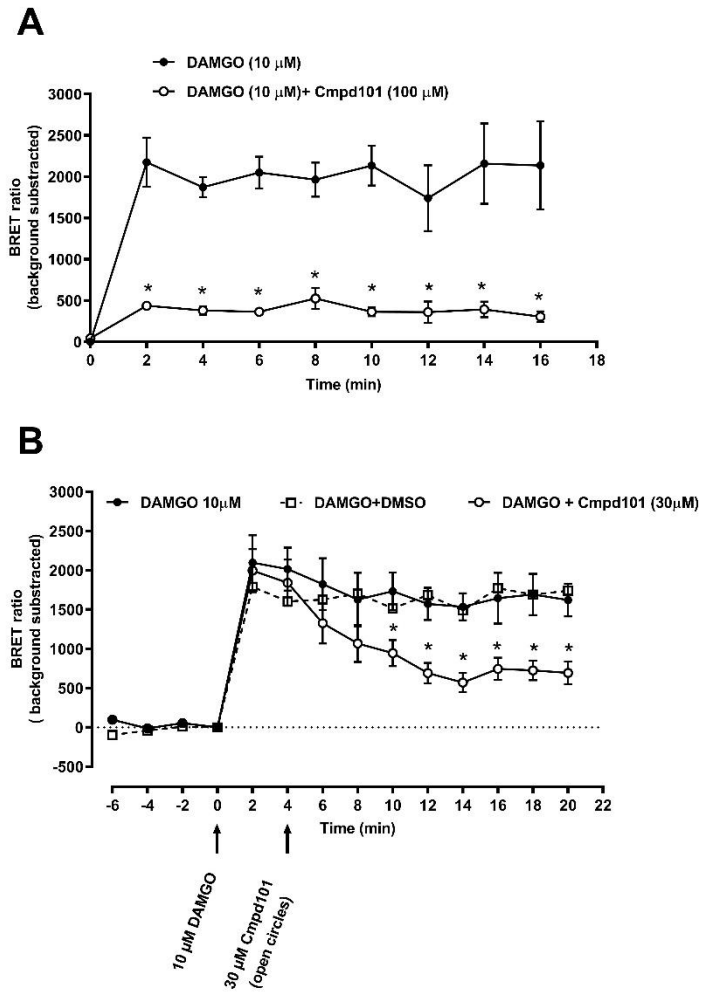

Figure 3.7 Inhibition of DAMGO-induced arrestin-3 recruitment by addition of cmpd101.

A) Time course of DAMGO-induced arrestin-3 recruitment in the absence (●) or presence of cmpd101 (100 μM, ○). HEK293 cells expressing MOPr-RLuc2 and Arr3-GFP were preincubated with cmpd101 (100 μM) for 30 min and then stimulated with DAMGO (10 μM) for 10 min and the BRET measurements were taken every 2 minutes for up to 16 min. (B) HEK293 cells expressing MOPr-RLuc2 and Arr3-GFP were stimulated with DAMGO (10 μM) for 4 min before the addition of cmpd101 (30 μM) and then BRET measurements were taken every 2 minutes for up to 16 min. The BRET ratio of nontreated cells at time zero was subtracted. Data are presented as mean ± SEM from four independent experiments performed in duplicate. (A) * $P < 0.05$ vs DAMGO at the same time point, two-way ANOVA followed by Bonferroni post hoc test; (B) * $P < 0.05$ vs DAMGO + DMSO, two-way ANOVA followed by Tukey post hoc test for multiple comparisons.

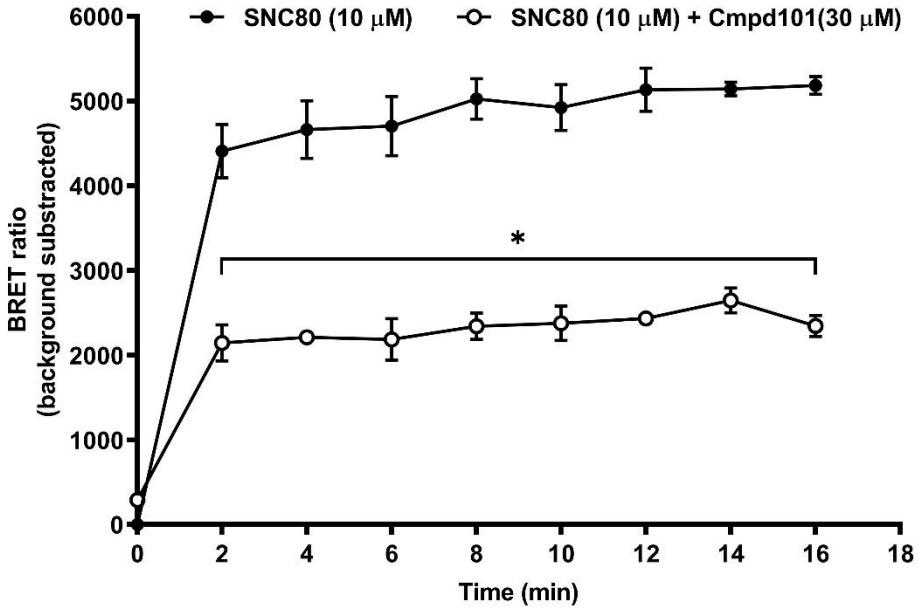

Figure 3.8 Inhibition of SNC80-induced arrestin-3 recruitment by addition of cmpd101.

Time course of SNC80-induced arrestin-3 recruitment in the absence (●) and in the presence of cmpd101 (30 μM, ○). HEK293 cells expressing DOPr-RLuc2 and Arr3-GFP were preincubated with cmpd101 (30 μM) for 30 min and then stimulated with SNC80 (10 μM) for 10 min in the continued presence of vehicle or cmpd101, and the BRET measurements were taken every 2 minutes for up to 16 min. The BRET ratio of nontreated cells at time zero was subtracted. Data are presented as mean ± SEM from three independent experiments performed in duplicate. * $P < 0.05$ vs SNC80 at the same time point, two-way ANOVA followed by Bonferroni post hoc test.

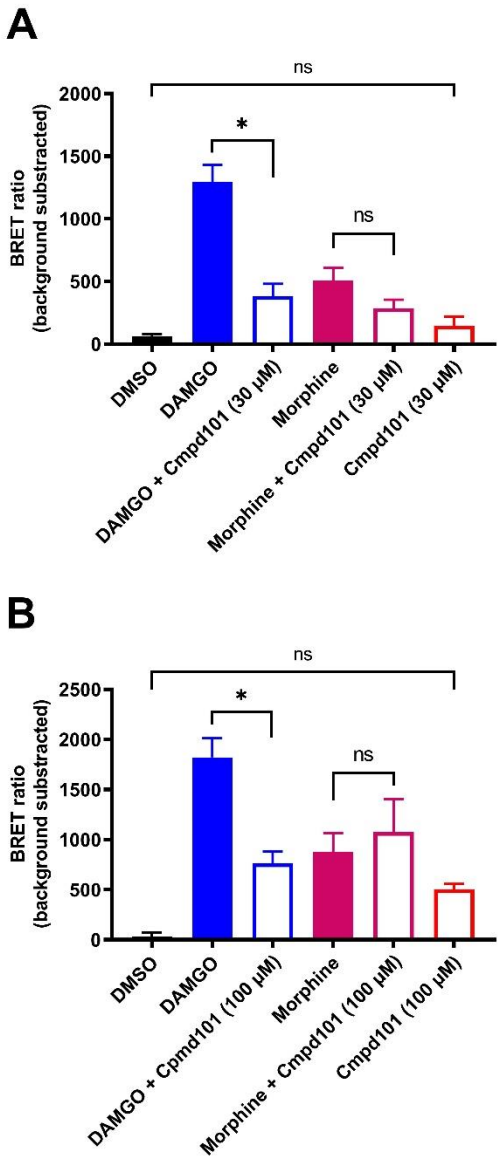

Figure 3.9 Effect of different concentrations of cmpd101 on DAMGO- and morphine-induced arrestin-3 recruitment to MOPr.

HEK293 cells expressing MOPr-RLuc2 and Arr3-GFP were preincubated with cmpd101 (30 µM) (A) or (100 µM) (B) for 30 min and cells then stimulated with DAMGO (10 µM) or morphine (30 µM) for 10 min and the BRET signals recorded. The BRET ratio of nontreated cells was subtracted. Data are presented as mean ± SEM from four independent experiments performed in duplicate. * $P < 0.05$, one-way ANOVA followed by Tukey post hoc test for multiple comparisons; ns, not statistically significant.

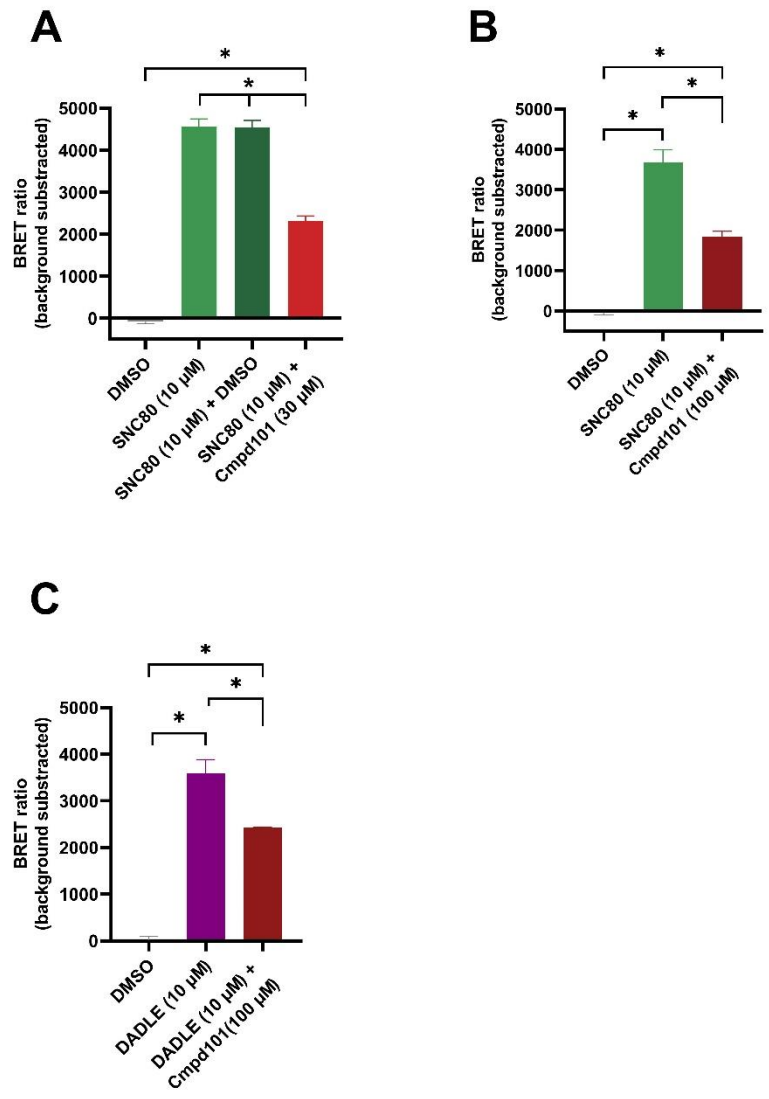

Figure 3.10 Effect of cmpd101 on SNC80- and DADLE-induced arrestin-3 recruitment to DOPr.

HEK293 cells expressing DOPr-RLuc2 and Arr3-GFP were preincubated with cmpd101 (30 µM) (A) or (100 µM) (B) for 30 min and cells were then stimulated with SNC80 (10 µM) or DADLE (10 µM) for 10 min and the BRET signal recorded. The BRET ratio of nontreated cells was subtracted. Data are presented as mean ± SEM from four independent experiments performed in duplicate. * P < 0.05, one-way ANOVA followed by Tukey post hoc test for multiple comparisons; ns, not statistically significant.

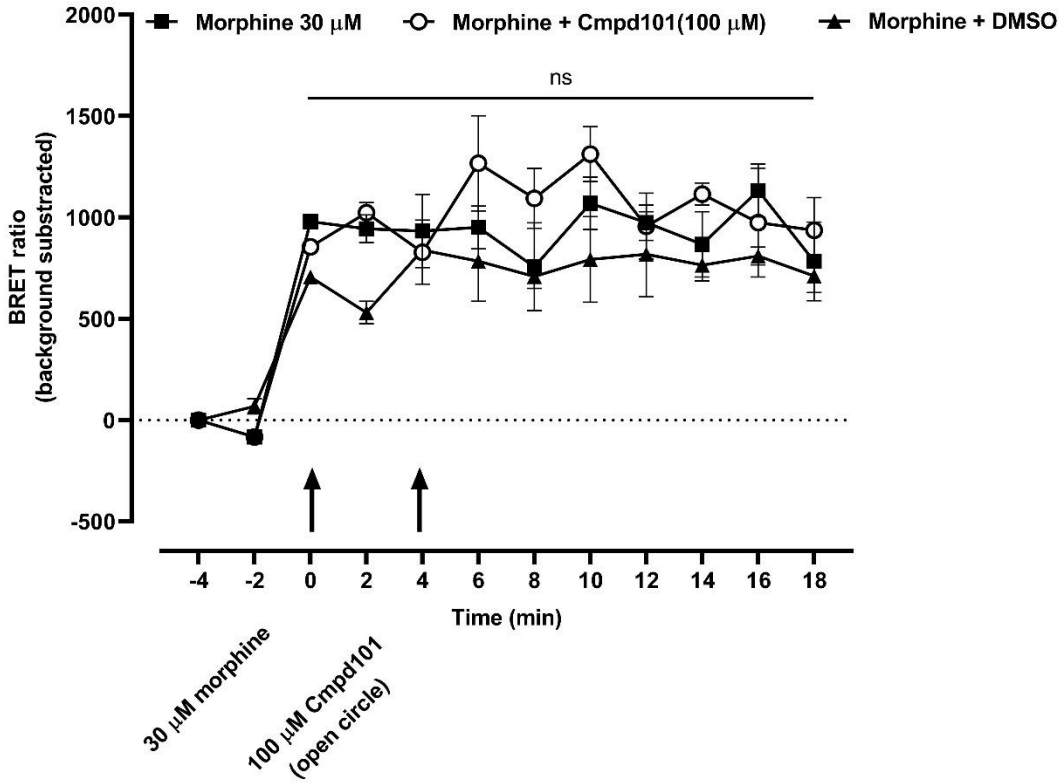

Figure 3.11 Effect of cmpd101 on morphine-induced arrestin-3 recruitment to MOPr

HEK293 cells expressing MOPr-RLuc2 and Arr3-GFP were stimulated with morphine (30 μM) for four minutes before the addition of cmpd101 (100 μM), and the BRET measurements taken every 2 minutes for a further 16 min. The BRET ratio of nontreated cells was subtracted. Data are presented as mean ± SEM from four independent experiments performed in duplicate. ns, not statistically significant, morphine + cmpd101 vs morphine + DMSO, two-way ANOVA.

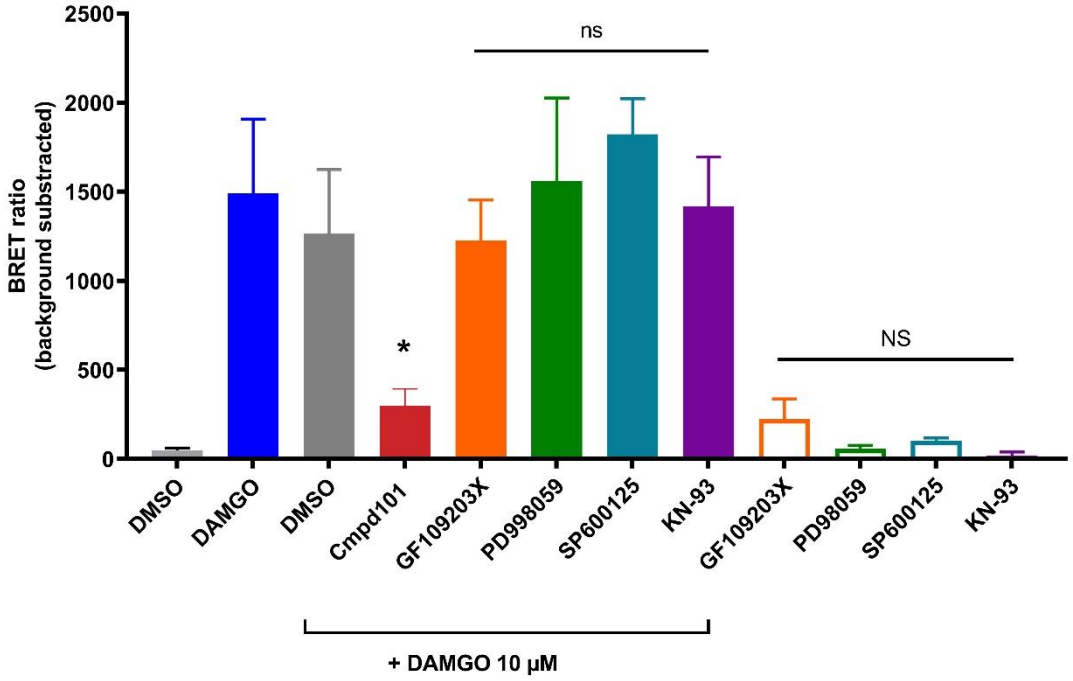

Figure 3.12 Lack of effect of various kinase inhibitors on DAMGO-induced arrestin-3 recruitment to MOPr

HEK293 cells expressing MOPr-RLuc2 and Arr3-GFP were preincubated with a PKC inhibitor (GF109203X, 1 µM), a JNK inhibitor (SP600125, 30 µM), an ERK1/2 inhibitor (PD998059, 10 µM), or a CaMKII inhibitor (KN-93, 1 µM), for 30 min before the addition of DAMGO (10 µM) or media for a further 10 min. The BRET ratio of no agonist-treated cells was subtracted. Data are presented as mean ± SEM of non-normalised results from four independent experiments performed in duplicate. * $P < 0.05$ compared to DAMGO or DAMGO + DMSO; cmpd101 statistically significant inhibits DAMGO-induced arrestin-3 recruitment; ns, not statistically significant compared to DAMGO + DMSO or DAMGO alone, one-way ANOVA followed by Tukey post hoc test for multiple comparisons; NS, not statistically significant vs DMSO, one-way ANOVA followed by Tukey post hoc test for multiple comparisons.

3.2.2 Effect of cmpd101 on DAMGO-induced G Protein Activation at MOPr

To investigate the effect of cmpd101 on the G_i activation and to determine the selectivity of cmpd101 towards arrestin/G protein pathway, agonist-induced G_i protein activation was measured in HEK293 cells expressing HA-MOPr using a BRET assay. DAMGO concentration-response curves were constructed in cells expressing MOPr in order to determine its potency and to determine whether cmpd101 had any effect on DAMGO-induced G protein signalling (Figure 3.13). The results showed that DAMGO induced G_i activation, with an EC_{50} of 0.40 ± 0.01 µM (Figure 3.13). In HEK293 cells pretreated with 30 µM cmpd101, the maximum response was not significantly changed from DAMGO-treated cells without cmpd101 (Figure 3.13). However, cmpd101 pretreated cells displayed a three-fold right shift of the curve (Figure 3.13), the DAMGO EC_{50} value was significantly different ($P < 0.05$) between cells with DAMGO and cmpd101 (1.20 ± 0.26 µM) and DAMGO-only treated cells (0.40 ± 0.01 µM) (Figure 3.13).

3.2.3 Effect of cmpd101 on Agonist-induced Cell Surface Loss of MOPr

Agonist-induced MOPr internalisation was measured by ELISA as described in Chapter 2, Section 2.2.6. HEK293 cells were treated with DAMGO (10 µM), a full MOPr agonist, or morphine (30 µM), a partial MOPr agonist, to induce surface receptor loss, which was measured by ELISA. The time course of internalisation induced by DAMGO (10 µM) is shown in Figure 3.14A. DAMGO produced a time-dependent loss of surface receptor, with a 22% loss of surface receptor at 30 min (Figure 3.14A). DAMGO induced surface receptor loss with an EC_{50} of 3.3 ± 1.0 µM and E_{max} of 35.2 ± 1.5 % (Figure 3.14B). Morphine induced negligible internalisation (Figure 3.15). We assumed that DAMGO reached the maximum of receptor internalisation at 30 min, which was not statistically significantly different from receptor loss at 60 min; thus, we used this time point (30 min) to construct a DAMGO concentration-response curve for MOPr surface receptor loss (Figure 3.14B).

To investigate the effect of cmpd101 on DAMGO-induced surface receptor loss, HEK293 cells expressing HA-MOPr were pretreated with cmpd101 (30 µM) for 30 min and then stimulated with DAMGO (10 µM) for a further 30 min. The addition of

cmpd101 on its own did not affect MOPr internalisation, as shown in Figure 3.15. However, cmpd101 significantly reduced DAMGO-induced MOPr internalisation by 65% (Figure 3.15).

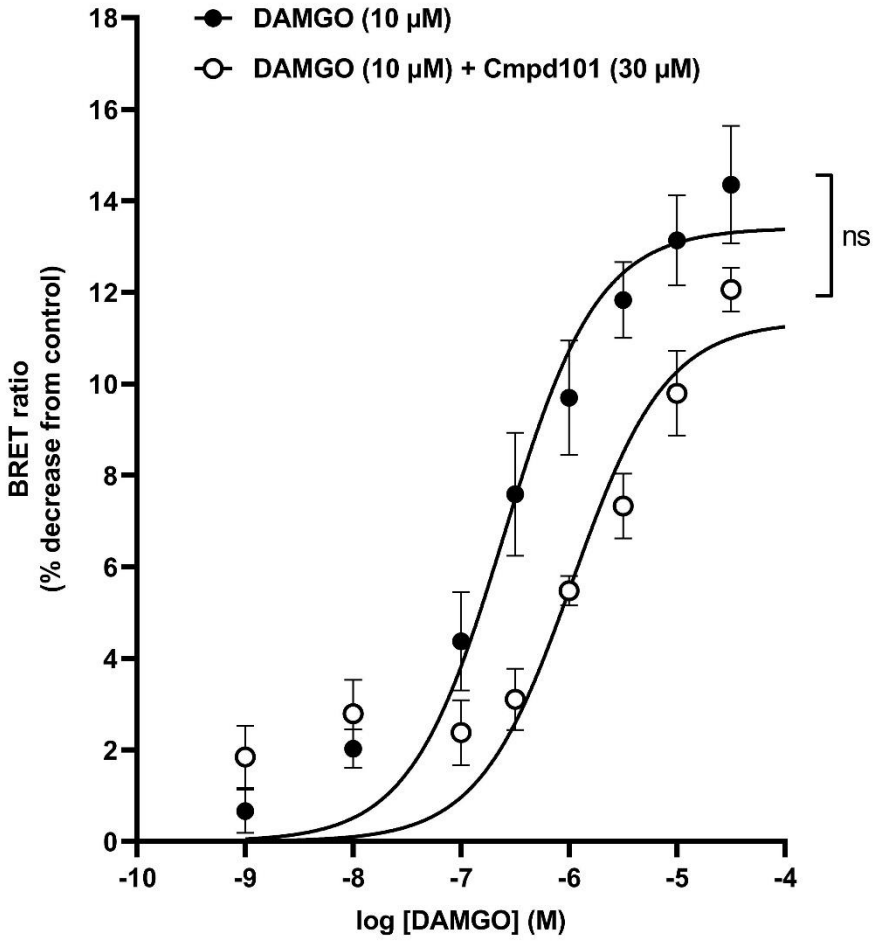

Figure 3.13 Effect of cmpd101 on G_i activation induced by DAMGO at MOPr.

HEK293 cells were transiently transfected with HA-MOPr, $G_{\alpha i}$-RLuc2 and G_{γ}-GFP. Cmpd101 (30 µM) (○) was added 30 min before the addition of DAMGO (10 µM) for two minutes. DAMGO-induced BRET ratios were expressed as the percentage decrease from nontreated cells. Data were fitted to a non-linear regression model with three parameters. ns; not statistically significant, one-sample Student's t-test. Data are presented as mean ± SEM from four independent experiments performed in duplicate.

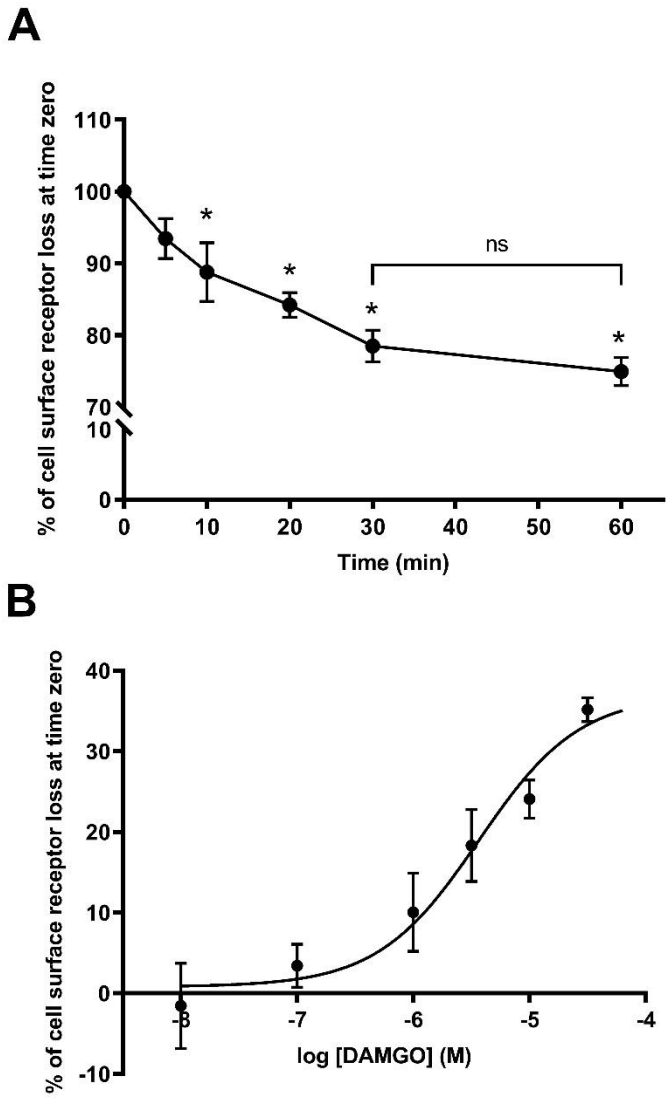

Figure 3.14 DAMGO-induced MOPr cell surface loss.

HEK293 cells were transiently transfected with HA-MOPr and were stimulated with DAMGO (10 µM) for up to 60 min at 37°C. The cell surface receptor expression was measured by ELISA. (A) Time course of DAMGO-induced internalisation of MOPr. (B) Concentration-response of DAMGO-induced internalisation of MOPr at 30 min. Data were fitted to a non-linear regression model with four parameters using GraphPad Prism software. The minimum response was constrained to zero. Data are presented as mean ± SEM of four independent experiments performed in triplicate. * $P < 0.05$ vs time zero, one-way ANOVA followed by Tukey post hoc test for multiple comparisons; ns, not statistically significant.

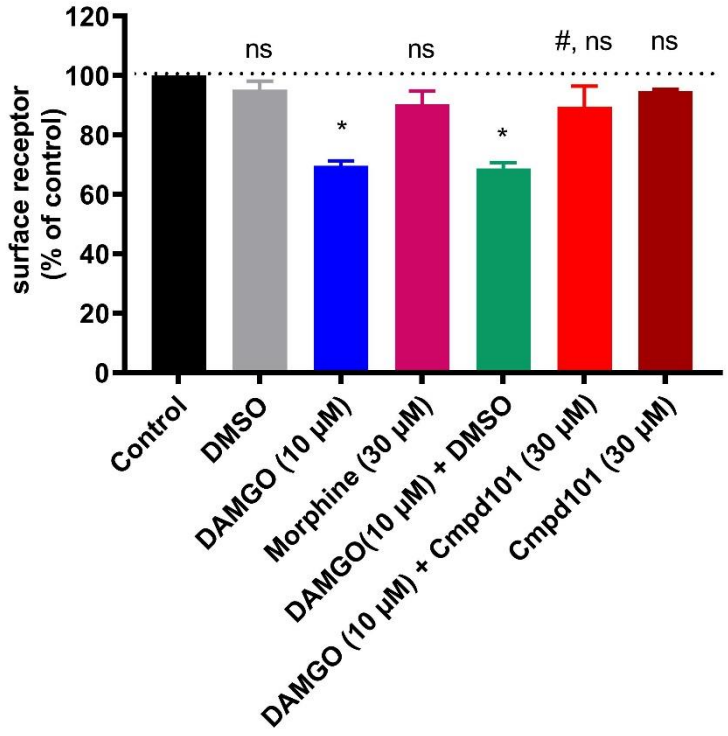

Figure 3.15 Inhibition of DAMGO-induced MOPr internalisation by cmpd101.

HEK293 cells were transiently transfected with HA-MOPr and were pretreated with cmpd101 (30 µM) or DMSO (where is indicated in the graph) for 30 min and then were stimulated with DAMGO (10 µM) or morphine (30 µM) for 30 min in the continued presence of cmpd101 or vehicle at 37°C. The cell surface receptor expression was measured by ELISA. Data are presented as mean ± SEM of four independent experiments performed in triplicate. Statistical analysis was performed by one-way ANOVA followed by Tukey post hoc test for multiple comparisons (* $P < 0.05$, compared to control; $^{\#}$ $P < 0.05$, compared to DAMGO; ns, not statistically significant compared to control).

3.3 Discussion

In this chapter, HEK293 cells expressing MOPr-RLuc2 or DOPr- RLuc2 and Arr3-GFP were used to study arrestin-3 recruitment to the receptor, measured by BRET assay. The ratio of MOPr-RLuc2 or DOPr-RLuc2 to Arr3-GFP (1:1) was determined previously in our laboratory where a fixed amount of MOPr-RLuc2 or DOPr-RLuc2 (a donor) was coexpressed with an increasing amount of Arr3-GFP (an acceptor) to determine the plateau of the donor saturation. The FACS results (Figure 3.1) showed that the GFP positive cells represented 22% of the transfected cells, which was somewhat less than expected, but was more than adequate to perform the BRET experiments in this thesis. We investigated two MOPr agonists, DAMGO, a full agonist, and morphine, a partial agonist and how they affect arrestin-3 recruitment to MOPr. We used another important opioid receptor, DOPr, to compare it with MOPr data and to widen our understanding of the effect of cmpd101 on the function of a different receptor. Also, we determined the ability of cmpd101, a GRK2/3 inhibitor, to inhibit agonist-induced arrestin-3 recruitment. We also measured agonist-induced G_i activation and the effects of cmpd101 on this, and finally, the agonist-induced internalisation of MOPr was measured in HEK293 cells using ELISA.

HEK293 cells are widely used in biomedical research because they are easy to grow, maintain and to transfect (Gharagozlou et al. 2003; Hill et al. 2018; Manglik et al. 2016). The BRET assay was chosen to measure the arrestin-3 recruitment to MOPr and DOPr in HEK293 cells because it is sensitive and is a relatively high throughput assay (El Khamlichi et al. 2019).

The results of BRET assay for arrestin-3 recruitment confirmed that DAMGO is likely to be a full agonist at MOPr compared to morphine which is a partial agonist. Similarly, SNC80 appeared to be a full agonist at DOPr and DADLE is a partial agonist. These findings align with previously published studies (Groer et al. 2011; Miess et al. 2018), as well as previous results from this laboratory (Conibear et al. 2020; Hill et al. 2018; McPherson et al. 2010; Sutcliffe et al. 2017). The addition of naloxone completely reversed the DAMGO-induced arrestin-3 recruitment to MOPr.

This indicates that arrestin-3 recruitment requires ongoing receptor activation, which is blocked by naloxone.

Cmpd101 at 30 and 100 μM similarly inhibited DAMGO-induced arrestin-3 recruitment to MOPr or SNC80-induced arrestin-3 recruitment to DOPr. However, we did not observe full inhibition of DAMGO or SNC80-induced arrestin-3 recruitment, being around 60% and 50%, respectively. One possibility that another GRK isoform/s involved in the receptor phosphorylation (e.g., GRK5/6) (Li, J et al. 2003) is not inhibited by cmpd101 and, thus, some phosphorylation and arrestin recruitment can take place. Another possible explanation is that arrestin-3 recruitment may depend on the active conformation of the receptor as well as on the GRK-mediated phosphorylation of the receptor. There are also studies suggesting that PKC activation is involved in morphine desensitisation and tolerance (Levitt & Williams 2012; Yousuf et al. 2015). These possibilities could explain why cmpd101 at 30 and 100 μM did not affect morphine-induced arrestin-3 recruitment. Also, it can be explained that proportion of morphine-induced arrestin-3 recruitment to MOPr is due to interaction with the active state of the receptor, as opposed to the GRK phosphorylation of the receptor. Under these conditions, cmpd101 might be less effective. Also, morphine may recruit a different GRK (e.g., GRK5) which is not inhibited by cmpd101 (Doll et al. 2012).

Cmpd101 at 1 μM in a cell-free system has been reported to inhibit a small number of non-GRK kinases by more than 50%, including protein kinase C-related protein kinase (PRK2), mitogen- and stress-activated kinases (MSK1), serum and glucocorticoid-related kinase (SGK1), ribosomal S6 kinase 1 (S6K1), and p90 ribosomal protein S6 kinase (RSK1) (Lowe et al. 2015). Additionally, the same study reported that cmpd101 at 1 μM inhibited PKC, ERK1/2, JNK and CaMKII by less than 20% (Lowe et al. 2015). While these kinase inhibitors are widely used, we observed that these kinases, often associated with receptor cell signalling, did not affect DAMGO-induced arrestin-3 recruitment to MOPr in HEK293 cells (Figure 3.12), which indicates that arrestin-3 recruitment is independent of PKC, ERK1/2, JNK or CaMKII activity in our BRET assay. It should however be acknowledged that we did not provide positive controls for the effects of these kinase inhibitors,

however the effectiveness of such inhibitors has previously been widely demonstrated.

DAMGO-induced G_i activation in HEK293 cells was measured by BRET assay, with DAMGO-induced G_i activation indicated by a decrease in the BRET signal. A decrease in the BRET signal indicates the dissociation of G_α and $G_{\beta\gamma}$. Pretreatment of the cells with cmpd101 (30 µM) led to a three-fold rightward shift of the curve, indicating a reduction in the potency of DAMGO. However, the maximum response of DAMGO upon addition of cmpd101 was not reduced. The crystallisation of GRK2 with $G_{\beta\gamma}$ revealed that the pleckstrin homology (PH) domain of GRK2 binds to the $G_{\beta\gamma}$ subunit (Lodowski et al. 2003). This binding contributes to the recruitment of GRK2 to the plasma membrane where GRK2 can phosphorylate the agonist-activated receptor and recruit arrestins. Ultimately, arrestin binding blocks G proteins signalling (Gurevich, V. V. & Gurevich 2019; Li, J et al. 2003). It is possible that cmpd101 could affect the fucnction of the $G_{\beta\gamma}$ subunits of the heterotrimeric G protein. GRK2 could facilitate the orientation of G protein with the receptor and when GRK2 is inhibited it partly disrupt the ability of GRK2 to facilitate the interaction of the G protein with the receptor. Hence, a small inhibition of G_i activation could be observed. Apart from an indirect effect of cmpd101 via GRK2, a direct inhibitory effect of cmpd101 or the other inhibitors on G protein function cannot be excluded.

Cmpd101 is a commercially available selective small molecule inhibitor of GRK2 and GRK3 (Thal et al. 2011). It has been reported to be selective for GRK2 and GRK3 with an IC_{50} of 35 nM (Ikeda, S, Keneko & Fujiwara 2007) and 290 nM (Thal et al. 2011) in different *in vitro* assays. Also, cmpd101 has no significant inhibitory activity at GRK1 or GRK5 at concentrations up to 125 µM in a purified enzyme assay (Thal et al. 2011). In HEK293 cells, cmpd101 inhibits DAMGO-induced arrestin-3 recruitment to MOPr with an IC_{50} value of 8 ± 3.5 µM. Cmpd101 has been used since then as a selective GRK2/3 inhibitor in different biochemical assays (Abraham et al. 2018; Jung et al. 2016; Lowe et al. 2015). To the best of our knowledge, no study has conducted a thorough investigation of the selectivity of cmpd101 in different assay conditions apart from that of Thal et al. (2011). The finding that cmpd101 affected the DAMGO-induced G_i activation in our study (Figure

3.13) raised questions regarding the selectivity of cmpd101. This finding supports the previous results that cmpd101 partially inhibits agonist-induced desensitisation in LC neurons (Lowe et al. 2015). Moreover, a recent study conducted on prostate smooth muscle has shown that cmpd101 (50 µM) failed to inhibit the agonist-induced phosphorylation state of β_2AR, which is phosphorylated and desensitised by GRK2 (Yu et al. 2018). In the same study, the author concluded that cmpd101 inhibited agonist-induced contraction in prostate smooth muscle by a GRK-independent mechanism (Yu et al. 2018). However, in human uterine smooth muscle cells (ULTR), Rainbow et al. (2018) reported that cmpd101 (30 µM) partially inhibited GRK2-medited histamine H_1 receptor desensitisation. This discrepancy could be attributed to the different cell types used. Collectively, these studies suggested that cmpd101 (and presumably the other experimental compounds used) may have off-target effects and the results should be interpreted with caution when using different cell lines and conditions.

The internalisation of HA-MOPr was assessed by ELISA using an anti-HA antibody to label surface receptors. DAMGO (10 µM) induced time-dependent loss of receptor surface, whereas morphine did not induce significant MOPr internalisation. These results are consistent with previously published data from this laboratory (Johnson, EA et al. 2006; McPherson et al. 2010). DAMGO-induced MOPr internalisation reaches a steady state at 30 min, which is not different from that at 60 min (22% and 25%, respectively). Previous studies have reported that agonist-induced MOPr internalisation reaches the maximum at 30 min which is thought to involve recycling MOPr back to the plasma membrane (Alvarez et al. 2002; Minnis et al. 2003). Cmpd101 significantly reduced DAMGO-induced MOPr internalisation. This result may be explained by the ability of cmpd101 to inhibit GRK function (Lowe et al. 2015; Thal et al. 2011). DAMGO has been shown to induce phosphorylation at both Thr^{370} and Ser^{375} on the C-terminus of MOPr while morphine induces relatively weak phosphorylation at Ser^{375} only (Doll et al. 2011; Gluck et al. 2014; Just et al. 2013). DAMGO-induced phosphorylation at Ser^{375} is mediated by GRK2 and GRK3; however, morphine-induced phosphorylation at Ser^{375} appears to be mediated at least in part by GRK5 (Doll et al. 2012). A prior study showed that cmpd101 inhibited DAMGO-induced phosphorylation at Ser^{375} and, thus, inhibited

receptor internalisation in HEK293 cells (Lowe et al. 2015). Furthermore, the Ser^{375} residue is believed to be the initial site on the C-terminus of MOPr for agonist-induced phosphorylation and then phosphorylation of the flanking residues, Thr^{370}, Thr^{376} and Thr^{379} ((Lau et al. 2011; Lowe et al. 2015; Miess et al. 2018). This also accords with other observations, which showed that isoproterenol, a full agonist at β_2 adrenoreceptor (β_2AR), has been shown to increase phosphorylation levels of the established multiple 13 β_2AR phosphorylation sites (Nobles et al. 2011). On the other hand, carvedilol increased the phosphorylation levels of only Ser^{355} and Ser^{356} (Nobles et al. 2011). These findings support the notion that different agonists induce different phosphorylation patterns of GPCRs. Thus, cmpd101 was able to inhibit DAMGO-induced internalisation of MOPr due to inhibition of GRK isoforms that involved in the phosphorylation of Ser^{375} (Miess et al. 2018).

3.4 Conclusion

In this chapter, we have described the effect of cmpd101 on agonist-induced arrestin-3 recruitment to MOPr and DOPr. In HEK293 cells, DAMGO, a full MOPr agonist, and SNC80, a full DOPr agonist, induce high levels of arrestin-3 recruitment while morphine, a partial MOPr agonist, and DADLE, a partial DOPr agonist, show less arrestin-3 recruitment. In addition, we have investigated the effect of cmpd101, a proposed GRK2/3 inhibitor, on arrestin-3 recruitment to MOPr and DOPr upon addition of MOPr agonists (DAMGO or morphine) or DOPr agonists (SNC80 or DADLE). Cmpd101 inhibits DAMGO- or SNC80-induced arrestin-3 recruitment by about 60% and 50%, respectively, while it inhibits DADLE-induced arrestin-3 recruitment by 33%. However, it failed to inhibit morphine-induced arrestin-3 recruitment. The ability of the cmpd101 to inhibit arrestin-3 recruitment appears to be governed by the agonist employed.

I also have determined the effect of cmpd101 on G_i activation. I have demonstrated that cmpd101 can inhibit DAMGO-induced G_i activation. Finally, the internalisation of MOPr in response to DAMGO and morphine has been investigated. It is well-established that morphine induces much less MOPr internalisation in comparison with DAMGO, which induces robust internalisation. Cmpd101 greatly inhibits

DAMGO-induced MOPr internalisation in HEK293 cells. Our data, therefore, confirm the role of GRKs in mediating agonist-induced MOPr internalisation.

These findings contribute to the existing knowledge of GRK inhibitor, cmpd101, by providing new evidence of the use of cmpd101 in the cell-based settings. The results demonstrate that cmpd101 gives the opportunity to study the roles of GRKs in opioid receptors (MOPr and DOPr) and other GPCRs signalling.

In the next chapter, I will examine the utility of novel GRK inhibitors to determine their effects on the arrestin-3 recruitment to MOPr and DOPr and to compare their activity with the established GRK inhibitor, cmpd101.

CHAPTER 4 Effect of Novel Compound101 Analogues on Arrestin-3 Recruitment to MOPr and DOPr

4.1 Introduction

Several small molecule inhibitors for GRKs, particularly GRK2, have been reported. Polyanionic and polycationic compounds, such as heparin, were the first to be reported to have inhibitory activity on GRK2 (Benovic et al. 1989). Since the crystallisation of human GRK2 with the natural product balanol (Tesmer, JJ et al. 2010), the search for selective GRK2 inhibitors has been focused on the ATP binding site in the GRK (Murga et al. 2019). Balanol inhibits GRK2 with an IC_{50} of 50 nM, but it also inhibits PKA with an IC_{50} of 110 nM (Tesmer, JJ et al. 2010). Paroxetine (Figure 4.1), an FDA-approved serotonin selective reuptake inhibitor (SSRI), has modest inhibitory activity against GRK2 (IC_{50} =1.1 μM) and is more than 6-fold selective over other GRK isoforms (Thal et al. 2012). The Takeda compounds, cmpd101 (Table 4.1) and cmpd103 were reported to be somewhat selective for the GRK2/3 subfamily, although they did not proceed to clinical trials because of their limited bioavailability (Ikeda, S, Keneko & Fujiwara 2007; Okawa et al. 2017). Recently, a compound derived from paroxetine (CCG258747) (Figure 4.1) was developed that showed potent inhibition of GRK2 (IC_{50}= 0.018 μM) and modest inhibition of GRK1 and GRK5 with IC_{50} values of 9.3 and 1.5 μM, respectively (Bouley, RA et al. 2020). CCG258747 also inhibited ROCK1 with an IC_{50} of 27 μM (Bouley, RA et al. 2020).

Understanding the structure and functions of GRKs will facilitate the development of potent and selective GRK inhibitors. Also, developing a selective inhibitor for individual GRKs/ or subfamilies is a critical step that could be used in advancing the therapy of diseases where GRKs may play a role. Furthermore, inhibitors of GRK phosphorylation of opioid receptors could represent drugs that suppress tolerance, a common problem observed with the use of opioid receptor agonists. Finally, selective GRK inhibitors will be important to explore the physiological function of these kinases in living systems.

In this chapter, I will study the ability of the novel compounds (Table 4.1), analogues of cmpd101, to inhibit GRK/s, principally by assessing their ability to inhibit agonist-induced arrestin-3 recruitment to μ and δ opioid receptors. In addition, to further

explore the selectivity of theses analogues in cell signalling, I will investigate their effect on both agonist-induced G_i activation and MOPr internalisation. In these experiments, cmpd101 will serve as a standard GRK inhibitor, in order to compare its activity with that of the novel compounds.

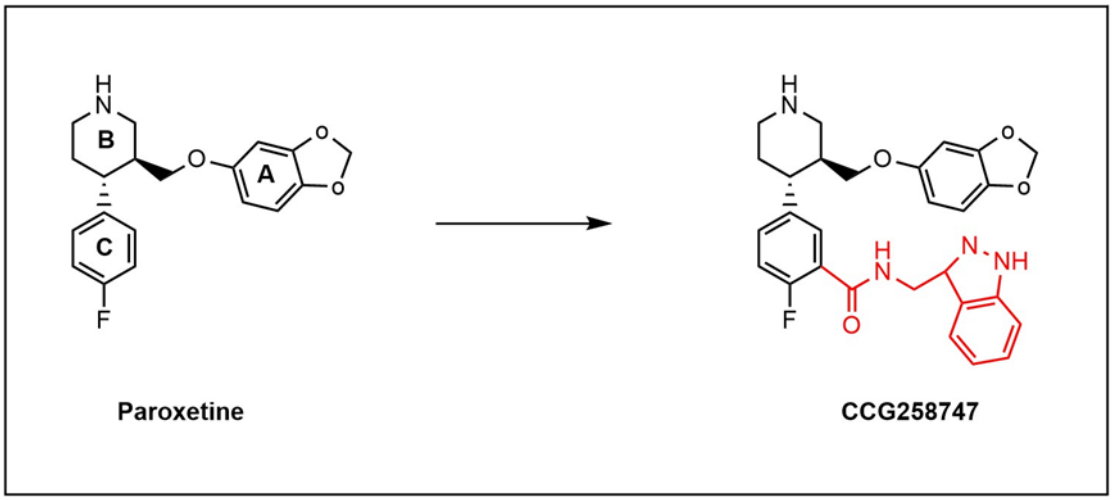

Figure 4.1 Structures of paroxetine and CCG258747

Substitution on paroxetine is shown in red.

Table 4.1 Chemical structures of cmpd101 and novel analogues

Compound	Molecular weight	LogP[(a)]	Structure
Cmpd101	466.2	3.72	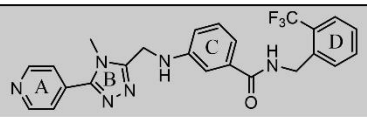
BU14016	434.5	1.65	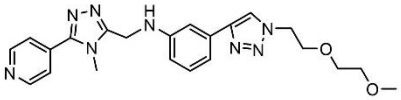
BU16005	435.5	5.14	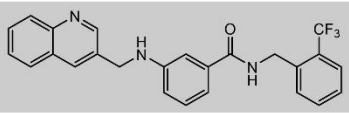
BU16007	434.5	6.06	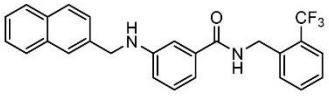
BU16006	367.5	3.80	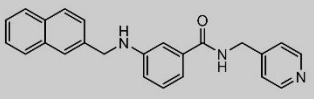
BU14017	422.5	3.7	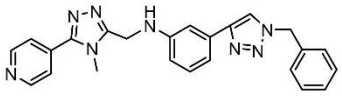
BU16009	465.5	4.69	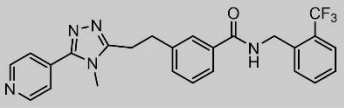
BU14013	435.5	5.03	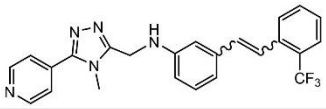
BU14014	463.5	4.68	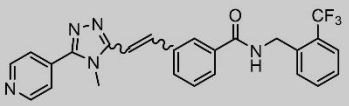

[(a)] The logP values were calculated using ChemDraw Professional 16 software.

4.2 Results

4.2.1 Effect of the Novel Compounds on Agonist-induced Arrestin-3 Recruitment to MOPr and DOPr

The novel compounds were screened as well as cmpd101 (a standard GRK inhibitor) at 30 and 100 µM using the BRET arrestin-3 recruitment assay. The novel compounds were initially tested at 100 µM, to observe as maximum an effect if possible. I compared the ability of these novel compounds to inhibit both DAMGO- and morphine-induced arrestin-3 recruitment to MOPr. DAMGO is a high efficacy peptide agonist at MOPr, whilst morphine is a lower efficacy non-peptide agonist and is, of course, widely used clinically. In further experiments, their effects on agonist-induced arrestin-3 recruitment to another opioid GPCR receptor, the δ receptor (DOPr), was investigated. For these experiments, the high efficacy agonists: SNC80 and DADLE were employed, with both being high efficacy agonists, but SNC80 being a synthetic agonist and DADLE a peptide (Conibear et al. 2020).

At a concentration of 100 µM, most of the inhibitors reduced DAMGO-induced (10 µM) arrestin-3 recruitment to MOPr (Figure 4.2). Compounds BU14016, BU16005 and BU16007 showed slightly higher inhibition (82%, 71% and 71%, respectively) than cmpd101 (58%), while compounds BU16006, BU14017 and BU16009 showed similar inhibition (61%, 56% and 52%, respectively) to cmpd101. The other compounds, BU14013 and BU14014, showed less inhibition (26%) (Figure 4.2). Likewise, when these novel compounds were applied at a lower concentration of 30 µM, most of them, including cmpd101, showed a similar level of inhibition as they did at 100 µM (Figure 4.3).

I also investigated whether the novel compounds might have an effect on basal arrestin-3 recruitment to MOPr (Figure 4.4). They induced an apparent increase in the basal arrestin-3 recruitment at both 30 µM and 100 µM, while 100 µM showed a higher apparent increase than at 30 µM; however, one-way ANOVA found no significant differences between the mean of the inhibitors and DMSO or basal value (Figure 4.4).

To further investigate the effect of other MOPr agonists on arrestin-3 recruitment in the presence of these novel compounds, HEK293 cells expressing MOPr were pretreated with cmpd101 or novel compounds (100 μM), and then the cells were stimulated with the lower efficacy agonist morphine (30 μM) for 10 min (Figure 4.5). Morphine-induced recruitment of arrestin-3 to MOPr was assessed using BRET and was significantly less than that seen with DAMGO (about 50%). Surprisingly, at 100 μM most of the compounds showed little or no inhibition of arrestin-3 recruitment induced by morphine (Figure 4.5). In addition, cmpd101 did not inhibit morphine-induced arrestin-3 recruitment whilst BU14016, BU16005 and BU16007, which showed the highest inhibition of DAMGO-induced arrestin-3 recruitment, also showed negligible inhibition (Figure 4.5). Unexpectedly, BU14017 significantly *enhanced* morphine-induced arrestin-3 recruitment (Figure 4.5). Interestingly, when compounds were screened at 30 μM, most compounds did not show inhibition of morphine-induced arrestin-3 recruitment, although, there is a trend towards inhibition, except for BU14013 which remained an activator rather than an inhibitor (Figure 4.6).

To explore these findings further, a time course was performed for morphine-induced arrestin-3 recruitment with BU14017 and BU14014 because these two compounds exerted an apparent enhancing effect on arrestin-3 recruitment induced by morphine when applied at 100 μM (that by BU14017 was statistically significant; Figure 4.5). The responses over time are shown in Figure 4.7, indicating that BU14017 and BU14014 appeared to enhance morphine-induced arrestin-3 recruitment throughout the time course of morphine activation (Figure 4.7). In contrast, it should be noted that I had previously found that 100 μM BU14017 inhibited DAMGO-induced arrestin-3 recruitment by about 60% (see Figures 4.2 and 4.3 above). Also, when cells were stimulated by DAMGO, 100 μM BU14014 inhibited arrestin-3 recruitment by about 20% (Figures 4.2 and 4.3).

I next investigated the ability of cmpd101 and the novel compounds to inhibit agonist-induced arrestin-3 recruitment to the closely related δ receptor (DOPr). The agonists used were SNC80 and DADLE (each 10 μM), using HEK293 cells cotransfected this time with DOPr. The results showed that SNC80 (10 μM) induced a high maximal level of arrestin-3 recruitment as compared to DADLE (10 μM)

(Figures 4.8 and 4.10). In addition, SNC80-induced arrestin-3 recruitment to DOPr signal was about 2-fold higher than that generally obtained for DAMGO-induced arrestin-3 recruitment to MOPr (see Figures 4.2 and 4.8).

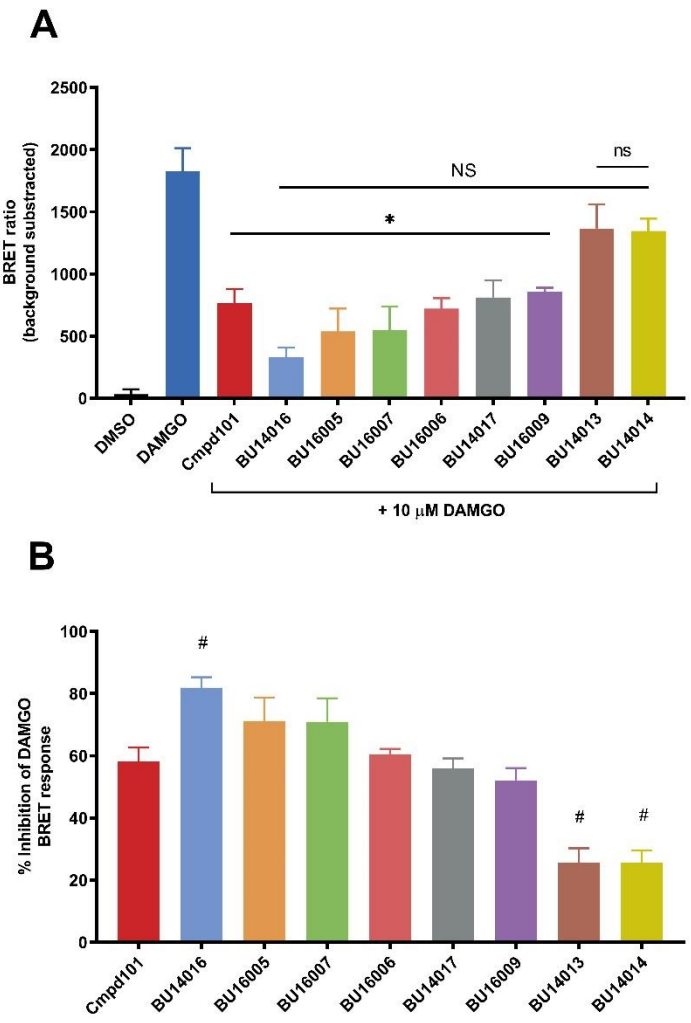

Figure 4.2 Cmpd101 and novel compounds at 100 µM inhibit DAMGO-induced arrestin-3 recruitment to MOPr.

HEK293 cells were cotransfected with MOPr-RLuc2 and Arr3-GFP. A) Cells were preincubated with cmpd101 or novel compounds (all at 100 µM) or DMSO as a vehicle for 30 min and then stimulated with DAMGO (10 µM) for a further 10 min. B) Data from A were normalised to the response induced by 10 µM DAMGO, to give % inhibition of the agonist-induced response. BRET ratio of no agonist-treated cells was subtracted from agonist-treated cells. * $P < 0.05$ compared to DAMGO alone; $^{\#}$ $P < 0.05$ compared to cmpd101; ns, not statistically significant compared to DAMGO alone, NS, not statistically significant compared to cmpd101, one-way ANOVA followed by Tukey's multiple comparison test. Data represented as mean ± SEM from four independent experiments.

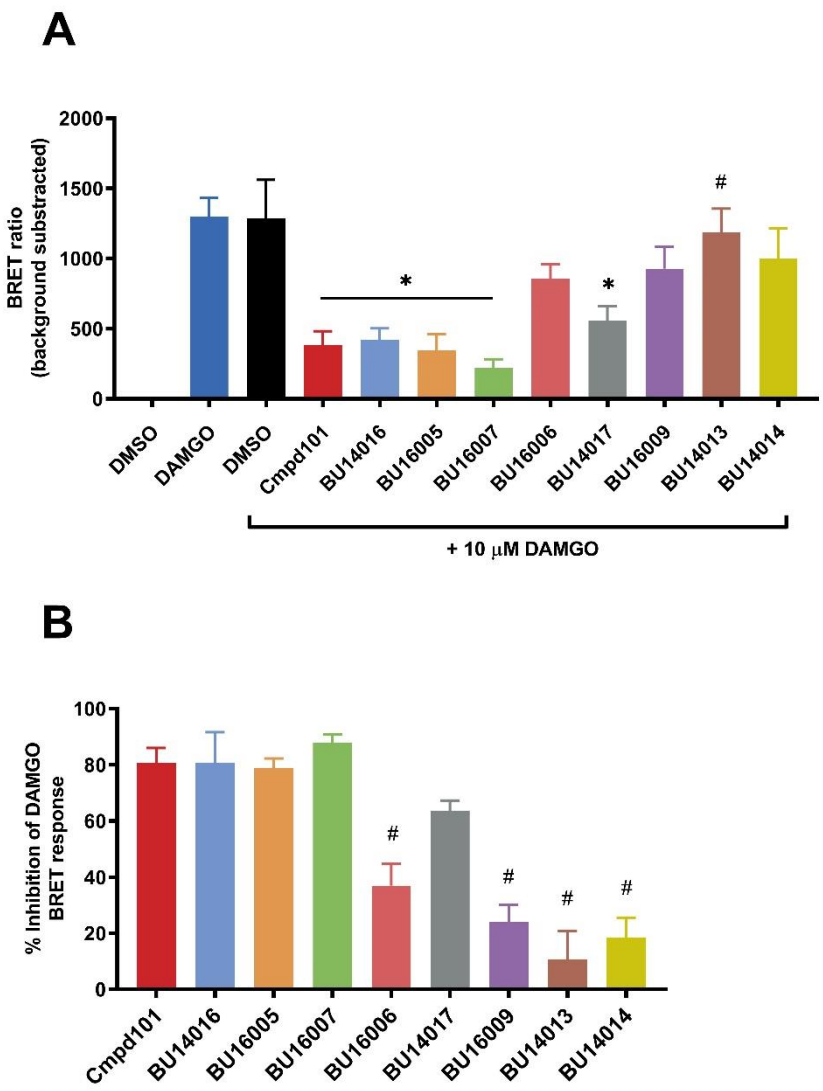

Figure 4.3 Cmpd101 and novel Compounds at 30 μM inhibit DAMGO-induced arrestin-3 recruitment to MOPr.

HEK293 cells were cotransfected with MOPr-RLuc2 and Arr3-GFP. A) Cells were preincubated with cmpd101 or novel compounds (all at 30 μM) for 30 min and then stimulated with DAMGO (10 μM) for a further 10 min. B) Data from A were normalised to the response induced by 10 μM DAMGO, to give % inhibition of the agonist-induced response. BRET ratio of no agonist-treated cells was subtracted from agonist-treated cells. * $P < 0.05$ compared to DAMGO or DAMGO+DMSO; # $P < 0.05$ compared to cmpd101; one-way ANOVA followed by Tukey's multiple comparison test. Data represented as mean ± SEM from four independent experiments.

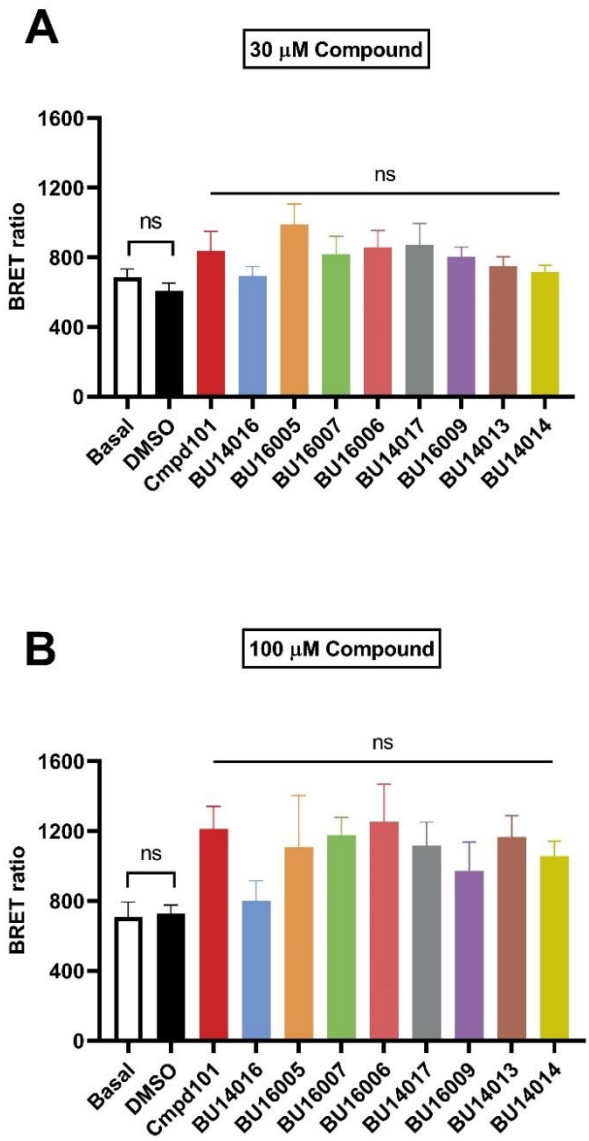

Figure 4.4 Effect of 30 or 100 μM cmpd101 and novel compounds on the basal level of arrestin-3 recruitment to MOPr.

HEK293 cells were transiently cotransfected with MOPr-RLuc2 and Arr3-GFP. Cells were preincubated with cmpd101 or novel compounds at A) 30 μM or B) 100 μM for 30 min. ns, not statistically significant compared to basal, one-way ANOVA. Data represented as mean ± SEM from four independent experiments.

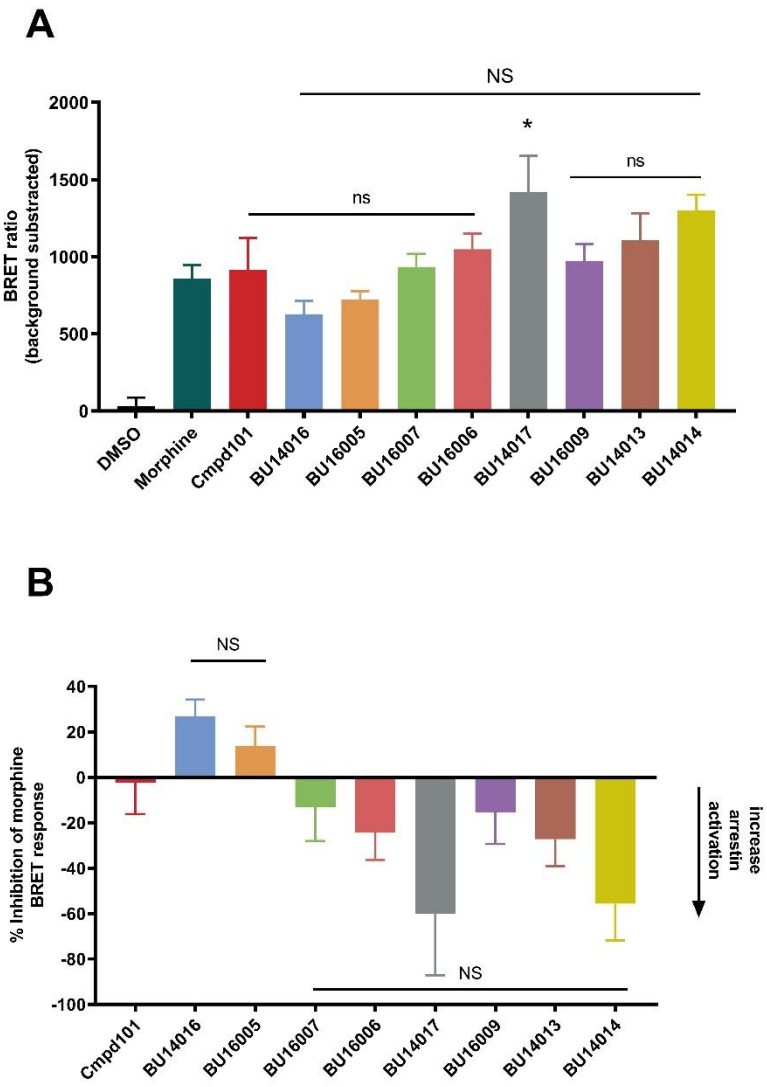

Figure 4.5 Effect of 100 µM cmpd101 and novel compounds on morphine-induced arrestin-3 recruitment to MOPr.

HEK293 cells were transiently transfected with MOPr-RLuc2 and Arr3-GFP. A) Cells were preincubated with cmpd101 (100 µM), novel compounds (100 µM) or DMSO as a vehicle for 30 min and then stimulated with morphine (30 µM) for a further 10 min. BRET ratio of no agonist-treated cells was subtracted from agonist-treated cells. B) Data were normalised to the response induced by 30 µM morphine, to give % of the morphine-induced response. Arrow indicates an increase in morphine-induced arrestin-3 recruitment. * $P < 0.05$ compared to morphine; ns, not statistically significant compared to morphine; NS, not statistically significant compared to cmpd101, one-way ANOVA followed by Dunnett's multiple comparison test. Data represented as mean ± SEM from four independent experiments.

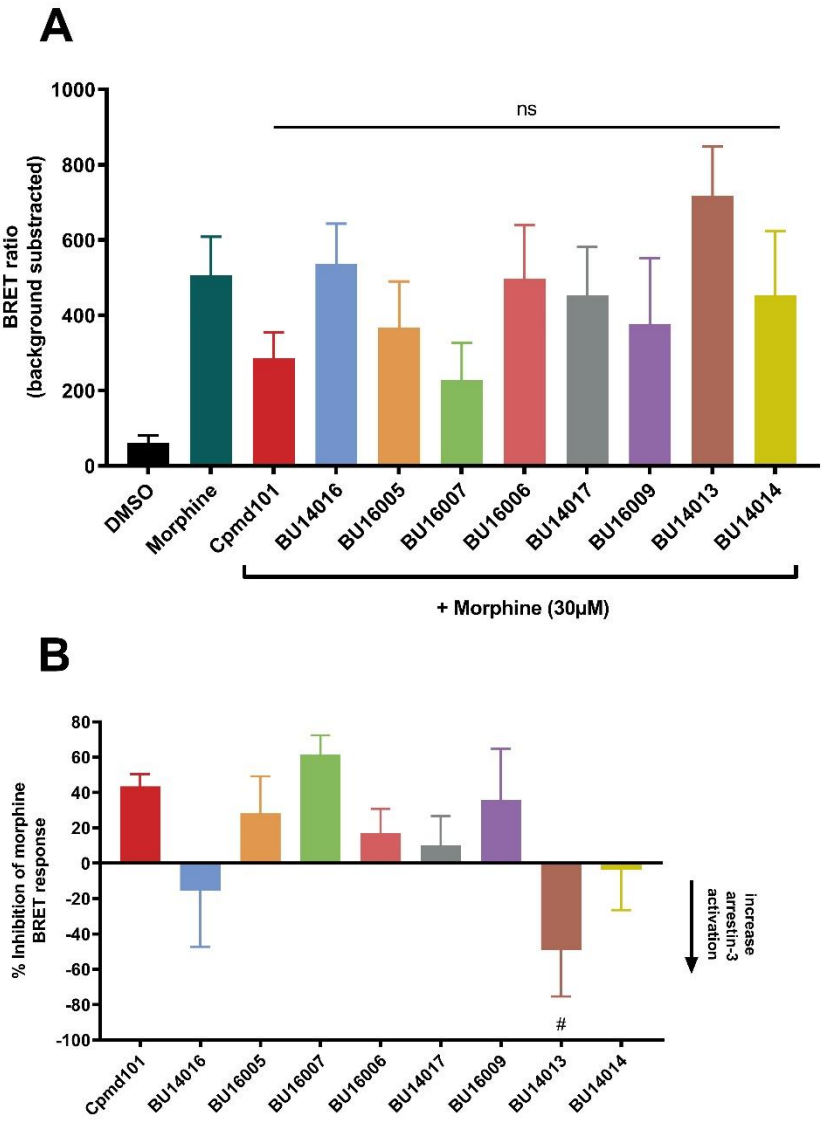

Figure 4.6 Effect of 30 μM of cmpd101 and novel compounds on morphine-induced arrestin-3 recruitment to MOPr.

HEK293 cells were transiently transfected with MOPr-RLuc2 and Arr3-GFP. A) Cells were preincubated with 30 μM cmpd101 or novel compounds for 30 min and then stimulated with morphine (30 μM) for a further 10 min. BRET ratio of no agonist-treated cells was subtracted from agonist-treated cells. B) Data from A were normalised to the response induced by 30 μM morphine, to give % of the morphine-induced response. $^{\#}P < 0.05$ compared to cmpd101; ns, not statistically significant compared to morphine, one-way ANOVA followed by Dunnett's multiple comparison test. Data represented as mean ± SEM from four independent experiments.

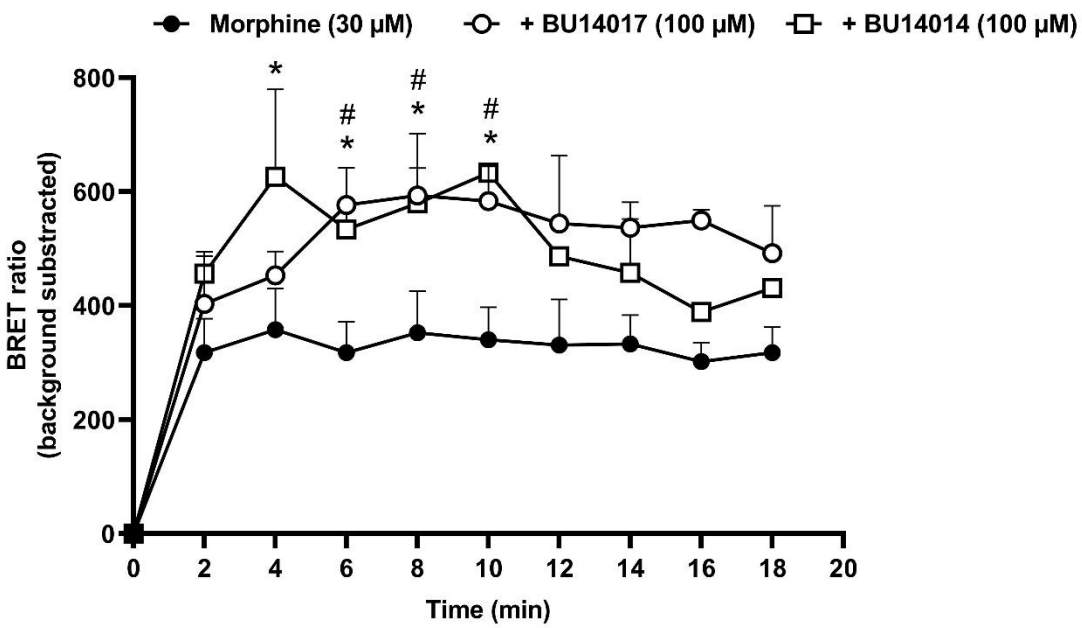

Figure 4.7 Effect of BU14017 and BU14014 on 30 µM morphine-induced arrestin-3 recruitment to MOPr.

HEK293 cells were transiently transfected with MOPr-RLuc2 and Arr3-GFP and preincubated with BU14017 (100 µM, ○) or BU14014 (100 µM, □) for 30 min. Cells were then stimulated with morphine (30 µM) and BRET measurements were taken every 2 min up to 18 min. The BRET ratio of vehicle-treated cells was subtracted from morphine-stimulated values. Data are represented as mean ± SEM of four independent experiments. * $P < 0.05$ BU14014 compared to respective morphine value; $^{\#}$ $P < 0.05$ BU14017 compared to morphine, two-way ANOVA followed by Dunnett's multiple comparisons test.

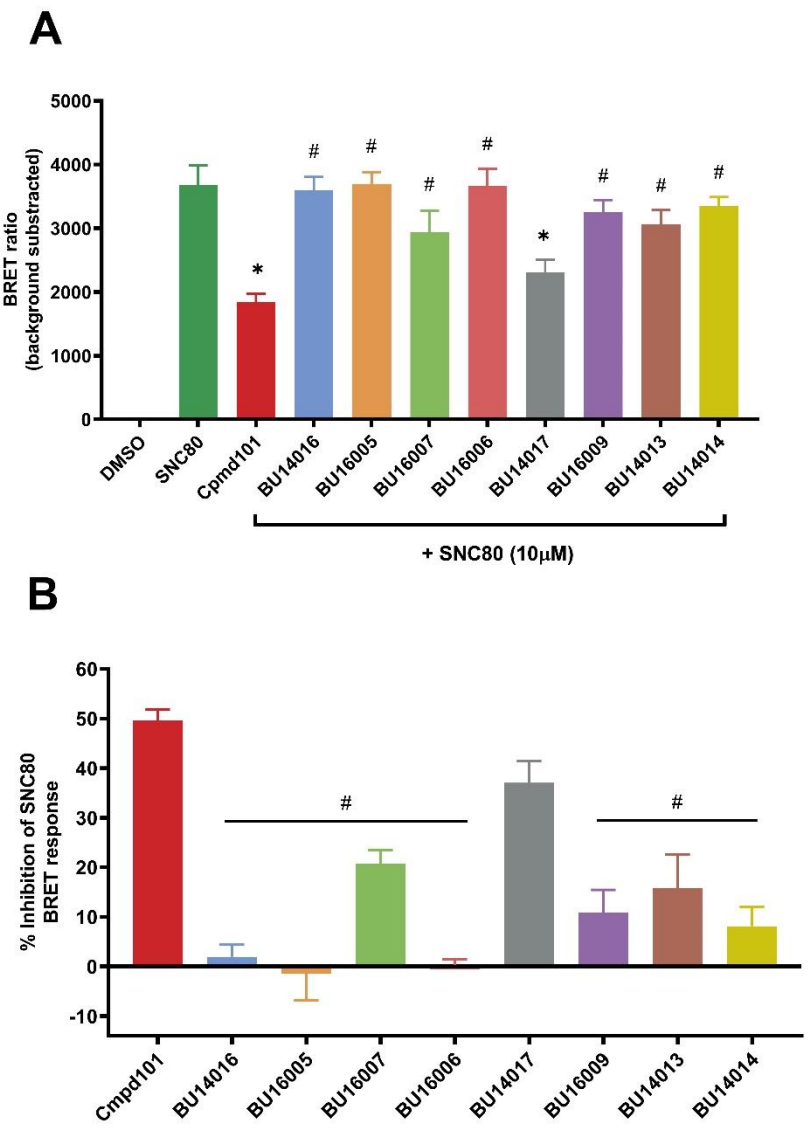

Figure 4.8 Effect of 100 μM cmpd101 or novel compounds on SNC80-induced arrestin-3 recruitment to DOPr.

HEK293 cells were transiently transfected with DOPr-RLuc2 and Arr3-GFP. A) Cells were preincubated with 100 μM cmpd101 or novel compounds for 30 min and then stimulated with SNC80 (10 μM) for a further 10 min. B) Data from A were normalised to the response induced by 10 μM SNC80, with the BRET ratio of no agonist-treated cells was subtracted from agonist-treated cells. * $P < 0.05$ compared to SNC80; $^{\#}$ $P < 0.05$ compared to cmpd101, one-way ANOVA followed by Dunnett's multiple comparison test. Data represented as mean ± SEM from four independent experiments.

Interestingly, whereas at 100 µM cmpd101 inhibited SNC80-induced arrestin-3 recruitment to DOPr by about 50%, of the novel compounds only BU14017 was able to significantly inhibit (~ 40%) the SNC80 signal (Figure 4.8). Furthermore, using the inhibitors at 30 µM, only cmpd101 was able to inhibit the SNC80 response (Figure 4.9). Using DADLE as the agonist, cmpd101, BU16007 and BU14017 at 100 µM each inhibited arrestin-3 recruitment by 30, 30 and 40%, respectively; however, the overall general pattern of inhibition did resemble that obtained with SNC80 (compare Figure 4.8 and 4.10). These results with DOPr are different from those for DAMGO-induced arrestin-3 recruitment to MOPr. For example, BU14016 at 100 µM inhibited DAMGO-induced arrestin-3 recruitment to MOPr by 80%, but was unable to inhibit SNC80- or DADLE-induced arrestin-3 recruitment to DOPr (Figures 4.2, 4.8 and 4.10).

Next, the novel compounds were applied at 100 µM on their own to determine their effect on basal arrestin-3 recruitment to DOPr. The results indicated that adding most of these novel inhibitors at 100 µM produced around a 1.5-fold increase in basal arrestin-3 recruitment to DOPr (Figure 4.11). In contrast, BU14016 showed no effect on basal arrestin-3 recruitment to MOPr or DOPr when added at either 30 or 100 µM (Figures 4.4 and 4.11).

To further investigate the effect of these novel inhibitors on the agonist-induced arrestin-3 recruitment to MOPr or DOPr, full concentration inhibition curves were constructed for BU14016, BU16005 and BU16007; these compounds showed the greatest inhibition of DAMGO-induced arrestin-3 recruitment to MOPr (Figures 4.2 and 4.3). The inhibition curves are shown in Figures 4.12 and 4.13. The IC_{50} and maximum inhibition values are summarised in Table 4.2. The results confirmed our previous findings (Figure 4.3 and 4.9). Interestingly, BU16007, which showed higher inhibition of DAMGO-induced arrestin-3 recruitment to MOPr at a concentration of 30 µM than of cmpd101 (Figure 4.3), showed a higher potency with an IC_{50} of 0.7 ± 0.4 µM and maximum inhibition of 90% compared to cmpd101 IC_{50} 9.3 ± 0.9 µM and maximum inhibition of 50% (Figure 4.12). The other compounds, BU14016 and BU16005, showed an IC_{50} of 2.9 ± 2.3 µM and 7.6 ± 2.0 µM and maximum inhibition of 90 and 60%, respectively (Figure 4.12). Conversely and intriguingly, BU14016,

BU16005 and BU16007 failed to inhibit SNC80-induced arrestin-3 recruitment to DOPr (Figure 4.13). However, cmpd101 showed a maximum 50% inhibition of SNC80-induced arrestin-3 recruitment to DOPr (Figure 4.13), which is similar to the inhibition of cmpd101 of DAMGO-induced arrestin-3 recruitment to MOPr (Figure 4.12).

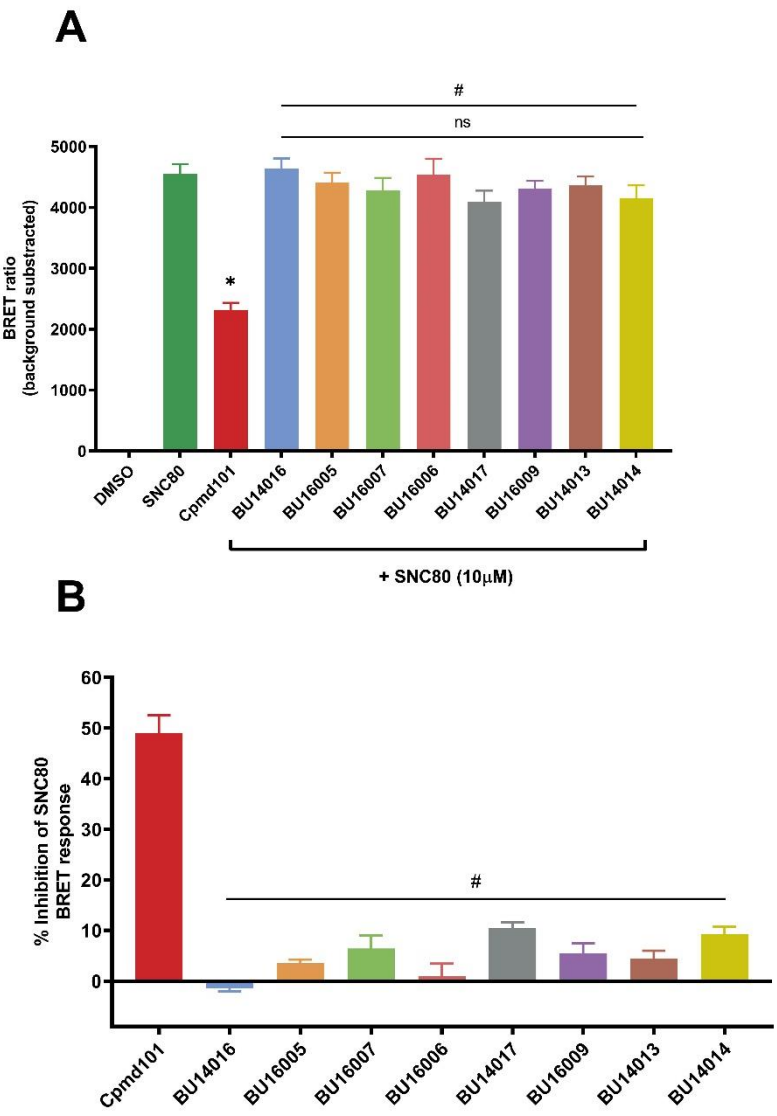

Figure 4.9 Effect of 30 μM cmpd101 and novel compounds on SNC80-induced arrestin-3 recruitment to DOPr

HEK293 cells were transiently transfected with DOPr-RLuc2 and Arr3-GFP. A) Cells were preincubated with 30 μM cmpd101 or novel compounds for 30 min and then stimulated with SNC80 (10 μM) for a further 10 min. The BRET ratio of no agonist-treated cells was subtracted from agonist-treated cells. B) Data were normalised to the response induced by 10 μM SNC80. * $P < 0.05$ compared to SNC80; $^{\#}$ $P < 0.05$ compared to cmpd101; ns, not statistically significant compared to SNC80, one-way ANOVA followed by Dunnett's multiple comparison test. Data represented as mean ± SEM from four independent experiments.

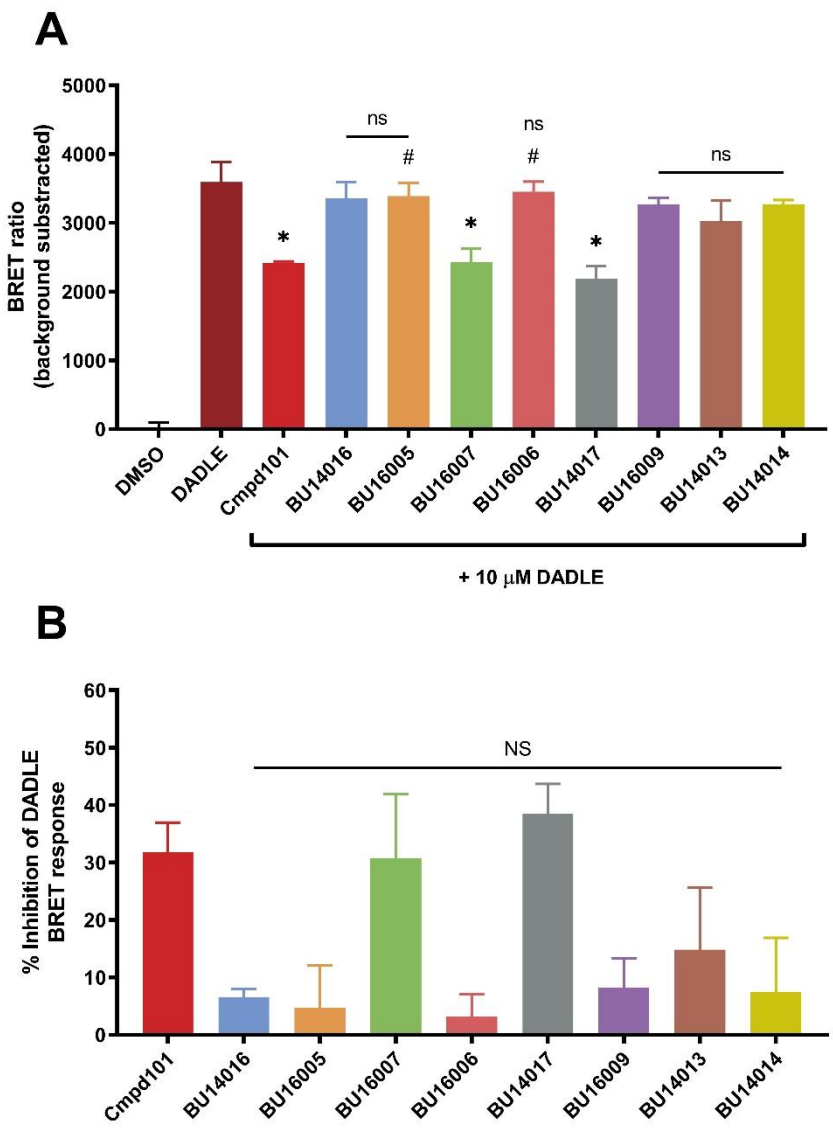

Figure 4.10 Effect of cmpd101 or novel compounds on DADLE-induced arrestin-3 recruitment to DOPr

HEK293 cells were transiently transfected with DOPr-RLuc2 and Arr3-GFP. A) Cells were preincubated with 100 µM cmpd101 or novel compounds for 30 min and then stimulated with DADLE (10 µM) for further 10 min. The BRET ratio of no agonist-treated cells was subtracted from agonist-treated cells. B) Data were normalised to the response induced by 10 µM DADLE. * $P < 0.05$ compared to DADLE; $^{\#}$ $P < 0.05$ compared to cmpd101; ns, not statistically significant compared to DADLE; NS, not statistically significant compared to cmpd101, one-way ANOVA followed by Dunnett's multiple comparison test. Data represented as mean ± SEM from four independent experiments.

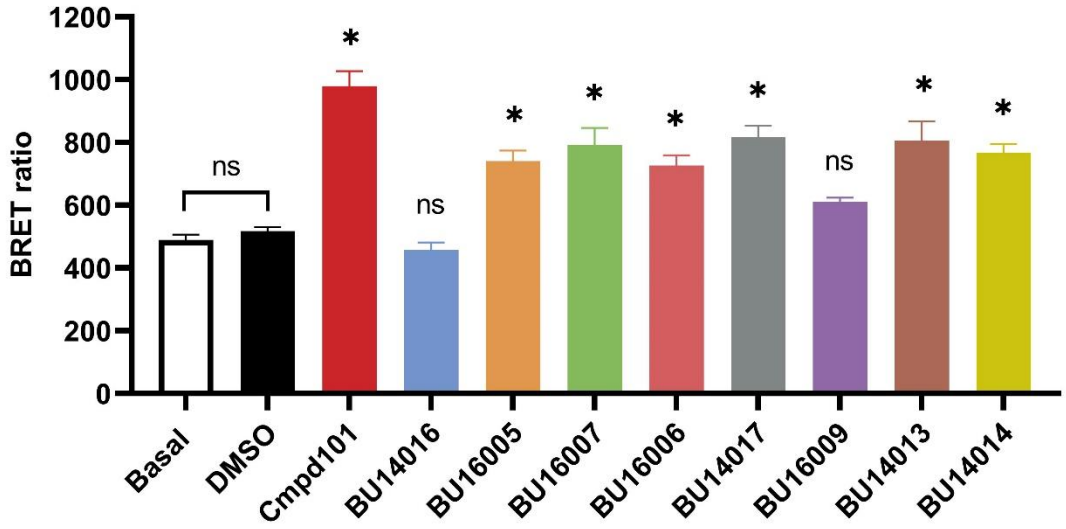

Figure 4.11 Effect of cmpd101 and novel compounds on basal arrestin-3 recruitment to DOPr

HEK293 cells were transiently cotransfected with DOPr-RLuc2 and Arr3-GFP. Cells were preincubated with cmpd101 or novel compounds (30 µM) for 30 min and BRET measurements made. * $P < 0.05$ compared to DMSO or basal; ns, not statistically significant compared to DMSO or basal, one-way ANOVA followed by Tukey's multiple comparison test. Data represented as mean ± SEM from four independent experiments.

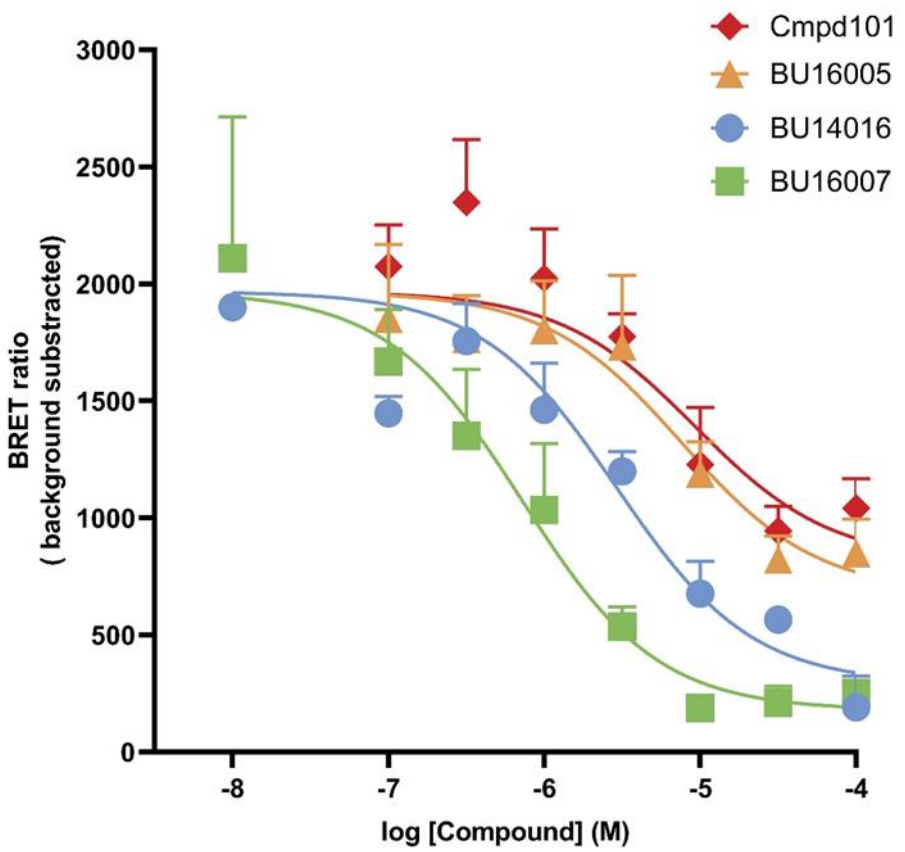

Figure 4.12 Concentration-dependent inhibition of 10 µM DAMGO-induced arrestin-3 recruitment to MOPr by cmpd101 and selected novel compounds.

HEK293 cells were cotransfected with MOPr-RLuc2 and Arr3-GFP. Cells were preincubated with cmpd101 (0.1 - 100 µM) or novel compounds (0.01 - 100 µM) for 30 min and then stimulated with DAMGO (10 µM) for further 10 min. The BRET ratio of no agonist-treated cells was subtracted from agonist-treated cells. Data were fitted to a non-linear regression model with three parameters using GraphPad Prism v8 software. Data are represented as mean ± SEM of results from four independent experiments each performed in duplicate.

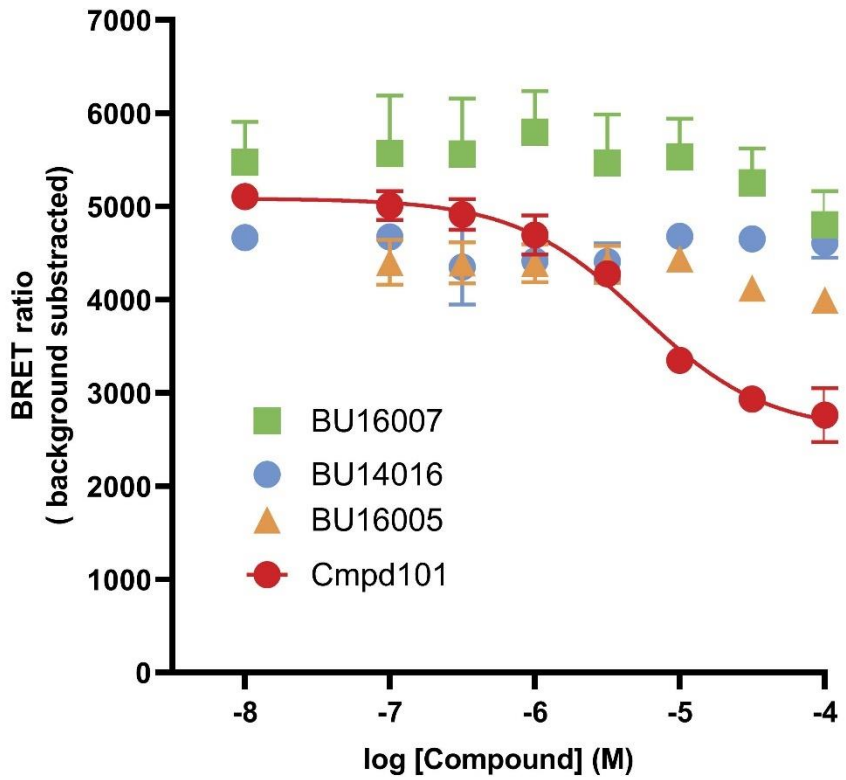

Figure 4.13 Concentration-inhibition curves for the ability of cmpd101 and novel compounds to inhibit 10 µM SNC80-induced arrestin-3 recruitment to DOPr.

HEK293 cells were cotransfected with DOPr-RLuc2 and Arr3-GFP. Cells were preincubated with cmpd101 or novel compounds (0.01- 100 µM) for 30 min and then stimulated with SNC80 (10 µM) for further 10 min. The BRET ratio of no agonist-treated cells was subtracted from agonist-treated cells. Where possible, data were fitted to a non-linear regression model with three parameters using GraphPad Prism v8 software. Data are represented as mean ± SEM of results from four independent experiments each performed in duplicate.

Table 4.2 IC_{50} and maximum inhibition of cmpd101 and novel compounds

	DAMGO-induced arrestin-3 recruitment to MOPr (10 μM)		SNC80-induced arrestin-3 recruitment to DOPr (10 μM)	
	IC_{50} (μM) ± SEM	**Maximum inhibition (%)**	**IC_{50} (μM) ± SEM**	**Maximum inhibition (%)**
Cmpd101	9.3 ± 0.9	50	5.6 ± 0.8	50
BU14016	2.9 ± 2.2	90	ND	ND
BU16007	0.7 ± 0.4	90	ND	ND
BU16005	7.5 ± 2.0	60	ND	ND

The IC_{50} and maximum inhibition values are taken from Figures 4.12 and 4.13. ND, not determined.

4.2.2 Effect of Novel Compounds on DAMGO-induced G_i Activation at MOPr

Next, I investigated the effect of these inhibitors on G_i activation to determine their selectivity in the arrestin/G protein signalling pathways. Some compounds were chosen that were either very effective at inhibiting DAMGO-induced arrestin-3 recruitment to MOPr, or, alternatively, were weak inhibitors. G protein subunit dissociation was assessed by BRET assay, which measures the separation of G_α and βγ during receptor activation and the BRET signal is reduced (Masuho, Martemyanov & Lambert 2015). The agonist concentration-response curves of the compounds are shown in Figure 4.14. DAMGO increased G protein dissociation (i.e., activated G protein) with an EC_{50} of 0.4 ± 0.1 µM, which is similar to the EC_{50} for DAMGO (0.8 ± 0.4 µM) obtained in the arrestin-3 recruitment assay (see Chapter 3, Figure 3.2B). These experiments showed that cmpd101 and BU14016 modestly inhibited DAMGO-induced $G_\alpha/G_{\beta\gamma}$ dissociation as depicted by a decrease in the BRET ratio (Figure 4.14). The EC_{50} and E_{max} values are summarised in Table 4.3. Cmpd101 and BU14016 shifted the DAMGO curve to the right by 3- and 6- fold, respectively (Figure 4.14). On the other hand, compounds BU14014 and BU14013, which were weak at inhibiting DAMGO-induced arrestin-3 recruitment to MOPr, did not significantly affect DAMGO-induced $G_\alpha/G_{\beta\gamma}$ dissociation (Table 4.3 and Figure 4.14).

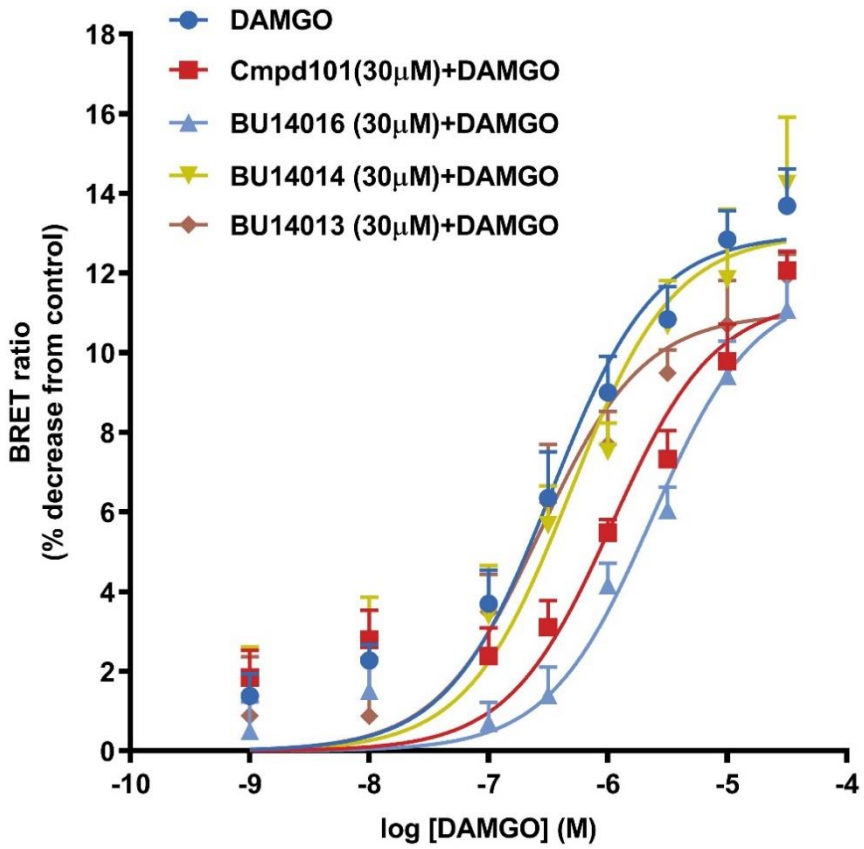

Figure 4.14 Effect of cmpd101 and novel compounds on log concentration-response curves of DAMGO-induced G_i activation.

HEK293 cells were transiently transfected with HA-MOPr, $G_{\alpha i}$-RLuc2 and $G_{\beta\gamma}$-GFP. Cmpd101 (30 μM) or novel compounds (30 μM) was added 30 min before the addition of DAMGO (0.001-30 μM) for a further 2 minutes. DAMGO-induced BRET ratios were expressed as the percentage decrease compared to nontreated cells. Data were fitted to a non-linear regression model with three parameters with the minimum constrained to zero. Data are presented as mean ± SEM from four independent experiments performed in duplicate.

Table 4.3 EC_{50} and E_{max} values of DAMGO in the presence of cmpd101 and the novel compounds

Inhibitor	DAMGO EC_{50} (μM)	E_{max} (BRET ratio, no units)
no inhibitor	0.4 ± 0.1	13.1 ± 0.7
Cmpd101	1.2 ± 0.3	11.5 ± 0.4
BU14016	2.4 ± 0.5*	11.7 ± 1.4
BU14014	0.8 ± 0.4	13.6 ± 2.0
BU14013	0.3 ± 0.1	11.1 ± 0.8

EC_{50} and E_{max} values are taken from Figure 4.14. * $P < 0.05$ compared to no inhibitor (DAMGO alone), one way ANOVA followed by Dunnett's multiple comparison test.

4.2.3 Effect of the Novel Compounds on the Cell Surface Loss of MOPr

Next, I want to determine the ability of cmpd101 and selected novel compounds to inhibit cell surface loss of MOPr as a result of DAMGO-induced internalisation of the receptor (Johnson, EA et al. 2006). ELISA was used to determine the effect of cmpd101 and some of the novel compounds on cell surface loss of MOPr. The results are shown in Figure 4.15. DAMGO at 10 μM clearly increased surface receptor loss of the receptor in HEK293 cells expressing HA-MOPr by about 30% (Figure 4.15). Applying cmpd101 and the selected novel compounds (all at 30 μM) on their own did not affect the basal level of surface MOPr loss (Figure 4.15B). On the other hand, compound BU16007 significantly reduced the DAMGO-induced surface receptor loss by 87% whilst cmpd101 and BU14016 reduced loss by 77% and 47%, respectively (Figure 4.15). In contrast, the compound BU16013, which failed to inhibit DAMGO-arrestin-3 recruitment to MOPr, did not reduce the DAMGO-induced surface receptor loss (Figure 4.15).

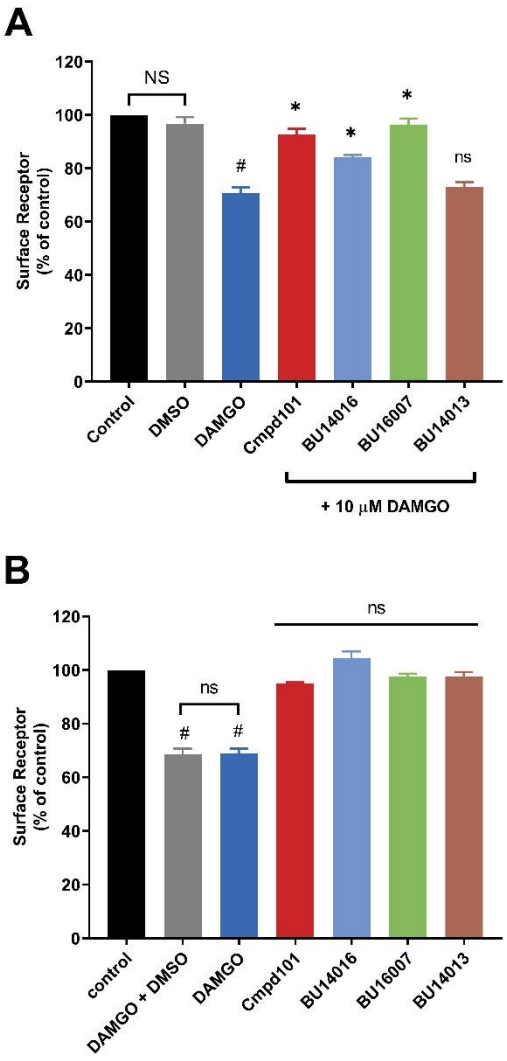

Figure 4.15 Inhibition of DAMGO-induced MOPr surface loss by cmpd101 and novel compounds

A) HEK293 cells were transiently transfected with HA-MOPr and were pretreated with cmpd101 (30 µM) or the novel compounds (30 µM) or DMSO for 30 min and then were stimulated with DAMGO (10 µM) (as indicated in the graph) for a further 30 min at 37°C. B) Cells were preincubated with cmpd101 (30 µM), novel compounds (30 µM) or DMSO for 30 min, DAMGO was added as indicated in the graph. The cell surface receptor expression was measured by ELISA. Control (basal) was set to 100%. Data are represented as mean ± SEM of four independent experiments performed in triplicate. Statistical analysis was performed by one-way ANOVA followed by Tukey post hoc test for multiple comparisons (* $P < 0.05$, compared to DAMGO; $^{\#}$ $P < 0.05$, compared to control; NS, not statistically significant compared to control; ns, not statistically significant compared to DAMGO).

4.3 Discussion

This thesis sought to identify more potent or more selective GRK inhibitors based on the structure of cmpd101. Here, colleagues at the University of Bath synthesised some novel cmpd101 analogues (see Table 4.1 for their structures), with the aim of determining their abilities to inhibit agonist-induced arrestin-3 recruitment to MOPr or DOPr; as a proxy of GRK-induced phosphorylation of the receptor. These novel compounds were screened to determine their ability to inhibit arrestin-3 recruitment in HEK239 cells transiently expressing MOPr or DOPr. In the initial screening, each compound was tested at a single high concentration (100 µM). I found that, at this concentration, compounds BU14016, BU16005 and BU16007 showed slightly higher inhibition than cmpd101; however, it was not a statistically significant difference from cmpd101 (Figure 4.2), while compounds BU16006, BU14017 and BU16009 showed similar inhibition to cmpd101 (Figure 4.2). The other compounds, BU14013 and BU14014, showed less inhibition (Figure 4.2). Among the compounds, BU14016, BU16005 and BU16007 inhibit arrestin-3 recruitment to MOPr by more than 60% at 100 µM. Therefore, I report here new potential GRK inhibitors, BU14016, BU16005 and BU16007, effective at inhibiting DAMGO-induced arrestin-3 recruitment to MOPr. I show that these compounds exhibit effective inhibition of arrestin-3 recruitment when applied at concentrations of 100 µM as well as 30 µM.

Surprisingly, when compounds were applied at 100 µM with regard to morphine-induced arrestin-3 recruitment, most of the inhibitors appeared to either have no effect or to be activators rather than inhibitors, except for BU14016 and BU16005, which are weak inhibitors (Figure 4.5). However, at 30 µM, the trend for most of the inhibitors reversed, except for BU14013, which remains an activator (Figure 4.6). One possibility is that some of the inhibitors bind to GRK/s that involve and stabilise an active conformation. I further investigated this observation by undertaking time courses of BU14017 and BU14014 (Figure 4.7), which confirms BU14017 and BU14014 are modestly enhancing morphine-induced arrestin-3 recruitment.

The results showed that, at a high concentration (100 µM), compounds BU14016 and BU16007 achieved almost complete inhibition of arrestin recruitment (both ~

90%) while cmpd101 and BU16005 did not achieve complete inhibition of DAMGO-induced arrestin-3 recruitment to MOPr. It is possible that these compounds do not inhibit another GRK/s involved in MOPr phosphorylation; therefore, some phosphorylation and arrestin recruitment takes place. Alternatively, the unexpected modest increase in arrestin recruitment that high concetration of some of these compounds produced could oppose the expected inhibition of recruitmetnt.

The results also show that cmpd101 and the novel compounds have distinct effect on of inhibition of arrestin-3 recruitment to MOPr depending upon the agonist used. Studies have found that Ser^{375} is the primary phosphorylation site in MOPr (Doll et al. 2011). In addition, it was reported that DAMGO stimulates the phosphorylation of multiple sites in MOPr, including Thr^{370} and Ser^{375}, while morphine stimulates the significant phosphorylation of Ser^{375} only (Doll et al. 2012). It has been reported that DAMGO phosphorylates Thr^{370} and Ser^{375} with GRK2 and GRK3 while morphine phosphorylates Ser^{375} with GRK5 (Doll et al. 2012). In addition, DAMGO phosphorylates the receptor more efficiently than morphine; thus, the level of DAMGO-arrestin-3 recruitment is higher (> 2-fold) than of morphine-induced as measured by BRET assay. Morphine-induced arrestin-3 recruitment to MOPr may not just depend upon phosphorylation, but instead on morphine-induced changes in receptor activation. This may in part explain why the inhibitors have no effect on arrestin-3 recruitment induced by morphine.

In the present study, I also investigated the activity of SNC80 and DADLE using HEK293 cells cotransfected with DOPr. The findings showed that cmpd101, BU16007, and BU14017 displayed a similar pattern in the inhibition of arrestin-3 recruitment induced by each agonist (see Figures 4.8 and 4.10). The compounds cmpd101, BU16007, and BU14017 exhibited comparable ability to inhibition of arrestin-3 recruitment to DOPr induced by either SNC80 or DADLE. However, the rest of the compounds did not show any inhibition of arrestin-3 recruitment to DOPr induced by SNC80 or DADLE. The reasons for this are presently unclear, but could be attributed to the possibility that SNC80- and DADLE-induced phosphorylation of DOPr involve the GRK/s that are not inhibited by the other experimental inhibitors. In HEK293 cells stably expressing HA-DOPr, both SNC80 and DADLE induced

robust phosphorylation of Thr^{361} and Ser^{363}, which are the major phosphorylation sites of DOPr (Mann et al. 2020).

One unanticipated finding was that the novel compounds showed relatively little inhibition of arrestin-3 recruitment to DOPr. Studies have shown that MOPr and DOPr are phosphorylated at different sites (Doll et al. 2011; Doll et al. 2012; Guo et al. 2000). It has been shown that DOPr is hierarchically phosphorylated by GRK2 at Ser^{363} and then at Thr^{358} (Guo et al. 2000). Using phosphosite-specific antibodies for the carboxy-terminal residues of the MOPr, it has been revealed that MOPr is phosphorylated at Ser^{363}, Thr^{370} and Ser^{375} (Doll et al. 2011). Based on these findings, the differences between MOPr and DOPr in terms of phosphorylation sites and different GRKs involved may explain why these analogues showed little inhibition. Further studies are needed to determine their selectivity and potency for GRK subtypes and explore their action on the downstream signalling.

It was observed that, at high concentration (100 μM), the novel compounds slightly increased basal (i.e., agonist-independent) arrestin-3 recruitment to MOPr, while at 30 μM the increase is much less; however, these changes were not statistically significant. Likewise, the novel compounds significantly increase basal arrestin-3 recruitment to DOPr at 100 μM except for BU14016 and BU16009. This could be that these inhibitors induce a receptor conformational change that able to engage with the arrestins in an agonist-independent manner.

BU14014 and BU14013 show the least inhibition of DAMGO-induced arrestin-3 recruitment compared to cmpd101 and other novel compounds. As expected, BU14014 and BU14013 did not affect G_i activation, while cmpd101 and BU14016 make 3- and 6-fold shift to the right of DAMGO-induced G_i activation curve. These findings are in line with the reported action of cmpd101 on G protein-coupled inwardly potassium channel (GIRK) activation. The previous study from our laboratory reported that cmpad101 (30 μM) partially reduced desensitisation of opioid-activated GIRK in locus coeruleus neurons. The reason for this is not clear, but it may have something to do with the non-specific effect of cmpd101 and BU14016.

Compounds BU14016 and BU16007, which show more effective or similar inhibition to cmpd101 with regard to DAMGO-induced arrestin-3 recruitment to MOPr, also significantly reduced DAMGO-induced internalisation, possibly through inhibiting GRK/s. On the other hand, compound BU14013, which fails to inhibit DAMGO-induced arrestin-3 recruitment to MOPr, was not able to block MOPr internalisation. A possible explanation for this might be that BU14013 is not able to inhibit GRK/s that involved in MOPr internalisation. Alternatively, cell permeability plays a major role in determining the efficacy of compounds in cells. For example, the recently developed GRK inhibitor compounds CCG224406 and CCG215022, potent GRK2 inhibitors with IC_{50} values of 0.13 μM and 0.15 μM respectively, show poor cell permeability when tested in a parallel artificial membrane permeation assay; thus, they have failed to inhibit DAMGO-induced MOPr internalisation in HEK293 and U2OS cell line (Bouley, RA et al. 2020). However, Rainbow et al. (2018) reported that CCG215022 strongly inhibited Ang-II induced desensitisation of AT1R. Since we do not have the facility to measure the lipophilicity, which is an indicator of cell permeability, of the novel compounds, the partition coefficient (LogP) values were calculated using ChemDraw professional 16 (PerkinElmer Informatics). The summary of the cell permeability parameters of the cmpd101 and the novel compounds are shown in Table 4.1. Most novel compounds have estimated logP values under 5 (Table 4.1), which are considered cell permeable (Lipinski et al. 2001). We would not expect BU16005 and BU16007 to penenterate the cell particularly well because they have logP values of 5.1 and 6.1, respectively (Table 4.1). However, BU16005 and BU16007 are the most effective at inhibiting DAMGO-induced arrestin-3 recruitment to MOPr. Hence, the estimated logP values do not correlate with the cellular activity of the novel compounds; nevertheless, the influence of cell permeability cannot be ruled out.

This thesis sought to investigate the importance of the pyridinyl-triazole moiety and the role of hydrogen bond donor and acceptor groups in their activity. To explore this idea, the A/B rings of cmpd101 were replaced by naphthyl rings, as in BU16007 and BU16006, or quinoline ring, as in BU16005 (see Table 4.1). Also, looking at the importance of the hydrogen bond donor and acceptor groups in the middle of the

molecule, the amide group and CH_2NH group were replaced by a double bond, as in compounds BU14013 and BU14014, respectively (Table 4.1).

Molecular modelling conducted by Mehrnoosh Ostovar (University of Bath; unpublished) of selected analogues (BU14014 and BU16009) with GRK2 (Figure 4.16) revealed that the lack of an NH group between rings B and C might contribute to the lower potency for inhibition of GRK activity and, hence, arrestin-3 recruitment. This is supported by our results where BU14014 and BU16009 exhibited reduced abilities to inhibit arrestin-3 recruitment. Another example, BU14013, which is missing an amide group between ring C and D compared to cmpd101, shows lower inhibition of DAMGO-induced arrestin-3 recruitment to MOPr. The low inhibition of BU14013 could be explained by the lack of hydrogen bond formation in this region with the GRK2. On the other hand, BU16006, which contains a naphthyl group (A/B rings) instead of the pyridyl 1,2,4-triazole (A/B rings) in cmpd101, shows similar inhibition of DAMGO-induced arrestin-3 recruitment to MOPr as cmpd101. This suggests that the formation of hydrogen bond in this region with GRK2 does not seem to give any advantage in enhancing the potency of the inhibitor.

The ATP binding site of the kinase is composed of the adenine, ribose, triphosphate and hydrophobic subsites (Thal et al. 2011). The amino group and C ring of cmpd101 occupy the triphosphate subsite forming hydrogen bonds with the side chain of Asp^{335} and Lys^{220} (Homan & Tesmer 2015; Thal et al. 2011). In addition, replacing the pyridyl 1,2,4-triazole in cmpd101 with a naphthyl ring did not improve the potency towards GRK2. Thal et al. (2011) observed that compounds forming fewer hydrogen bonds are more selective for GRK2. Thus, H-bond formation does not play a major role in the potency of cmpd101. Our results supported this idea that neither BU16007 nor BU16006 displayed significant improvements in the inhibition of arrestin-3 recruitment to MOPr compared to cmpd101.

Bouley, RA et al. (2020) developed a new paroxetine derivative (CCG258747) (Figure 4.1) that showed potent and selective inhibition of GRK2 (IC_{50}= 18 nM) over GRK1, GRK5, PKA and ROCK1. The crystal structure of CCG258747 complexed with GRK2-$G_{\beta\gamma}$ showed the interactions of the inhibitor with the GRK2 kinase domain. Importantly, the addition of the indazole D-ring of CCG258747 played a role

in the potency of the inhibitor while the benzodioxole ring influenced the selectivity (Bouley, RA et al. 2020). Previous studies of GRK2 inhibitors have revealed that interactions with hydrophobic subsites of the kinase influence the potency of inhibition (Homan & Tesmer 2015). The synthesis of a compound that is structurally related to GSK180736A, a compound analogue to paroxetine, by mimicking the difluoro benzyl amide of compound103 has shown great potency and selectivity for GRK2 (Waldschmidt et al. 2016). Thus, modification of the D-ring of cmpd101 plays a major role in the potency and selectivity. This can be reflected in our results that BU14016 displayed more effective inhibition of arrestin-3 recruitment to MOPr than cmpd101.

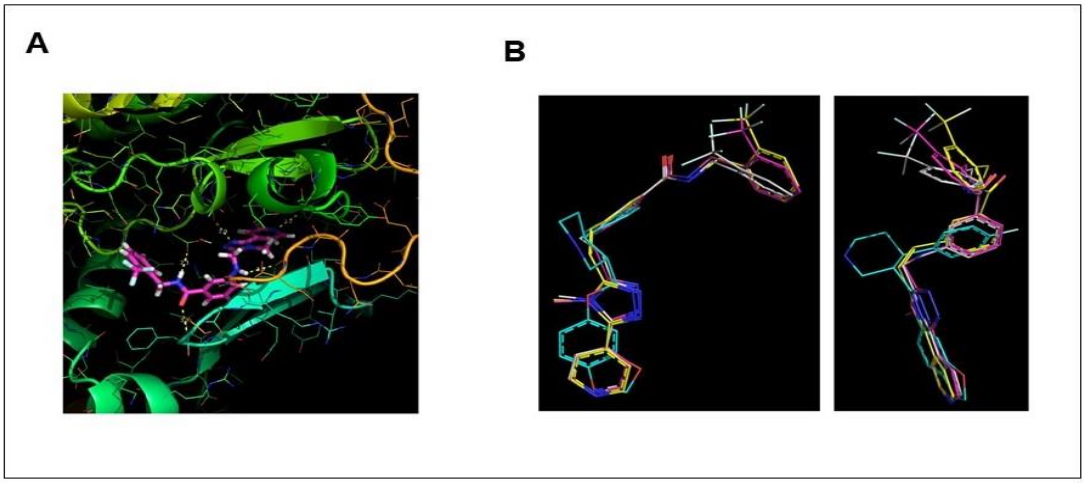

Figure 4.16 Molecular docking of cmpd101, BU14014 and BU16009

The molecular docking studies show: A) The docked pose of cmpd101 (purple) in the GRK2 binding site. The dashed yellow lines indicate hydrogen bonds (lengths are shown in Å). The protein secondary structure is shown as an animation coloured red at the C-terminus, through orange, yellow and green to blue at the N-terminus. B) Overlay of the crystal structure (PDB Code 3V5W) ligand (cyan) with the docked poses of cmpd101 (pink), BU14014 (cis) (yellow), and BU16009 (white). This docking study is taken from Ostovar et al. (University of Bath, unpublished).

4.4 Conclusion

Our colleagues at the University of Bath synthesised a small library of compounds based on the GRK inhibitor cmpd101 in which A/B rings, amide group, or D ring of cmpd101 were replaced by a variety of functional groups. I have determined in part

the ability of these compounds to inhibit GRK/s using arrestin-3 recruitment as a proxy assay. I show here that cmpd101 shows similar inhibition of agonist-induced arrestin-3 recruitment to MOPr and DOPr. I have found that modification of A/B or D rings of cmpd101 lead to a minor improvement in the inhibition of agonist-induced arrestin-3 recruitment. Also, I have found that the compounds BU14016, BU16007, BU16006 and BU16005 are just as effective as cmpd101 in inhibition of arrestin-3 recruitment to MOPr. However, the ability of the different test compounds to inhibit arrestin-3 recruitment to a GPCR is agonist-dependent (DAMGO versus morphine) and receptor-dependent (MOPr versus DOPr). The reasons for such differences are not always apparent and will require further study.

Furthermore, the data presented here suggest that compounds BU16007, BU16005 and BU14016 are effective inhibitors of GRKs. Based on these findings, it seems promising to further investigate the replacement of A/B or D ring of cmpd101 to further improve GRKs' potency. Altogether, these new cmpd101 analogues represent a good start to design small molecule inhibitors that can be used to explore the roles of the individual GRKs. In the next chapter, studies will be directed towards determining the selectivity of cmpd101 and the novel compounds for different GRK subtypes.

CHAPTER 5 The Selectivity of Compound101 and Novel Compounds for Inhibition of GRK Subtypes

5.1 Introduction

GRKs phosphorylate GPCRs on the C-terminus and/or intracellular loops, which plays a vital role in receptor desensitisation and trafficking (Gurevich, Vsevolod V., Gurevich & Tesmer 2016). In recent years, research has focused on GRKs due to the finding that altered levels or activity of some GRKs, in particular, GRK2 and GRK5, may play a role in certain diseases (Murga et al. 2019). Studies have shown that GRK2 and GRK5 play a critical role in heart failure (Belmonte & Blaxall 2011). Thus, selective GRK inhibitors could be used as therapeutic agents in diseases where GRKs play a role. Accumulating studies have confirmed the benefit of inhibition of GRK2 in an animal model of heart failure (Cannavo, Liccardo & Koch 2013). The first studies used β-ARKct, a peptide inhibitor of GRK2, expressed in mice which could enhance cardiac function (Koch, WJ et al. 1995). Also, β-ARKct expressed in mice has been reported to show beneficial effects in dilated cardiomyopathy (Rockman et al. 1998) and hypertrophic cardiomyopathy (Freeman et al. 2001; Harding et al. 2001). Recently, paroxetine, an FDA approved selective serotonin reuptake inhibitor, has been identified as GRK2 inhibitor (Thal et al. 2011). In mouse models, paroxetine has been shown to increase the myocyte contractility (Sato et al. 2015; Thal et al. 2012).

Apart from development as therapeutic agents, selective GRK inhibitors would help in studying the physiological functions of individual GRK isoform in the body as well as in specific tissues and cells. Several developed GRK inhibitors have already been used to study the role of GRKs in regulating GPCR signal (Birdsong & Williams 2020; Lowe et al. 2015; Rainbow et al. 2018; Thal et al. 2011). Using selective and potent individual GRK isoforms inhibitors would lead to a better understanding of the significance of the role of GRKs in regulating GPCR signalling and in modulating physiological processes. For example, there is increasing evidence of the beneficial effect of inhibition of GRK2 and probably GRK5 in heart failure patients has led to the search for the development of selective inhibitors of GRK2 and GRK5. However, studies on the role of other GRK isoforms (GRK1, GRK4 and GRK7) are limited because of their tissue-limited expression and lack of selective inhibitors. Despite

all efforts to find a small molecule GRK inhibitor, the selective inhibitor of particular GRKs has, however, yet to be developed.

In this chapter, I aim to determine the selectivity of the cmpd101 and novel inhibitors towards GRK isoforms. The arrestin-3 recruitment assay, with cellular overexpression of GRK isoforms (GRK2, GRK3, GRK5 and GRK6) will be employed to explore the kinase selectivity towards our inhibitors. The inhibitors to be used in this part of the study have been chosen because, in earlier chapters, they show either extensive inhibition of arrestin-3 recruitment compared to cmpd101, or alternatively little or no inhibition.

5.2 Results

5.2.1 GRK Overexpression Increases Agonist-induced Arrestin-3 Recruitment

An investigation of the selectivity of cmpd101 and its analogues towards arrestin-3 recruitment mediated by different GRK isoforms (GRK2, GRK3, GRK5 and GRK6) in HEK293 cells was first undertaken. HEK293 cells were transiently transfected with MOPr-RLuc2 or DOPr-RLuc2 and Arr3-GFP in the presence of overexpressed GRK isoforms. Again, the BRET assay was used to measure the interaction between the MOPr or DOPr and Arr3 in the presence of the overexpressed GRKs.

GRK isoform protein overexpression was assessed by Western blot. The GRK2 (80 kDa), GRK3 (80 kDa), GRK5 (66 kDa), and GRK6 (68 kDa) bands were detected at the expected molecular weights (Figure 5.1) in agreement with previously published reports (Doll et al. 2012). The results showed a marked increase of GRK2 expression compared to the endogenous GRK2 (Figure 5.1). The results also showed the overexpression of the GRK3, GRK5 and GRK6; however, the antibodies used were not able to detect endogenous GRK3, GRK5 or GRK6 (Figure 5.1).

The influence of overexpression of GRK isoforms on arrestin-3 recruitment was then investigated using the BRET assay. Compared to previous results reported in this thesis (Chapter 4, Figures 4.3 and 4.6), transfection with pcDNA3.1 had no effect on DAMGO- or morphine-induced arrestin-3 recruitment to MOPr. In pcDNA3.1-contransfected cells, DAMGO and morphine-induced arrestin recruitment similar to that induced in non-pcDNA3.1 transfected cells (compare Figures 5.4 and 5.7 with Figures 4.3 and 4.6). The overexpression of GRK isoforms resulted in an increase in both DAMGO- and morphine-induced arrestin-3 recruitment to MOPr (Figures 5.2, 5.3 and Table 5.1). It was observed that, although the overexpression of GRK isoforms increased the efficacy of DAMGO and morphine, it did not significantly change the basal levels of arrestin-3 recruitment (Figures 5.2, 5.3 and Table 5.1).

I then investigated arrestin-3 recruitment in HEK293 transfected with MOPr and different GRK isoforms (overexpression of GRK2, GRK3, GRK5 or GRK6). This

represented an attempt to investigate the selectivity of the novel compounds for different GRK subtypes, although, of course, any endogenous GRKs would presumably still be active. As a control, some cells were transfected with pcDNA3.1 alone (Figure 5.4). Cells were pretreated with cmpd101 or the novel compounds (30 μM) and then stimulated with DAMGO (10 μM). The results showed that cotransfection with pcDNA3.1 generally did not affect the ability of the novel inhibitors to inhibit arrestin-3 recruitment to MOPr as compared with previous results in this thesis (Chapter 4, Figure 4.3). Figures 5.5 and 5.6 show that cmpd101 at 30 μM seems to be a more effective inhibitor in cells where GRK2 (95%) and GRK3 (95%) are overexpressed, and less so in cells where GRK5 (70%) and GRK6 (70%) are overexpressed compared to pcDNA3.1-treated cells (Figure 5.10). These results also show that BU14016, BU16005 and BU16007 were effective inhibitors of arrestin-3 recruitment in the presence of overexpression of all four GRKs tested. Of these, BU14016 at 30 μM was in each case a somewhat weaker inhibitor than the other three compounds. Although BU16006 and BU14017 did not significantly inhibit DAMGO-stimulated arrestin-3 recruitment in vector-treated cells (Figure 5.4), they did significantly inhibit arrestin-3 recruitment in the presence of overexpression of all four of the GRKs tested (Figures 5.5 and 5.6). However, in the previous chapter BU14017 (30 μM) significantly inhibited DAMGO-stimulated arrestin-3 recruitment (Figure 4.3). Furthermore, in the presence of overexpression of GRK isoforms, BU16009, BU14013 and BU14914 remained unable to significantly inhibit DAMGO-induced arrestin-3 recruitment (apart from BU14013 versus GRK6) (Figures 5.5 and 5.6). The results also demonstrated an apparent lack of selectivity of the compounds for inhibition of the different GRKs, as the effective inhibitors displayed the same pattern of inhibition irrespective of the GRK subtype overexpressed. In summary, overexpression of GRK isoforms marginally changed the inhibition pattern of novel inhibitors of DAMGO-induced arrestin-3 recruitment (see summary in Figure 5.10).

In pcDNA3.1 cotransfected cells, only BU116007 showed significant inhibition of morphine-induced arrestin-3 recruitment while cmpd101 and other compounds were ineffective (Figure 5.7), which is similar to the results obtained in the previous chapter with no pcDNA3.1 transfected (Figure 4.5). In morphine-stimulated cells, cmpd101 significantly inhibited arrestin-3 recruitment in the presence of

overexpressed GRK2, GRK3, or GRK5 (Figures 5.8 and 5.9A). On the other hand, overexpression of GRK6 did not affect the ability of cmpd101 to inhibit morphine-induced arrestin-3 recruitment compared to pcDNA3.1-treated cells (Figure 5.9B). Compared to pcDNA3.1-treated cells (Figure 5.7), compounds BU16005 and BU16007 showed an increase in the inhibition of arrestin-3 recruitment in the presence of overexpressed GRK2 or GRK5 (Figures 5.8A and 5.9A). In contrast, overexpression of GRK3 or GRK6 did not affect the inhibitory ability of BU116005 compared to pcDNA3.1-treated cells. Overexpression of GRK3 or GRK6 also led to a decrease in the ability of BU116007 to inhibit arrestin-3 recruitment compared to vector-transfected cells (Figures 5.7, 5.8B and 5.9B). Overall, cmpd101, BU16005 and BU16007 only show an enhanced inhibition of morphine-induced arrestin-3 recruitment in overexpressed GRK cells compared to pcDNA3.1-treated cells (Figure 5.11).

5.2.2 Effect of GRK2 Overexpression on the Ability of cmpd101 or BU14016 to Inhibit concentration-dependent Arrestin-3 Recruitment to MOPr and DOPr

Next, I investigated the effect of GRK2 overexpression on the ability of cmpd101 and BU14016 to inhibit the concentration-dependent recruitment of arrestin-3 to MOPr and DOPr with DAMGO or SNC80 as agonists, respectively. The EC_{50}, E_{max} and Hill slope values from these experiments are summarised in Table 5.2. As expected, overexpression of GRK2 resulted in a marked increase in the potency of DAMGO, as well as the maximum response of this agonist (Figure 5.12). However, in marked contrast, in DOPr expressing cells, GRK2 overexpression did not lead to an increase in the potency of SNC80, or an increase in maximum response (Figure 5.13). As shown previously in this thesis, both cmpd101 and BU14016 (each 30 μM) effectively inhibited DAMGO-induced arrestin-3 recruitment to MOPr (see Figure 4.3). In the presence of overexpressed GRK2, cmpd101 remained a highly effective inhibitor of arrestin-3 recruitment to MOPr; however, BU14016 was less effective (Figure 5.12A). The EC_{50}, E_{max} and Hill slope values of DAMGO in the presence and absence of GRK2 overexpression are summarised in Table 5.3. For DOPr, whilst SNC80-induced arrestin-3 recruitment was inhibited by cmpd101 both in the

presence and absence of overexpressed GRK2, BU14016 was ineffective as an inhibitor in each case (Figure 5.13B and C). This latter reflected earlier findings in this thesis (see Figure 4.9). Moreover, overexpression of GRK2 significantly increased the basal level of arrestin-3 recruitment to DOPr (Figure 5.13A).

5.2.3 The Selectivity of cmpd101 and BU16007 for Inhibition of Arrestin-3 Recruitment Driven by Different GRK Isoforms

Next, the ability of cmpd101 and BU16007 (which in most cases appears to be a more potent inhibitor of DAMGO-induced arrestin-3 to MOPr than cmpd101) to inhibit DAMGO-induced arrestin-3 to MOPr in the presence of overexpressed GRKs was investigated. HEK293 cells were cotransfected with MOPr and GRK isoforms (GRK2, GRK3, GRK5, or GRK6). Cells were pretreated with cmpd101(0.001- 100 µM) or BU16007 (0.001- 100 µM) for 30 min and then stimulated with DAMGO (10 µM) for a further 10 min. Perhaps surprisingly, cmpd101 and BU16007 showed similar IC_{50} values irrespective of the GRK isoform tested (Figure 5.14). The IC_{50} values are summarised in Table 5.4. Moreover, the results also showed that BU16007 was more potent than cmpd101 in the presence of all GRK isoforms (Figure 5.14 and Table 5.4).

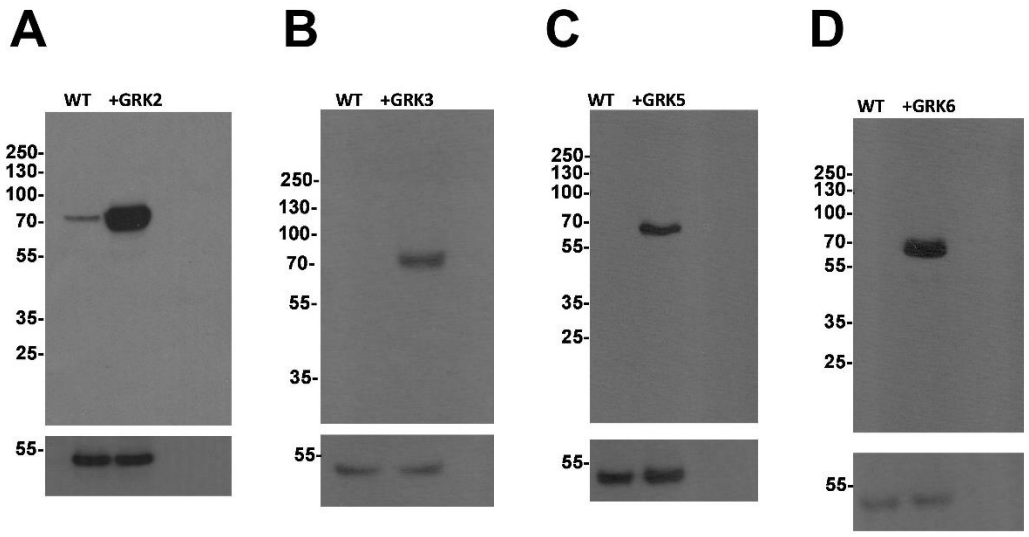

Figure 5.1 Analysis of GRK isoforms expression in HEK293 cells

Immunoblotting for GRK isoforms expressed endogenously (WT) in HEK293 cells, or transfected with A) GRK2, B) GRK3, C) GRK5 or D) GRK6. After 48h of transfection, cells were lysed and immunoblotted with antibodies to GRK2, GRK3, GRK5 or GRK6. Blots were then stripped and probed with anti-α-tubulin antibody to ensure equal loading. Representative blots of two independent experiments for each isoform are shown.

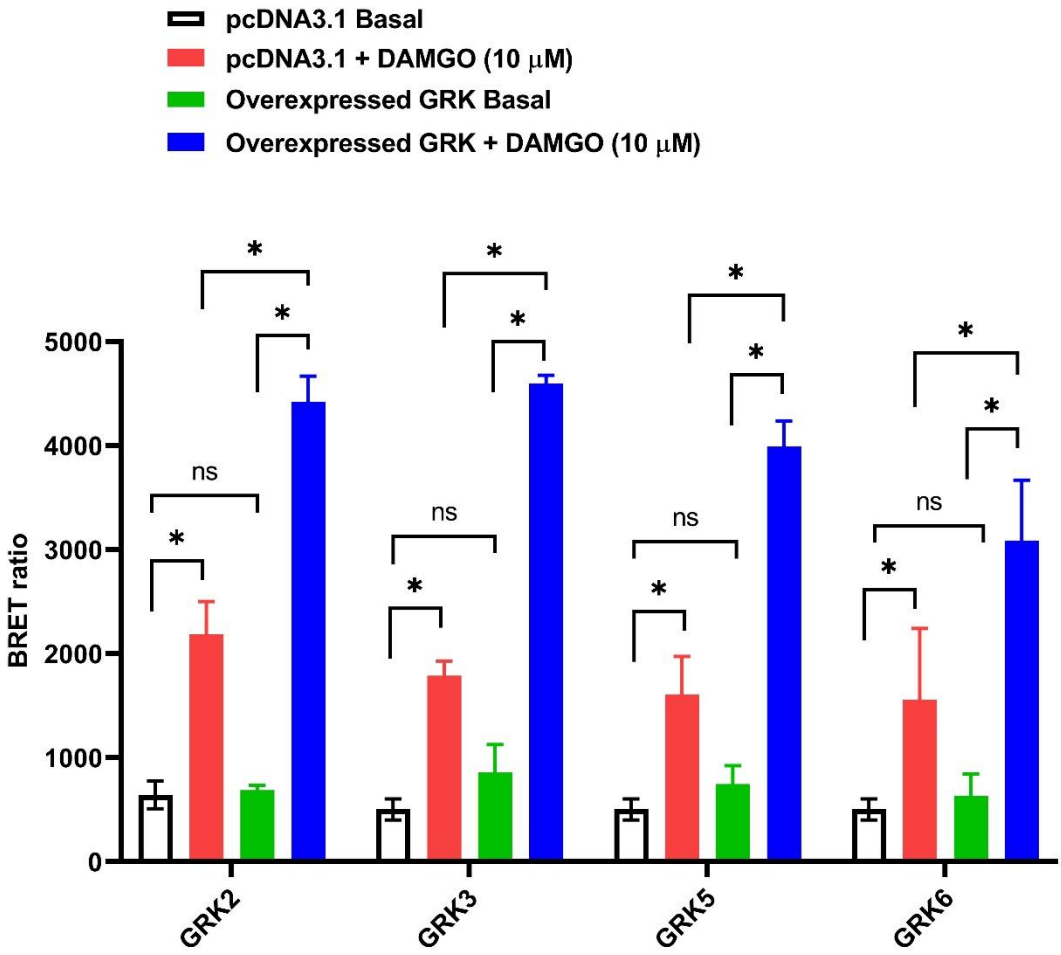

Figure 5.2 DAMGO-induced arrestin-3 recruitment to MOPr in the presence of overexpressed GRKs

HEK293 cells were transiently transfected with MOPr-RLuc2, Arr3-GFP and either pcDNA3.1, GRK2, GRK3, GRK5 or GRK6. Cells were stimulated with a saturating concentration of DAMGO (10 μM, where indicated in the graph legend) for 10 min and BRET measurements were then taken. * $P < 0.05$; ns, not statistically significant, two-way ANOVA followed by Tukey's multiple comparison test. Data are represented as mean ± SEM from four independent experiments, each performed in duplicate.

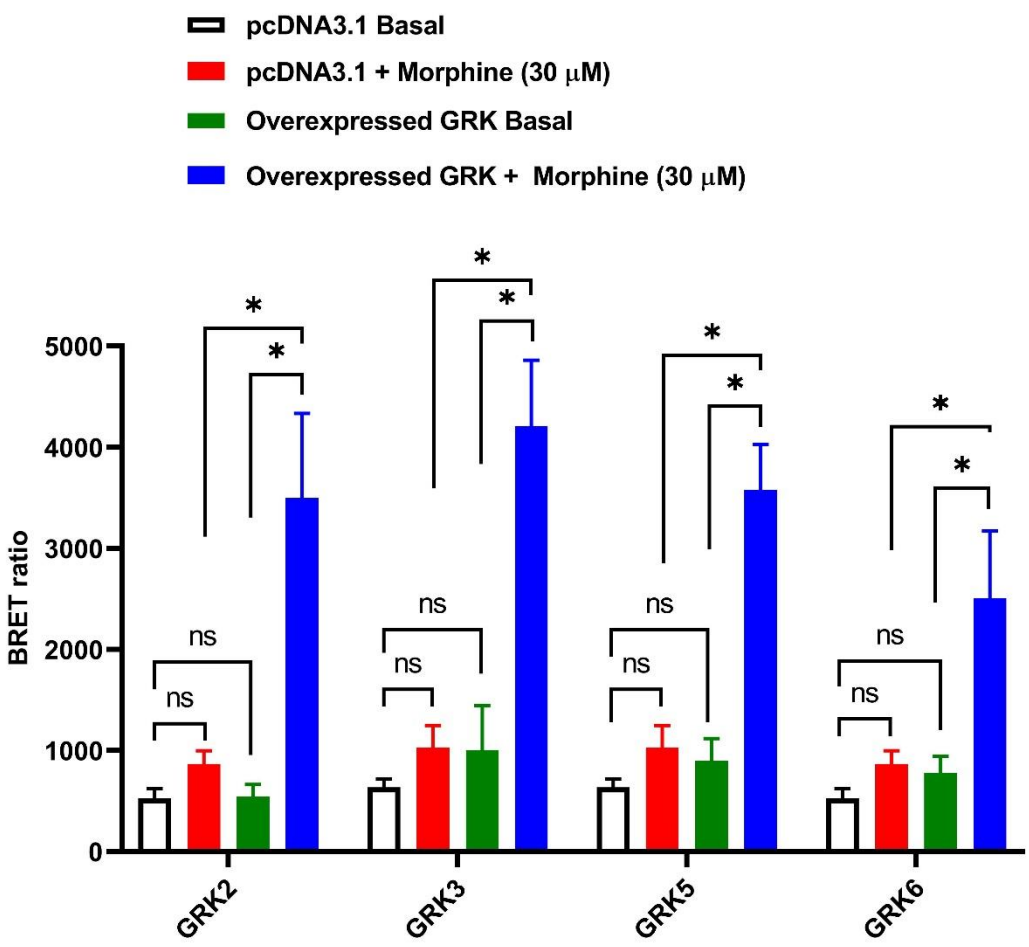

Figure 5.3 Morphine-induced arrestin-3 recruitment to MOPr in the presence of overexpressed GRKs

HEK293 cells were transiently transfected with MOPr-RLuc2, Arr3-GFP and either pcDNA3.1, GRK2, GRK3, GRK5 or GRK6. Cells were stimulated with morphine (30 μM, where indicated in the graph legend) for 10 min and BRET measurements were then taken. * $P < 0.05$; ns, not statistically significant, two-way ANOVA followed by Tukey's multiple comparison test. Data are represented as mean ± SEM from four independent experiments, each performed in duplicate.

Table 5.1 Fold change of agonist-induced arrestin recruitment in the presence of overexpressed GRK isoforms

	DAMGO	
	Basal	DAMGO
GRK2	1.1	2.3
GRK3	1.7	2.9
GRK5	1.5	3.7
GRK6	1.2	5.4
	Morphine	
	Basal	Morphine
GRK2	1.0	9.0
GRK3	1.4	10.3
GRK5	1.4	7.3
GRK6	1.5	2.6

The fold change values are taken from Figures 5.2 and 5.3.

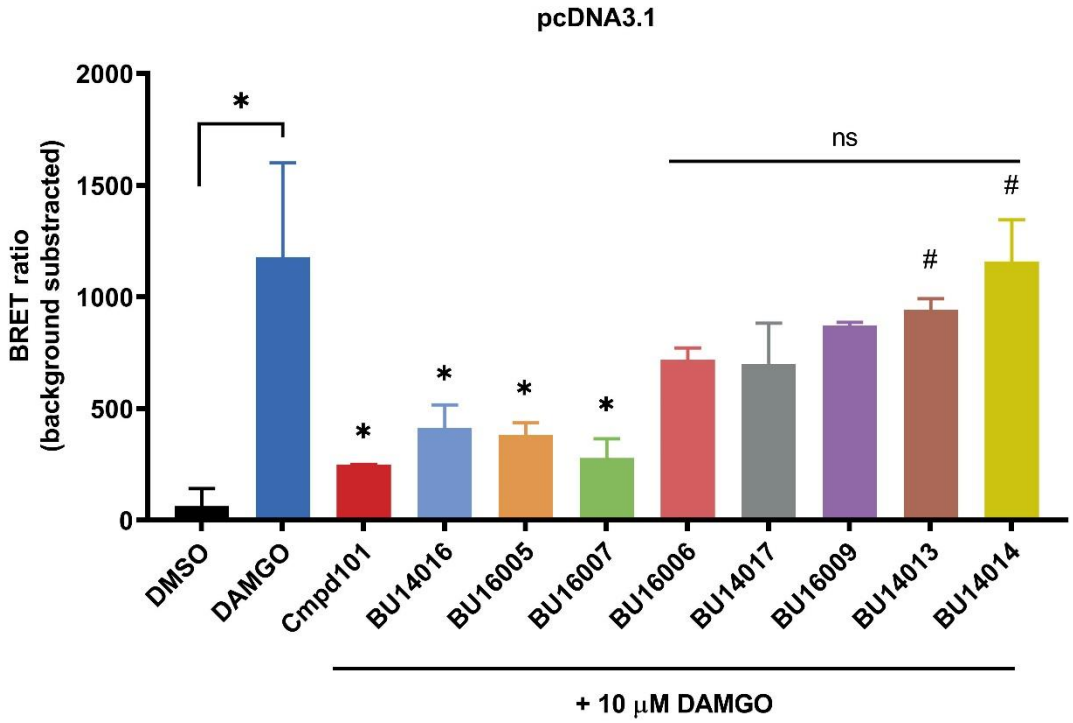

Figure 5.4 Effect of cmpd101 and novel compounds on DAMGO-induced arrestin-3 recruitment to MOPr in HEK293 cells transfected with pcDNA3.1

HEK293 cells were cotransfected with MOPr-RLuc2, Arr3-GFP and pcDNA3.1. Cells were preincubated with cmpd101 or novel compounds (all 30 µM) for 30 min and then stimulated with DAMGO (10 µM) for a further 10 min. The BRET ratio of no agonist-treated cells was subtracted from vehicle- or DAMGO-treated cells. * $P < 0.05$, compared to DAMGO; $^{\#}$ $P < 0.05$ compared to cmpd101; ns, not statistically significant compared to DAMGO, one-way ANOVA followed by Tukey's multiple comparison test. Data are represented as mean ± SEM from four independent experiments, each performed in duplicate.

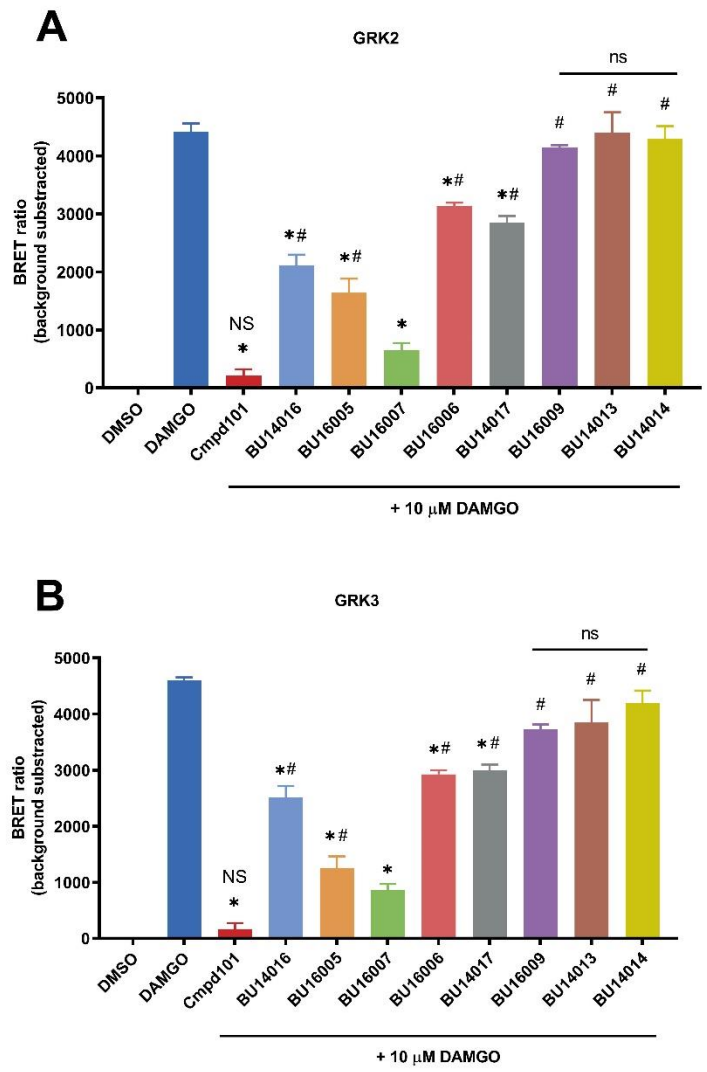

Figure 5.5 Effect of cmpd101 and novel compounds on DAMGO-induced arrestin-3 recruitment to MOPr in HEK293 cells transfected with GRK2 or GRK3

HEK293 cells were cotransfected with MOPr-RLuc2, Arr3-GFP and A) GRK2 or B) GRK3. Cells were preincubated with cmpd101 or novel compounds (all 30 µM) for 30 min and then stimulated with DAMGO (10 µM) for a further 10 min. The BRET ratio of no agonist-treated cells was subtracted from vehicle- or DAMGO-treated cells. * $P < 0.05$ compared to respective DAMGO; # $P < 0.05$ compared to cmpd101; ns, not statistically significant compared to DAMGO; NS, not statistically significant compared to DMSO, one-way ANOVA followed by Tukey's multiple comparison test. Data are represented as mean ± SEM from four independent experiments, each performed in duplicate.

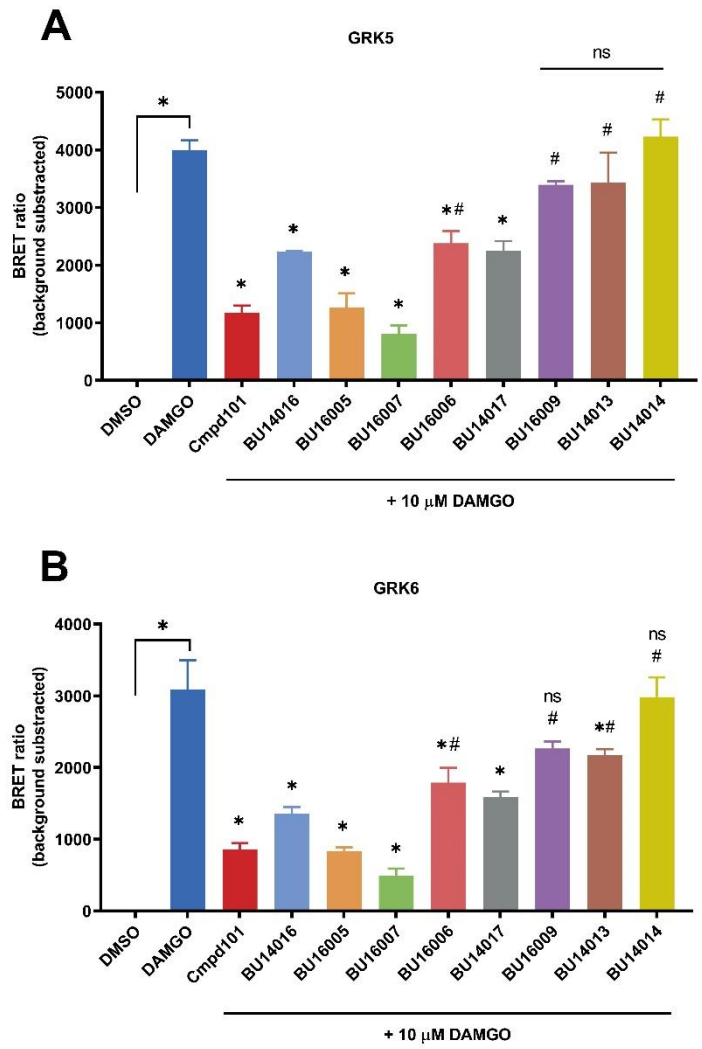

Figure 5.6 Effect of cmpd101 and novel compounds on DAMGO-induced arrestin-3 recruitment to MOPr in HEK293 cells transfected with GRK5 or GRK6

HEK293 cells were cotransfected with MOPr-RLuc2, Arr3-GFP and A) GRK5 or B) GRK6. Cells were preincubated with cmpd101 or novel compounds (all 30 μM) for 30 min and then stimulated with DAMGO (10 μM) for a further 10 min. The BRET ratio of no agonist-treated cells was subtracted from vehicle- or DAMGO-treated cells. * $P < 0.05$, compared to DAMGO, $^{\#}$ $P < 0.05$ compared to cmpd101; ns, not statistically significant compared to DAMGO, one-way ANOVA followed by Tukey's multiple comparison test. Data are represented as mean ± SEM from four independent experiments, each performed in duplicate.

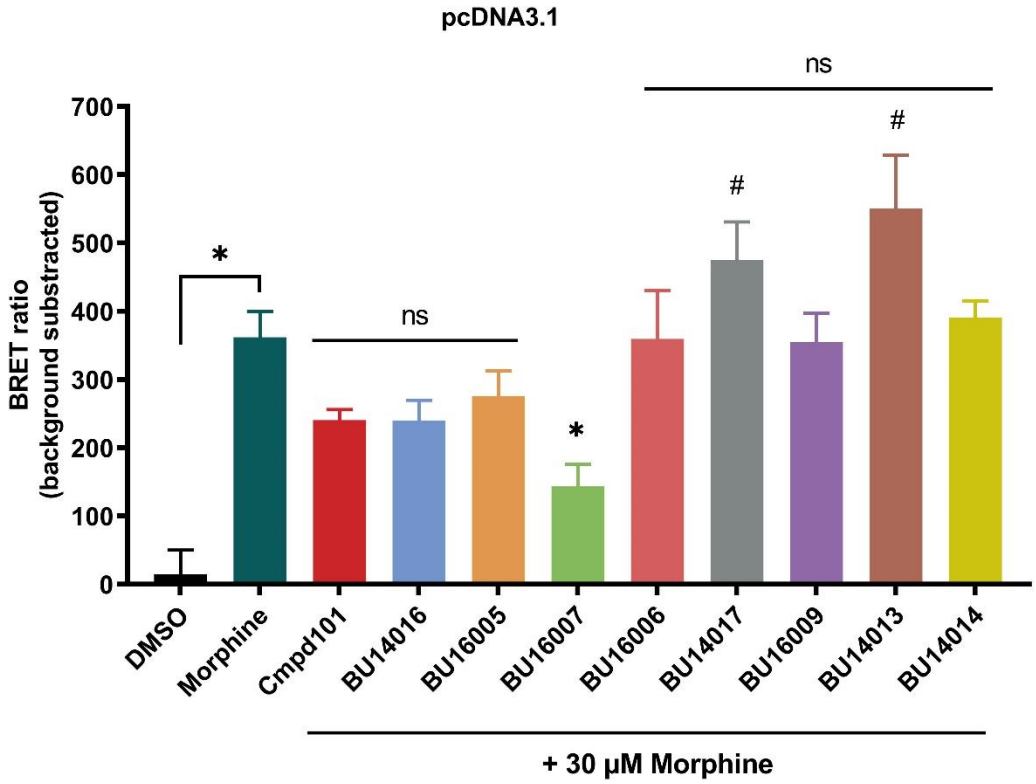

Figure 5.7 Effect of cmpd101 and novel compounds on morphine-induced arrestin-3 recruitment to MOPr in HEK293 cells transfected with pcDNA3.1

HEK293 cells were cotransfected with MOPr-RLuc2, Arr3-GFP and pcDNA3.1. Cells were preincubated with cmpd101 or novel compounds (all 30 µM) for 30 min and then stimulated with morphine (30 µM) for a further 10 min. The BRET ratio of no agonist-treated cells was subtracted from vehicle- or morphine-treated cells. * $P < 0.05$ compared to morphine; $^{\#}$ $P < 0.05$ compared to cmpd101; ns, not statistically significant compared to morphine, one-way ANOVA followed by Tukey's multiple comparison test. Data are represented as mean ± SEM from four independent experiments, each performed in duplicate.

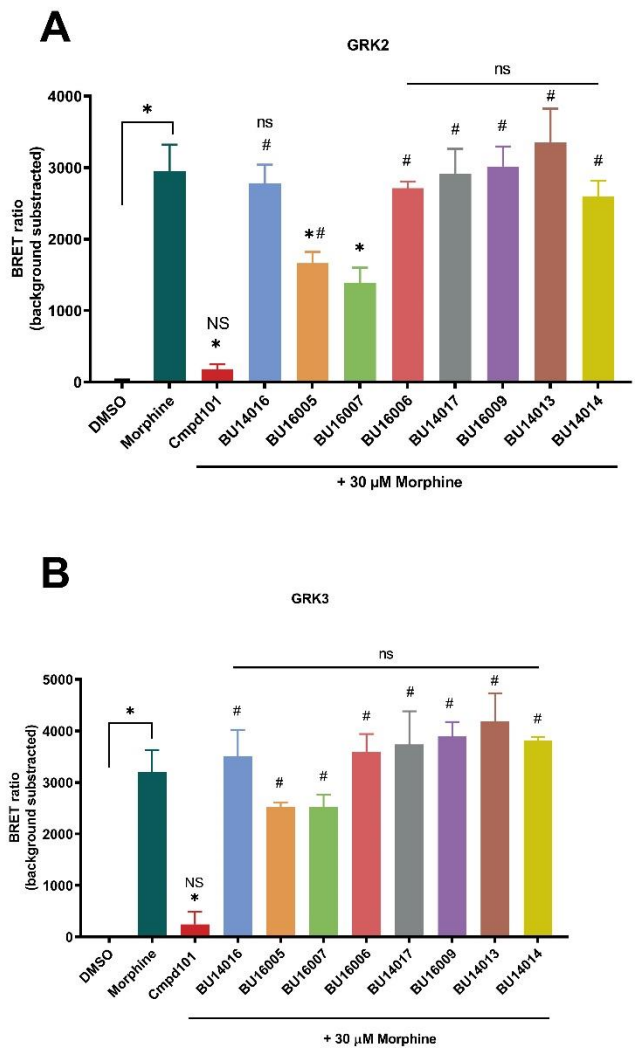

Figure 5.8 Effect of cmpd101 and novel compounds on morphine-induced arrestin-3 recruitment to MOPr in HEK293 cells transfected with GRK2 or GRK3

HEK293 cells were cotransfected with MOPr-RLuc2, Arr3-GFP and A) GRK2 or B) GRK3. Cells were preincubated with cmpd101 or novel compounds (each 30 µM) for 30 min and then stimulated with morphine (30 µM) for a further 10 min. The BRET ratio of no agonist-treated cells was subtracted from vehicle- or morphine-treated cells. * $P < 0.05$ compared to respective morphine alone; $^{\#}$ $P < 0.05$ compared to cmpd101; ns, not statistically significant compared to respective morphine, NS, not statistically significant compared to DMSO, one-way ANOVA followed by Tukey's multiple comparison test. Data are represented as mean ± SEM from four independent experiments, each performed in duplicate.

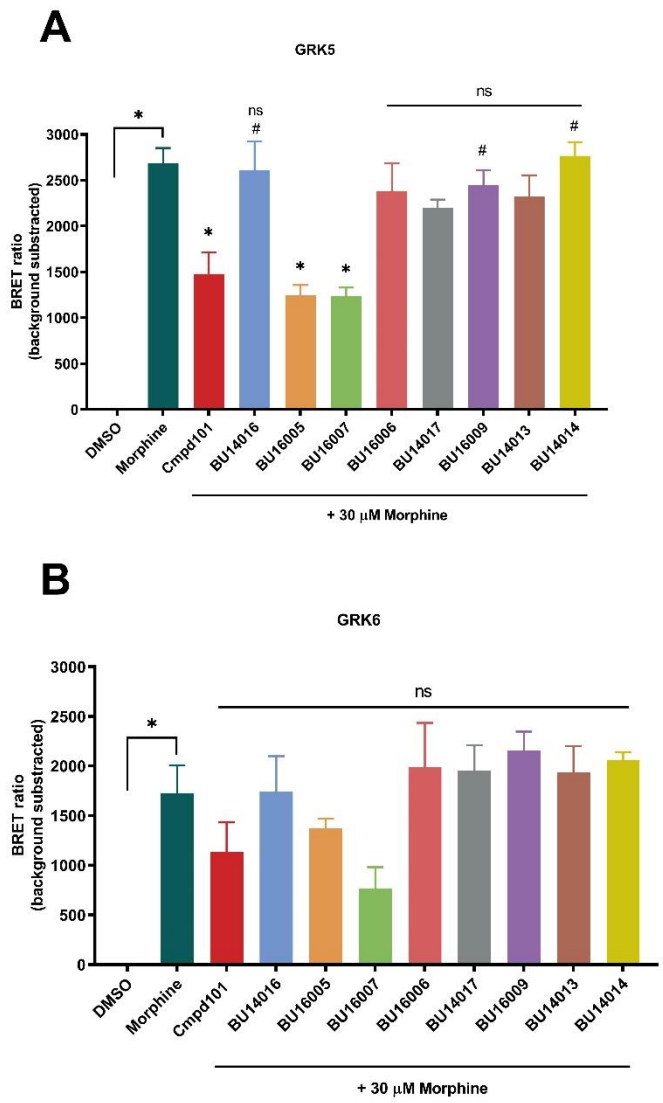

Figure 5.9 Effect of cmpd101 and novel compounds on morphine-induced arrestin-3 recruitment to MOPr in HEK293 cells transfected with GRK5 or GRK6

HEK293 cells were cotransfected with MOPr-RLuc2, Arr3-GFP and A) GRK5 or B) GRK6. Cells were preincubated with cmpd101 or novel compounds (each 30 μM) for 30 min and then stimulated with morphine (30 μM) for a further 10 min. The BRET ratio of no agonist-treated cells was subtracted from vehicle- or morphine-treated cells. * $P < 0.05$ compared to morphine alone, $^{\#}$ $P < 0.05$ compared to cmpd101; ns, not statistically significant compared to morphine, one-way ANOVA followed by Tukey's multiple comparison test. Data are represented as mean ± SEM from four independent experiments, each performed in duplicate.

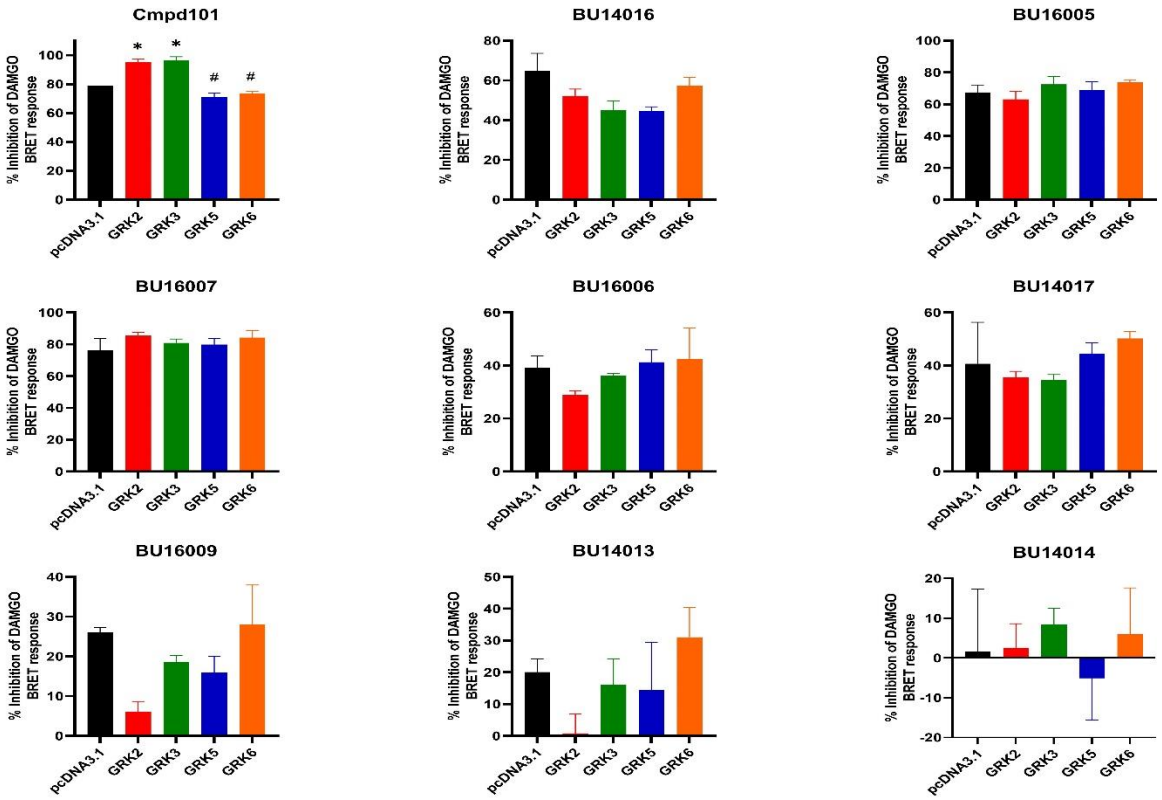

Figure 5.10 Percentage inhibition of DAMGO-induced arrestin-3 recruitment by cmpd101 and the novel compounds

This is a summary of Figures 5.4, 5.5 and 5.6. Data were normalised to the response induced by 10 μM DAMGO to give percentage inhibition of DAMGO-induced response. * $P < 0.05$ compared to pcDNA3.1, $^{\#}$ $P < 0.05$ compared to GRK2; one-way ANOVA followed by Tukey's multiple comparison test. Data are represented as mean ± SEM from four independent experiments, each performed in duplicate.

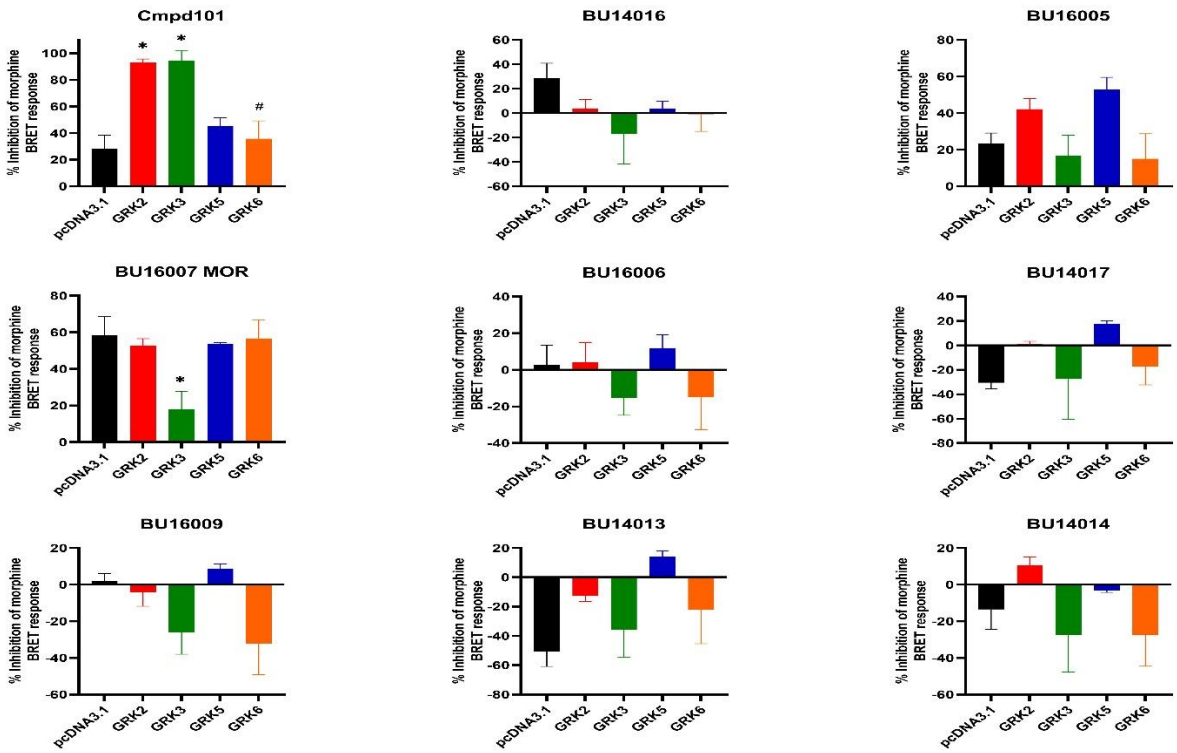

Figure 5.11 Percentage inhibition of morphine-induced arrestin-3 recruitment by cmpd101 and the novel compounds

This is a summary of Figures 5.7, 5.8 and 5.9. Data were normalised to the response induced by 30 µM morphine to give a percentage of morphine-induced response. * $P < 0.05$ compared to pcDNA3.1, $^{\#}$ $P < 0.05$ compared to GRK2; one-way ANOVA followed by Tukey's multiple comparison test. Data are represented as mean ± SEM from four independent experiments, each performed in duplicate.

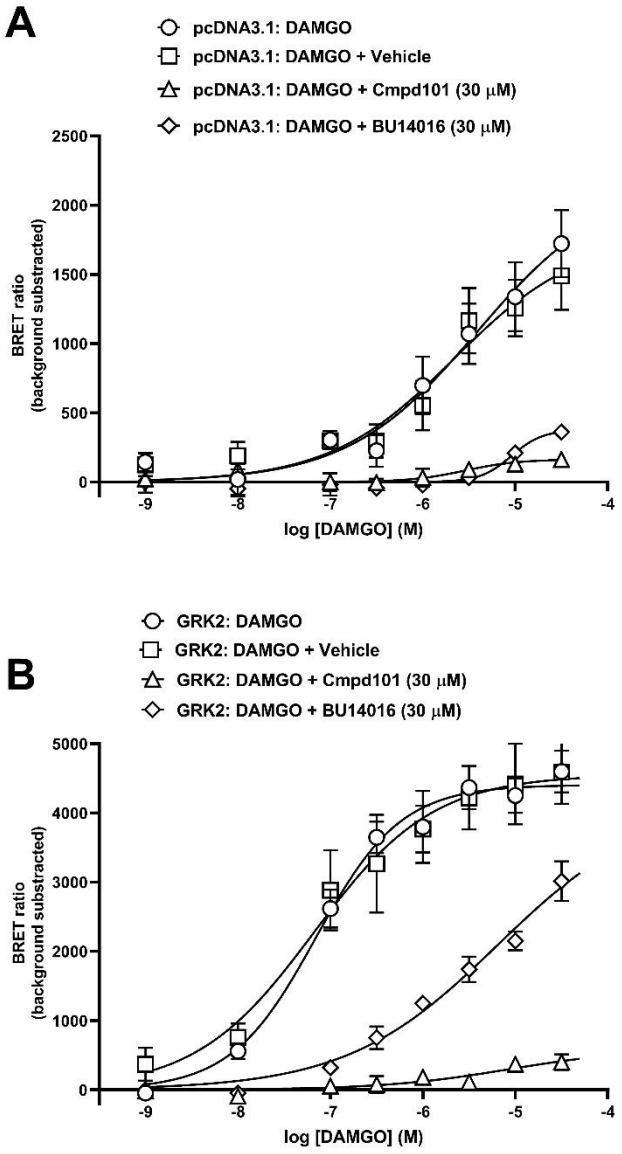

Figure 5.12 Inhibition of DAMGO-induced arrestin-3 recruitment to MOPr by 30 μM cmpd101 or BU14016 in absence or presence of GRK2 overexpression

HEK293 cells were transiently transfected with MOPr-RLuc2, Arr3-GFP and A) pcDNA3.1 or B) GRK2. Following this, Cmpd101 (30 μM), BU14016 (30 μM) or vehicle (0.3% DMSO) was added 30 min before the addition of DAMGO (0.001- 30 μM) for a further 10 min. The BRET ratio of non-agonist-treated cells was subtracted from that of DAMGO-treated cells. A and B, data were fitted to a non-linear regression model with four-parameters using GraphPad Prism v8 software and the bottom values of the curves constrained to zero. The resulting EC_{50}, E_{max} and Hill slope values are summarised in Table 5.1. Data are presented as mean ± SEM from four independent experiments, each performed in duplicate.

Table 5.2 EC_{50} and maximum response (E_{max}) values of DAMGO in the arrestin-3 recruitment assay

pcDNA3.1				
	DAMGO	DAMGO+ vehicle	DAMGO+ Cmpd101 (30 µM)	DAMGO+ BU14016 (30 µM)
EC_{50} (µM)	3.9 ± 2.0	2.2 ± 1.3	2.8 ± 1.5	9.1 ± 0.9
E_{max} (BRET ratio)	2,165 ± 663	1,779 ±312	163 ± 71	376 ± 43
Hill slope	0.6 ± 0.1	0.6 ± 0.4	1.5 ± 0.9	2.6 ± 2.1
GRK2 Overexpression				
	DAMGO	DAMGO+ vehicle	DAMGO+ Cmpd101 (30 µM)	DAMGO+ BU14016 (30 µM)
EC_{50} (µM)	0.1± 0.02	0.1 ± 0.06	8.6 ± 1.6	5.08 ± 0.2
E_{max} (BRET ratio)	4,406 ± 324	4,554 ± 341	598 ± 170*	3,016 ± 411
Hill slope	0.9 ± 0.08	0.7 ± 0.1	0.6 ± 0.7	0.6 ± 0.1

The values are taken from Figure 5.10. Data are expressed as mean ± SEM of four independent experiments, each performed in duplicate. * $P < 0.05$, compared to the respective DAMGO + vehicle or DAMGO alone, one-way ANOVA, followed by Tukey's multiple comparison test.

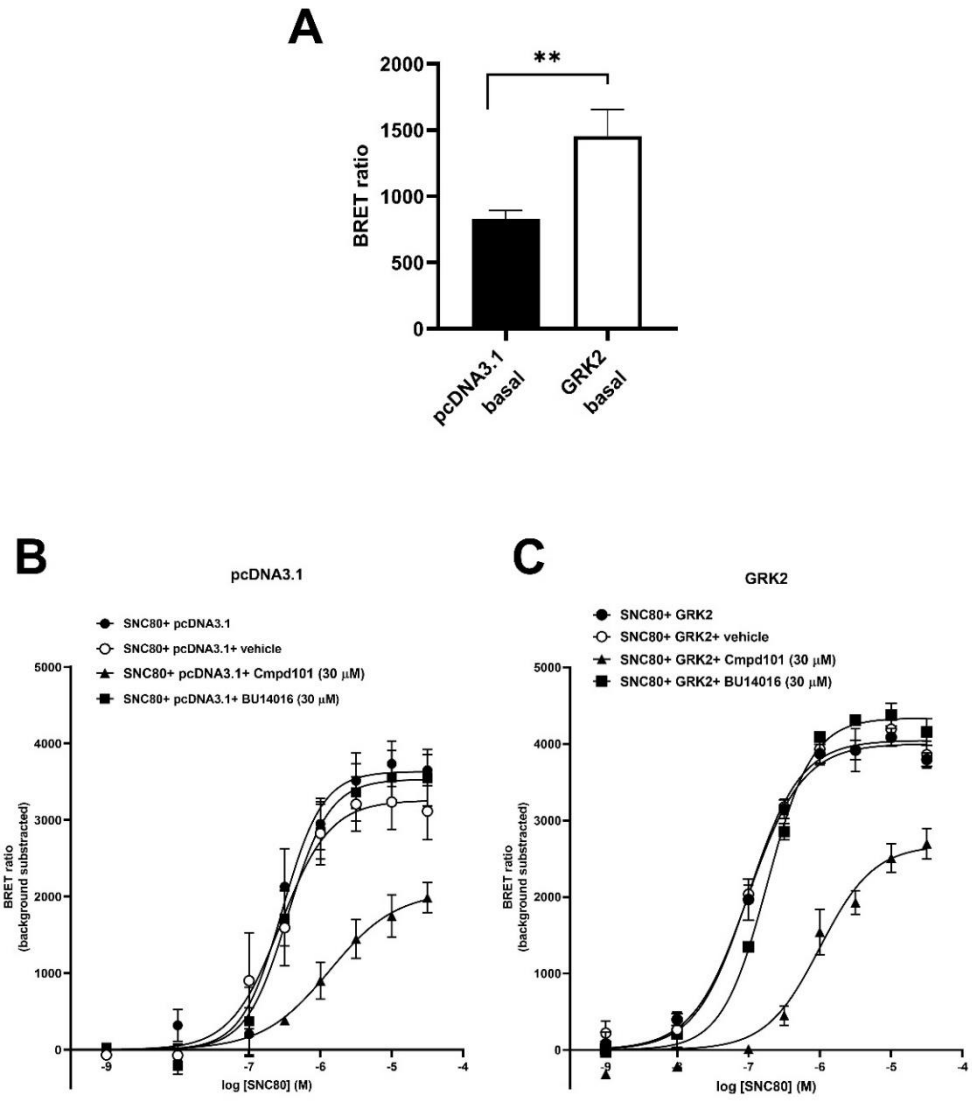

Figure 5.13 Inhibition of SNC80-induced arrestin-3 recruitment to DOPr by cmpd101 and BU14016 in the presence or absence of GRK2 overexpression

HEK293 cells were transiently transfected with DOPr-RLuc2, Arr3-GFP and A) pcDNA3.1 or B) GRK2. Cmpd101 (30 µM), BU14016 (30 µM) or vehicle (0.3% DMSO) was added 30 min before the addition of SNC80 (0.001- 30 µM) for a further 10 min. The BRET ratio of no agonist-treated cells was subtracted SNC80-treated cells. C) the BRET ratio of untreated cells of A and B. Data in A and B were fitted to a non-linear regression model with four-parameters using GraphPad Prism v8 software and the bottom values of the curves were constrained to zero. The EC_{50}, E_{max} and Hill slope values are summarised in Table 5.2. Data are presented as mean ± SEM from four independent experiments, each performed in duplicate.

Table 5.3 EC_{50} and maximum response (E_{max}) values of SNC80 in the arrestin-3 recruitment assay

	pcDNA3.1			
	SNC80	SNC80+ vehicle	SNC80+ Cmpd101 (30 μM)	SNC80+ BU14016 (30 μM)
EC_{50} (μM)	0.3 ± 0.1	0.3 ± 0.06	1.3 ± 0.7*	0.4 ± 0.07
E_{max} (BRET ratio)	3,635 ± 107	3,258 ± 371	2,065 ± 197	3,533 ± 404
Hill slope	1.5 ± 0.7	1.3 ± 0.6	0.9 ± 0.1	1.5 ± 0.3
	GRK2 Overexpression			
	SNC80	SNC80+ vehicle	SNC80+ Cmpd101 (30 μM)	SNC80+ BU14016 (30 μM)
EC_{50} (μM)	0.1 ± 0.02	0.1 ± 0.01	1.0 ±0.2	0.2 ± 0.02
E_{max} (BRET ratio)	4,002 ± 62	4,046 ± 229	2,677 ± 149*	4,339 ± 115
Hill slope	1.1 ± 0.1	1.2 ± 0.2	1.2 ± 0.01*	1.4 ± 0.1

The values are taken from Figure 5.11. Data are expressed as mean ± SEM of four independent experiments, each performed in duplicate. * $P < 0.05$, compared to respective SNC80 or SNC80 + vehicle; one-way ANOVA, followed by Tukey's multiple comparison test.

Table 5.4 IC_{50} values of cmpd101 and BU16007 for inhibition of arrestin-3 recruitment to MOPr in the presence of GRK isoforms

	GRK2	GRK3	GRK5	GRK6
Cmpd101 (μM)	7.4 ± 1.7	11.5 ± 12.4	16.9 ± 1.8	6.3 ± 6.5
BU16007 (μM)	2.9 ± 1.3	1.5 ± 1.0	2.3 ± 0.3	2.0 ± 1.1

The IC_{50} values are taken from Figure 5.14. The IC_{50} measurements are an average of four independent experiments, each performed in duplicate. Data are represented as mean ± SEM.

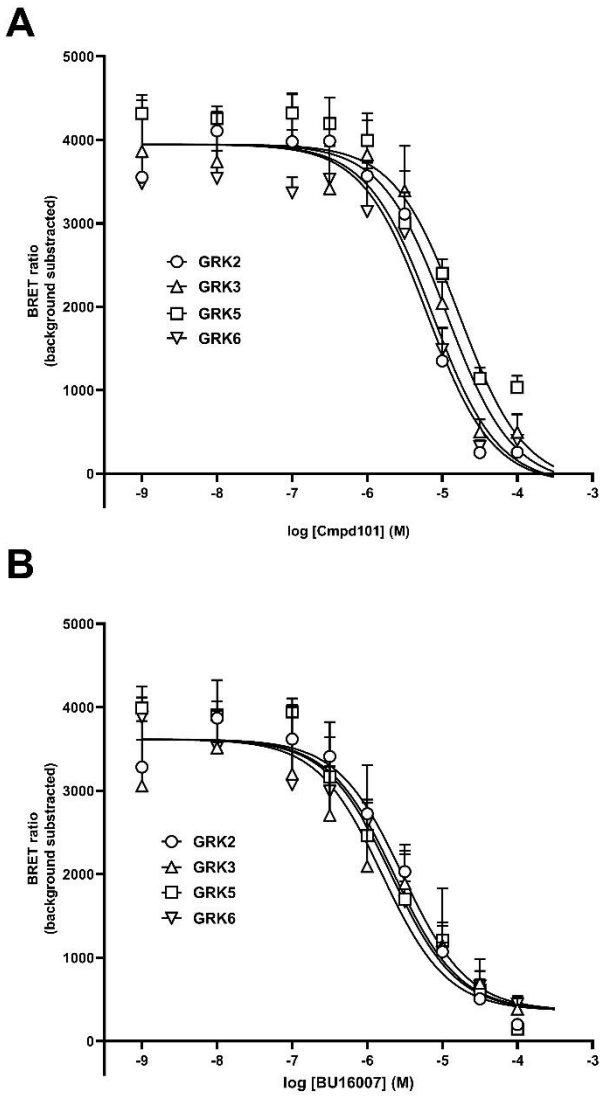

Figure 5.14 Concentration-dependent inhibition of DAMGO-stimulated arrestin-3 recruitment to MOPr by cmpd101 and BU16007 in the presence of overexpressed GRK isoforms

HEK293 cells were cotransfected with MOPr-RLuc2, Arr3-GFP and GRK2, GRK3, GRK5, or GRK6. Cells were preincubated with A) cmpd101 (0.001- 100 µM) or B) BU16007 (0.001- 100 µM) for 30 min and then stimulated with DAMGO (10 µM) for a further 10 min. The BRET ratio of no agonist-treated cells was subtracted DAMGO-treated cells. Data were fitted to a non-linear regression model with three parameters using GraphPad Prism v8 software. Data are represented as mean ± SEM of results from four independent experiments performed in duplicate.

5.3 Discussion

Cmpd101 has been used as a GRK inhibitor and often assumed to be a selective of GRK2/3 in many studies; however, our findings in previous chapters suggest that cmpd101 may also affect non-GRK targets. The selectivity of cmpd101 for GRKs has only been determined in a cell-free system (Thal et al. 2011). Thus, in this chapter, I have determined the selectivity of cmpd101 and novel inhibitors towards GRK isoforms (GRK2, GRK3, GRK5 and GRK6) in intact HEK293 cells transfected with MOPr or DOPr and overexpressed GRK isoforms, and the arrestin-3 recruitment was assessed by the BRET technique. Studying the effect of these inhibitors in HEK293 cells cotransfected with specific GRKs provides a simple means to initially detect differences in the selectivity of the novel compounds for GRK subtypes.

The selectivity of GRK inhibitors has previously been determined using different assays. For instance, purified GRK isoforms are convenient in studying the selectivity of an inhibitor for individual GRK isoform (Thal et al. 2011). However, the potency determined in a cell-free assay does not always correlate with that obtained in a cell-based assay. Another approach is using GRK knockout cells in order to overcome the influence of endogenous GRKs. One way to study inhibitor selectivity is using overexpressed GRK in cell-based assay, which is the assay used in this thesis because the other methods were not at this time feasible in our laboratory. Instead, HEK293 cells were used in the presence of transfected and overexpressed GRK isoforms. HEK293 endogenously express GRK2, GRK3, GRK5 and GRK6 (Violin, Ren & Lefkowitz 2006). Endogenous GRK2 was detectable in HEK293 cells using western blot, but it was not possible to detect endogenous GRK3, GRK5, or GRK6. This could be attributed to low expression of the GRK in question, or the lack of sensitivity of the antibodies used. Whilst it is also possible that endogenously expressed GRKs 3, 5 and 6 are absent from these particular HEK293 cells, this seems unlikely as other studies report their presence (Doll et al. 2012; Just et al. 2013).

Overexpression of GRKs enhanced the maximal efficacy of DAMGO and morphine. Also, overexpression of GRK2 enhanced the potency of DAMGO. This is in

agreement with the previous report that overexpression of GRK2/3 increased potency and efficacy of DAMGO- and morphine-induced arrestin-2 and -3 recruitment to MOPr (Miess et al. 2018). This can be explained by the efficiency and extent of arrestin-3 recruitment being largely dependent on the extent of GRK phosphorylation of the receptor (Miess et al. 2018). On the other hand, in the DOPr-transfected cells, overexpression of GRK2 enhanced neither the potency nor efficacy of SNC80 (Figure 5.12). Several reasons can explain these findings. One possibility is that DOPr is expressed in these cells at a greater level than MOPr; thus, the signal is enhanced. Another possible reason is due to the fact that DOPr is more efficient in recruiting arrestin-3 than MOPr (Lowe et al. 2002); therefore, DOPr recruits more arrestins that reflected in increasing the signal. Also, it is possible that SNC80 is more efficient in inducing DOPr phosphorylation (Mann et al. 2020), which is a prerequisite for arrestin recruitment and, thus, the signal is enhanced. Alternatively, these findings can be explained by the fact that I used a limited system where SNC80 is considered a full agonist and already recruits arrestin-3 to the maximum capacity. Thus, overexpression of GRK2 does not affect SNC80-induced arrestin-3 recruitment.

Nickolls et al. (2013) and Manglik et al. (2016) reported that the overexpression of GRK2 increased the basal arrestin-3 recruitment to MOPr. This differs from the findings presented here that overexpression of GRK2 does not cause an increase in the basal of DAMGO-induced arrestin-3 recruitment. On the other hand, overexpression of GRK2 enhanced the basal arrestin-3 recruitment to DOPr. It seems possible that these results are due to the high constitutive activity of DOPr (Mann et al. 2020; Neilan et al. 1999). Another possible reason is that arrestin recruitment depends on the level of GRK expression (Miess et al. 2018), considering both experiments were conducted at different times.

Studies have focused on developing selective inhibitors for GRK2 and GRK5 (Bouley, RA et al. 2020; Waldschmidt et al. 2018; Waldschmidt et al. 2017; Waldschmidt et al. 2016) because such inhibitors could potentially benefit patients with heart disease (Cannavo, Liccardo & Koch 2013). All small molecule inhibitors of GRK so far work through binding to the active site of the GRK domain, which is

conserved in all AGC kinases (Johnson, LN 2009). For instance, cmpd101 exhibits its selectivity for GRK2 through binding to the active site of GRK2 (Thal et al. 2011) in a way similar to that of balanol, a nonselective GRK inhibitor (Figure 5.15A and B) (Murga et al. 2019; Tesmer, JJ et al. 2010). The selectivity of cmpd101 mostly depends on the overall conformation of the GRK2 active site as opposed to cmpd101 interactions with specific GRK residues (Tesmer, VM et al. 2012; Thal et al. 2011). Recently, Bouley, R et al. (2017) have developed indazole and benzodioxole compounds derived from paroxetine to improve potency and selectivity towards inhibition of GRK2. Compared to paroxetine, the crystal structure of these compounds in complex with GRK2-$G_{\beta\gamma}$ shows a stronger interaction with the hinge of GRK2 and they also stabilise a different conformation of the kinase (Figure 5.15C and D) (Bouley, R et al. 2017; Murga et al. 2019). The compound CCG224061, one example of the indazole-paroxetine derivatives, shows a dramatic increase in potency for inhibition of GRK2 (20-fold) compared to paroxetine (Bouley, R et al. 2017). However, it also retains selectivity for GRK1, GRK5, PKA and ROCK1 (Bouley, R et al. 2017). Thus, the selectivity towards GRKs is not always easy to predict from the chemical structure of the inhibitors. Thus, finding potent and selective inhibitors for individual GRK remains a major aim in the field.

Cmpd101 is a commercially available small molecule inhibitor selective for GRK2/3 with an IC_{50} of 35 nM (Ikeda, S, Keneko & Fujiwara 2007) and 290 nM (Thal et al. 2011) determined in different *in vitro* assays. Also, cmpd101 has no significant inhibitory activity at GRK1 or GRK5 at concentrations up to 125 µM in a purified enzyme assay (Thal et al. 2011). However, our studies revealed surprisingly that cmpd101 does not appear to show any selectivity towards different GRK isoforms as assessed in these GRK isoform overexpression studies. These findings lead us to two possible conclusions: first, cmpd101 is not GRK2/3 selective, at least in HEK293 cells, or second, that, in our experimental system, GRK2 (endogenously present) initiates the phosphorylation of MOPr and this is followed by phosphorylation by other GRK isoforms leading to greater arrestin-3 recruitment. Therefore, this effect of endogenous GRKs cannot be ruled out in our study model. Also, it was observed that the pattern of inhibition by the novel compounds was similar across all overexpressed GRKs. Again, it seems possible that endogenous

GRK2/3 induces phosphorylation of Ser^{375} followed by multi-phosphorylation of flanking residues Thr^{370}, Thr^{376} and Thr^{379}, possibly by other kinases. This is evident when both cmpd101 and BU16007 showed similar IC_{50} values for inhibition of arrestin-3 recruitment regardless of overexpressed GRK isoform.

It is interesting to note that overexpression of GRKs did not affect inhibition of cmpd101 or BU14016 of arrestin-3 recruitment to DOPr, whereas it enhanced their inhibition in arrestin recruitment to MOPr. There are, however, several possible reasons for this inconsistency. First, it could be that DOPrs were expressed at a much higher level than MOPr in the cells. Second, it may be receptor-dependent where DOPr is more efficient in recruiting arrestin than MOPr upon stimulation with agonist, so that enhances the arrestin to the maximum. Third, it is possible that it is an agonist-dependent where SNC80 induced robust phosphorylation of the receptor, and thus enhanced arrestin affinity.

Cmpd101 has been reported to have an IC_{50} for GRK2/3 in the nanomolar range (Thal et al. 2011) while our studies in intact cells report IC_{50} values within the micromolar range. The likely reason for this is that our data are obtained from intact cells so that an inhibitor has to cross the cell membrane before reaching its target on the GRK (Rainbow et al. 2018). There is no published experimental measurement of the cell permeability parameters for cmpd101, only the predicted ones using professional software. The widely used measure of lipophilicity is log of the partition coefficient (logP), which is defined as the partition coefficient of a molecule between aqueous (water) and lipophilic (octanol) phases. The reported logP values of cmpd101 are 5.46 (XLogP; GuidetoPharmacology) and 3.2 (XLogP3-AA; PubChem). Since the data on the cell permeability parameters of the novel compounds are not available, the LogP values were calculated using ChemDraw Professional 16.0 software (PerkinElmer Informatics). The LogP values are summarised in Chapter 4, Table 4.1. The calculated LogP of cmpd101 is 3.7, which is considered to be a cell-permeable. Most of the LogP values of the novel compounds are under 5 (Table 4.1), which supposed to cross the cell membrane. However, some compounds have LogP value of more than 5, such as BU16005, BU16007 and BU14013. Surprisingly, BU16007, which is the most potent inhibitor,

has a LogP value of 6 (Table 4.1). Therefore, the calculated LogP values do not straightforwardly reflect the cellular action of the novel compounds.

Phosphorylation of opioid receptors plays a major role in receptor desensitisation and internalisation (Gurevich, Vsevolod V., Gurevich & Tesmer 2016). MOPr and DOPr are phosphorylated at different residues mediated mainly by GRK2/3 (Brackley et al. 2016; Doll et al. 2012; Lemos Duarte & Devi 2020). About 20 phosphorylatable residues have been identified in the intracellular regions of MOPr, including Thr^{357},(which is within $^{354}TSST^{357}$ cassette), Thr^{370}, Ser^{375}, Thr^{376} and Thr^{379}, which are within $^{370}TREHPSTANT^{379}$ cassette (Figure 5.16A) (Chen, YJ et al. 2013; Gluck et al. 2014; Lau et al. 2011; Miess et al. 2018). It has been reported that alanine mutation of $^{354}TSST^{357}$ residues does not affect desensitisation or internalisation of MOPr (Lau et al. 2011; Yousuf et al. 2015). On the other hand, DOPr has been shown to be phosphorylated at the Thr^{358} and Ser^{363} residues in the C-terminus of the receptor (Law et al. 2000; Mann et al. 2020; Navratilova et al. 2005; Zhang et al. 2005). Also, different agonists promote phosphorylation of distinct residues on the C-terminal of MOPr. For instance, DAMGO phosphorylates MOPr at multiple residues, including Thr^{370} and Ser^{375}, which appears to be mainly mediated by GRK2/3, while morphine weakly phosphorylates MOPr at Ser^{375} residue, which appears to be mediated in part by GRK5 (Doll et al. 2012). Additionally, MOPr and DOPr are also phosphorylated by agonist-independent mechanisms (Mann et al. 2015; Xiang et al. 2001). For example, MOPr and DOPr are phosphorylated at Thr^{370} and Ser^{344} residues, respectively, which is mainly mediated by PKC (Mann et al. 2015; Xiang et al. 2001).

It has been shown that agonist-induced phosphorylation of Ser^{375} occurs faster than at other residues, and this is mainly mediated by GRK2/3 (Just et al. 2013). Therefore, phosphorylation of Ser^{375} is the primary site of phosphorylation followed by phosphorylation of the flanking residues, Thr^{370}, Thr^{376} and Thr^{379}. This could explain the observed increase in arrestin recruitment upon overexpression of GRK2/3. In the case of overexpression of GRK5/6, the endogenous GRK2/3 could phosphorylate Ser^{375} followed by phosphorylation of the flanking residues by other

GRKs, hence increasing arrestin recruitment to the receptor as reflected by an increase in the BRET signal.

Also, it was observed that the pattern of inhibition by the novel compounds was almost similar across all overexpressed GRK. Again, it seems possible that endogenous GRK2/3 phosphorylates Ser^{375} followed by multi-phosphorylation of flanking residues. This is evident when both cmpd101 and BU16007 showed similar IC_{50} values for GRK regardless of overexpressed isoform.

Also, it is noteworthy to note that cmpd101 and BU14016 seem effective in pcDNA3.1 cotransfected cells. However, in GRK2 overexpressed cells, BU14016 was less effective. For example, at 1 µM, BU14016 gave 75% inhibition and at 30 µM gave only about 20% inhibition. This suggests that the amount of inhibition of BU14016 depends on the size of the signal; thereby, BU14016 may be a weak inhibitor, depending upon the magnitude of the arrestin-3 induced signal.

5.4 Conclusion

I have used the arrestin-3 recruitment assay to study the selectivity of cmpd101 and a series of novel compounds towards GRK isoforms when overexpressed in HEK293 cells. Two opioid receptors, MOPr and DOPr, were used as representative of GPCRs in the presence of overexpressed GRKs. In these experiments, cmpd101 and novel compounds did not appear to show selectivity towards individual GRK isoforms. On the one hand, these findings could suggest that cmpd101 and some of the novel compounds can be used as pan-GRK inhibitors to study the role of GRKs in GPCR signalling and other cellular processes. On the other hand, however, the results and apparent lack of selectivity could reflect the complexities of sequential phosphorylation of MOPr. Further studies will be required to resolve these possibilities.

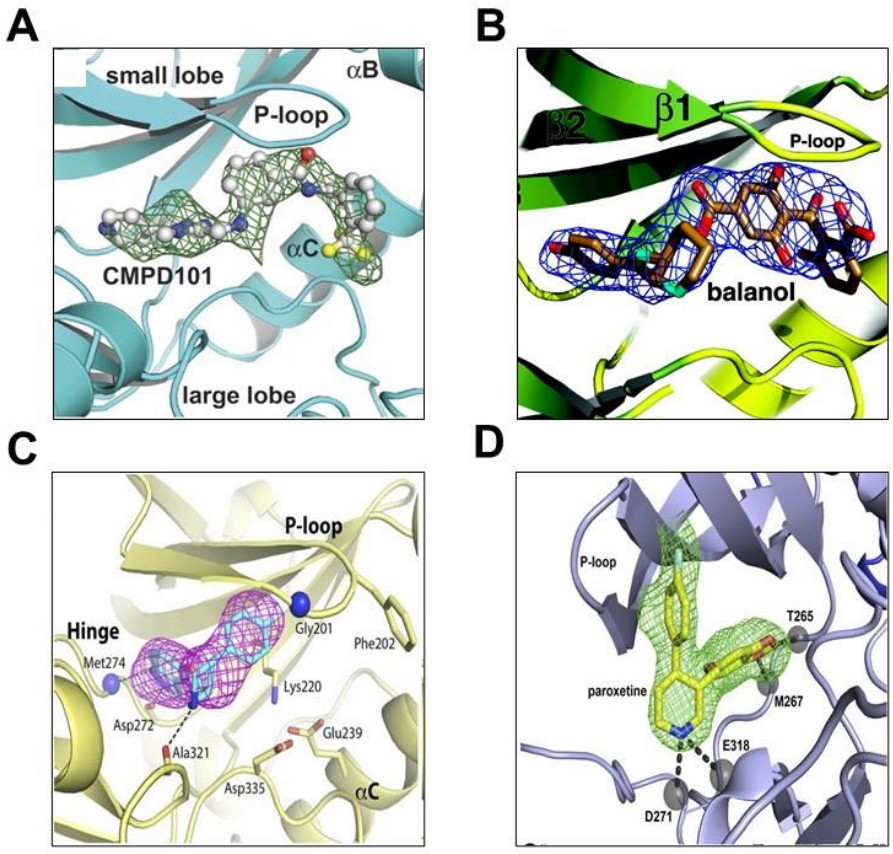

Figure 5.15 Crystal structures of inhibitors bound to the active site of GRK2

The crystal structures of inhibitors bound to GRK2-$G_{\beta\gamma}$. Cmpd101 (A) is shown as a ball and stick model carbons, oxygens, nitrogens, and fluorines are shown in white, red, blue, and yellow, respectively. Balanol (B) is drawn with carbons (tan), oxygens (red), and nitrogens (cyan). CCG2224061 (C) is shown with carbon atoms in cyan. Hydrogen bonds are shown as black dashed lines and backbone nitrogens are shown as blue spheres. Paroxetine (D) is shown as a stick model, carbons, oxygens, and nitrogens are shown in cyan, red, and blue, respectively. Hydrogen bonds are drawn as black dashed lines. Upon inhibitor binding, small conformational changes occur in the large lobe, the P-loop, and the αB-αC-loop. The crystal structure of (A) was taken from (Thal et al. 2011); (B) from (Tesmer, JJ et al. 2010); (C) from (Bouley, R et al. 2017); and (D) from (Homan et al. 2014).

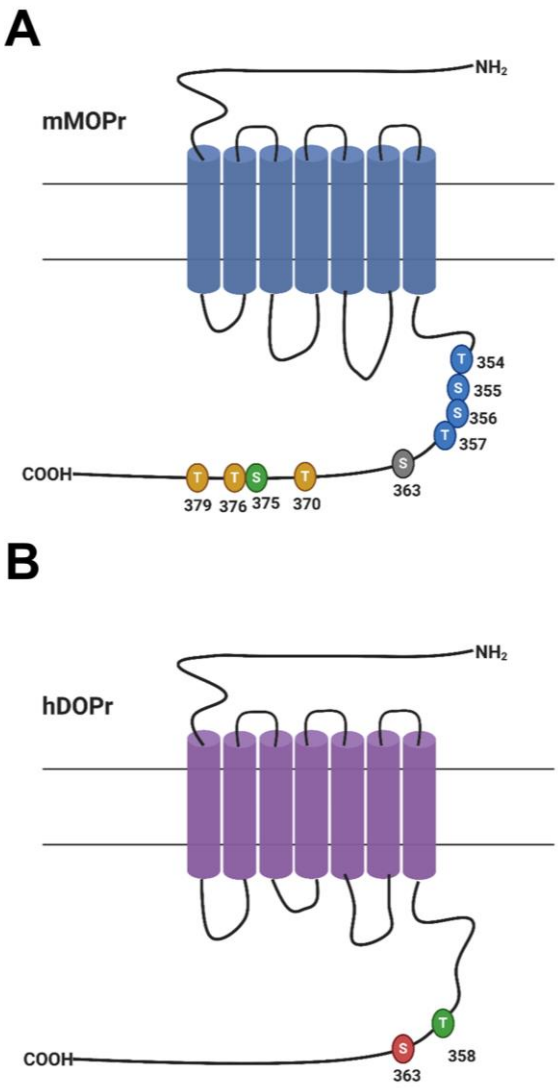

Figure 5.16 Phosphorylation sites

A schematic showing the intracellular regions of A) mouse MOPr, TSST residues are shown in blue, Ser^{375} residue is shown in green which is the primary site of phosphorylation of MOPr. Flaking residues Thr^{370}, Thr^{376} and Thr^{379} are shown in yellow. B) human DOPr, the primary phosphorylation site Ser^{363} (red) and Thr^{358} (green).

CHAPTER 6 General Discussion

6.1 Summary

GRKs phosphorylate-activated GPCRs leading to an increase in the affinity of arrestin to bind to the receptor and block further G protein activation. Therefore, the G protein-dependent signalling of a GPCR is terminated and the receptor undergoes desensitisation, often followed by internalisation and recycling. Besides their role in regulating GPCR signalling, GRKs also can bind to non-GPCR substrates in a phosphorylation-independent manner. Moreover, GRKs have been implicated in the progression of many diseases. Particularly, GRK2 and GRK5, which are the most studied GRK isoforms, are the main kinases upregulated in heart failure. GRK2 also mediates the desensitisation of MOPr, which is the main target of acute pain therapy with opioid agonist drugs.

Many studies have attempted to modulate the activity of GRK2 using various strategies. For instance, using small interfering RNA (siRNA) (Just et al. 2013), a truncated peptide (Raake et al. 2013), and a dominant-negative mutant of GRK2 (DNM-GRK2) (Celver et al. 2004; Cooke et al. 2015). However, the most promising and practical strategy to date is the use of small molecule inhibitors, such as cmpd101 (Lowe et al. 2015). The search for selective and potent inhibitors for individual GRK isoforms could be beneficial in intervening in heart diseases, in the case of GRK2 and GRK5, and serve as research tools for studying the function of GRK isoforms in the physiological regulation of GPCRs. However, the development of potent and selective GRK inhibitors, with good cell permeability, remains a challenge.

The main goal of this thesis was to investigate the ability of cmpd101 and some novel compounds, analogues of cmpd101, to inhibit agonist-induced arrestin-3 recruitment to MOPr, which is an indirect means of assessing GRK phosphorylation of receptor, in a cell-based system. The results of this thesis have demonstrated that cmpd101 and BU14016, BU14007 and BU16005 were effective at inhibiting DAMGO-induced arrestin-3 recruitment to MOPr (Table 6.1). In other words, cmpd101 and some of the novel compounds are in all likelihood able to inhibit GRK/s involved in phosphorylation of MOPr in HEK293 cells.

A second aim was to compare the inhibitory effect of the novel compounds on agonist-induced arrestin-3 recruitment to MOPr by different agonists. Namely, whether the inhibition of arrestin recruitment by potential GRK inhibitors is an agonist-dependent phenomenon. For MOPr, the research reported in this thesis has demonstrated that the inhibition of arrestin-3 recruitment to MOPr is indeed agonist-dependent (Table 6.1). As reported, some of the novel compounds inhibited DAMGO-induced arrestin-3 recruitment and failed to inhibit morphine-induced arrestin-3 recruitment. Possibly, morphine is a partial agonist at MOPr which could contribute to the inability of the compounds to inhibit morphine-induced arrestin-3 recruitment. For DOPr, the novel compounds show a similar pattern of inhibition of SNC80- and DADLE-induced arrestin-3 recruitment to DOPr (Table 6.2). A caveat of the studies is that both DOPr agonists used are considered full agonists at the arrestin-3 recruitment assay in HEK293.

A third aim of the thesis was to investigate whether the inhibition of arrestin recruitment by novel compounds is a receptor-dependent phenomenon. The results of this thesis show that cmpd101 inhibited agonist-induced arrestin-3 recruitment to MOPr and DOPr at similar potency. It is interesting to note that the novel compounds showed different inhibition capacity of agonist-induced arrestin-3 recruitment to DOPr. These results do not explain whether the inhibition of arrestin-3 recruitment is receptor-dependent or not in the case of cmpd101.

This thesis also sought to investigate the selectivity of cmpd101 and the novel compounds towards individual GRK isoforms. Our attempts, however, using arrestin-3 recruitment assay with HEK293 cells expressing MOPr and overexpressing GRK isoforms, failed to detect selectivity of cmpd101 and the novel inhibitors towards individual GRK isoforms (see Tables 6.3 and 6.4).

Table 6.1 Percent inhibition of DAMGO- and morphine-induced arrestin-3 recruitment to MOPr by cmpd101 and novel inhibitors

	MOPr			
	DAMGO (10μM)		Morphine (30μM)	
Compound	30 μM	100 μM	30 μM	100 μM
Cmpd101	81	58	43	-2
BU14016	81	82*	-15	27
BU16005	79	71	28	14
BU16007	88	71	61	-13
BU16006	37*	61	17	-24
BU14017	64	56	10	-60
BU16009	24*	52	36	-16
BU14013	11*	26*	-49*	-27
BU14014	18*	26*	-4	-56

This table is a summary of Figures 4.2-3, 4.5-6. (-) sign indicates activation of agonist-induced arrestin-3 recruitment. The table highlights the different effects of cmpd101 and the novel inhibitors on arrestin-3 recruitment to MOPr by DAMGO versus morphine. * $P < 0.05$ compared to respective cmpd101, one-way ANOVA followed by Dunnett's multiple comparison test.

Table 6.2 Percent inhibition of SNC80- and DADLE-induced arrestin-3 recruitment to DOPr by cmpd101 and novel inhibitors

	DOPr		
	SNC80 (10μM)		DADLE (10μM)
Compound	30 μM (%)	100 μM (%)	100 μM (%)
Cmpd101	49	50	32
BU14016	-1*	2*	7
BU16005	4*	-1*	5
BU16007	6*	21*	31
BU16006	1*	-0.3*	3
BU14017	10*	37	39
BU16009	5*	11*	8
BU14013	4*	16*	15
BU14014	9*	8*	7

This table is a summary of Figures 4.8-10. (-) sign indicates activation of agonist-induced arrestin-3 recruitment. The table highlights the broadly similar effects of cmpd101 and the novel inhibitors on arrestin-3 recruitment to DOPr by the two high efficacy agonists. * $P < 0.05$ compared to respective cmpd101, one-way ANOVA followed by Dunnett's multiple comparison test.

Table 6.3 Percent inhibition of DAMGO-induced arrestin-3 recruitment to MOPr in the presence of overexpressed GRK isoforms by cmpd101 and novel inhibitors

	Overexpressed GRKs				
	DAMGO (10μM)				
Compound (30μM)	pcDNA3.1(%)	GRK2 (%)	GRK3 (%)	GRK5 (%)	GRK6 (%)
Cmpd101	79	95	96	71	74
BU14016	65	52	45	45	57
BU16005	68	63	73	69	74
BU16007	76	85	81	80	84
BU16006	39	29	36	41	42
BU14017	41	36	35	45	50
BU16009	26	6	19	16	28
BU14013	20	0.7	16	14	31*
BU14014	2	2.6	8	-5	6

This table is a summary of Figures 5.4-6. (-) sign indicates activation of agonist-induced arrestin-3 recruitment. The table highlights that the inhibitors have the same effect irrespective of which GRK subtype is overexpressed. * $P < 0.05$ compared to respective pcDNA3.1, two-way ANOVA followed by Tukey's multiple comparison test.

Table 6.4 Percent inhibition of morphine-induced arrestin-3 recruitment to MOPr in the presence of overexpressed GRK isoforms by cmpd101 and novel inhibitors

	Overexpressed GRKs				
	Morphine (30μM)				
Compound (30μM)	pcDNA3.1(%)	GRK2 (%)	GRK3 (%)	GRK5 (%)	GRK6 (%)
Cmpd101	28	93*	95*	45	36^
BU14016	29	4	-17*	3	-1
BU16005	23	42	17	53	15
BU16007	59	53	18	54	57
BU16006	3	4	-15	12	-15
BU14017	-30	1	-28	18	-17
BU16009	2	-4	-26	9	-32
BU14013	-51	-13	-36	14*	-22
BU14014	-14	11	-27	-3	-28

This table is a summary of Figures 5.7-9. (-) sign indicates activation of agonist-induced arrestin-3 recruitment. * $P < 0.05$ compared to respective pcDNA3.1, ^ $P < 0.05$ compared to respective GRK2, two-way ANOVA followed by Tukey's multiple comparison test.

6.2 The Selectivity of cmpd101 Against Arrestin/GRK Pathway

Since the development of cmpd101 (Ikeda, S, Keneko & Fujiwara 2007), it has been used as a selective GRK2/3 inhibitor. Thal et al. (2011) determined the selectivity of cmpd101 towards GRK isoforms in an isolated enzyme assay. Some published reports contain evidence of the non-selective action of cmpd101. Moller et al. (2020) reported that cmpd101 at 10 µM did not affect the basal internalisation or arrestin-3 recruitment to MOPr. However, at 30 µM, cmpd101 decreased both basal internalisation and arrestin-3 recruitment to MOPr (Moller et al. 2020). The authors concluded that cmpd101 might have off-target effects at a concentration higher than 30 µM (Moller et al. 2020). There has been no specific attempt within the published literature (except of some observations) to explore the selectivity of cmpd101 towards GRK isoforms in a cell-based system. This thesis builds upon these reported findings, showing other sites of action of cmpd101 at the cellular level. Using cmpd101 at a concentration of more than 30 µM is not recommended, as suggested by the findings of this thesis where cmpd101 inhibit DAMGO-induced activation of G protein, and previously reported studies (Moller et al. 2020; Yu et al. 2018). A caveat of the experiments in this thesis is that the work is limited to HEK293 cells and opioid receptors. Future studies should extend these studies to involve other cell lines and receptors.

6.3 The Novel Inhibitors

Several potential GRK inhibitors have been developed, such as paroxetine (Thal et al. 2012), balanol (Homan & Tesmer 2015), compd101 (Ikeda, S, Keneko & Fujiwara 2007), GSK180736A (Homan et al. 2015). All these inhibitors either lack the selectivity over other GRK isoforms and other kinases such as PKA, ROCK1 or they are not good candidates for clinical use due to poor bioavailability. The novel inhibitors reported in this thesis are chemically modified versions (analogues) of cmpd101, assumed to be a GRK2/3 inhibitor. In our study, most of the compounds inhibited arrestin-3 recruitment due to overexpression of GRK isoforms, with no apparent selectivity towards individual isoforms. However, a preliminary study conducted by our collaborator, Prof. Stefan Schulz at the Friedrich Schiller Universität Jena, Germany, has shown that compound BU16007 strongly inhibited

the DAMGO-induced phosphorylation of Ser^{375}, Thr^{370}, Thr^{376}, and Thr^{379} (unpublished results) (Figure 6.1A). These results align with findings reported in this thesis that BU16007 strongly inhibited DAMGO-induced arrestin-3 recruitment to MOPr (Chapter 4, Figures 4.3 and 4.12). Cmpd101 inhibited DAMGO-induced phosphorylation of Thr^{370}, Thr^{376}, and Thr^{379} and modest inhibition of Thr^{375} (Figure 6.1A) Unexpectedly, compounds BU14016 and BU16005, which show strong inhibition of DAMGO-induced arrestin-3 recruitment to MOPr (Figure 4.3), did not inhibit DAMGO-induced phosphorylation of Ser^{375}, Thr^{370}, Thr^{376}, or Thr^{379}. In morphine stimulated cells, cmpd101 and BU16007 strongly inhibited morphine-induced phosphorylation at Ser^{375} (Figure 6.1B). Of note, these results are from one experiment. During my thesis research years, new inhibitors have been developed, in particular CCG258747 which shows potent and selective inhibition of GRK2 versus other GRK isoforms as well as other kinases such as PKA and ROCK1 (Bouley, RA et al. 2020). Our compound BU16007 stands out from the other compounds as it shows better selectively inhibition of DAMGO-induced arrestin-3 to MOPr over morphine. However, it is not possible to compare the potency of our compounds with that of the recently developed inhibitor CCG258747 because they were tested under different conditions. Our compounds were tested in cell-based assay whilst CCG258747 was tested in isolated GRK enzymes. Studies are needed to investigate compound BU16007 in more detail as it can serve as a scaffold for developing more potent and selective GRK inhibitors.

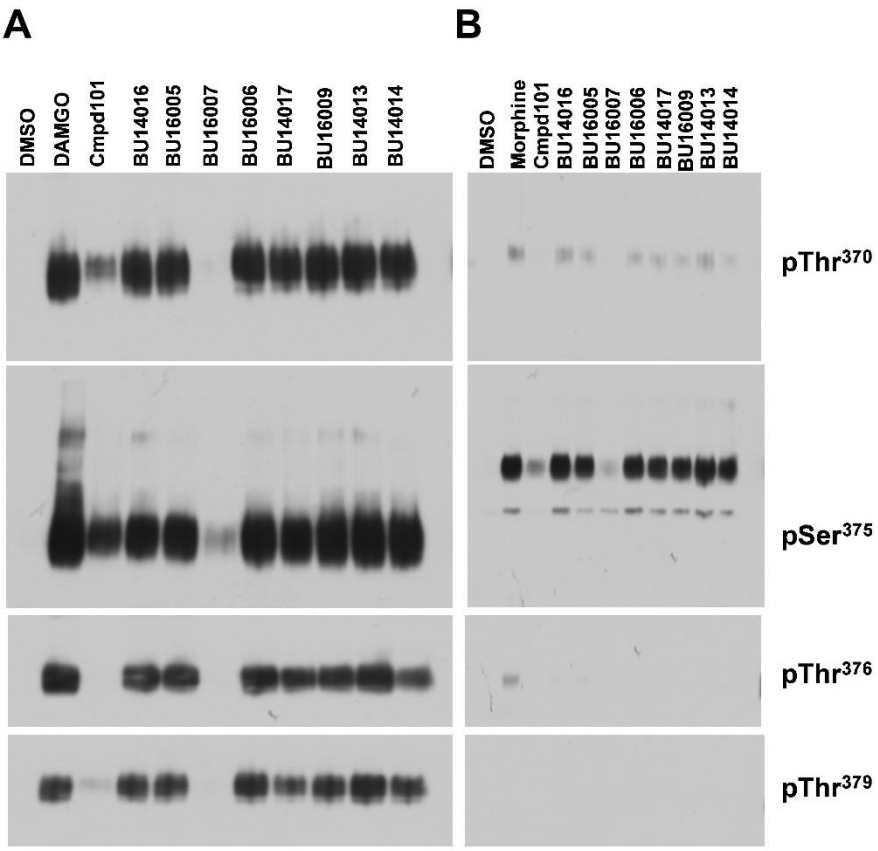

Figure 6.1 Effect of cmpd101 and the novel inhibitors on agonist-induced phosphorylation of MOPr

HEK293 cells stably expressing hemagglutinin (HA)–tagged MOPr, were pretreated with cmpd101 or the novel inhibitors (each 30 µM) for 30 min, then cells were stimulated with (A) 10 µM DAMGO or (B) 30 µM morphine for a further 30 min. Cells were lysed and immunoblotted with anti-pThr^{370}, anti-pSer^{375}, anti-pThr^{376}, or anti-pThr^{379} antibodies. This is a representative blot of two independent experiments, but the same effects were observed in each experiment. These studies were conducted by Nina Cathleen Blum, a PhD student of Prof. Stefan Schulz at the Friedrich Schiller Universität Jena, Germany.

6.4 The Selectivity of cmpd101 and Novel Inhibitors Towards GRK Isoforms

In this thesis, I have tried to investigate the selectivity of cmpd101 and the novel compounds towards individual GRK isoforms, using the arrestin-3 recruitment assay. However, cmpd101 and the novel compounds showed no apparent selectivity towards individual GRK isoforms in this assay. These findings illustrate the likely complexity of the phosphorylation mechanism of MOPr. It has been reported that high efficacy agonists, such as DAMGO and fentanyl, induce phosphorylation of multiple sites on the C-terminus of MOPr (Just et al. 2013; Miess et al. 2018), which occurs in a hierarchal manner. When Ser^{375} was mutated to alanine, there was no apparent phosphorylation of the flanking residues upon stimulation of the mutant MOPr with DAMGO (Just et al. 2013). In overexpression GRK experiments, the influence of endogenous GRKs cannot be excluded in our studies and that could explain in part the findings presented in this thesis.

One caveat of the studies in this thesis is that the effects of the novel inhibitors on the activity of the other kinases such as PKA, PKC and others are not known, and future studies should explore these effects. Importantly, cmpd101 at 1μM inhibits PKA, PKC, CaMKII, ERK1/2 and JNK by less than 20% in purified kinase screening assay (Lowe et al. 2015).

Attempts have been made to develop selective inhibitors of GRKs since the accumulating findings linked them to many diseases, in particular, heart failure. These attempts have had modest success in developing modest inhibitors for GRK2. Very recently, Bouley, RA et al. (2020) have developed a promising potent and selective GRK2 inhibitor. Preliminary results obtained from GRK2/3 knockout cells show that BU16007 could also inhibit GRK5/6. However, with all these efforts, selective GRK4/5/6 inhibitors have yet to be developed.

Instead of attempting to completely inhibit the action of a GRK, it could be more effective to modulate the GRK activity. It has been established that GRKs can bind to $G_{\beta\gamma}$, and the alpha subunit of G_q, these can be inhibited by using small molecule

inhibitors, rather than inhibiting GRK (Gurevich, EV et al. 2012). With the growing list of substrates that GRK can bind to, developing another strategy may be possible. One way is to target the substrate that binds to GRK, so there would be no need to inhibit GRK activity. PKC is also known to regulate GRK2 activity (Bailey, Oldfield, et al. 2009). Thus, targeting PKC by selective inhibitors is another way of modulating GRKs (Ghanemi 2015). In addition, overexpression of GRK activity has been reported in many diseases and decrease in the activity of GRK has also has been reported in other illnesses, such as depression (Gurevich, EV et al. 2012). Therefore, inhibition of GRK is not an ideal strategy in several diseases. Thus, the need to develop other methods to modulate GRK activity.

Another method that is promising is using a gene therapy technique to selectively target specific GRKs (Gurevich, EV et al. 2012). In psychiatric diseases, it has been reported that GRK activity is reduced so, in some cases, enhancing GRK activity could be used to manage psychiatric diseases (Ahmed et al. 2010; Gurevich, EV et al. 2012). In practical terms, at present, the only way to enhance GRK activity by using gene therapy. Briefly, gene therapy concept is based on using non-infectious viral or nonviral vectors to carry the gene of interest (in this context GRK2) into a specific cell type in a specific tissue (Kieserman et al. 2019). Most commonly used viral vectors are lentiviral and adenoviral vectors, where circular plasmid DNA vectors are examples of nonviral vectors (Kieserman et al. 2019). Some viral vectors have been successfully used to deliver βARKct, a peptide inhibitor of GRK2, to the heart of pig model of heart failure after subjected to left ventricular myocardial infarction (Raake et al. 2013). The βARKct expression in heart showed an improvement in cardiac function (Raake et al. 2013).

Many mechanisms of GRK are still unexplored in detail, such as how GRKs are synthesised in the cell and how they are degraded. Knowing these processes could open new avenues of targeting GRKs (Gurevich, EV et al. 2012).

6.5 Future Experiments

The search for selective and potent GRK inhibitors is still understudied. Here I will include a brief discussion on potential future studies to explore further the results presented in this thesis:

6.5.1 Short-Term Goals:

Ongoing studies are looking at the ability of the novel compounds to inhibit agonist-induced phosphorylation of the residues on MOPr. As shown in Figure 6.1, the preliminary results are interesting and can explain some of the results presented in this thesis, such as the potent inhibitory effect of BU16007. Also, another ongoing study in the laboratory is an examination of the effect of these novel inhibitors on the potential role of GRKs in desensitisation of the MOPr-activated G protein-activated inwardly-rectifying potassium (GIRK) current in locus coeruleus (LC) neurons. They measure the potassium current (K^+) induced by Met-enkephalin by using whole-cell patch-clamp recording in LC from rat brain slices. These studies will investigate the ability of these compounds to inhibit the acute MOPr desensitisation induced by an agonist.

To explore further the results of this thesis, it would be good to investigate the effect of cmpd101 and BU16007 on the recruitment of GRK to the receptor, which provides a direct measurement of GRK recruitment to the activated receptor and, presumably, phosphorylation. The MOPr can be fused with a donor (e.g., RLuc8) and GRK isoform can be fused with an acceptor (Venus). The recruitment of GRK to the receptor after stimulation by an agonist can be monitored by BRET. This method will give a clear picture of the selectivity of the novel compounds.

6.5.2 Medium-Term Goals:

For MOPr, it is well-documented that GRK2 and probably GRK3 are the main phosphorylation kinases. To further study the selectivity of individual GRKs, one way is to conduct the experiment by using GRK2/3-knockout cells to rule out the effect of GRK2/3 and to study selectivity of the inhibitor for GRK5/6 isoforms.

6.5.3 Long-Term Goals:

A complete pharmacokinetic profile is not available for cmpd101 and the novel compounds; a further study could be conducted to determine the pharmacokinetic parameters of cmpd101 and the novel compounds *in vitro* and *in vivo*. These kinds of studies give a great idea of the bioavailability of the compounds which can be related to their cellular effects.

Compound BU16007 is a promising GRK inhibitor and it can be structurally optimised to develop new molecules that are more potent and have better selectivity for GRKs. Besides, the nature of the interaction of BU16007 with GRK2 is not known; it would be useful to do docking studies to reveal the nature of the interactions with GRK2 and possibly with other GRK isoforms.

6.6 Conclusion

In summary, although much has been done, at present there remains no selective and potent inhibitor for individual GRK isoforms. This indicates how complex is developing potent and selective GRK inhibitors and it is a long-term process.

The findings of this thesis suggest that cmpd101 might affect off-targets when used at or more than 30 µM, so it is recommended to use it at a lower concentration to give the intended action as selective GRK2/3 inhibitor. Also, using arrestin-3 recruitment assay in HEK293 cells, the data in this thesis has shown that cmpd101 and the novel compounds do not show selectivity for individual GRK isoforms. Moreover, the studies of this thesis, along with the preliminary studies of Prof Stefan Schulz, have shown that compound BU16007 is a promising GRK inhibitor. Our studies have expanded our understanding of the action of cmpd101 in cell-based settings. Also, the findings suggest that phosphorylation is a complicated process whereby it can be a receptor-dependent, agonist-dependent and possibly also cell-dependent.

References

Abraham, AD, Schattauer, SS, Reichard, KL, Cohen, JH, Fontaine, HM, Song, AJ, Johnson, SD, Land, BB & Chavkin, C 2018, 'Estrogen Regulation of GRK2 Inactivates Kappa Opioid Receptor Signaling Mediating Analgesia, But Not Aversion', *J Neurosci*, vol. 38, no. 37, pp. 8031-8043.

Ahmed, MR, Berthet, A, Bychkov, E, Porras, G, Li, Q, Bioulac, BH, Carl, YT, Bloch, B, Kook, S, Aubert, I, Dovero, S, Doudnikoff, E, Gurevich, VV, Gurevich, EV & Bezard, E 2010, 'Lentiviral overexpression of GRK6 alleviates L-dopa-induced dyskinesia in experimental Parkinson's disease', *Sci Transl Med*, vol. 2, no. 28, p. 28ra28.

Al-Hasani, R & Bruchas, MR 2011, 'Molecular mechanisms of opioid receptor-dependent signaling and behavior', *Anesthesiology*, vol. 115, no. 6, pp. 1363-1381.

Alexander, SP, Christopoulos, A, Davenport, AP, Kelly, E, Marrion, NV, Peters, JA, Faccenda, E, Harding, SD, Pawson, AJ, Sharman, JL, Southan, C, Davies, JA & Collaborators, C 2017, 'THE CONCISE GUIDE TO PHARMACOLOGY 2017/18: G protein-coupled receptors', *Br J Pharmacol*, vol. 174 Suppl 1, pp. S17-S129.

Allouche, S, Noble, F & Marie, N 2014, 'Opioid receptor desensitization: mechanisms and its link to tolerance', *Front Pharmacol*, vol. 5, p. 280.

Alvarez, VA, Arttamangkul, S, Dang, V, Salem, A, Whistler, JL, Von Zastrow, M, Grandy, DK & Williams, JT 2002, 'mu-Opioid receptors: Ligand-dependent activation of potassium conductance, desensitization, and internalization', *J Neurosci*, vol. 22, no. 13, pp. 5769-5776.

Anderson, KM, Eckhart, AD, Willette, RN & Koch, WJ 1999, 'The myocardial beta-adrenergic system in spontaneously hypertensive heart failure (SHHF) rats', *Hypertension*, vol. 33, no. 1 Pt 2, pp. 402-407.

Arttamangkul, S, Leff, ER, Koita, O, Birdsong, WT & Williams, JT 2019, 'Separation of Acute Desensitization and Long-Term Tolerance of micro-Opioid Receptors Is Determined by the Degree of C-Terminal Phosphorylation', *Mol Pharmacol*, vol. 96, no. 4, pp. 505-514.

Ayoub, MA & Pfleger, KD 2010, 'Recent advances in bioluminescence resonance energy transfer technologies to study GPCR heteromerization', *Curr Opin Pharmacol*, vol. 10, no. 1, pp. 44-52.

Bailey, CP & Connor, M 2005, 'Opioids: cellular mechanisms of tolerance and physical dependence', *Curr Opin Pharmacol*, vol. 5, no. 1, pp. 60-68.

Bailey, CP, Llorente, J, Gabra, BH, Smith, FL, Dewey, WL, Kelly, E & Henderson, G 2009, 'Role of protein kinase C and mu-opioid receptor (MOPr) desensitization in tolerance to morphine in rat locus coeruleus neurons', *Eur J Neurosci*, vol. 29, no. 2, pp. 307-318.

Bailey, CP, Oldfield, S, Llorente, J, Caunt, CJ, Teschemacher, AG, Roberts, L, McArdle, CA, Smith, FL, Dewey, WL, Kelly, E & Henderson, G 2009, 'Involvement of PKC alpha and G-protein-coupled receptor kinase 2 in agonist-selective desensitization of mu-opioid receptors in mature brain neurons', *Br J Pharmacol*, vol. 158, no. 1, pp. 157-164.

Belcheva, MM, Vogel, Z, Ignatova, E, Avidor-Reiss, T, Zippel, R, Levy, R, Young, EC, Barg, J & Coscia, CJ 1998, 'Opioid modulation of extracellular signal-regulated protein kinase activity is ras-dependent and involves Gbetagamma subunits', *J Neurochem*, vol. 70, no. 2, pp. 635-645.

Belmonte, SL & Blaxall, BC 2011, 'G protein coupled receptor kinases as therapeutic targets in cardiovascular disease', *Circ Res*, vol. 109, no. 3, pp. 309-319.

Benovic, JL, Stone, WC, Caron, MG & Lefkowitz, RJ 1989, 'Inhibition of the beta-adrenergic receptor kinase by polyanions', *J Biol Chem*, vol. 264, no. 12, pp. 6707-6710.

Birdsong, WT & Williams, JT 2020, 'Recent progress in opioid research from an electrophysiological perspective', *Mol Pharmacol*, vol.

Borroto-Escuela, DO, Flajolet, M, Agnati, LF, Greengard, P & Fuxe, K 2013, 'Bioluminescence resonance energy transfer methods to study G protein-coupled receptor-receptor tyrosine kinase heteroreceptor complexes', *Methods Cell Biol*, vol. 117, pp. 141-164.

Borsodi, A, Bruchas, M, Caló, G, Chavkin, , C., C, M. J., C, O., C, M., C, B. M., D, L. A., E, C., H, V., , Henderson, G, Husbands, S, Kelly, E, Kieffer,, B., K, I., K, M.-J., Liu-Chen, L.-Y., Massot, D, Meunier, J.-C., P, P. S., S, S., S, T. S., S, E. J., T, L., T, J. R., U, H., W, Y. H., Z & N. and Zimmer 2019, 'Opioid receptors (version 2019.4) in the IUPHAR/BPS Guide to Pharmacology Database', *IUPHAR/BPS Guide to Pharmacology CITE*, vol. 4.

Bouley, R, Waldschmidt, HV, Cato, MC, Cannavo, A, Song, J, Cheung, JY, Yao, XQ, Koch, WJ, Larsen, SD & Tesmer, JJG 2017, 'Structural Determinants Influencing the Potency and Selectivity of Indazole-Paroxetine Hybrid G Protein-Coupled Receptor Kinase 2 Inhibitors', *Mol Pharmacol*, vol. 92, no. 6, pp. 707-717.

Bouley, RA, Weinberg, ZY, Waldschmidt, HV, Yen, YC, Larsen, SD, Puthenveedu, MA & Tesmer, JJG 2020, 'A New Paroxetine-Based GRK2 Inhibitor Reduces Internalization of the mu-Opioid Receptor', *Mol Pharmacol*, vol. 97, no. 6, pp. 392-401.

Bowman, SL, Soohoo, AL, Shiwarski, DJ, Schulz, S, Pradhan, AA & Puthenveedu, MA 2015, 'Cell-autonomous regulation of mu-opioid receptor recycling by substance P', *Cell Reports*, vol. 10, no. 11, pp. 1925-1936.

Brackley, AD, Gomez, R, Akopian, AN, Henry, MA & Jeske, NA 2016, 'GRK2 Constitutively Governs Peripheral Delta Opioid Receptor Activity', *Cell Reports*, vol. 16, no. 10, pp. 2686-2698.

Brandt, MR, Furness, MS, Rice, KC, Fischer, BD & Negus, SS 2001, 'Studies of tolerance and dependence with the delta-opioid agonist SNC80 in rhesus monkeys

responding under a schedule of food presentation', *J Pharmacol Exp Ther*, vol. 299, no. 2, pp. 629-637.

Brinks, H, Boucher, M, Gao, E, Chuprun, JK, Pesant, S, Raake, PW, Huang, ZM, Wang, X, Qiu, G, Gumpert, A, Harris, DM, Eckhart, AD, Most, P & Koch, WJ 2010, 'Level of G protein-coupled receptor kinase-2 determines myocardial ischemia/reperfusion injury via pro- and anti-apoptotic mechanisms', *Circ Res*, vol. 107, no. 9, pp. 1140-1149.

Bristow, MR, Hershberger, RE, Port, JD, Gilbert, EM, Sandoval, A, Rasmussen, R, Cates, AE & Feldman, AM 1990, 'Beta-adrenergic pathways in nonfailing and failing human ventricular myocardium', *Circulation*, vol. 82, no. 2 Suppl, pp. I12-25.

Butcher, AJ, Prihandoko, R, Kong, KC, McWilliams, P, Edwards, JM, Bottrill, A, Mistry, S & Tobin, AB 2011, 'Differential G-protein-coupled receptor phosphorylation provides evidence for a signaling bar code', *J Biol Chem*, vol. 286, no. 13, pp. 11506-11518.

Cahill, TJ, 3rd, Thomsen, AR, Tarrasch, JT, Plouffe, B, Nguyen, AH, Yang, F, Huang, LY, Kahsai, AW, Bassoni, DL, Gavino, BJ, Lamerdin, JE, Triest, S, Shukla, AK, Berger, B, Little, Jt, Antar, A, Blanc, A, Qu, CX, Chen, X, Kawakami, K, Inoue, A, Aoki, J, Steyaert, J, Sun, JP, Bouvier, M, Skiniotis, G & Lefkowitz, RJ 2017, 'Distinct conformations of GPCR-beta-arrestin complexes mediate desensitization, signaling, and endocytosis', *Proc Natl Acad Sci U S A*, vol. 114, no. 10, pp. 2562-2567.

Cannavo, A, Liccardo, D & Koch, WJ 2013, 'Targeting cardiac beta-adrenergic signaling via GRK2 inhibition for heart failure therapy', *Front Physiol*, vol. 4, p. 264.

Cannavo, A, Marzano, F, Elia, A, Liccardo, D, Bencivenga, L, Gambino, G, Perna, C, Rapacciuolo, A, Cittadini, A, Ferrara, N, Paolocci, N, Koch, WJ & Rengo, G 2019, 'Aldosterone Jeopardizes Myocardial Insulin and beta-Adrenergic Receptor Signaling via G Protein-Coupled Receptor Kinase 2', *Front Pharmacol*, vol. 10, p. 888.

Carter, BD & Medzihradsky, F 1993, 'Go mediates the coupling of the mu opioid receptor to adenylyl cyclase in cloned neural cells and brain', *Proceedings of the National Academy of Sciences of the United States of America*, vol. 90, no. 9, pp. 4062-4066.

Celver, J, Xu, M, Jin, W, Lowe, J & Chavkin, C 2004, 'Distinct domains of the mu-opioid receptor control uncoupling and internalization', *Mol Pharmacol*, vol. 65, no. 3, pp. 528-537.

Chen, EP, Bittner, HB, Akhter, SA, Koch, WJ & Davis, RD 1998, 'Myocardial recovery after ischemia and reperfusion injury is significantly impaired in hearts with transgenic overexpression of beta-adrenergic receptor kinase', *Circulation*, vol. 98, no. 19 Suppl, pp. II249-253; discussion II253-244.

Chen, EP, Bittner, HB, Akhter, SA, Koch, WJ & Davis, RD 2001, 'Myocardial function in hearts with transgenic overexpression of the G protein-coupled receptor kinase 5', *Ann Thorac Surg*, vol. 71, no. 4, pp. 1320-1324.

Chen, YJ, Oldfield, S, Butcher, AJ, Tobin, AB, Saxena, K, Gurevich, VV, Benovic, JL, Henderson, G & Kelly, E 2013, 'Identification of phosphorylation sites in the COOH-terminal tail of the mu-opioid receptor', *J Neurochem*, vol. 124, no. 2, pp. 189-199.

Ciccarelli, M, Chuprun, JK, Rengo, G, Gao, E, Wei, Z, Peroutka, RJ, Gold, JI, Gumpert, A, Chen, M, Otis, NJ, Dorn, GW, 2nd, Trimarco, B, Iaccarino, G & Koch, WJ 2011, 'G protein-coupled receptor kinase 2 activity impairs cardiac glucose uptake and promotes insulin resistance after myocardial ischemia', *Circulation*, vol. 123, no. 18, pp. 1953-1962.

Comer, SD, Hoenicke, EM, Sable, AI, McNutt, RW, Chang, KJ, De Costa, BR, Mosberg, HI & Woods, JH 1993, 'Convulsive effects of systemic administration of the delta opioid agonist BW373U86 in mice', *J Pharmacol Exp Ther*, vol. 267, no. 2, pp. 888-895.

Conibear, AE, Asghar, J, Hill, R, Henderson, G, Borbely, E, Tekus, V, Helyes, Z, Palandri, J, Bailey, C, Starke, I, von Mentzer, B, Kendall, D & Kelly, E 2020, 'A Novel G Protein-Biased Agonist at the delta Opioid Receptor with Analgesic Efficacy in Models of Chronic Pain', *J Pharmacol Exp Ther*, vol. 372, no. 2, pp. 224-236.

Cooke, AE, Oldfield, S, Krasel, C, Mundell, SJ, Henderson, G & Kelly, E 2015, 'Morphine-induced internalization of the L83I mutant of the rat mu-opioid receptor', *Br J Pharmacol*, vol. 172, no. 2, pp. 593-605.

Corder, G, Castro, DC, Bruchas, MR & Scherrer, G 2018, 'Endogenous and Exogenous Opioids in Pain', *Annu Rev Neurosci*, vol. 41, pp. 453-473.

Dang, VC, Napier, IA & Christie, MJ 2009, 'Two distinct mechanisms mediate acute mu-opioid receptor desensitization in native neurons', *J Neurosci*, vol. 29, no. 10, pp. 3322-3327.

Dhami, GK, Anborgh, PH, Dale, LB, Sterne-Marr, R & Ferguson, SS 2002, 'Phosphorylation-independent regulation of metabotropic glutamate receptor signaling by G protein-coupled receptor kinase 2', *J Biol Chem*, vol. 277, no. 28, pp. 25266-25272.

Doll, C, Konietzko, J, Poll, F, Koch, T, Hollt, V & Schulz, S 2011, 'Agonist-selective patterns of micro-opioid receptor phosphorylation revealed by phosphosite-specific antibodies', *Br J Pharmacol*, vol. 164, no. 2, pp. 298-307.

Doll, C, Poll, F, Peuker, K, Loktev, A, Gluck, L & Schulz, S 2012, 'Deciphering micro-opioid receptor phosphorylation and dephosphorylation in HEK293 cells', *Br J Pharmacol*, vol. 167, no. 6, pp. 1259-1270.

Downes, GB & Gautam, N 1999, 'The G protein subunit gene families', *Genomics*, vol. 62, no. 3, pp. 544-552.

Dzimiri, N, Muiya, P, Andres, E & Al-Halees, Z 2004, 'Differential functional expression of human myocardial G protein receptor kinases in left ventricular cardiac diseases', *Eur J Pharmacol*, vol. 489, no. 3, pp. 167-177.

El Khamlichi, C, Reverchon-Assadi, F, Hervouet-Coste, N, Blot, L, Reiter, E & Morisset-Lopez, S 2019, 'Bioluminescence Resonance Energy Transfer as a Method to Study Protein-Protein Interactions: Application to G Protein Coupled Receptor Biology', *Molecules*, vol. 24, no. 3.

Evans, CJ 2004, 'Secrets of the opium poppy revealed', *Neuropharmacology*, vol. 47 Suppl 1, pp. 293-299.

Evron, T, Daigle, TL & Caron, MG 2012, 'GRK2: multiple roles beyond G protein-coupled receptor desensitization', *Trends Pharmacol Sci*, vol. 33, no. 3, pp. 154-164.

Fan, Q, Chen, M, Zuo, L, Shang, X, Huang, MZ, Ciccarelli, M, Raake, P, Brinks, H, Chuprun, KJ, Dorn, GW, 2nd, Koch, WJ & Gao, E 2013, 'Myocardial Ablation of G Protein-Coupled Receptor Kinase 2 (GRK2) Decreases Ischemia/Reperfusion Injury through an Anti-Intrinsic Apoptotic Pathway', *PLoS One*, vol. 8, no. 6, p. e66234.

Ferguson, SS 2001, 'Evolving concepts in G protein-coupled receptor endocytosis: the role in receptor desensitization and signaling', *Pharmacol Rev*, vol. 53, no. 1, pp. 1-24.

Fredriksson, R, Lagerstrom, MC, Lundin, LG & Schioth, HB 2003, 'The G-protein-coupled receptors in the human genome form five main families. Phylogenetic analysis, paralogon groups, and fingerprints', *Mol Pharmacol*, vol. 63, no. 6, pp. 1256-1272.

Freeman, K, Lerman, I, Kranias, EG, Bohlmeyer, T, Bristow, MR, Lefkowitz, RJ, Iaccarino, G, Koch, WJ & Leinwand, LA 2001, 'Alterations in cardiac adrenergic signaling and calcium cycling differentially affect the progression of cardiomyopathy', *J Clin Invest*, vol. 107, no. 8, pp. 967-974.

Galasinski, SC, Resing, KA, Goodrich, JA & Ahn, NG 2002, 'Phosphatase inhibition leads to histone deacetylases 1 and 2 phosphorylation and disruption of corepressor interactions', *J Biol Chem*, vol. 277, no. 22, pp. 19618-19626.

Gallantine, EL & Meert, TF 2005, 'A comparison of the antinociceptive and adverse effects of the mu-opioid agonist morphine and the delta-opioid agonist SNC80', *Basic Clin Pharmacol Toxicol*, vol. 97, no. 1, pp. 39-51.

Gasiunaite G 2017, 'Galanin receptor dimerisation', PhD thesis, University of Bristol.

Gendron, L, Mittal, N, Beaudry, H & Walwyn, W 2015, 'Recent advances on the delta opioid receptor: from trafficking to function', *Br J Pharmacol*, vol. 172, no. 2, pp. 403-419.

Ghanemi, A 2015, 'Targeting G protein coupled receptor-related pathways as emerging molecular therapies', *Saudi Pharm J*, vol. 23, no. 2, pp. 115-129.

Gharagozlou, P, Demirci, H, David Clark, J & Lameh, J 2003, 'Activity of opioid ligands in cells expressing cloned mu opioid receptors', *BMC Pharmacol*, vol. 3, p. 1.

Gluck, L, Loktev, A, Mouledous, L, Mollereau, C, Law, PY & Schulz, S 2014, 'Loss of morphine reward and dependence in mice lacking G protein-coupled receptor kinase 5', *Biol Psychiatry*, vol. 76, no. 10, pp. 767-774.

Groer, CE, Schmid, CL, Jaeger, AM & Bohn, LM 2011, 'Agonist-directed interactions with specific beta-arrestins determine mu-opioid receptor trafficking, ubiquitination, and dephosphorylation', *J Biol Chem*, vol. 286, no. 36, pp. 31731-31741.

Guccione, M, Ettari, R, Taliani, S, Da Settimo, F, Zappala, M & Grasso, S 2016, 'G-Protein-Coupled Receptor Kinase 2 (GRK2) Inhibitors: Current Trends and Future Perspectives', *J Med Chem*, vol. 59, no. 20, pp. 9277-9294.

Guo, J, Wu, Y, Zhang, W, Zhao, J, Devi, LA, Pei, G & Ma, L 2000, 'Identification of G protein-coupled receptor kinase 2 phosphorylation sites responsible for agonist-stimulated delta-opioid receptor phosphorylation', *Mol Pharmacol*, vol. 58, no. 5, pp. 1050-1056.

Gurevich, EV, Tesmer, JJ, Mushegian, A & Gurevich, VV 2012, 'G protein-coupled receptor kinases: more than just kinases and not only for GPCRs', *Pharmacol Ther*, vol. 133, no. 1, pp. 40-69.

Gurevich, VV & Gurevich, EV 2019, 'GPCR Signaling Regulation: The Role of GRKs and Arrestins', *Front Pharmacol*, vol. 10, p. 125.

Gurevich, VV & Gurevich, EV 2020, 'Biased GPCR signaling: Possible mechanisms and inherent limitations', *Pharmacol Ther*, vol. 211, p. 107540.

Gurevich, VV, Gurevich, EV & Tesmer, J 2016, *G protein-coupled receptor kinases*, /z-wcorg/ database.

Gutstein, HB, Rubie, EA, Mansour, A, Akil, H & Woodgett, JR 1997, 'Opioid effects on mitogen-activated protein kinase signaling cascades', *Anesthesiology*, vol. 87, no. 5, pp. 1118-1126.

Hamdan, FF, Percherancier, Y, Breton, B & Bouvier, M 2006, 'Monitoring protein-protein interactions in living cells by bioluminescence resonance energy transfer (BRET)', *Curr Protoc Neurosci*, vol. Chapter 5, p. Unit 5 23.

Hanyaloglu, AC & von Zastrow, M 2008, 'Regulation of GPCRs by endocytic membrane trafficking and its potential implications', *Annu Rev Pharmacol Toxicol*, vol. 48, pp. 537-568.

Harding, VB, Jones, LR, Lefkowitz, RJ, Koch, WJ & Rockman, HA 2001, 'Cardiac beta ARK1 inhibition prolongs survival and augments beta blocker therapy in a mouse model of severe heart failure', *Proc Natl Acad Sci U S A*, vol. 98, no. 10, pp. 5809-5814.

Hathaway, GM, Lubben, TH & Traugh, JA 1980, 'Inhibition of casein kinase II by heparin', *J Biol Chem*, vol. 255, no. 17, pp. 8038-8041.

Hauser, AS, Attwood, MM, Rask-Andersen, M, Schioth, HB & Gloriam, DE 2017, 'Trends in GPCR drug discovery: new agents, targets and indications', *Nat Rev Drug Discov*, vol. 16, no. 12, pp. 829-842.

Hilger, D, Masureel, M & Kobilka, BK 2018, 'Structure and dynamics of GPCR signaling complexes', *Nat Struct Mol Biol*, vol. 25, no. 1, pp. 4-12.

Hill, R, Disney, A, Conibear, A, Sutcliffe, K, Dewey, W, Husbands, S, Bailey, C, Kelly, E & Henderson, G 2018, 'The novel mu-opioid receptor agonist PZM21 depresses

respiration and induces tolerance to antinociception', *Br J Pharmacol*, vol. 175, no. 13, pp. 2653-2661.

Homan, KT, Larimore, KM, Elkins, JM, Szklarz, M, Knapp, S & Tesmer, JJ 2015, 'Identification and structure-function analysis of subfamily selective G protein-coupled receptor kinase inhibitors', *ACS Chem Biol*, vol. 10, no. 1, pp. 310-319.

Homan, KT & Tesmer, JJ 2015, 'Molecular basis for small molecule inhibition of G protein-coupled receptor kinases', *ACS Chem Biol*, vol. 10, no. 1, pp. 246-256.

Homan, KT, Wu, E, Wilson, MW, Singh, P, Larsen, SD & Tesmer, JJ 2014, 'Structural and functional analysis of g protein-coupled receptor kinase inhibition by paroxetine and a rationally designed analog', *Mol Pharmacol*, vol. 85, no. 2, pp. 237-248.

Hu, GM, Mai, TL & Chen, CM 2017, 'Visualizing the GPCR Network: Classification and Evolution', *Sci Rep*, vol. 7, no. 1, p. 15495.

Huang, W, Manglik, A, Venkatakrishnan, AJ, Laeremans, T, Feinberg, EN, Sanborn, AL, Kato, HE, Livingston, KE, Thorsen, TS, Kling, RC, Granier, S, Gmeiner, P, Husbands, SM, Traynor, JR, Weis, WI, Steyaert, J, Dror, RO & Kobilka, BK 2015, 'Structural insights into μ-opioid receptor activation', *Nature*, vol. 524, no. 7565, pp. 315-321.

Huang, W, Masureel, M, Qu, Q, Janetzko, J, Inoue, A, Kato, HE, Robertson, MJ, Nguyen, KC, Glenn, JS, Skiniotis, G & Kobilka, BK 2020, 'Structure of the neurotensin receptor 1 in complex with beta-arrestin 1', *Nature*, vol. 579, no. 7798, pp. 303-308.

Ikeda, K, Kobayashi, T, Kumanishi, T, Niki, H & Yano, R 2000, 'Involvement of G-protein-activated inwardly rectifying K (GIRK) channels in opioid-induced analgesia', *Neurosci Res*, vol. 38, no. 1, pp. 113-116.

Ikeda, S, Keneko, M & Fujiwara, S 2007, *Cardiotonic agent comprising GRK Inhibitor*, US.

Illing, S, Mann, A & Schulz, S 2014, 'Heterologous regulation of agonist-independent mu-opioid receptor phosphorylation by protein kinase C', *Br J Pharmacol*, vol. 171, no. 5, pp. 1330-1340.

Ingram, SL & Traynor, JR 2009, 'Role of protein kinase C in functional selectivity for desensitization at the mu-opioid receptor: from pharmacological curiosity to therapeutic potential', *Br J Pharmacol*, vol. 158, no. 1, pp. 154-156.

Issad, T & Jockers, R 2006, 'Bioluminescence resonance energy transfer to monitor protein-protein interactions', *Methods Mol Biol*, vol. 332, pp. 195-209.

Jaber, M, Koch, WJ, Rockman, H, Smith, B, Bond, RA, Sulik, KK, Ross, J, Jr., Lefkowitz, RJ, Caron, MG & Giros, B 1996, 'Essential role of beta-adrenergic receptor kinase 1 in cardiac development and function', *Proc Natl Acad Sci U S A*, vol. 93, no. 23, pp. 12974-12979.

James, A & Williams, J 2020, 'Basic Opioid Pharmacology - An Update', *Br J Pain*, vol. 14, no. 2, pp. 115-121.

Johnson, EA, Oldfield, S, Braksator, E, Gonzalez-Cuello, A, Couch, D, Hall, KJ, Mundell, SJ, Bailey, CP, Kelly, E & Henderson, G 2006, 'Agonist-selective mechanisms of mu-opioid receptor desensitization in human embryonic kidney 293 cells', *Mol Pharmacol*, vol. 70, no. 2, pp. 676-685.

Johnson, LN 2009, 'Protein kinase inhibitors: contributions from structure to clinical compounds', *Q Rev Biophys*, vol. 42, no. 1, pp. 1-40.

Johnson, LR, Scott, MG & Pitcher, JA 2004, 'G protein-coupled receptor kinase 5 contains a DNA-binding nuclear localization sequence', *Mol Cell Biol*, vol. 24, no. 23, pp. 10169-10179.

Jung, SR, Seo, JB, Deng, Y, Asbury, CL, Hille, B & Koh, DS 2016, 'Contributions of protein kinases and beta-arrestin to termination of protease-activated receptor 2 signaling', *J Gen Physiol*, vol. 147, no. 3, pp. 255-271.

Just, S, Illing, S, Trester-Zedlitz, M, Lau, EK, Kotowski, SJ, Miess, E, Mann, A, Doll, C, Trinidad, JC, Burlingame, AL, von Zastrow, M & Schulz, S 2013, 'Differentiation of opioid drug effects by hierarchical multi-site phosphorylation', *Mol Pharmacol*, vol. 83, no. 3, pp. 633-639.

Kam, AY, Chan, AS & Wong, YH 2004, 'Phosphatidylinositol-3 kinase is distinctively required for mu-, but not kappa-opioid receptor-induced activation of c-Jun N-terminal kinase', *J Neurochem*, vol. 89, no. 2, pp. 391-402.

Kang, DS, Tian, X & Benovic, JL 2014, 'Role of beta-arrestins and arrestin domain-containing proteins in G protein-coupled receptor trafficking', *Curr Opin Cell Biol*, vol. 27, pp. 63-71.

Kang, Y, Zhou, XE, Gao, X, He, Y, Liu, W, Ishchenko, A, Barty, A, White, TA, Yefanov, O, Han, GW, Xu, Q, de Waal, PW, Ke, J, Tan, MH, Zhang, C, Moeller, A, West, GM, Pascal, BD, Van Eps, N, Caro, LN, Vishnivetskiy, SA, Lee, RJ, Suino-Powell, KM, Gu, X, Pal, K, Ma, J, Zhi, X, Boutet, S, Williams, GJ, Messerschmidt, M, Gati, C, Zatsepin, NA, Wang, D, James, D, Basu, S, Roy-Chowdhury, S, Conrad, CE, Coe, J, Liu, H, Lisova, S, Kupitz, C, Grotjohann, I, Fromme, R, Jiang, Y, Tan, M, Yang, H, Li, J, Wang, M, Zheng, Z, Li, D, Howe, N, Zhao, Y, Standfuss, J, Diederichs, K, Dong, Y, Potter, CS, Carragher, B, Caffrey, M, Jiang, H, Chapman, HN, Spence, JC, Fromme, P, Weierstall, U, Ernst, OP, Katritch, V, Gurevich, VV, Griffin, PR, Hubbell, WL, Stevens, RC, Cherezov, V, Melcher, K & Xu, HE 2015, 'Crystal structure of rhodopsin bound to arrestin by femtosecond X-ray laser', *Nature*, vol. 523, no. 7562, pp. 561-567.

Karageorgos, V, Venihaki, M, Sakellaris, S, Pardalos, M, Kontakis, G, Matsoukas, MT, Gravanis, A, Margioris, A & Liapakis, G 2018, 'Current understanding of the structure and function of family B GPCRs to design novel drugs', *Hormones (Athens)*, vol. 17, no. 1, pp. 45-59.

Katritch, V, Cherezov, V & Stevens, RC 2012, 'Diversity and modularity of G protein-coupled receptor structures', *Trends Pharmacol Sci*, vol. 33, no. 1, pp. 17-27.

Kelly, E 2013, 'Ligand bias at the mu-opioid receptor', *Biochem Soc Trans*, vol. 41, no. 1, pp. 218-224.

Kelly, E, Bailey, CP & Henderson, G 2008, 'Agonist-selective mechanisms of GPCR desensitization', *Br J Pharmacol*, vol. 153 Suppl 1, pp. S379-388.

Kieserman, JM, Myers, VD, Dubey, P, Cheung, JY & Feldman, AM 2019, 'Current Landscape of Heart Failure Gene Therapy', *J Am Heart Assoc*, vol. 8, no. 10, p. e012239.

Kishimoto, A, Brown, MS, Slaughter, CA & Goldstein, JL 1987, 'Phosphorylation of serine 833 in cytoplasmic domain of low density lipoprotein receptor by a high molecular weight enzyme resembling casein kinase II', *J Biol Chem*, vol. 262, no. 3, pp. 1344-1351.

Kliewer, A, Schmiedel, F, Sianati, S, Bailey, A, Bateman, JT, Levitt, ES, Williams, JT, Christie, MJ & Schulz, S 2019, 'Phosphorylation-deficient G-protein-biased mu-opioid receptors improve analgesia and diminish tolerance but worsen opioid side effects', *Nat Commun*, vol. 10, no. 1, p. 367.

Koch, T, Kroslak, T, Mayer, P, Raulf, E & Hollt, V 1997, 'Site mutation in the rat mu-opioid receptor demonstrates the involvement of calcium/calmodulin-dependent protein kinase II in agonist-mediated desensitization', *J Neurochem*, vol. 69, no. 4, pp. 1767-1770.

Koch, WJ, Inglese, J, Stone, WC & Lefkowitz, RJ 1993, 'The binding site for the beta gamma subunits of heterotrimeric G proteins on the beta-adrenergic receptor kinase', *J Biol Chem*, vol. 268, no. 11, pp. 8256-8260.

Koch, WJ, Rockman, HA, Samama, P, Hamilton, RA, Bond, RA, Milano, CA & Lefkowitz, RJ 1995, 'Cardiac function in mice overexpressing the beta-adrenergic receptor kinase or a beta ARK inhibitor', *Science*, vol. 268, no. 5215, pp. 1350-1353.

Kohout, TA & Lefkowitz, RJ 2003, 'Regulation of G protein-coupled receptor kinases and arrestins during receptor desensitization', *Molecular Pharmacology*, vol. 63, no. 1, pp. 9-18.

Komolov, KE & Benovic, JL 2018, 'G protein-coupled receptor kinases: Past, present and future', *Cell Signal*, vol. 41, pp. 17-24.

Kouhen, OM, Wang, G, Solberg, J, Erickson, LJ, Law, PY & Loh, HH 2000, 'Hierarchical phosphorylation of delta-opioid receptor regulates agonist-induced receptor desensitization and internalization', *J Biol Chem*, vol. 275, no. 47, pp. 36659-36664.

Kozielewicz, P, Turku, A & Schulte, G 2020, 'Molecular Pharmacology of Class F Receptor Activation', *Mol Pharmacol*, vol. 97, no. 2, pp. 62-71.

Kuhn, H, Hall, SW & Wilden, U 1984, 'Light-induced binding of 48-kDa protein to photoreceptor membranes is highly enhanced by phosphorylation of rhodopsin', *FEBS Lett*, vol. 176, no. 2, pp. 473-478.

Latek, D, Modzelewska, A, Trzaskowski, B, Palczewski, K & Filipek, S 2012, 'G protein-coupled receptors--recent advances', *Acta Biochim Pol*, vol. 59, no. 4, pp. 515-529.

Lau, EK, Trester-Zedlitz, M, Trinidad, JC, Kotowski, SJ, Krutchinsky, AN, Burlingame, AL & von Zastrow, M 2011, 'Quantitative encoding of the effect of a partial agonist on individual opioid receptors by multisite phosphorylation and threshold detection', *Sci Signal*, vol. 4, no. 185, p. ra52.

Law, PY, Kouhen, OM, Solberg, J, Wang, W, Erickson, LJ & Loh, HH 2000, 'Deltorphin II-induced rapid desensitization of delta-opioid receptor requires both phosphorylation and internalization of the receptor', *J Biol Chem*, vol. 275, no. 41, pp. 32057-32065.

Le Merrer, J, Becker, JA, Befort, K & Kieffer, BL 2009, 'Reward processing by the opioid system in the brain', *Physiol Rev*, vol. 89, no. 4, pp. 1379-1412.

Lee, Y, Warne, T, Nehme, R, Pandey, S, Dwivedi-Agnihotri, H, Chaturvedi, M, Edwards, PC, Garcia-Nafria, J, Leslie, AGW, Shukla, AK & Tate, CG 2020, 'Molecular basis of beta-arrestin coupling to formoterol-bound beta1-adrenoceptor', *Nature*, vol.

Lefkowitz, RJ 2000, 'The superfamily of heptahelical receptors', *Nat Cell Biol*, vol. 2, no. 7, pp. E133-136.

Lemos Duarte, M & Devi, LA 2020, 'Post-translational Modifications of Opioid Receptors', *Trends Neurosci*, vol. 43, no. 6, pp. 417-432.

Levine, JD & Taiwo, YO 1989, 'Involvement of the mu-opiate receptor in peripheral analgesia', *Neuroscience*, vol. 32, no. 3, pp. 571-575.

Levitt, ES & Williams, JT 2012, 'Morphine desensitization and cellular tolerance are distinguished in rat locus ceruleus neurons', *Mol Pharmacol*, vol. 82, no. 5, pp. 983-992.

Li, H, Eishingdrelo, A, Kongsamut, S & Eishingdrelo, H 2016, 'G-protein-coupled receptors mediate 14-3-3 signal transduction', *Signal Transduct Target Ther*, vol. 1, p. 16018.

Li, J, Xiang, B, Su, W, Zhang, X, Huang, Y & Ma, L 2003, 'Agonist-induced formation of opioid receptor-G protein-coupled receptor kinase (GRK)-G beta gamma complex on membrane is required for GRK2 function in vivo', *J Biol Chem*, vol. 278, no. 32, pp. 30219-30226.

Lipinski, CA, Lombardo, F, Dominy, BW & Feeney, PJ 2001, 'Experimental and computational approaches to estimate solubility and permeability in drug discovery and development settings', *Adv Drug Deliv Rev*, vol. 46, no. 1-3, pp. 3-26.

Lodowski, DT, Pitcher, JA, Capel, WD, Lefkowitz, RJ & Tesmer, JJ 2003, 'Keeping G proteins at bay: a complex between G protein-coupled receptor kinase 2 and Gbetagamma', *Science*, vol. 300, no. 5623, pp. 1256-1262.

Lowe, JD, Celver, JP, Gurevich, VV & Chavkin, C 2002, 'mu-Opioid receptors desensitize less rapidly than delta-opioid receptors due to less efficient activation of arrestin', *J Biol Chem*, vol. 277, no. 18, pp. 15729-15735.

Lowe, JD, Sanderson, HS, Cooke, AE, Ostovar, M, Tsisanova, E, Withey, SL, Chavkin, C, Husbands, SM, Kelly, E, Henderson, G & Bailey, CP 2015, 'Role of G Protein-Coupled Receptor Kinases 2 and 3 in mu-Opioid Receptor Desensitization and Internalization', *Mol Pharmacol*, vol. 88, no. 2, pp. 347-356.

Manglik, A, Lin, H, Aryal, DK, McCorvy, JD, Dengler, D, Corder, G, Levit, A, Kling, RC, Bernat, V, Hubner, H, Huang, XP, Sassano, MF, Giguere, PM, Lober, S, Da, D, Scherrer, G, Kobilka, BK, Gmeiner, P, Roth, BL & Shoichet, BK 2016, 'Structure-based discovery of opioid analgesics with reduced side effects', *Nature*, vol. 537, no. 7619, pp. 185-190.

Mann, A, Illing, S, Miess, E & Schulz, S 2015, 'Different mechanisms of homologous and heterologous mu-opioid receptor phosphorylation', *Br J Pharmacol*, vol. 172, no. 2, pp. 311-316.

Mann, A, Liebetrau, S, Klima, M, Dasgupta, P, Massotte, D & Schulz, S 2020, 'Agonist-induced phosphorylation bar code and differential post-activation signaling of the delta opioid receptor revealed by phosphosite-specific antibodies', *Sci Rep*, vol. 10, no. 1, p. 8585.

Massoud, TF, Paulmurugan, R, De, A, Ray, P & Gambhir, SS 2007, 'Reporter gene imaging of protein-protein interactions in living subjects', *Curr Opin Biotechnol*, vol. 18, no. 1, pp. 31-37.

Masuho, I, Martemyanov, KA & Lambert, NA 2015, 'Monitoring G Protein Activation in Cells with BRET', *Methods Mol Biol*, vol. 1335, pp. 107-113.

Matkovich, SJ, Diwan, A, Klanke, JL, Hammer, DJ, Marreez, Y, Odley, AM, Brunskill, EW, Koch, WJ, Schwartz, RJ & Dorn, GW, 2nd 2006, 'Cardiac-specific ablation of G-

protein receptor kinase 2 redefines its roles in heart development and beta-adrenergic signaling', *Circ Res*, vol. 99, no. 9, pp. 996-1003.

Mayer, G, Wulffen, B, Huber, C, Brockmann, J, Flicke, B, Neumann, L, Hafenbradl, D, Klebl, BM, Lohse, MJ, Krasel, C & Blind, M 2008, 'An RNA molecule that specifically inhibits G-protein-coupled receptor kinase 2 in vitro', *RNA*, vol. 14, no. 3, pp. 524-534.

McPherson, J, Rivero, G, Baptist, M, Llorente, J, Al-Sabah, S, Krasel, C, Dewey, WL, Bailey, CP, Rosethorne, EM, Charlton, SJ, Henderson, G & Kelly, E 2010, 'mu-opioid receptors: correlation of agonist efficacy for signalling with ability to activate internalization', *Mol Pharmacol*, vol. 78, no. 4, pp. 756-766.

Melief, EJ, Miyatake, M, Bruchas, MR & Chavkin, C 2010, 'Ligand-directed c-Jun N-terminal kinase activation disrupts opioid receptor signaling', *Proc Natl Acad Sci U S A*, vol. 107, no. 25, pp. 11608-11613.

Metaye, T, Gibelin, H, Perdrisot, R & Kraimps, JL 2005, 'Pathophysiological roles of G-protein-coupled receptor kinases', *Cell Signal*, vol. 17, no. 8, pp. 917-928.

Metaye, T, Levillain, P, Kraimps, JL & Perdrisot, R 2008, 'Immunohistochemical detection, regulation and antiproliferative function of G-protein-coupled receptor kinase 2 in thyroid carcinomas', *J Endocrinol*, vol. 198, no. 1, pp. 101-110.

Miess, E, Gondin, AB, Yousuf, A, Steinborn, R, Mosslein, N, Yang, Y, Goldner, M, Ruland, JG, Bunemann, M, Krasel, C, Christie, MJ, Halls, ML, Schulz, S & Canals, M 2018, 'Multisite phosphorylation is required for sustained interaction with GRKs and arrestins during rapid mu-opioid receptor desensitization', *Sci Signal*, vol. 11, no. 539.

Minnis, JG, Patierno, S, Kohlmeier, SE, Brecha, NC, Tonini, M & Sternini, C 2003, 'Ligand-induced mu opioid receptor endocytosis and recycling in enteric neurons', *Neuroscience*, vol. 119, no. 1, pp. 33-42.

Moller, TC, Pedersen, MF, van Senten, JR, Seiersen, SD, Mathiesen, JM, Bouvier, M & Brauner-Osborne, H 2020, 'Dissecting the roles of GRK2 and GRK3 in mu-opioid

receptor internalization and beta-arrestin2 recruitment using CRISPR/Cas9-edited HEK293 cells', *Sci Rep*, vol. 10, no. 1, p. 17395.

Monto, F, Oliver, E, Vicente, D, Rueda, J, Aguero, J, Almenar, L, Ivorra, MD, Barettino, D & D'Ocon, P 2012, 'Different expression of adrenoceptors and GRKs in the human myocardium depends on heart failure etiology and correlates to clinical variables', *Am J Physiol Heart Circ Physiol*, vol. 303, no. 3, pp. H368-376.

Moore, CA, Milano, SK & Benovic, JL 2007, 'Regulation of receptor trafficking by GRKs and arrestins', *Annu Rev Physiol*, vol. 69, pp. 451-482.

Mundell, SJ, Benovic, JL & Kelly, E 1997, 'A dominant negative mutant of the G protein-coupled receptor kinase 2 selectively attenuates adenosine A2 receptor desensitization', *Mol Pharmacol*, vol. 51, no. 6, pp. 991-998.

Mundell, SJ, Nisar, SP & Kelly, E 2010, 'Measurement and Visulization of G Protein-coupled Receptor Trafficking by Enzyme-linked Immunosorbent Assay and Immunofluorence', in D Poyner & M Wheatley (eds), *G Protein-Coupled Receptors : Essential Methods*, John Wiley & Sons, The Atrium, Southern Gate, Chichester, West Sussex, UK ; Hoboken, NJ, pp. 215-228.

Murga, C, Arcones, AC, Cruces-Sande, M, Briones, AM, Salaices, M & Mayor, F, Jr. 2019, 'G Protein-Coupled Receptor Kinase 2 (GRK2) as a Potential Therapeutic Target in Cardiovascular and Metabolic Diseases', *Front Pharmacol*, vol. 10, p. 112.

Nagi, K & Pineyro, G 2014, 'Kir3 channel signaling complexes: focus on opioid receptor signaling', *Front Cell Neurosci*, vol. 8, p. 186.

Navratilova, E, Eaton, MC, Stropova, D, Varga, EV, Vanderah, TW, Roeske, WR & Yamamura, HI 2005, 'Morphine promotes phosphorylation of the human delta-opioid receptor at serine 363', *Eur J Pharmacol*, vol. 519, no. 3, pp. 212-214.

Negus, SS, Gatch, MB, Mello, NK, Zhang, X & Rice, K 1998, 'Behavioral effects of the delta-selective opioid agonist SNC80 and related compounds in rhesus monkeys', *J Pharmacol Exp Ther*, vol. 286, no. 1, pp. 362-375.

Neilan, CL, Akil, H, Woods, JH & Traynor, JR 1999, 'Constitutive activity of the delta-opioid receptor expressed in C6 glioma cells: identification of non-peptide delta-inverse agonists', *Br J Pharmacol*, vol. 128, no. 3, pp. 556-562.

Nickolls, SA, Humphreys, S, Clark, M & McMurray, G 2013, 'Co-expression of GRK2 reveals a novel conformational state of the micro-opioid receptor', *PLoS One*, vol. 8, no. 12, p. e83691.

Nobles, KN, Xiao, K, Ahn, S, Shukla, AK, Lam, CM, Rajagopal, S, Strachan, RT, Huang, TY, Bressler, EA, Hara, MR, Shenoy, SK, Gygi, SP & Lefkowitz, RJ 2011, 'Distinct phosphorylation sites on the beta(2)-adrenergic receptor establish a barcode that encodes differential functions of beta-arrestin', *Sci Signal*, vol. 4, no. 185, p. ra51.

O'Connell, TD, Jensen, BC, Baker, AJ & Simpson, PC 2014, 'Cardiac alpha1-adrenergic receptors: novel aspects of expression, signaling mechanisms, physiologic function, and clinical importance', *Pharmacol Rev*, vol. 66, no. 1, pp. 308-333.

Okawa, T, Aramaki, Y, Yamamoto, M, Kobayashi, T, Fukumoto, S, Toyoda, Y, Henta, T, Hata, A, Ikeda, S, Kaneko, M, Hoffman, ID, Sang, BC, Zou, H & Kawamoto, T 2017, 'Design, Synthesis, and Evaluation of the Highly Selective and Potent G-Protein-Coupled Receptor Kinase 2 (GRK2) Inhibitor for the Potential Treatment of Heart Failure', *J Med Chem*, vol. 60, no. 16, pp. 6942-6990.

Pack, TF, Orlen, MI, Ray, C, Peterson, SM & Caron, MG 2018, 'The dopamine D2 receptor can directly recruit and activate GRK2 without G protein activation', *J Biol Chem*, vol. 293, no. 16, pp. 6161-6171.

Pasternak, GW & Pan, YX 2013, 'Mu opioids and their receptors: evolution of a concept', *Pharmacol Rev*, vol. 65, no. 4, pp. 1257-1317.

Penela, P, Murga, C, Ribas, C, Lafarga, V & Mayor, F, Jr. 2010, 'The complex G protein-coupled receptor kinase 2 (GRK2) interactome unveils new physiopathological targets', *Br J Pharmacol*, vol. 160, no. 4, pp. 821-832.

Penela, P, Murga, C, Ribas, C, Tutor, AS, Peregrin, S & Mayor, F, Jr. 2006, 'Mechanisms of regulation of G protein-coupled receptor kinases (GRKs) and cardiovascular disease', *Cardiovasc Res*, vol. 69, no. 1, pp. 46-56.

Penela, P, Ruiz-Gomez, A, Castano, JG & Mayor, F, Jr. 1998, 'Degradation of the G protein-coupled receptor kinase 2 by the proteasome pathway', *J Biol Chem*, vol. 273, no. 52, pp. 35238-35244.

Pfleger, KD & Eidne, KA 2006, 'Illuminating insights into protein-protein interactions using bioluminescence resonance energy transfer (BRET)', *Nat Methods*, vol. 3, no. 3, pp. 165-174.

Pfleger, KD, Seeber, RM & Eidne, KA 2006, 'Bioluminescence resonance energy transfer (BRET) for the real-time detection of protein-protein interactions', *Nat Protoc*, vol. 1, no. 1, pp. 337-345.

Pierce, KL, Premont, RT & Lefkowitz, RJ 2002, 'Seven-transmembrane receptors', *Nat Rev Mol Cell Biol*, vol. 3, no. 9, pp. 639-650.

Pitcher, JA, Freedman, NJ & Lefkowitz, RJ 1998, 'G protein-coupled receptor kinases', *Annual Review of Biochemistry*, vol. 67, pp. 653-692.

Pitcher, JA, Inglese, J, Higgins, JB, Arriza, JL, Casey, PJ, Kim, C, Benovic, JL, Kwatra, MM, Caron, MG & Lefkowitz, RJ 1992, 'Role of beta gamma subunits of G proteins in targeting the beta-adrenergic receptor kinase to membrane-bound receptors', *Science*, vol. 257, no. 5074, pp. 1264-1267.

Pradhan, AA, Perroy, J, Walwyn, WM, Smith, ML, Vicente-Sanchez, A, Segura, L, Bana, A, Kieffer, BL & Evans, CJ 2016, 'Agonist-Specific Recruitment of Arrestin Isoforms

Differentially Modify Delta Opioid Receptor Function', *J Neurosci*, vol. 36, no. 12, pp. 3541-3551.

Premont, RT & Gainetdinov, RR 2007, 'Physiological roles of G protein-coupled receptor kinases and arrestins', *Annu Rev Physiol*, vol. 69, pp. 511-534.

Qiu, Y, Loh, HH & Law, PY 2007, 'Phosphorylation of the delta-opioid receptor regulates its beta-arrestins selectivity and subsequent receptor internalization and adenylyl cyclase desensitization', *J Biol Chem*, vol. 282, no. 31, pp. 22315-22323.

Raake, PW, Schlegel, P, Ksienzyk, J, Reinkober, J, Barthelmes, J, Schinkel, S, Pleger, S, Mier, W, Haberkorn, U, Koch, WJ, Katus, HA, Most, P & Muller, OJ 2013, 'AAV6.betaARKct cardiac gene therapy ameliorates cardiac function and normalizes the catecholaminergic axis in a clinically relevant large animal heart failure model', *Eur Heart J*, vol. 34, no. 19, pp. 1437-1447.

Rainbow, RD, Brennan, S, Jackson, R, Beech, AJ, Bengreed, A, Waldschmidt, HV, Tesmer, JJG, Challiss, RAJ & Willets, JM 2018, 'Small-Molecule G Protein-Coupled Receptor Kinase Inhibitors Attenuate G Protein-Coupled Receptor Kinase 2-Mediated Desensitization of Vasoconstrictor-Induced Arterial Contractions', *Mol Pharmacol*, vol. 94, no. 3, pp. 1079-1091.

Rang, HP 2006, 'The receptor concept: pharmacology's big idea', *British Journal of Pharmacology*, vol. 147 Suppl 1, no. Suppl 1, pp. S9-S16.

Rankovic, Z, Brust, TF & Bohn, LM 2016, 'Biased agonism: An emerging paradigm in GPCR drug discovery', *Bioorg Med Chem Lett*, vol. 26, no. 2, pp. 241-250.

Rasmussen, SG, DeVree, BT, Zou, Y, Kruse, AC, Chung, KY, Kobilka, TS, Thian, FS, Chae, PS, Pardon, E, Calinski, D, Mathiesen, JM, Shah, ST, Lyons, JA, Caffrey, M, Gellman, SH, Steyaert, J, Skiniotis, G, Weis, WI, Sunahara, RK & Kobilka, BK 2011, 'Crystal structure of the beta2 adrenergic receptor-Gs protein complex', *Nature*, vol. 477, no. 7366, pp. 549-555.

Reyes-Alcaraz, A, Lee, YN, Yun, S, Hwang, JI & Seong, JY 2018, 'Conformational signatures in beta-arrestin2 reveal natural biased agonism at a G-protein-coupled receptor', *Commun Biol*, vol. 1, p. 128.

Rezazadeh, S, Claydon, TW & Fedida, D 2006, 'KN-93 (2-[N-(2-hydroxyethyl)]-N-(4-methoxybenzenesulfonyl)]amino-N-(4-chlorocinnamyl)-N -methylbenzylamine), a calcium/calmodulin-dependent protein kinase II inhibitor, is a direct extracellular blocker of voltage-gated potassium channels', *J Pharmacol Exp Ther*, vol. 317, no. 1, pp. 292-299.

Rockman, HA, Chien, KR, Choi, DJ, Iaccarino, G, Hunter, JJ, Ross, J, Jr., Lefkowitz, RJ & Koch, WJ 1998, 'Expression of a beta-adrenergic receptor kinase 1 inhibitor prevents the development of myocardial failure in gene-targeted mice', *Proc Natl Acad Sci U S A*, vol. 95, no. 12, pp. 7000-7005.

Rockman, HA, Choi, DJ, Rahman, NU, Akhter, SA, Lefkowitz, RJ & Koch, WJ 1996, 'Receptor-specific in vivo desensitization by the G protein-coupled receptor kinase-5 in transgenic mice', *Proc Natl Acad Sci U S A*, vol. 93, no. 18, pp. 9954-9959.

Rowlands, RA, Cato, MC, Waldschmidt, HV, Bouley, RA, Chen, Q, Avramova, L, Larsen, SD, Tesmer, JJG & White, AD 2019, 'Structure-Based Design of Selective, Covalent G Protein-Coupled Receptor Kinase 5 Inhibitors', *ACS Med Chem Lett*, vol. 10, no. 12, pp. 1628-1634.

Sallese, M, Iacovelli, L, Cumashi, A, Capobianco, L, Cuomo, L & De Blasi, A 2000, 'Regulation of G protein-coupled receptor kinase subtypes by calcium sensor proteins', *Biochim Biophys Acta*, vol. 1498, no. 2-3, pp. 112-121.

Sallese, M, Mariggiò, S, D'Urbano, E, Iacovelli, L & De Blasi, A 2000, 'Selective regulation of Gq signaling by G protein-coupled receptor kinase 2: Direct interaction of kinase N terminus with activated G(αq)', *Molecular Pharmacology*, vol. 57, no. 4, pp. 826-831.

Santulli, G, Trimarco, B & Iaccarino, G 2013, 'G-protein-coupled receptor kinase 2 and hypertension: molecular insights and pathophysiological mechanisms', *High Blood Press Cardiovasc Prev*, vol. 20, no. 1, pp. 5-12.

Sato, PY, Chuprun, JK, Schwartz, M & Koch, WJ 2015, 'The evolving impact of g protein-coupled receptor kinases in cardiac health and disease', *Physiol Rev*, vol. 95, no. 2, pp. 377-404.

Schmidt, H, Schulz, S, Klutzny, M, Koch, T, Händel, M & Höllt, V 2000, 'Involvement of mitogen-activated protein kinase in agonist-induced phosphorylation of the μ-opioid receptor in HEK 293 cells', *Journal of Neurochemistry*, vol. 74, no. 1, pp. 414-422.

Schroeder, JE, Fischbach, PS, Zheng, D & McCleskey, EW 1991, 'Activation of mu opioid receptors inhibits transient high- and low-threshold Ca2+ currents, but spares a sustained current', *Neuron*, vol. 6, no. 1, pp. 13-20.

Schumacher, SM, Gao, E, Zhu, W, Chen, X, Chuprun, JK, Feldman, AM, Tesmer, JJ & Koch, WJ 2015, 'Paroxetine-mediated GRK2 inhibition reverses cardiac dysfunction and remodeling after myocardial infarction', *Sci Transl Med*, vol. 7, no. 277, p. 277ra231.

Setyawan, J, Koide, K, Diller, TC, Bunnage, ME, Taylor, SS, Nicolaou, KC & Brunton, LL 1999, 'Inhibition of protein kinases by balanol: specificity within the serine/threonine protein kinase subfamily', *Mol Pharmacol*, vol. 56, no. 2, pp. 370-376.

Seward, E, Hammond, C & Henderson, G 1991, 'Mu-opioid-receptor-mediated inhibition of the N-type calcium-channel current', *Proc Biol Sci*, vol. 244, no. 1310, pp. 129-135.

Shenoy, SK & Lefkowitz, RJ 2011, 'beta-Arrestin-mediated receptor trafficking and signal transduction', *Trends Pharmacol Sci*, vol. 32, no. 9, pp. 521-533.

Shukla, AK & Dwivedi-Agnihotri, H 2020, 'Structure and function of beta-arrestins, their emerging role in breast cancer, and potential opportunities for therapeutic manipulation', *Adv Cancer Res*, vol. 145, pp. 139-156.

Singh, J, Petter, RC, Baillie, TA & Whitty, A 2011, 'The resurgence of covalent drugs', *Nat Rev Drug Discov*, vol. 10, no. 4, pp. 307-317.

Siryk-Bathgate, A, Dabul, S & Lymperopoulos, A 2013, 'Current and future G protein-coupled receptor signaling targets for heart failure therapy', *Drug Des Devel Ther*, vol. 7, pp. 1209-1222.

Smith, JS & Rajagopal, S 2016, 'The beta-Arrestins: Multifunctional Regulators of G Protein-coupled Receptors', *J Biol Chem*, vol. 291, no. 17, pp. 8969-8977.

Staus, DP, Hu, H, Robertson, MJ, Kleinhenz, ALW, Wingler, LM, Capel, WD, Latorraca, NR, Lefkowitz, RJ & Skiniotis, G 2020, 'Structure of the M2 muscarinic receptor-beta-arrestin complex in a lipid nanodisc', *Nature*, vol. 579, no. 7798, pp. 297-302.

Steury, MD, McCabe, LR & Parameswaran, N 2017, 'G Protein-Coupled Receptor Kinases in the Inflammatory Response and Signaling', *Adv Immunol*, vol. 136, pp. 227-277.

Stevenson, GW, Folk, JE, Rice, KC & Negus, SS 2005, 'Interactions between delta and mu opioid agonists in assays of schedule-controlled responding, thermal nociception, drug self-administration, and drug versus food choice in rhesus monkeys: studies with SNC80 [(+)-4-[(alphaR)-alpha-((2S,5R)-4-allyl-2,5-dimethyl-1-piperazinyl)-3-methoxybenz yl]-N,N-diethylbenzamide] and heroin', *J Pharmacol Exp Ther*, vol. 314, no. 1, pp. 221-231.

Stoeber, M, Jullié, D, Lobingier, BT, Laeremans, T, Steyaert, J, Schiller, PW, Manglik, A & von Zastrow, M 2018, 'A Genetically Encoded Biosensor Reveals Location Bias of Opioid Drug Action', *Neuron*, vol. 98, no. 5, pp. 963-976.e965.

Stoffel, RH, Randall, RR, Premont, RT, Lefkowitz, RJ & Inglese, J 1994, 'Palmitoylation of G protein-coupled receptor kinase, GRK6. Lipid modification diversity in the GRK family', *J Biol Chem*, vol. 269, no. 45, pp. 27791-27794.

Sutcliffe, KJ, Henderson, G, Kelly, E & Sessions, RB 2017, 'Drug Binding Poses Relate Structure with Efficacy in the mu Opioid Receptor', *J Mol Biol*, vol. 429, no. 12, pp. 1840-1851.

Tang, J, Dong, J, Yang, L, Gao, L & Zheng, J 2015, 'Paroxetine alleviates rat limb post-ischemia induced allodynia through GRK2 upregulation in superior cervical ganglia', *International Journal of Clinical and Experimental Medicine*, vol. 8, no. 2, pp. 2065-2076.

Tesmer, JJ, Tesmer, VM, Lodowski, DT, Steinhagen, H & Huber, J 2010, 'Structure of human G protein-coupled receptor kinase 2 in complex with the kinase inhibitor balanol', *J Med Chem*, vol. 53, no. 4, pp. 1867-1870.

Tesmer, VM, Kawano, T, Shankaranarayanan, A, Kozasa, T & Tesmer, JJ 2005, 'Snapshot of activated G proteins at the membrane: the Galphaq-GRK2-Gbetagamma complex', *Science*, vol. 310, no. 5754, pp. 1686-1690.

Tesmer, VM, Lennarz, S, Mayer, G & Tesmer, JJ 2012, 'Molecular mechanism for inhibition of g protein-coupled receptor kinase 2 by a selective RNA aptamer', *Structure*, vol. 20, no. 8, pp. 1300-1309.

Thal, DM, Homan, KT, Chen, J, Wu, EK, Hinkle, PM, Huang, ZM, Chuprun, JK, Song, J, Gao, E, Cheung, JY, Sklar, LA, Koch, WJ & Tesmer, JJ 2012, 'Paroxetine is a direct inhibitor of g protein-coupled receptor kinase 2 and increases myocardial contractility', *ACS Chem Biol*, vol. 7, no. 11, pp. 1830-1839.

Thal, DM, Yeow, RY, Schoenau, C, Huber, J & Tesmer, JJ 2011, 'Molecular mechanism of selectivity among G protein-coupled receptor kinase 2 inhibitors', *Mol Pharmacol*, vol. 80, no. 2, pp. 294-303.

Tian, X, Kang, DS & Benovic, JL 2014, 'beta-arrestins and G protein-coupled receptor trafficking', *Handb Exp Pharmacol*, vol. 219, pp. 173-186.

Toubia, T & Khalife, T 2019, 'The Endogenous Opioid System: Role and Dysfunction Caused by Opioid Therapy', *Clin Obstet Gynecol*, vol. 62, no. 1, pp. 3-10.

Ungerer, M, Bohm, M, Elce, JS, Erdmann, E & Lohse, MJ 1993, 'Altered expression of beta-adrenergic receptor kinase and beta 1-adrenergic receptors in the failing human heart', *Circulation*, vol. 87, no. 2, pp. 454-463.

Ungerer, M, Parruti, G, Bohm, M, Puzicha, M, DeBlasi, A, Erdmann, E & Lohse, MJ 1994, 'Expression of beta-arrestins and beta-adrenergic receptor kinases in the failing human heart', *Circ Res*, vol. 74, no. 2, pp. 206-213.

Usui, I, Imamura, T, Satoh, H, Huang, J, Babendure, JL, Hupfeld, CJ & Olefsky, JM 2004, 'GRK2 is an endogenous protein inhibitor of the insulin signaling pathway for glucose transport stimulation', *EMBO J*, vol. 23, no. 14, pp. 2821-2829.

Vicente-Sanchez, A, Dripps, IJ, Tipton, AF, Akbari, H, Akbari, A, Jutkiewicz, EM & Pradhan, AA 2018, 'Tolerance to high-internalizing delta opioid receptor agonist is critically mediated by arrestin 2', *Br J Pharmacol*, vol. 175, no. 14, pp. 3050-3059.

Violin, JD, Ren, XR & Lefkowitz, RJ 2006, 'G-protein-coupled receptor kinase specificity for beta-arrestin recruitment to the beta2-adrenergic receptor revealed by fluorescence resonance energy transfer', *J Biol Chem*, vol. 281, no. 29, pp. 20577-20588.

Vroon, A, Heijnen, CJ & Kavelaars, A 2006, 'GRKs and arrestins: regulators of migration and inflammation', *J Leukoc Biol*, vol. 80, no. 6, pp. 1214-1221.

Vroon, A, Heijnen, CJ, Lombardi, MS, Cobelens, PM, Mayor, F, Jr., Caron, MG & Kavelaars, A 2004, 'Reduced GRK2 level in T cells potentiates chemotaxis and signaling in response to CCL4', *J Leukoc Biol*, vol. 75, no. 5, pp. 901-909.

Waldhoer, M, Bartlett, SE & Whistler, JL 2004, 'Opioid receptors', *Annu Rev Biochem*, vol. 73, pp. 953-990.

Waldschmidt, HV, Bouley, R, Kirchhoff, PD, Lee, P, Tesmer, JJG & Larsen, SD 2018, 'Utilizing a structure-based docking approach to develop potent G protein-coupled

receptor kinase (GRK) 2 and 5 inhibitors', *Bioorg Med Chem Lett*, vol. 28, no. 9, pp. 1507-1515.

Waldschmidt, HV, Homan, KT, Cato, MC, Cruz-Rodriguez, O, Cannavo, A, Wilson, MW, Song, J, Cheung, JY, Koch, WJ, Tesmer, JJ & Larsen, SD 2017, 'Structure-Based Design of Highly Selective and Potent G Protein-Coupled Receptor Kinase 2 Inhibitors Based on Paroxetine', *J Med Chem*, vol. 60, no. 7, pp. 3052-3069.

Waldschmidt, HV, Homan, KT, Cruz-Rodriguez, O, Cato, MC, Waninger-Saroni, J, Larimore, KM, Cannavo, A, Song, J, Cheung, JY, Kirchhoff, PD, Koch, WJ, Tesmer, JJ & Larsen, SD 2016, 'Structure-Based Design, Synthesis, and Biological Evaluation of Highly Selective and Potent G Protein-Coupled Receptor Kinase 2 Inhibitors', *J Med Chem*, vol. 59, no. 8, pp. 3793-3807.

Wang, J, Gareri, C & Rockman, HA 2018, 'G-Protein-Coupled Receptors in Heart Disease', *Circ Res*, vol. 123, no. 6, pp. 716-735.

Wei, Z, Hurtt, R, Ciccarelli, M, Koch, WJ & Doria, C 2012, 'Growth inhibition of human hepatocellular carcinoma cells by overexpression of G-protein-coupled receptor kinase 2', *J Cell Physiol*, vol. 227, no. 6, pp. 2371-2377.

Williams, JT, Ingram, SL, Henderson, G, Chavkin, C, von Zastrow, M, Schulz, S, Koch, T, Evans, CJ & Christie, MJ 2013, 'Regulation of mu-opioid receptors: desensitization, phosphorylation, internalization, and tolerance', *Pharmacol Rev*, vol. 65, no. 1, pp. 223-254.

Wingler, LM & Lefkowitz, RJ 2020, 'Conformational Basis of G Protein-Coupled Receptor Signaling Versatility', *Trends Cell Biol*, vol.

Woo, AY & Xiao, RP 2012, 'beta-Adrenergic receptor subtype signaling in heart: from bench to bedside', *Acta Pharmacol Sin*, vol. 33, no. 3, pp. 335-341.

Xiang, B, Yu, GH, Guo, J, Chen, L, Hu, W, Pei, G & Ma, L 2001, 'Heterologous activation of protein kinase C stimulates phosphorylation of delta-opioid receptor at serine 344,

resulting in beta-arrestin- and clathrin-mediated receptor internalization', *J Biol Chem*, vol. 276, no. 7, pp. 4709-4716.

Xiao, RP 2001, 'Beta-adrenergic signaling in the heart: dual coupling of the beta2-adrenergic receptor to G(s) and G(i) proteins', *Sci STKE*, vol. 2001, no. 104, p. re15.

Yang, Z, Yang, F, Zhang, D, Liu, Z, Lin, A, Liu, C, Xiao, P, Yu, X & Sun, JP 2017, 'Phosphorylation of G Protein-Coupled Receptors: From the Barcode Hypothesis to the Flute Model', *Mol Pharmacol*, vol. 92, no. 3, pp. 201-210.

Yao, XQ, Cato, MC, Labudde, E, Beyett, TS, Tesmer, JJG & Grant, BJ 2017, 'Navigating the conformational landscape of G protein-coupled receptor kinases during allosteric activation', *J Biol Chem*, vol. 292, no. 39, pp. 16032-16043.

Yi, XP, Zhou, J, Baker, J, Wang, X, Gerdes, AM & Li, F 2005, 'Myocardial expression and redistribution of GRKs in hypertensive hypertrophy and failure', *Anat Rec A Discov Mol Cell Evol Biol*, vol. 282, no. 1, pp. 13-23.

Yin, W, Li, Z, Jin, M, Yin, YL, de Waal, PW, Pal, K, Yin, Y, Gao, X, He, Y, Gao, J, Wang, X, Zhang, Y, Zhou, H, Melcher, K, Jiang, Y, Cong, Y, Edward Zhou, X, Yu, X & Eric Xu, H 2019, 'A complex structure of arrestin-2 bound to a G protein-coupled receptor', *Cell Res*, vol. 29, no. 12, pp. 971-983.

Yoo, SM, Bhardwaj, A & Benovic, JL 2020, 'Arresting Developments in Biased Signaling', *Trends Pharmacol Sci*, vol. 41, no. 6, pp. 387-389.

Yousuf, A, Miess, E, Sianati, S, Du, YP, Schulz, S & Christie, MJ 2015, 'Role of phosphorylation sites in desensitization of μ-opioid receptor', *Molecular Pharmacology*, vol. 88, no. 4, pp. 825-835.

Yu, Q, Gratzke, C, Wang, Y, Herlemann, A, Strittmatter, F, Rutz, B, Stief, CG & Hennenberg, M 2018, 'Inhibition of prostatic smooth muscle contraction by the inhibitor of G protein-coupled receptor kinase 2/3, CMPD101', *Eur J Pharmacol*, vol. 831, pp. 9-19.

Zhang, X, Wang, F, Chen, X, Chen, Y & Ma, L 2008, 'Post-endocytic fates of delta-opioid receptor are regulated by GRK2-mediated receptor phosphorylation and distinct beta-arrestin isoforms', *J Neurochem*, vol. 106, no. 2, pp. 781-792.

Zhang, X, Wang, F, Chen, X, Li, J, Xiang, B, Zhang, YQ, Li, BM & Ma, L 2005, 'Beta-arrestin1 and beta-arrestin2 are differentially required for phosphorylation-dependent and -independent internalization of delta-opioid receptors', *J Neurochem*, vol. 95, no. 1, pp. 169-178.

Zhou, XE, He, Y, de Waal, PW, Gao, X, Kang, Y, Van Eps, N, Yin, Y, Pal, K, Goswami, D, White, TA, Barty, A, Latorraca, NR, Chapman, HN, Hubbell, WL, Dror, RO, Stevens, RC, Cherezov, V, Gurevich, VV, Griffin, PR, Ernst, OP, Melcher, K & Xu, HE 2017, 'Identification of Phosphorylation Codes for Arrestin Recruitment by G Protein-Coupled Receptors', *Cell*, vol. 170, no. 3, pp. 457-469 e413.